

# Assessing the controls on long-term organic carbon preservation in soils

A field study in intertidal landscapes  
and a model assessment



**Marijn Van de Broek**

Supervisor: Prof. dr. G. Govers  
Co-supervisor: Prof. dr. R. Merckx

Dissertation presented in partial  
fulfilment of the requirements for the  
degree of Doctor of Science (PhD):  
Geography

June 2018

---



# **Assessing the controls on long-term organic carbon preservation in soils**

A field study in intertidal landscapes and a model assessment

**Marijn Van de Broek**

Supervisor: prof. dr. G. Govers (KU Leuven)  
Co-supervisor: prof. dr. R. Merckx (KU Leuven)

Members of the examination committee:  
Prof. dr. J. Poesen (Chairman) (KU Leuven)  
Prof. dr. K. Van Oost (UCL)  
Prof. dr. S. Temmerman (UAntwerpen)  
Prof. dr. S. Bouillon (KU Leuven)  
Prof. dr. J. Diels (KU Leuven)  
Prof. dr. B. Jansen (Universiteit van Amsterdam)  
dr. M. Schrumpf (Max-Planck-Institute, Germany)

Dissertation presented in partial  
fulfilment of the requirements for the  
degree of Doctor of Science (PhD):  
Geography

June 2018

© 2018 KU Leuven, Science, Engineering & Technology

Uitgegeven in eigen beheer, Marijn Van de Broek, Leuven

Afbeelding op de voorpagina: schorrand van het Schor bij Waarde (Nederland)

Alle rechten voorbehouden. Niets uit deze uitgave mag worden vermenigvuldigd en/of openbaar gemaakt worden door middel van druk, fotokopie, microfilm, elektronisch of op welke andere wijze ook zonder voorafgaandelijke schriftelijke toestemming van de uitgever.

All rights reserved. No part of the publication may be reproduced in any form by print, photoprint, microfilm, electronic or any other means without written permission from the publisher.

## Preface

---

Het schrijven van een dankwoord kondigt vaak het einde van iets belangrijks aan. Enerzijds voelt het afwerken van dit doctoraat dan ook aan als het einde aan een periode waar ik vier jaar naar heb toegeleefd. De reis die me naar dit moment heeft geleid was echter veel belangrijker dan de eindmeet. Het was er een door vele landen met leerrijke ontmoetingen die mijn leven op veel vlakken hebben verrijkt. Anderzijds is dit ook de start van een nieuw avontuur. Voor ik daar aan begin, zou ik graag enkele mensen willen bedanken.

Een enorme dank u gaat uit naar mijn promotor, Gerard. Met je onuitputtelijke energie en optimisme heb je er niet alleen voor gezorgd dat dit doctoraat tot een goed einde kwam, maar ook dat ik de afgelopen 4 jaar met zeer veel vrijheid mijn eerste stappen in de wetenschappelijk wereld kon zetten. Ondanks je drukke agenda maakte je steeds tijd om snel wat raad te geven, voor een vergadering of om zeer uitgebreide feedback op elke nieuwe versie van een paper te geven. Ook tijdens koffiepauzes, op excursie of tijdens de lessen die je gaf was er steeds tijd voor een ontspannende babbel of een analyse van de grote problemen van deze wereld. Van onze eerste samenwerking, toen ik in 2010 koos om mijn bachelorproef te schrijven rond koolstof in polderbodems, tot het einde van dit doctoraat was het een zeer aangename samenwerking waarvan ik hoop dat we ze in de toekomst nog kunnen verderzetten.

Een speciale dank gaat uit naar Roel, om mij als co-promotor te begeleiden tijdens de afgelopen jaren. Bovendien wil ik Stijn enorm bedanken voor de begeleiding tijdens dit doctoraat. Ook onze samenwerking gaat terug naar mijn bachelorproef en werd intensiever toen ik besloot mijn masterthesis te schrijven rond polderbodems en jouw geliefde terrein: de schorren van de Schelde. Ik was steeds welkom in Antwerpen voor een vergadering, waarop duidelijk werd dat jouw enorme kennis van deze ecosystemen onmisbaar was om dit doctoraat tot een goed einde te brengen. Hopelijk kunnen we deze samenwerking in de toekomst blijven verderzetten. Daarnaast zou ik ook Boris hartelijk willen bedanken voor de warme welkom in Amsterdam en jouw groep. De interessante en leuke discussies waren keer op keer zeer leerrijk en hebben me veel kennis bijgebracht over de chemische kant van bodemkoolstof. Marion, I also want to thank you for the interesting discussions together with Bernhard about the COMISSION model and the feedback on the SOILcarb- RM model. I would furthermore like to thank all my jury members for being a part of my examination committee and for the very useful feedback on the first version of this manuscript.

Om van een doctoraatsperiode een leuke tijd te maken is een leuke werkomgeving een onmisbaar element, en dat was zeker het geval in 'de E'. Er heerste steeds een gemoedelijke sfeer, er kon altijd worden gelachen en de dagelijkse koffiepauzes zorgden voor de nodige ontspanning. Bedankt collega's, dat ik mijn doctoraat samen met een vriendengroep kon maken in plaats van louter collega's, wat op zijn minst uniek te noemen is. De werkomgeving in het geo-instituut werd recent nog aangenamer gemaakt door de aanleg van de 'geogarden', met Anton als drijvende kracht, waardoor de middagpauze vanaf nu kan doorgaan in onze tuin in plaats van op de stenen vloer. Een speciale vernoeming gaat uit naar mijn bureaugenoten: Benjamin, Armando, Veronique, Xiaoyan, Bright en Kristof. Merci voor de leuke momenten die we in 03.264 hebben meegemaakt! Ook de collega's uit de onze onderzoeksgroep zou ik heel graag willen bedanken voor de steun en de vele interessante seminaries die we hadden: Benjamin, Jérémy, Jianlin, Taciana, Liesa, Lies, Xiaoyan, Man, Jiaqian en Arthur. Een welgemeende dankjewel is weggelegd voor Lore, zonder wie dit doctoraat nooit op 4 jaar had kunnen worden afgewerkt. Bedankt voor de enorme hulp en het aangename gezelschap tijdens het vele veldwerk op de schorren, in de polders en in een occasionele plaggenbodem, en bij de verwerking van de stalen in het labo.

Another special 'thank you' is reserved for the international PhD students in our group. Fred, thanks a lot for the great time, both inside and outside the lab! Jianlin, your enthusiasm made our office a great place to work, and brightened many trips and Chinese dinners. Taciana (and of course João), thanks a lot for the many great moments we shared, both in the office and in Rock Café! Kristien and myself had a great time while being in Piracicaba, thanks again for having us and showing us how wonderful Brazil is! I also want to thank the members of the SOGLO project, with whom I shared a great time in Brazil during the fieldwork campaign! Although none of the data made it into this manuscript, it was a very interesting experience and it was great getting to know all of you! Also the meetings afterwards contributed greatly to this PhD, as it was very inspiring to learn about the different fields everyone worked in and to apply that in my own research.

De afgelopen 4 jaar heb ik het genoeg gehad om verschillende studenten te begeleiden tijdens het maken van hun MSc thesis, wat mij veel kennis heeft bijgebracht. Bovendien was het geweldig om jullie te leren kennen en te zien hoe jullie interesse in bodems, koolstof, erosie en modelleren groeide gedurende deze periode. Hoewel de samenwerking met elk van jullie plezant was, wil ik toch graag Caroline, Lotte en Dries extra vernoemen. Zij hebben zich met een ongezien enthousiasme op de schorren en de polders van de Schelde gestort. De data die uit deze thesissen zijn voortgekomen hebben een belangrijke bijdrage geleverd aan dit doctoraat. Enorm veel bedankt dus!

De begeleider van mijn eigen thesis, Wim, zou ik ook heel graag bedanken om mij enkele weken te ontvangen in Lund, voor het enthousiasme en de interessante gesprekken over wetenschap en vele andere zaken.

Om een doctoraat tot een goed einde te brengen is de tijd die je ontspant zeker zo belangrijk als de tijd die je al werkend spendeert. Ondanks een verhuis naar Leuven werd er voor ontspanning vaak teruggegaan naar Herk, waar ik steeds kon rekenen op een grote groep vrienden die voor de nodige afleiding zorgden. De leuke avonden bij Willy, bij iemands thuis

of op een feestje waren steeds onvergetelijk. Lotte, jij verdient hierbij een zeer speciaal bedankje: dankzij jouw oneindig optimisme, je luisterend oor en goede raad ben je een enorme steun voor mij geweest, niet alleen tijdens de afgelopen 4 jaren, maar al veel langer. Enorm bedankt voor alles!

Ondanks het feit dat mijn leidingsfluit al enkele jaren ligt opgeborgen, bracht ik een groot deel van mijn vrije tijd nog steeds door met de (oud)leiding van de chiro. Of het nu op de chiro was, bij de opbouw van de fuif of op weekend, er was altijd tijd voor een goede babbel bij een stevige pint, waar ik telkens naar uitkeek. Hopelijk kunnen we dit nog lang zou houden!

Ik wil natuurlijk ook heel graag mijn ouders bedanken. Voor de kans die ik heb gekregen om geografie te gaan studeren, wat de uiteindelijk basis vormde voor dit doctoraat. Bedankt om er altijd voor mij te zijn, mij alle vrijheid te geven om te gaan en staan waar ik wou, of dat nu in Herk, Leuven, Stockholm, Amsterdam of waar ook ter wereld was. Ook het gezin van Kristien was er steeds om mij te steunen, waarvoor enorm veel dank!

Kristien, jij bent de belangrijkste persoon die er voor heeft gezorgd dat dit doctoraatsproject tot een goed einde is gekomen. Jij bent er van in het begin bij betrokken geweest en hebt van op de eerste rij alle makkelijke en moeilijke momenten meegemaakt. Bedankt om me altijd te blijven steunen wanneer het allemaal even tegen zat of wanneer ik de zoveelste keer naar het buitenland ging, of het nu voor een korte of langere tijd was. Zelfs op de momenten dat ik gefrustreerd was wanneer de modelcodes weer niet werkten. Bedankt om me er, zeker tijdens de laatste maanden van dit project, op te wijzen dat ontspannen ook belangrijk is en me af en toe van mijn computer weg te trekken om het doctoraat in te wisselen voor een ijsje, een terrasje of een ontspannende wandeling. Ik ben je enorm dankbaar voor je steun tijdens de afgelopen jaren en ook voor het nieuwe avontuur in Zürich waar we binnenkort aan beginnen! Ik kan niet wachten om deze ervaring samen met jou te delen!

Marijn



## Samenvatting

---

De bodem maakt enkel de bovenste meters van onze aarde uit, maar toch is ze vitaal voor het leven op aarde. Vanuit het standpunt van de mens is een gezonde bodem noodzakelijk om gewassen te telen en om vegetatie te onderhouden, die CO<sub>2</sub> uit de atmosfeer omzet naar de lucht die wij inademen. Vanuit het standpunt van de natuur is de bodem een belangrijke habitat, want in elke gram bodem leven duizenden verschillende soorten micro-organismen, een densiteit die hoger is dan in de meeste andere ecosystemen ter wereld. Ondanks het feit dat deze micro-organismen (voornamelijk bacteriën en schimmels) onzichtbaar zijn voor het menselijke oog, spelen ze een belangrijke rol in de globale cyclus van koolstof. Wanneer ze organische moleculen opnemen uit hun omgeving, voornamelijk afkomstig van de wortels en bovengrondse delen van planten, zetten ze een deel van de organische bestanddelen om naar CO<sub>2</sub>. Dit ontsnapt vervolgens naar de atmosfeer, waar het een belangrijk broeikasgas is. Een goed begrip van hoe bodems fungeren is dus niet enkel belangrijk vanuit een agronomisch perspectief, maar is ook een onmisbare schakel in de kennis die ons toelaat te begrijpen hoe de globale cyclus van koolstof werkt en dus om betrouwbare voorspellingen te kunnen maken van hoe het klimaat op onze planeet in de toekomst zal veranderen.

Het doel van dit doctoraat was het bijbrengen van kennis over hoe organische koolstof (dit is koolstof afkomstig van voornamelijk vegetatie, vervat in organische bestanddelen) zich in bodems gedraagt, om zo een beter beeld te krijgen van de mechanismen die de snelheid bepalen waarmee deze organische bestanddelen worden omgezet naar CO<sub>2</sub> door micro-organismen om zo betere voorspellingen te kunnen maken over hoe het klimaat er in de toekomst zal uitzien. Dit is gedaan voor twee specifieke omgevingen: schorren en polders in het estuarium van de Schelde (België en Nederland). Schorren zijn gebieden begroeid met vegetatie, te vinden langsheen kustlijnen en in estuaria (dit is het deel van een rivier dat beïnvloed wordt door getijdenwerking). Polders ontstaan wanneer een schor wordt bedijkt om zo te kunnen worden aangewend voor landbouw. Het grootste gedeelte van de oppervlakte van de Nederlandse provincie Zeeland is bijvoorbeeld een polder. Een deel van deze dissertatie draait verder rond de manier waarop organische koolstof in bodems wordt voorgesteld in numerische modellen. Dit is een belangrijk thema met betrekking tot het maken van voorspelling over hoe het klimaat zal veranderen gedurende de komende decennia. Dat laatste gebeurt met behulp van modellen van het systeem aarde (*Engels*: Earth system models). Dit zijn modellen die simulaties maken van fluxen van verschillende elementen, waaronder koolstof, tussen de grootste reservoirs op Aarde: de oceanen, de atmosfeer, vegetatie en bodems. Een laatste deel van dit doctoraat draait rond mid-infrarood

spectroscopy, een techniek die de laatste jaren aan belang heeft gewonnen als een alternatieve methode om de concentratie van organische koolstof in bodemstalen te voorspellen.

Het empirische deel van deze dissertatie heeft nieuwe inzichten aangebracht met betrekking tot de mechanismen die het gedrag van organische koolstof in de bodems van schorren controleren. Er is aangetoond dat het grootste deel van deze organische koolstof niet afkomstig is van lokale vegetatie (wat in bijvoorbeeld een bosbodem steeds het geval is), maar dat een groot gedeelte van deze koolstof wordt aangevoerd van buitenaf. Schorren worden immers overspoeld met water tijdens hoogtij, waarbij tijdens deze overstromingen sediment wordt afgezet aan het oppervlak van schorren. Dit sediment bevat organische koolstof, die dus een groot deel van de koolstof in schorbodems uitmaakt. Er is aangetoond dat deze koolstof afkomstig is uit terrestrische (in dit geval bijvoorbeeld akkers in het Scheldebekken) en mariene (bijvoorbeeld sedimenten langsheen de kustlijn) ecosystemen. Bovendien is er aangetoond dat de koolstof die aan dit sediment vasthangt tot duizenden jaren oud is. Deze bevindingen hebben belangrijke gevolgen voor berekeningen van de hoeveelheid CO<sub>2</sub> die door schorren aan de atmosfeer wordt onttrokken. Deze CO<sub>2</sub> wordt vervolgens opgeslagen in de bodems van deze schorren als organisch materiaal. Wanneer er geen rekening gehouden wordt met het feit dat een groot deel van de organische koolstof in schorsedimenten is aangevoerd, zal de hoeveelheid lokale CO<sub>2</sub> opslag sterk worden overschat. Verder heeft dit onderzoek aangetoond dat wanneer schorren worden ingepolderd er een groot deel (zo'n 60 %) van de organische koolstof in deze bodems verloren gaat, vermoedelijk voornamelijk als CO<sub>2</sub> naar de atmosfeer. In feite gaat een groter gedeelte van de oorspronkelijke hoeveelheid organische koolstof verloren, maar deze wordt deels vervangen door organische koolstof afkomstig van de geteelde gewassen. Verder is er aangetoond dat wanneer men een nauwkeurige begroting wil maken van de verandering in de totale hoeveelheid organische koolstof in de bodems van gebieden die door inpoldering worden gevormd, men rekening moet houden met historische veranderingen in de oppervlakte ingenomen door polders (die weinig koolstof bevatten) en schorren (die net veel koolstof bevatten). In het laatste empirische stuk van dit doctoraat wordt verder getoond dat mid-infrarood spectroscopy een goed alternatief is om het gehalte organische koolstof van schorsedimenten te voorspellen.

In het modelleergedeelte van dit proefschrift werd er nagegaan hoe correct de structuur van bestaande koolstofmodellen is (dit zijn modellen die het gedrag van organische koolstof in bodems simuleren). Meer specifiek is er nagegaan in welke mate twee reeds bestaande modellen in staat zijn om naast de totale hoeveelheid koolstof ook de hoeveelheid <sup>14</sup>C ('koolstof 14', wat een proxy is voor de leeftijd van de koolstof is) en stabiele isotopen van koolstof (aangeduid als δ<sup>13</sup>C) te simuleren. De motivatie van deze oefening was dat een koolstofmodel met een correcte interne structuur in staat moet zijn om de drie natuurlijk voorkomende isotopen van koolstof (<sup>12</sup>C, <sup>13</sup>C en <sup>14</sup>C) correct te simuleren. De resultaten toonden aan dat ondanks het feit dat deze modellen realistische voorspellingen maakten voor totale koolstof en <sup>14</sup>C, de stabiele isotopen (<sup>13</sup>C) niet correct werden gesimuleerd. Op basis van de inzichten die in deze oefening zijn verworven werd in het laatste deel van deze dissertatie een nieuw koolstofmodel ontwikkeld. Het nieuwe aan dit model is dat het een onderscheid maakt tussen het gedrag van koolstof in het gedeelte van bodems dat

rechtstreeks door wortels wordt beïnvloed (dat is het deel van de bodem waar er zich het meeste leven bevindt) en de minerale bodem (waar koolstof voornamelijk gebonden is aan mineralen en het daardoor niet beschikbaar is als bron van energie voor micro-organismen). Deze modelstructuur zorgt er voor dat er realistische voorspellingen gemaakt kunnen worden voor zowel totale koolstof,  $^{14}\text{C}$  als  $\delta^{13}\text{C}$ .



## Summary

---

The soil constitutes only the uppermost meter of our planet, yet it's vital to life on Earth. From a human perspective, a healthy soil is necessary for people to grow crops and to sustain vegetation, which convert CO<sub>2</sub> from the atmosphere to the oxygen we all breathe. From a natural perspective, soils are an important habitat and have a species richness higher than most other ecosystems, with a gram of soil containing several thousands of species of microorganisms. Despite being invisible to the human eye, these heterotrophic microorganisms in soils (mostly fungi and bacteria) are an important component of the global carbon cycle. When these organisms take up organic molecules from their environment, mostly derived from plant roots and litter, they convert a portion of these molecules to CO<sub>2</sub> which is subsequently transferred to the atmosphere where it acts as a greenhouse gas. Understanding how soils function is thus not only important from an agronomic perspective, but is also necessary to understand the global carbon cycle and thus to predict how the future climate on Earth will look.

The aim of this PhD dissertation is to contribute to knowledge on organic carbon cycling in soils, to better understand the mechanisms controlling the rate at which soil organic carbon is converted to CO<sub>2</sub> by microorganisms and to better predict how the amount of organic carbon in soils will change when the climate changes. This was done for two specific environments: tidal marshes and polders of the Scheldt estuary (Belgium and The Netherlands). The former are vegetated platforms found along coastlines and estuaries. The latter are tidal marshes which have been embanked and drained for agricultural purposes. A portion of this dissertation also focused on how soil organic carbon is represented in numerical models. This is an important issue regarding predictions of future climate change, which is done using Earth system models. These models simulate fluxes of elements, such as carbon, between the most important global reservoirs: the atmosphere, oceans, vegetation and soils. In addition, a part of this dissertation was centered on mid-infrared spectroscopy, which is used as an alternative method to predict the organic carbon concentration of soil samples.

The empirical part of this dissertation has provided novel insights with regard to the controls of soil organic carbon dynamics in tidal marsh sediments. It has been shown that the majority of organic carbon in these sediments does not originate from local vegetation, but is imported to these environments when tidal marshes are flooded and sediments, containing organic carbon, are deposited at the marsh surface. This deposited organic carbon has been shown

to originate from terrestrial and marine environments and to be fixed from atmospheric CO<sub>2</sub> up to millennia ago. This has important consequences for calculated rates at which these ecosystems remove CO<sub>2</sub> from the atmosphere, which may be greatly overestimated if these calculations do not account for the fact that a large portion of the organic carbon present in these sediments has not been fixed by the vegetation present on these tidal marshes. When these tidal marshes are converted to arable land after embanking these vegetated platforms, to prevent inundation by tidal water, it is shown in this dissertation that an important portion of the organic carbon present in these sediments (ca. 60 %) is lost. In fact, a larger portion of the original organic carbon is lost, but is replaced by organic carbon origination from the crops that are grown in these fields. In addition, it is shown that in order to correctly assess how much organic carbon is lost from these landscapes as a consequence of tidal marsh embankments, spatial variations in the historical extent of both tidal marshes and polders need to be taken into account. Furthermore, it has been shown that mid-infrared spectroscopy is able to accurately predict the concentration of organic carbon present in sediment samples obtained from tidal marshes.

The modelling part of this dissertation focused on the structure of existing soil organic carbon models. Specifically, it was assessed if two established numerical models were able to simulate depth profiles of total organic carbon, its <sup>14</sup>C content (a proxy for the age of this carbon) and stable carbon isotopes ( $\delta^{13}\text{C}$ ). The rationale behind this exercise was that a model that represents soil organic carbon dynamics correctly needs to simulate the dynamics of these 3 naturally-occurring isotopes of carbon correctly. Although the established models simulate realistic depth profiles of total organic carbon and its <sup>14</sup>C content, both models failed to simulate realistic depth profiles of  $\delta^{13}\text{C}$ . Based on the insights gained from this exercise, a new model structure was proposed. The novelty of this model is that it makes a distinction between soil organic carbon cycling in the rhizosphere and the mineral soil. In addition, the majority of organic carbon that is stabilized in the soil environment is assumed to originate from dead microorganisms. This allowed for the simulation of realistic depth profiles of total organic carbon, its <sup>14</sup>C content and  $\delta^{13}\text{C}$ .

## Abbreviations

---

C	Carbon
OC	Organic carbon
SOC	Soil organic carbon
$\delta^{13}\text{C}$	Delta 13-carbon
$F^{14}\text{C}$	Fraction modern 14-C
$\Delta^{14}\text{C}$	Delta 14-carbon
ESM	Earth system model
s	Salinity
M	Macroaggregates and particulate organic matter
m	Microaggregates, sand and particulate organic matter
sc	Silt and clay
scM	Silt and clay in macroaggregates
mM	Microaggregates, sand and particulate organic matter in macroaggregates
m + S	Microaggregates and sand
POM	Particulate organic matter
DW	Dry weight
GOF	Goodness of fit
$\text{OC}\%_{\text{m-IR}}$	Organic carbon concentration predicted using mid-infrared spectroscopy
$\text{OC}\%_{\text{meas}}$	Organic carbon concentration measured using a mass spectrometer
PLSR	Partial least squares regression



---

## Contents

---

Preface .....	I
Samenvatting .....	V
Summary .....	IX
Abbreviations .....	XI
Contents .....	XIII
List of Figures .....	XIX
List of Tables .....	XXIII
<b>Chapter 1 Introduction .....</b>	<b>1</b>
1.1 Soils in the global carbon cycle .....	1
1.1.1 The global carbon cycle.....	1
1.1.2 Organic carbon storage in soils.....	2
1.1.3 The effect of land use changes on soil organic carbon stocks.....	4
1.1.4 Soil organic carbon in a changing climate .....	5
1.2 A new paradigm on soil organic carbon cycling.....	6
1.2.1 The historical view .....	7
1.2.2 The emerging view.....	8
1.2.3 Consequences for soil organic carbon models .....	9
1.3 The application of carbon isotopes in soil organic carbon research .....	12
1.3.1 Stable carbon isotopes ( $\delta^{13}\text{C}$ ) .....	12
1.3.2 Radioactive isotopes ( $^{14}\text{C}$ ).....	18
1.4 Environments in which soil organic carbon is studied .....	20
1.4.1 Tidal marshes .....	20
1.4.2 Polders .....	23
1.5 Current gaps in soil organic carbon research.....	25
1.6 Research questions .....	26

1.7	Dissertation outline.....	28
<b>Chapter 2 Controls on soil organic carbon stocks in tidal marshes along an estuarine salinity gradient .....</b>		<b>31</b>
2.1	Introduction.....	32
2.2	Materials and methods .....	33
2.2.1	Study sites .....	33
2.2.2	Sample collection .....	36
2.2.3	Soil and biomass analysis .....	36
2.2.4	Data analysis .....	37
2.3	Results .....	37
2.3.1	Soil characteristics .....	37
2.3.2	Vegetation biomass production .....	38
2.3.3	Soil organic carbon depth profiles .....	39
2.3.4	Soil organic carbon inventories .....	39
2.3.5	Stable carbon isotopes.....	40
2.4	Discussion.....	40
2.4.1	Observed patterns in SOC storage.....	40
2.4.2	Explanations for the observed patterns in soil organic carbon stocks.....	42
2.4.3	Effect of sampling procedure on reported estuarine OC stocks .....	46
2.4.4	Implications of sea level rise for estuarine soil organic carbon stocks .....	47
2.5	Conclusion .....	48
<b>Chapter 3 Long-term organic carbon sequestration in tidal marsh sediments is dominated by old-aged allochthonous inputs in a macro-tidal estuary.....</b>		<b>51</b>
3.1	Introduction.....	52
3.2	Materials and Methods .....	53
3.2.1	Study site.....	53
3.2.2	Biomass .....	55
3.2.3	Soil samples.....	56
3.2.4	Collection of deposited sediments .....	57
3.2.5	Physical fractionation of organic carbon .....	57
3.2.6	Statistical analysis .....	59
3.3	Results .....	59

---

3.3.1	Grain size.....	59
3.3.2	Biomass .....	59
3.3.3	Organic carbon characteristics of deposited sediments .....	60
3.3.4	Soil organic carbon stocks.....	61
3.3.5	Radiocarbon content of deposits and SOC .....	61
3.3.6	Organic carbon fractionation.....	63
3.4	Discussion.....	65
3.4.1	Autochthonous organic carbon inputs along the estuary .....	65
3.4.2	Allochthonous organic carbon deposits along the estuary .....	65
3.4.3	Preservation mechanisms of organic carbon in tidal marsh sediments.....	67
3.4.4	Consequences for calculated CO <sub>2</sub> sequestration rates .....	69
<b>Chapter 4 Soil organic carbon stocks in a tidal marsh landscape are largely affected by human marsh embankment and subsequent marsh progradation.....</b>		<b>73</b>
4.1	Introduction.....	74
4.2	Material and methods.....	76
4.2.1	Study area .....	76
4.2.2	Field sampling .....	77
4.2.3	Lab analyses .....	78
4.2.4	Data analyses .....	79
4.2.5	Landscape-scale soil organic carbon model .....	79
4.3	Results .....	80
4.3.1	Grain size, pH and inorganic carbon content .....	80
4.3.2	Organic carbon and $\delta^{13}\text{C}$ depth profiles .....	81
4.3.3	Changes in soil bulk density .....	83
4.3.4	Changes in organic carbon stocks and $\delta^{13}\text{C}$ values.....	83
4.3.5	Temporal changes in landscape-scale organic carbon stocks .....	85
4.4	Discussion.....	87
4.4.1	Organic carbon losses from embanked coastal marsh sediments .....	87
4.4.2	Additional organic carbon storage during stepwise embankments.....	90
4.4.3	Limitations and opportunities .....	92
4.5	Conclusion .....	93

<b>Chapter 5 Assessing the uncertainty on predictions of soil organic carbon stocks in tidal marsh sediments using mid-infrared spectroscopy</b> .....	<b>95</b>
5.1 Introduction.....	96
5.2 Material and methods.....	97
5.2.1 Study site and sample processing.....	97
5.2.2 Spectroscopy measurements.....	98
5.2.3 Data analyses .....	98
5.3 Results and discussion.....	100
5.3.1 Characterization of the dataset .....	100
5.3.2 Determination of the optimal PLSR model.....	101
5.3.3 Minimal size of the calibration dataset .....	102
5.3.4 Errors associated with predicted organic carbon stocks.....	103
5.4 Conclusion .....	107
<b>Chapter 6 Assessment of the capacity of soil organic carbon models to simulate depth profiles of stable carbon isotopes (<math>\delta^{13}\text{C}</math>)</b> .....	<b>109</b>
6.1 Introduction.....	110
6.2 Material and methods.....	113
6.2.1 Model set-up.....	113
6.2.2 ICBM-DE model structure .....	113
6.2.3 COMISSION model structure .....	117
6.2.4 Additional modelled processes.....	121
6.3 Results and discussion.....	124
6.3.1 The potential of ICBM-DE to simulate $\delta^{13}\text{C}$ depth profiles.....	124
6.3.2 The potential of COMISSION to simulate $\delta^{13}\text{C}$ depth profiles.....	128
6.4 Conclusion .....	132
<b>Chapter 7 Development of a soil organic carbon model to simulate depth profiles of stable carbon isotopes (<math>\delta^{13}\text{C}</math>)</b> .....	<b>133</b>
7.1 Introduction.....	134
7.2 Material and methods.....	136
7.2.1 General overview of the SOILcarb – RM.....	136
7.2.2 Carbon dynamics in SOILcarb - RM.....	137
7.2.3 Simulation of $^{13}\text{C}$ and $^{14}\text{C}$ in SOILcarb – RM.....	140

---

7.3	Results .....	141
7.3.1	The potential of SOILcarb - RM to simulate $\delta^{13}\text{C}$ depth profiles .....	141
7.4	Discussion .....	145
7.4.1	Novelties of the SOILcarb – RM model .....	145
7.4.2	The added value of the simulation of $\delta^{13}\text{C}$ values .....	147
7.4.3	Increasing model complexity implies a trade-off with data availability.....	148
7.4.4	Considerations for future work .....	149
7.5	Conclusions.....	151
<b>Chapter 8 Conclusions .....</b>		<b>153</b>
8.1	Implications for future soil organic carbon research .....	153
8.1.1	Assessment of the organic carbon sink capacity of intertidal vegetated ecosystems .....	153
8.1.2	Assessing the influence of environmental changes on future tidal marsh organic carbon stocks: the role of organic carbon models .....	154
8.2	Concluding summary .....	156
8.3	Future research perspectives .....	160
Data availability.....		165
Supporting figures and tables .....		167
References.....		193



## List of Figures

### Chapter 1

<b>Figure 1-1</b> Organic carbon stocks in the major global reservoirs .....	2
<b>Figure 1-2</b> The spatial distribution of soil organic carbon down to a depth of 1 m .....	3
<b>Figure 1-3</b> Organic carbon depth profiles for a forest soil in Hesse (NE France), from Schrumpf et al. (2013) .....	4
<b>Figure 1-4</b> Graphical representation of the ‘historical view’ (a) and ‘emerging view’ (b) on soil organic carbon cycling, from Schmidt et al. (2011, p. 52) .....	8
<b>Figure 1-5</b> Structure of the RothC soil organic carbon model (Coleman and Jenkinson, 1999) .....	10
<b>Figure 1-6</b> Example of a soil organic carbon model structure which explicitly simulates soil microbes (MIC) and the enzymes they produce (ENZ), which are used to depolymerize polymeric soil organic carbon (SOC) to dissolved organic carbon (DOC). From Allison et al. (2010, p. 336) .....	11
<b>Figure 1-7</b> Record of historical $\delta^{13}\text{C}$ values of atmospheric $\text{CO}_2$ (data source: Keller et al. (2017)) .....	13
<b>Figure 1-8</b> The range in $\delta^{13}\text{C}$ values of atmospheric $\text{CO}_2$ , C3 and C4 vegetation .....	13
<b>Figure 1-9</b> Record of historical $\Delta^{14}\text{C}$ values of atmospheric $\text{CO}_2$ .....	19
<b>Figure 1-10</b> View on a tidal marsh in the salt portion of the Scheldt estuary .....	20
<b>Figure 1-11</b> Historical topographic maps .....	24
<b>Figure 1-12</b> Picture of a polder landscape .....	24
<b>Figure 1-13</b> Flowchart of the outline of the dissertation .....	29

### Chapter 2

<b>Figure 2-1</b> Map of the Scheldt estuary showing the salinity zones and the location of the sampled tidal marshes in a western European context. ....	34
<b>Figure 2-2</b> Evolution of marsh surface elevation at the sampled locations .....	35
<b>Figure 2-3</b> Depth profiles of the sampled tidal marshes showing the vegetation history at each location .....	36
<b>Figure 2-4</b> Annual biomass production ( $\text{g dry weight m}^{-2} \text{ yr}^{-1}$ ) .....	38
<b>Figure 2-5</b> Depth profiles of organic carbon concentration for all study sites .....	39
<b>Figure 2-6</b> Depth profiles of $\delta^{13}\text{C}$ , together with the $\delta^{13}\text{C}$ signal of above-ground (circles) and below-ground (triangles) biomass .....	41

**Figure 2-7** Conceptual diagram of the effect of both sediment deposition rate ( $dE/dt$ ,  $E =$  elevation) and the relative inputs of recalcitrant allochthonous organic carbon and labile autochthonous organic carbon on the fate of buried OC in a tidal freshwater marsh (a) and salt marsh (b) .....45

### Chapter 3

**Figure 3-1** Map of the Scheldt estuary. ....54

**Figure 3-2** Organic carbon fractionation scheme .....58

**Figure 3-3** Grain size distribution of disaggregated topsoil sediments of tidal marshes along the Scheldt estuary .....59

**Figure 3-4** Total biomass ( $g\ DW\ m^{-2}$ ) present at the sampled freshwater (green), brackish (brown) and saltmarshes (blue).....60

**Figure 3-5** Organic carbon concentration and  $\delta^{13}C$  values of sediments deposited at the tidal marsh surface during flooding events .....61

**Figure 3-6** Total organic carbon stock ( $kg\ OC\ m^{-2}$ ) in the top 0.6 m of tidal marsh sediments along the Scheldt estuary.. .....62

**Figure 3-7** Fraction modern  $^{14}C$  ( $F^{14}C$ ) of deposited sediments at the surface of tidal marshes in summer and winter, and sediments at different depths .....63

**Figure 3-8** Final OC fractions of topsoil and subsoil tidal marsh sediments along the estuary .....64

**Figure 3-9** Conceptual framework of OC dynamics in tidal saltmarsh sediments and measurements of OC accumulation rates. ....70

### Chapter 4

**Figure 4-1** Map of the sampled salt and brackish polders along the Scheldt estuary and associated tidal marshes and sandflats.. .....76

**Figure 4-2** Depth profiles of organic carbon concentration (%) and  $\delta^{13}C$  values (‰) of selected polder soils in the brackish and salt region with a different time since embankment .....82

**Figure 4-3** Average bulk density in the top 0.3 m of present-day tidal marsh sediments and embanked polders .....83

**Figure 4-4** Mass of organic carbon ( $kg\ OC\ m^{-2}$ ) in the uppermost  $400\ kg\ m^{-2}$  of sediments in both present-day tidal marsh sediments and embanked polder soils. ....85

**Figure 4-5**  $\delta^{13}C$  values (‰) of OC in the uppermost  $400\ kg\ m^{-2}$  of sediments in both present-day tidal marsh sediments and embanked polder soils. ....85

**Figure 4-6** Results of the landscape-scale OC model for the brackish and salt polders .....86

**Figure 4-7** Results of the landscape-scale SOC model for the brackish polder region. ....86

**Figure 4-8** Results of the landscape-scale SOC model for the salt polder region. ....87

### Chapter 5

**Figure 5-1** Modelled versus the measured OC concentrations.....103

<b>Figure 5-2</b> $R^2$ , root mean square error (RMSE) and the average absolute difference between $OC\%_{meas}$ and $OC\%_{m-IR}$ in function of the number of calibration samples used to construct the general PLSR model..	104
<b>Figure 5-3</b> Depth profiles of $OC\%_{m-IR}$ and $OC\%_{meas}$	105
<b>Figure 5-4</b> Modelled and measured sedimentary organic carbon stocks using different methods..	106
<b>Chapter 6</b>	
<b>Figure 6-1</b> Organic carbon fractionation results from Schrumpf et al. (2013) for the forest site in Hesse	112
<b>Figure 6-2</b> Model structure of ICBM-DE	115
<b>Figure 6-3</b> The effect of the $r$ profile on simulated depth profiles of organic carbon concentration and fraction modern carbon	116
<b>Figure 6-4</b> Model structure of the COMISSION model.	117
<b>Figure 6-5</b> Atmospheric levels of $\delta^{13}C$ and $\Delta^{14}C$ over the past centuries as used as an input in the model simulations	122
<b>Figure 6-6</b> Results of the ICBM simulations	126
<b>Figure 6-7</b> Simulated depth profiles of organic carbon concentration, fraction modern $^{14}C$ and $\delta^{13}C$ with ICBM - DE, assuming unlimited bioturbation with depth	127
<b>Figure 6-8</b> Modelled depth profiles using the COMISSION model	130
<b>Chapter 7</b>	
<b>Figure 7-1</b> Model structure of the SOILcarb – RM model.	137
<b>Figure 7-2</b> Modelled depth profiles using the SOILcarbon - RM model	142
<b>Figure 7-3</b> Simulation of the SOILcarb - RM model without advection of DOC	143
<b>Figure 7-4</b> The trade-off between complexity of environmental models and data availability	149



## List of Tables

### Chapter 2

<b>Table 2.1</b> Main properties of the sampled tidal marshes .....	35
<b>Table 2.2</b> General characteristics of the soil profiles at the studied sites.. .....	37
<b>Table 2.3</b> Total organic carbon (OC) stock (kg OC m <sup>-2</sup> ) and standard deviations calculated for the full vertical sampling profiles and the upper 0.6m. ....	40
<b>Table 2.4</b> Reported SOC stocks (kg OC m <sup>-2</sup> ) of tidal marsh soils along estuarine salinity gradients .....	46

### Chapter 3

<b>Table 3.1</b> General characteristics of the sampled tidal marshes and indication of the locations where different analyses are performed. ....	55
--	----

### Chapter 4

<b>Table 4.1</b> Characteristics of the sampled polders per region.....	77
<b>Table 4.2</b> Depths down to which SOC stocks are calculated (for a mass of 400 kg of bulk soil) and the average SOC stocks of soils in the different regions.. .....	84

### Chapter 5

<b>Table 5.1</b> Results of the determination of the optimal PLSR model. ....	102
---	-----

### Chapter 6

<b>Table 6.1:</b> ICBM-DE model parameter values .....	116
<b>Table 6.2:</b> Overview of the parameters, their names and units of the COMISSION model.	119
<b>Table 6.3:</b> Parameter values for the COMISSION model.....	121

### Chapter 7

<b>Table 7.1</b> Overview of the parameters, their names and units of the SOILcarb - RM model .....	140
<b>Table 7.2</b> Parameter values for the SOILcarb - RM model .....	141



## Chapter 1 Introduction

---

### 1.1 Soils in the global carbon cycle

#### 1.1.1 The global carbon cycle

Over the past decades, carbon (C) has received an increasing amount of attention in scientific research and news reports, as a consequence of the intimate link between this element and the global climate. More specifically, the accumulation of this element in the atmosphere as carbon dioxide (CO<sub>2</sub>) and methane (CH<sub>4</sub>) is being held responsible for a large portion of the increase in global temperature that has been observed since the onset of the industrial era. There is indeed no doubt that humans have significantly increased the amount of CO<sub>2</sub> in the atmosphere as a consequence of mainly combustion of fossil fuels and cement production. The concentration of atmospheric CO<sub>2</sub> has increased from an average of ca. 280 ppm (parts per million, cm<sup>3</sup> · m<sup>-3</sup>) throughout the Holocene (the period that followed the last ice age, starting ca. 11 650 years ago) (Ciais et al., 2013) to 406.5 ppm averaged over 2017 (as measured on Mauna Loa, Hawaii). Atmospheric CO<sub>2</sub> is an important driver for the climate on Earth, as it traps a portion of the energy that is emitted from the Earth surface and sends it back to Earth, thus acting as a greenhouse gas.

Despite its importance in regulating the global climate, the amount of C elements present in the atmosphere constitute only a small portion of all C atoms in the Earth system (589 Pg C (Petagram, 1 Pg = 10<sup>15</sup> g), 1.3 % of the total C on Earth, Figure 1-1). C elements are indeed present in much larger quantities in different reservoirs on Earth, with the majority of C (ca. 40 350 Pg C, ca. 86.5 %) present in the ocean and ocean floor sediments. In the biosphere, the majority of C is present in soils (ca. 3500 Pg C, 7.5 %), while also global vegetation stores a considerable amount of C (550 Pg C, 1.2 %). It is noted that these numbers exclude carbon present in rocks. Carbon in the atmosphere (e.g. CO<sub>2</sub> or CH<sub>4</sub>) is generally referred to as mineral C, while C that has been biosynthesized by organisms through the process of photosynthesis (whereby atmospheric CO<sub>2</sub> is converted to organic molecules) is referred to as organic carbon (OC). The amount of carbon in these different reservoirs is not static, as carbon is continuously transferred between reservoirs on timescales ranging from seconds (e.g. photosynthesis) to millions of years (e.g. the release of OC stored in fossil reserves, assuming they would not be dug up and burned). The interactions between these different reservoirs play an important role in regulating the global climate. For example, from the ca. 420 ± 20 Pg C that has been emitted through fossil fuel combustion between 1750 and 2016 (note that this value approaches the total amount of C present in all vegetation globally, Figure 1-1), ca. 160 ± 20 Pg C has been absorbed by the ocean (Le Quéré et al., 2018). While this negative feedback

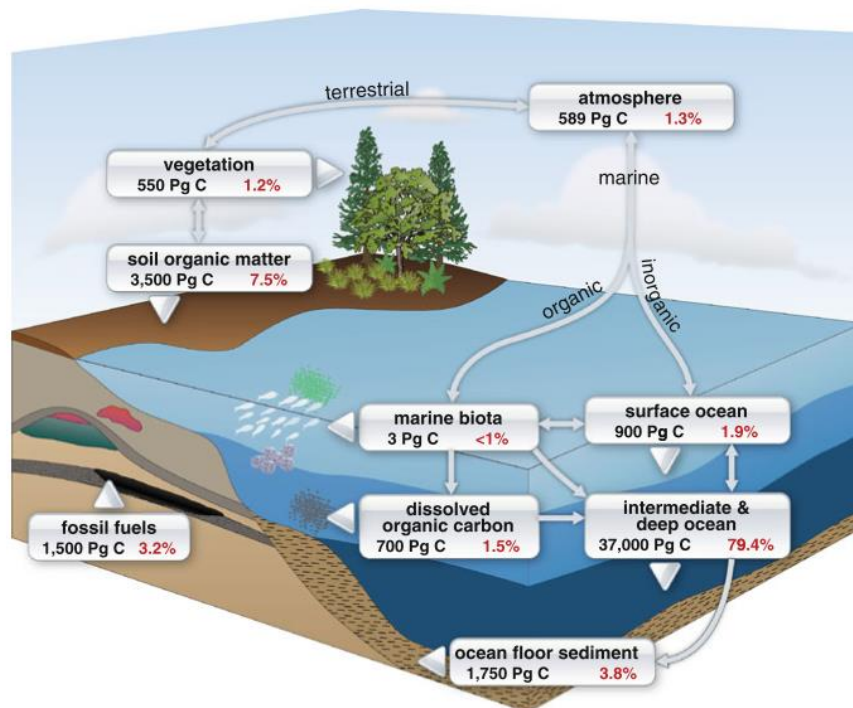


**Figure 1-1** Organic carbon stocks in the major global reservoirs (in Pg C (1 Pg =  $10^{15}$  g)) in black, the relative contribution of each pool to the total amount of C globally is shown in red. From Schuur et al. (2016, p. 5), who collected the data from (IPCC, 2013), while the soil organic stock was combined with estimates for permafrost soils from Schuur et al. (2015).

decreases the effect of fossil fuel combustion on global temperatures, also positive feedbacks are possible. For example, increasing global temperatures will potentially thaw frozen soils in the Arctic (Permafrost), which contain a similar amount of OC compared to all non-frozen soils globally (Scharlemann et al., 2014; Tarnocai et al., 2009). This might cause the release of additional  $\text{CO}_2$  and, even worse,  $\text{CH}_4$  to the atmosphere, thereby enhancing the increase in global atmospheric temperature (Schuur et al., 2015). Understanding the factors controlling the size of the different global carbon pools and the fluxes of carbon between these pools is thus a major prerequisite in order to assess how the climate on Earth will change in the future. The aim of this PhD thesis is to gain more understanding of the largest terrestrial C store, the soil, which is presented in more detail in the following sections.

### 1.1.2 Organic carbon storage in soils

Carbon constitutes ca. 50 % of soil organic matter (OM) (organic compounds and parts of vegetation), of which the presence in a soil is very important for its fertility. Although currently there is a tendency to increase the OC content of soils as a strategy to decrease the amount of atmospheric  $\text{CO}_2$  (Lal, 2018), OM in soils is also the main source of nutrients for plants and needs to decay before its nutrients can be taken up by vegetation (Janzen, 2006). Globally, soils store ca. 6 times more organic carbon compared to all vegetation combined and the amount of carbon present in the atmosphere (Schuur et al., 2016, 2015) (Figure 1-1). Of this soil organic carbon (SOC) about 50 % is stored in frozen soils (Permafrost) in the Arctic and sub-Arctic (Schuur et al., 2015) (Figure 1-2). Of the remaining soil organic carbon, ca. 50 % is

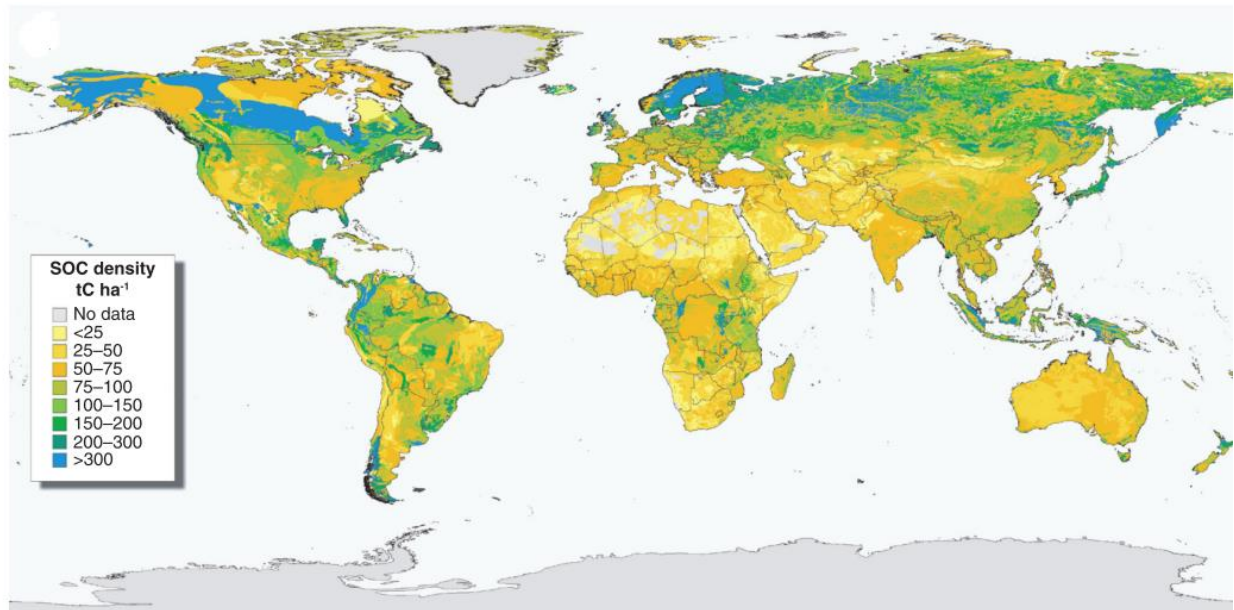


**Figure 1-2** The spatial distribution of soil organic carbon down to a depth of 1 m (expressed as ton C ha<sup>-1</sup>), from Scharlemann et al. (2014, p. 84)

stored in tropical soils (Scharlemann et al., 2014). The presence of soil organic carbon is not limited to the surface of soils (referred to as topsoil), but is often present down to a depth of multiple meters (referred to as subsoil). In a recent review, Lal (2018) estimated that globally ca. 77 % of total soil organic carbon is stored below a depth of 0.3 m, when accounting for soil organic carbon down to a depth of 3 m. The importance of this deep soil organic carbon is implicitly acknowledged throughout this dissertation, as depth profiles of soil organic carbon have been studied to assess controls on soil organic carbon cycling along the soil profile (chapters 2, 3, 4, 6 and 7).

To illustrate how soil organic carbon is distributed with depth in a soil profile, a depth profile from an undisturbed European forest is shown in Figure 1-3 (Schrumpf et al., 2013). The focus here will be on the depth profiles of organic carbon concentration (Figure 1-3a), while the depth profiles of  $\delta^{13}\text{C}$  and the fraction modern  $^{14}\text{C}$  (Figure 1-3b and c) are discussed in section 1.3. At the scale of the soil profile, an approximately exponentially decreasing organic carbon content is generally observed with depth (Figure 1-3a). This is mainly a consequence of the fact that roots, which are the main input of organic carbon in soils, together with litter at the soil surface, are most abundant in the topsoil and decrease with depth. This is the case in forest (Gill and Jackson, 2000) as well as in agricultural soils (Fan et al., 2016). However, organic carbon is generally also observed in soils below the depth to which roots extend. This process is generally attributed to a downward flux of dissolved organic carbon (DOC) (Kaiser and Kalbitz, 2012). Once organic carbon enters a soil, both at the top as litter or at depth due to root die-off or root exudates (organic substances excreted by roots), it serves as a source of energy for heterotrophic soil organisms (e.g. fungi and bacteria, but also larger meso and macrofauna, see Orgiazzi et al. (2016) for a comprehensive overview). These organisms utilize this organic matter as a source of energy, generally after reducing the size of the organic molecules using enzymes (e.g. Schimel and Schaeffer (2012)). During this process, a portion of the organic carbon is respired as  $\text{CO}_2$ , which is subsequently transferred to the atmosphere.

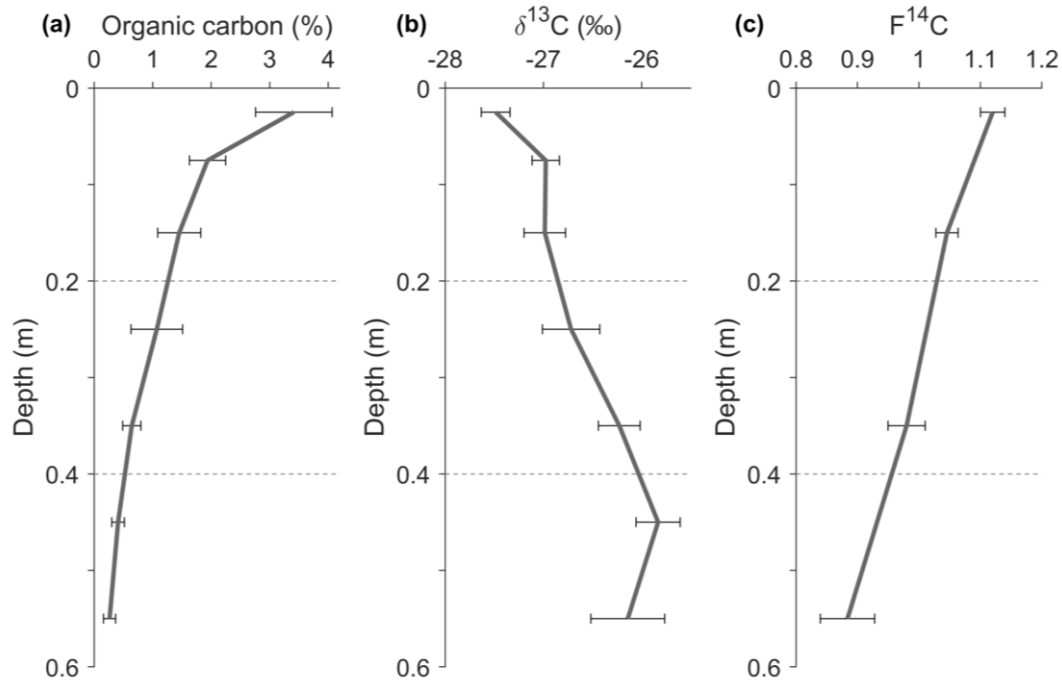


**Figure 1-3** Organic carbon depth profiles for a forest soil in Hesse (NE France), from Schrumpf et al. (2013): (a) organic carbon concentration, (b) stable carbon isotope ( $\delta^{13}\text{C}$ ) values and (c) fraction modern carbon ( $F^{14}\text{C}$ )

A portion of soil organic carbon is, however, not directly respired and can remain in the soil for timescales up to millennia (Rumpel et al., 2002; Schrumpf et al., 2013; Trumbore, 2000). The current view on why organic carbon can remain in the soil over such long timescales are related to mechanisms protecting soil organic carbon from decomposition by microorganisms, such as adsorption onto soil minerals (Kleber et al., 2015; Kögel-Knabner et al., 2008) and incorporation of organic matter in soil aggregates (Six et al., 2000). This is discussed in more detail in section 1.2.

### 1.1.3 The effect of land use change on soil organic carbon stocks

The amount of organic carbon in a soil is not static, but depends to a large extent on the land use to which the soil is subjected. Forest and grassland soils, for example, contain substantially more organic carbon compared to arable land (Jobbágy and Jackson, 2000). As a consequence, land use changes have a substantial influence on the amount of organic carbon stored in a soil and can cause both losses and gains in organic carbon depending of the type of land use change. For example, the conversion of native forest to cropland has been shown to lead to a reduction in the soil organic carbon stock in the top 0.3 m by  $32 \pm 20$  % in temperate areas (Poeplau et al., 2011) and by  $25 \pm 3$  % in the tropics (Don et al., 2011). In contrast, the conversion of cropland to secondary forest has been shown to increase topsoil organic carbon stock by  $83 \pm 39$  % in temperate areas (Poeplau et al., 2011) and by  $50 \pm 12$  % in the tropics (Don et al., 2011). As a consequence, the substantial increase in the area covered by cropland over the past centuries (Lal, 2018) has led to a substantial transfer of organic carbon from the biosphere (soils and vegetation combined) to the atmosphere, with estimates for the entire globe for the period since 1750 in the order of 70 – 230 Pg C (Le Quéré

et al., 2018), with current rates (calculated for the period 1990 – 2010) in the order of  $1.14 \pm 0.18 \text{ Pg C yr}^{-1}$  (although the additional uncertainty on this number is considerable,  $0.5 \text{ Pg C yr}^{-1}$ ) (Houghton et al., 2012). When comparing this number to estimates of the amount of C that has entered the atmosphere due to fossil fuel burning over the same period (1750 – 2016),  $420 \pm 20 \text{ Pg C}$ , it is clear that carbon emissions from anthropogenic land use changes have contributed substantially to increases in the concentration of  $\text{CO}_2$  over the past centuries (Le Quéré et al., 2018). Over the past two decades, however, there has been a small decrease in the global area covered by cropland (Lal, 2018), while for Europe it has been calculated that soils have taken up ca.  $7.6 \text{ Pg C}$  and emitted  $0.8 \text{ Pg C}$  due to land use changes over the period 1950 – 2010 as a consequence of an increase in the forest area and a decrease in the area covered by cropland (Fuchs et al., 2016). In this dissertation, the effect of a different type of land use change, the conversion of tidal marshes to arable land, on the amount of organic carbon stored in soils is studied (chapter 4), which is introduced in section 1.4.2.

#### 1.1.4 Soil organic carbon in a changing climate

Soils store considerably more organic carbon (ca.  $3500 \text{ Pg C}$ ) compared to the amount of carbon that is present in the atmosphere (ca.  $589 \text{ Pg C}$ ) (Figure 1-1). Therefore, small perturbations to the global soil system that cause the transfer of carbon to the atmosphere in the form of  $\text{CO}_2$  or  $\text{CH}_4$  can have a large effect on the global climate. This effect is generally referred to as the ‘carbon – climate feedback’ (Bauska et al., 2015; Friedlingstein et al., 2006; He et al., 2016). As a consequence, a thorough understanding of how environmental and anthropogenic perturbations to the soil system affect its carbon balance are an important prerequisite to study how the global climate will change in the future.

Soils have been shown to be important regulators of the global climate. For example, based on a reconstruction of the  $\delta^{13}\text{C}$  value (see section 1.3.1) of atmospheric  $\text{CO}_2$  for the past 1000 years, Bauska et al. (2015) argued that the biosphere is likely to have been the most important control on the atmospheric  $\text{CO}_2$  content of the past millennium. In addition, Kaplan (2015) argued that at least a portion of  $\text{CO}_2$  emissions over the past millennium had an anthropogenic cause, based on the co-occurrence of (i) the fluctuations in atmospheric  $\text{CO}_2$  and  $\delta^{13}\text{C}$  as measured by Bauska et al. (2015) and (ii) important events in human history. This has earlier also been proposed by Ruddiman (2003), who proposed that humans have been responsible for substantial emissions of  $\text{CO}_2$  due to land use changes from 8000 years ago onwards. Furthermore, Spahni et al. (2013) have shown that over the past millennium, northern peatland soils have taken up between 30 and 50 Pg of C, thereby acting as an important sink for atmospheric  $\text{CO}_2$ .

It is thus clear that soils play an important role as regulators of the global climate. In addition to changes in soil organic carbon stocks caused by land use changes, the amount of organic carbon stored in a soil and, more specifically, the rate at which this is mineralized (converted to  $\text{CO}_2$ ) by soil microorganisms is affected by natural factors such as temperature and soil moisture content. At very low levels of soil moisture (e.g. in desert environments), virtually no mineralization of organic carbon takes place, as microorganisms need a minimal amount of water to survive. In soils which are water saturated, in contrast, mineralization rates are

often also limited due to the limited availability of oxygen (although anaerobic microorganisms are able to mineralize organic carbon in the absence of oxygen). Different responses of organic carbon mineralization rates on soil moisture levels have been proposed in the past, but these responses are subject to large uncertainties (see e.g. Sierra et al., 2015). With regard to temperature, it is generally assumed that an increase in temperature will lead to an increase of the rate at which soil microorganisms mineralize organic carbon (Crowther et al., 2016), with more recalcitrant organic carbon being thought to be more sensitive to increases in temperature, compared to more labile organic carbon (see Davidson and Janssens (2006) and the discussion below). In addition, both variables occur together in natural systems, which makes predictions of the effect of both variables on soil organic carbon decomposition even more difficult (Carey et al., 2016; Sierra et al., 2015).

In order to predict how environmental factors will influence global soil organic carbon stocks, and consequentially global climate, models are used. These are referred to as Earth system models (ESMs), as they represent interactions between the global soil system, vegetation, the oceans and the atmosphere. As soils have been shown to be an important control on the global climate through uptake and emissions of CO<sub>2</sub>, a correct representation of soils in ESM is necessary to reliably predict how the future climate will look (Luo et al., 2015; Tian et al., 2015). However, the representation of soils in ESMs has been identified as one of the major sources of uncertainty on predictions of the future climate (Todd-Brown et al., 2014). This is clear from current estimates of the response of the global soil organic carbon pool to climatic changes, which range from small gains to enormous losses of 1/3 of the current pool by 2100 (as summarized by Bradford et al., 2016).

The effect of temperature on soil organic carbon mineralization has received considerably more research attention over the past decade compared to the effect of soil moisture, and has been shown to be prone to many uncertainties (Bradford et al., 2016; Carey et al., 2016). The current uncertainties about predictions of future soil organic carbon stocks under a changing climate require urgent research attention, as Bradford et al. (2016) state that 'we have neither the data nor the models required to reliably determine how soil C stocks will be affected by a warmer world'. Furthermore, another problem with the prediction of future soil organic carbon stocks by ESMs is what has been referred to as 'outdated assumptions about soil organic carbon turnover', which are currently incorporated in the sub-models simulating soil processes in ESMs (Bradford et al., 2016; Lehmann and Kleber, 2015). This is discussed below in section 1.2.3, and the representation of soil organic carbon in numerical models is the subject of chapters 6 and 7 of this dissertation.

### **1.2 A new paradigm on soil organic carbon cycling**

Over the past decades, there has been a shift in the concepts explaining soil organic carbon cycling and, more specifically, the mechanisms controlling the stabilization of organic carbon in soils. This involved a shift from the 'humification theory' to a paradigm which acknowledges different physical and chemical stabilization mechanisms in soils. The former will be referred to as the 'historical view' and the latter as the 'emerging view', based on the terminology used by Lehmann and Kleber (2015) and Schmidt et al. (2011). Although concepts from the

emerging view have been incorporated in empirical research for multiple years, most currently used soil organic carbon models still rely on concepts associated with the humification theory. In the sections below, first a brief overview of this paradigm shift is provided, after which the consequences for soil organic carbon models are briefly discussed. Both concepts are illustrated in the graphical representation by Schmidt et al. (2011) in Figure 1-4.

### **1.2.1 The historical view**

A first assumption on which the historical view was built is that a portion of plant inputs to the soils is intrinsically 'recalcitrant', rendering them inert to degradation by soil microorganisms (Cotrufo et al., 2013; Schmidt et al., 2011). This was based on the assumption that the fraction of litter loss, e.g. during litter bag experiments, represented C losses from the system, while the fraction of organic matter that remained after these experiments was interpreted as organic matter that would contribute to stable soil organic matter (Cotrufo et al., 2013). However, organic molecules which were assumed to be relatively resistant against decomposition, e.g. lignin, have in fact been shown to be broken down fastest in the early stages of decomposition (Cotrufo et al., 2013; Lehmann and Kleber, 2015 and references therein). In addition, although it has been shown that certain plant compounds may indeed persist longer during biomass decomposition (e.g. in litter bag experiments), in mineral soils these compounds often decay faster compared to bulk soil organic matter (Schmidt et al., 2011).

A second assumption the historical view relied on is the 'humification theory', which assumes that a portion of plant inputs is transformed into complex molecules (also referred to as 'humic substances'), which are resistant against microbial decomposition. Two mechanisms have been proposed to explain the formation of resistant organic molecules (often referred to as 'humus'), as summarized by Cotrufo et al. (2013): (i) biopolymer degradation, assuming selective preservation of macromolecules and recalcitrant compounds and (ii) abiotic condensation, assuming that low molecular weight compounds are abiotically condensed into humus, consisting of large polymers. The notion that a very stable organic carbon fraction exists, referred to as humus, originated from the use of alkaline extraction methods to separate soil organic matter from soil minerals (Lehmann and Kleber, 2015). This extraction resulted in the separation of soil organic matter fractions with different chemical characteristics: humic acid, fulvic acid and humin. However, citing Lehmann and Kleber (2015), 'Among the thousands of publications on 'humic substances', not one independently confirms - for example, by direct spectroscopic observation - that the 'humic substances' extracted by alkali are components of organic matter that exist separately in soil environments'. As a consequence, over the past years multiple authors have argued to abandon the 'humification theory', which assumes that the turnover rate of organic carbon in soils is determined by the chemical structure of the organic molecule, and to move to a new paradigm where the physical protection mechanism of soil organic carbon are explicitly acknowledged (Cotrufo et al., 2013; Lehmann and Kleber, 2015; Schmidt et al., 2011).

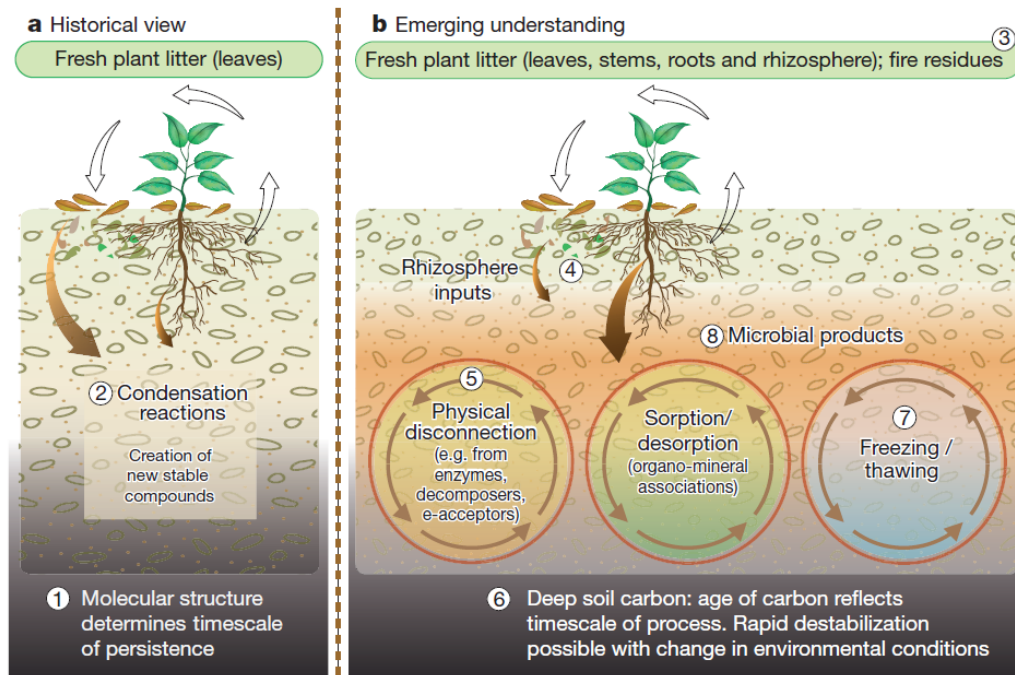


**Figure 1-4** Graphical representation of the ‘historical view’ (a) and ‘emerging view’ (b) on soil organic carbon cycling, from Schmidt et al. (2011, p. 52)

### 1.2.2 The emerging view

The emerging view on soil organic matter cycling is focused on different physical and chemical protection mechanisms in soils (Figure 1-4b), such as the incorporation of organic matter in aggregates (Six et al., 2000) and the adsorption of organic molecules on mineral surfaces (Kleber et al., 2015), e.g. on iron and aluminum oxides (Kögel-Knabner et al., 2008). In addition, in recent years evidence emerged of a mainly microbial origin of stable organic carbon in soils, as microbial necromass has been proposed to be the main source of stable organic carbon (Kiem and Kögel-Knabner, 2003; Kindler et al., 2006; Liang and Balser, 2011, 2008; Miltner et al., 2012; Simpson et al., 2007). This view is also incorporated in the Microbial Efficiency – Matrix Stabilization (MEMS) framework proposed by Cotrufo et al. (2013), as a way to synthesize emerging understanding of soil organic carbon cycling. Also Bradford et al. (2016) acknowledge the importance of microbial-derived organic carbon as the main precursor of organic carbon stabilized on soil minerals, and state that organic molecules have to pass through a ‘microbial funnel’ in order to be processed and subsequently stabilized on mineral surfaces.

The emergence of the view that the majority of organic carbon stabilized on mineral surfaces in soils has a microbial origin constitutes one of the major differences between the ‘historical view’ and the ‘emerging view’ on soil organic carbon cycling. Where the historical view assumes that mainly recalcitrant organic compounds are stabilized in soils while labile compounds are rapidly mineralized, the emerging view assumes the opposite. Indeed, as proposed by Cotrufo et al. (2013), the rapid incorporation of labile organic carbon into microbes, of which the necromass is seen as the most important precursor of stable organic carbon (Bradford et al., 2016; Miltner et al., 2012), leads to a larger contribution of labile

organic matter to stabilized organic matter. This in contrast to organic compounds of 'lower quality' (more difficult to be decomposed by microorganisms), which are hypothesized to indeed be decomposed at a slower rate but contribute less to stable soil organic carbon (Cotrufo et al., 2013). For a more detailed overview of differences between the 'historical' and 'emerging view' of soil organic carbon cycling, reference is made to Dungait et al. (2012), Bradford et al. (2016), Cotrufo et al. (2013), Lehmann and Kleber (2015) and Schmidt et al. (2011).

### 1.2.3 Consequences for soil organic carbon models

The advent of the 'emerging view' on soil organic carbon cycling was based on an increasing amount of empirical evidence that (i) the operationally-defined 'humic substances' have not been observed in soil but are an artefact of the alkaline extraction procedure (Lehmann and Kleber (2015) and references therein), (ii) soil organic carbon is preserved in soils through physical and chemical protection mechanisms and (iii) that a large portion of stable soil organic carbon is of microbial origin (see previous paragraph for references). However, most currently used soil organic carbon models (e.g. RothC (Coleman and Jenkinson, 1999), Century (Parton et al., 2001) or ICBM (Andr n and K tterer, 1997)) are based on the humification theory (Bradford et al., 2016; Cotrufo et al., 2013; Lehmann and Kleber, 2015; Schmidt et al., 2011). These models typically divide soil organic carbon into multiple pools with different intrinsic turnover rates, as a way to represent different physical and molecular properties of soil organic matter, in addition to limitations on the accessibility of soil organic matter by the microbial decomposer community (Dungait et al., 2012). For example, the model structure of RothC, as shown in Figure 1-5, explicitly includes a 'humified' and 'inert' organic matter pool to represent organic compounds which decay very slowly or not at all, respectively.

Over the past years, the validity of these traditional soil organic carbon models has been questioned based on the emerging evidence on dynamics of soil organic carbon cycling. First, although these model assume that organic carbon is processed by microorganisms, they are often not explicitly represented (Campbell and Paustian, 2015; Dungait et al., 2012). In the RothC model, in contrast, soil microbes are explicitly incorporated in a separate pool, but microbes are assumed to decay similar to other carbon pools while not having an influence on rates of organic carbon decay (Figure 1-5). In addition, microbes and their metabolites are generally included in the fastest cycling pools in these models, based on the assumption that microbial biomass is very labile and will rapidly decompose. As a consequence, microbial biomass cannot lead to long-term stabilized organic carbon, as has been proposed by many studies (see previous paragraph for references) (Dungait et al., 2012). Another criticism is related to the fact that predictions of changes in soil organic carbon stocks as a consequence of environmental disturbances by these models are not in line with empirical observations. For example, the soil organic carbon stock predicted by these models is generally a linear function of the amount of carbon inputs. This is a consequence of the simulation of decay rates using first order kinetics. Therefore, simulated increases in carbon inputs, for example as a consequence of the CO<sub>2</sub> fertilization effect, will lead to increases in simulated carbon stocks. This is however not in line with empirical evidence, as van Groenigen et al. (2017) have

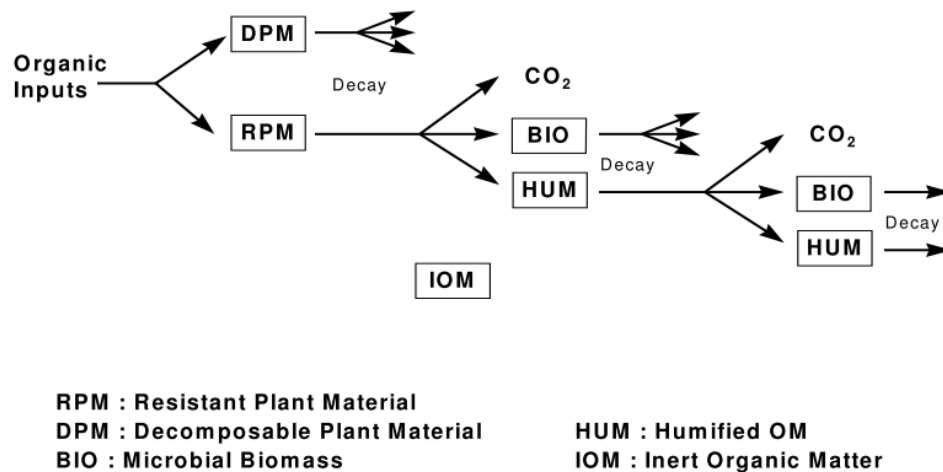


**Figure 1-5** Structure of the RothC soil organic carbon model (Coleman and Jenkinson, 1999)

shown that while the CO<sub>2</sub> fertilization effect indeed leads to increased carbon inputs to the soil, it does not lead to increased soil organic carbon stocks as a consequence of increased mineralization rates of organic matter under elevated CO<sub>2</sub> concentrations. The authors attributed this increase in the mineralization rate of mainly fresh organic carbon inputs to an increase in the supply of labile C from root exudates, which can stimulate the decomposition of plant litter, and higher rates of litter decomposition under elevated CO<sub>2</sub> concentrations, as reported by previous studies (see van Groenigen et al. (2017) and references therein). In addition, these models do not explicitly include preservation mechanisms of soil organic carbon, e.g. stabilization of organic carbon on soil minerals. This is a major shortcoming, as e.g. Doetterl et al. (2015) have proposed that soil geochemistry (the different chemical characteristics of these minerals) is a more important control on soil organic carbon stocks than temperature.

A last consequence of the emerging view on the representation of soil organic carbon in numerical models is related to the simulation of the effect of increasing temperature on decay rates of soil organic carbon. Based on the Arrhenius function, it has traditionally been assumed that the decay of more intrinsically recalcitrant organic carbon would be more sensitive to temperature increases. This is a consequence of the higher activation energy needed to depolymerize and mineralize these molecules by soil microbes (Davidson and Janssens, 2006), also referred to as the Carbon-Quality-Temperature theory (CQT). This has been incorporated in traditional soil organic carbon models by increasing the decay rate of different carbon pools in function of temperature, with multiple functions having been proposed (Sierra et al., 2015). The resulting increase in decomposition rate with temperature may, however, overestimate the release of carbon from soils, as organisms regulating decomposition of organic matter might adapt to these changes and render the initially observed effect of increased CO<sub>2</sub> emissions transient (Bradford et al., 2016). In addition, Lehmann and Kleber (2015) add to this that 'the CQT theory loses much of its explanatory potential for the carbon pools with slow turnover if the decomposition of organic matter is not creating complex and recalcitrant compounds'. This thus poses an urgent need for the development of a better representation of the response of soil organic carbon stocks to

increasing temperatures, which has been the subject of recent research efforts (e.g. Allison et al., 2018, 2010; Carey et al., 2016).

As a result of these shortcomings, over the past years there have been multiple calls to incorporate the mechanisms leading to organic carbon decay (microorganisms) and the protection of organic carbon (e.g. stabilization on soil minerals) explicitly into soil organic carbon models (Bradford et al., 2016; Cotrufo et al., 2013; Lehmann and Kleber, 2015; Schmidt et al., 2011). This has caused a shift in the rationale behind developed models over the past decade, from first-order decay models using conceptual pools with predefined turnover rates (e.g. ICBM, RothC and Century) to vertically explicit models which explicitly simulate microbial dynamics and represent mineral surfaces as a mechanisms for long-term organic carbon stabilization (Smith et al., 2018). An example of a relative simple model structure including microbes and enzyme-mediated soil organic matter depolymerisation is shown in Figure 1-6 (from Allison et al., 2010, p. 336). Recently developed models explicitly simulating microbial dynamics include efforts by Schimel and Weintraub (2003), Allison et al. (2010) and the DAMM model (Davidson et al., 2012). In addition, multiple models have included the explicit simulation of the stabilization of organic carbon on mineral surfaces (COMMISSION (Ahrens et al., 2015), BAMS1 (Riley et al., 2014), MIMICS (Wieder et al., 2014), CORPSE (Sulman et al., 2014), MEND (Wang et al., 2013) and the CLM microbial model (Wieder et al., 2013)) and the inclusion of organic matter in aggregates (AggModel (Segoli et al., 2013)). For more information about these models, reference is made to the cited literature.

Although these models clearly include a better representation of physical and chemical mechanisms controlling soil organic carbon dynamics, their complexity greatly outweighs available data for model calibration and validation, resulting in large uncertainties associated with these mechanistic soil organic carbon models. This was confirmed by Riley et al. (2014), who stated that ‘to our knowledge, observations do not exist to fully test such a complicated model structure [...]’, referring to their BAMS1 model. As a consequence, whether microbial-explicit soil organic carbon models represent a more accurate representation of soil organic carbon dynamics is currently still subject to debate (Bradford et al., 2016).

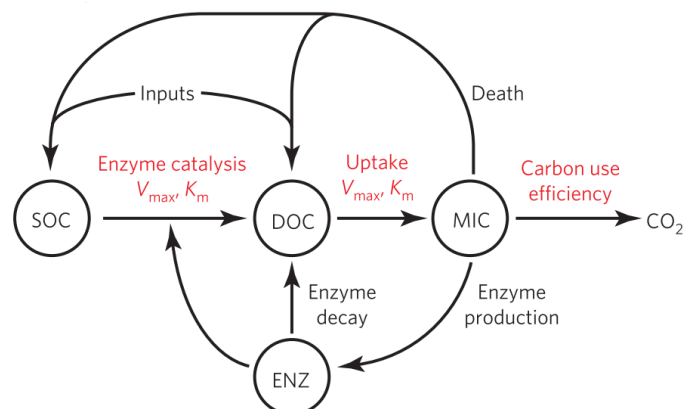


**Figure 1-6** Example of a soil organic carbon model structure which explicitly simulates soil microbes (MIC) and the enzymes they produce (ENZ), which are used to depolymerize polymeric soil organic carbon (SOC) to dissolved organic carbon (DOC). From Allison et al. (2010, p. 336)

### 1.3 The application of carbon isotopes in soil organic carbon research

Carbon (C) has two naturally occurring stable isotopes,  $^{12}\text{C}$  and  $^{13}\text{C}$ , and one radioisotope,  $^{14}\text{C}$ . The natural abundance of the stable C isotopes are 98.9 % for  $^{12}\text{C}$  and 1.1 % for  $^{13}\text{C}$ , while  $^{14}\text{C}$  is much less abundant, with less than 1 C atom for every  $10^{10}$  C atoms being  $^{14}\text{C}$ . Although the majority of C atoms in the biosphere is  $^{12}\text{C}$ , the abundance of  $^{12}\text{C}$  is often combined with both other isotopes in various ways to understand C cycling in the biosphere. The ratio of  $^{13}\text{C}$  to  $^{12}\text{C}$  (expressed as  $\delta^{13}\text{C}$ , see below), is used throughout this dissertation to derive information about the source of soil organic carbon (chapters 2, 3, 4) and to assess the accuracy of the structure of different soil organic carbon models (chapters 6 and 7). In addition, the  $^{14}\text{C}$  content of soil samples is used as a proxy for the age of soil organic carbon (chapter 3) and is incorporated in soil organic carbon models to assess the accuracy of these models (chapters 6 and 7). More information about  $^{13}\text{C}$  and  $^{14}\text{C}$ , and how they can be used to derive information about soil organic carbon dynamics is provided in the next sections.

#### 1.3.1 Stable carbon isotopes ( $\delta^{13}\text{C}$ )

##### 1.3.1.1 Stable carbon isotopes in the biosphere

The ratio of  $^{13}\text{C}$  and  $^{12}\text{C}$  atoms ( $^{13}\text{C}/^{12}\text{C}$ ) of various compounds containing C atoms is, as a standard, expressed relative to an internationally agreed upon standard, using the  $\delta$  notation and expressed as per mil (‰):

$$\delta^{13}\text{C} = \left[ \frac{\left( \frac{^{13}\text{C}}{^{12}\text{C}} \right)_{\text{sample}}}{\left( \frac{^{13}\text{C}}{^{12}\text{C}} \right)_{\text{standard}}} - 1 \right] \cdot 1000 \quad (1.1)$$

The standard is PDB (Pee Dee Belimnite), a carbonate from a marine Cretaceous formation found in South Carolina (USA), with an  $^{13}\text{C}/^{12}\text{C}$  ratio of 0.0112372 (IAEA, 2001). However, as this standard has been used up, a new standard has been decided upon, the Vienna PDB (VPDB), which differs < 0.01 % from the original PDB (IAEA, 2001). As a consequence of the high  $^{13}\text{C}/^{12}\text{C}$  ratio of this standard, organic matter generally has a negative  $\delta^{13}\text{C}$  value.

In 2014, atmospheric  $\text{CO}_2$  molecules had an average  $\delta^{13}\text{C}$  value of ca. -8.4 ‰ (Keeling et al., 2017). However, this value is not constant over time. Fossil fuel combustion since the start of the industrial era has added a substantial amount of fossil C to the atmosphere, which is typically depleted in  $^{13}\text{C}$  isotopes compared to the contemporary atmosphere. This process is known as the  $^{13}\text{C}$  – Suess effect (Keeling, 1979), and has decreased the  $\delta^{13}\text{C}$  value of atmospheric  $\text{CO}_2$  from its pre-industrial value of ca. -6.4 ‰ (Bauska et al., 2015; Keeling, 1979; Keller et al., 2017) to its current value (Figure 1-7).

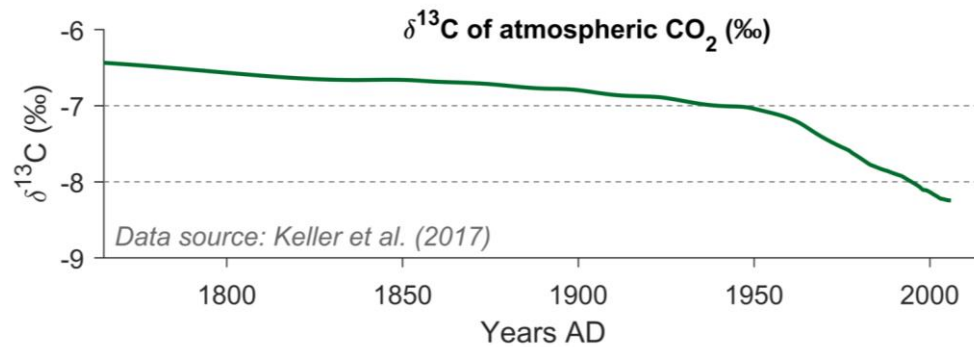


**Figure 1-7** Record of historical  $\delta^{13}\text{C}$  values of atmospheric  $\text{CO}_2$  (data source: Keller et al. (2017))

The  $\delta^{13}\text{C}$  value of organic compounds in the biosphere (e.g. vegetation) differs substantially from the  $\delta^{13}\text{C}$  value of atmospheric  $\text{CO}_2$ . This is a consequence of a process called isotopic fractionation, during which a certain isotope is preferentially taken up or removed from a substrate (the source of organic carbon, in this case atmospheric  $\text{CO}_2$ ). Typically, the  $\delta^{13}\text{C}$  value of terrestrial vegetation is enriched in  $^{12}\text{C}$  (thus having a more negative  $\delta^{13}\text{C}$  value) compared to atmospheric  $\text{CO}_2$ . This is the case because  $^{12}\text{C}$  atoms are preferentially taken up through the stomata of the photosynthesizing parts of plants during photosynthesis (Farquhar et al., 1982). However, the magnitude of this isotopic discrimination against  $^{13}\text{C}$  atoms greatly depends on the photosynthesis pathway plants follow. Plants following the C3 pathway (using the Calvin – Benson cycle) exhibit the largest discrimination against  $^{13}\text{C}$  and typically have  $\delta^{13}\text{C}$  values in the range of -22 - -32 ‰ (Figure 1-8). On the other hand, plants using a C4 pathway (using the Hatch – Slack pathway) discriminate much less against  $^{13}\text{C}$  and have  $\delta^{13}\text{C}$  values in the range of -9 - -17 ‰ (Figure 1-8). A third category of plants have the ability to switch between both pathways, using Crassulacean acid metabolism (CAM), having  $\delta^{13}\text{C}$  values in the range of -10 - -28 ‰ (as summarized by Werth and Kuzyakov (2010)). Globally, C3 plants cover an area ca. 4.5 times higher than C4 plants, while C3 plants are mostly present in temperate zones and make up all forest species and C4 plants are often herbaceous forms present in environments where a high water use efficiency is required (Still et al., 2003). In addition, there is a large variability in the average  $\delta^{13}\text{C}$  value of different plants following the same photosynthetic pathway depending on environmental factors such as temperature and precipitation, as e.g. shown for C3 vegetation (Kohn, 2010; Li et al., 2017). This difference in isotopic composition between C3 and C4 plants has often been the basis to detect historical changes in vegetation in multiple environments by studying organic remains of plants in soils (e.g. Dümig et al., 2008; Martinelli et al., 1996; Pessenda et al., 1996).

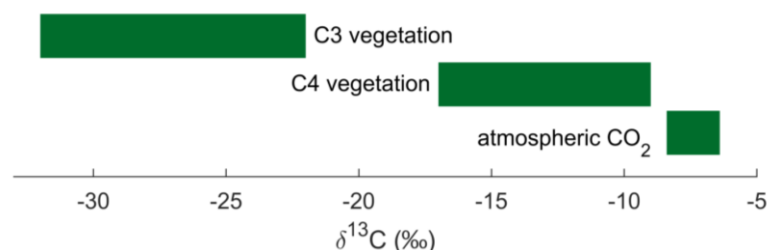


**Figure 1-8** The range in  $\delta^{13}\text{C}$  values of atmospheric  $\text{CO}_2$ , C3 and C4 vegetation

The variability in  $\delta^{13}\text{C}$  values however does not stop at the species level, as different compounds of the same plant also exhibit a large variation in isotopic signature. For example, roots are generally enriched in  $^{13}\text{C}$  compared to the aboveground part of plants as a consequence of the downward transport of  $^{13}\text{C}$ -enriched carbohydrates to plant roots (Ghashghaie and Badeck, 2014). Even at the compound scale, there are large differences in  $\delta^{13}\text{C}$  values, as lipids and lignin are generally depleted in  $^{13}\text{C}$  compared to the bulk plant biomass, while sugars, proteins and cellulose are generally enriched by up to multiple per mil (Bowling et al., 2008). As plant biomass is the largest source for organic carbon present in soils, the  $\delta^{13}\text{C}$  value of soil organic carbon is generally similar to its source material. However, substantial changes to the  $^{13}\text{C}/^{12}\text{C}$  ratio of soil organic carbon occur in soil, as explained in the next section.

### 1.3.1.2 *What controls the $\delta^{13}\text{C}$ value of soil organic carbon?*

The transition from plant biomass, over decomposing litter and potential incorporation into stable soil organic carbon is generally accompanied with an increase in the  $\delta^{13}\text{C}$  value of organic carbon (thus a relative enrichment in  $^{13}\text{C}$  compared to  $^{12}\text{C}$ ), as shown in Figure 1-3b. It is generally observed that the  $\delta^{13}\text{C}$  value of fresh litter at the soil surface has a  $\delta^{13}\text{C}$  value similar to that of aboveground biomass, while older litter can be slightly enriched in  $^{13}\text{C}$  (Balesdent et al., 1993; Ehleringer et al., 2000; von Fischer and Tieszen, 1995). However, organic carbon in the top centimeters of a soil are generally enriched in  $^{13}\text{C}$  (thus having a less negative  $\delta^{13}\text{C}$  value) compared to the litter layer (Acton et al., 2013; Balesdent et al., 1993; Powers and Schlesinger, 2002; Torn et al., 2003; von Fischer and Tieszen, 1995). In addition, when moving down the soil profile, even further  $^{13}\text{C}$  enrichment of soil organic carbon is generally observed with depth, indicated by increasing  $\delta^{13}\text{C}$  values with depth (thus becoming less negative) (Acton et al., 2013; Kohl et al., 2015; Nakanishi et al., 2012; Schrumpp et al., 2013). In most temperate soils under C3 type vegetation, the increase in the  $\delta^{13}\text{C}$  value of soil organic carbon from the topsoil to deep soil layers (> 0.5 m depth) is generally in the range of 2 – 4 ‰ (see many of the references cited above). However, it has been argued that tropical soils can exhibit increases in  $\delta^{13}\text{C}$  values of organic carbon with depth up to 4 – 6 ‰ without a shift from C4 to C3 vegetation having occurred in the past, although this generally cannot be ruled out (Martinelli et al., 1996). For soils under C4 vegetation, in contrast, no substantial increase in the  $\delta^{13}\text{C}$  value of soil organic carbon is generally observed (Dümig et al., 2008; Krull et al., 2005; Martin et al., 1990).

Although the increasing  $\delta^{13}\text{C}$  value of soil organic carbon with increasing soil depth is a feature observed in most well-drained soils around the globe, there has been a debate in literature over the past two decades about the mechanisms controlling this increase. In order to discuss these mechanisms, first an overview of the different mechanisms that have been proposed in literature is provided, after which the proposed mechanisms are discussed in function of the new view on soil organic carbon cycling, as discussed in section 1.2.2. It is noted that often multiple mechanisms are proposed to play a role together, while they are presented here separately.

- a) Differences in the isotopic signature between aboveground biomass and roots, with the former being up to 1.5 ‰  $^{13}\text{C}$ -depleted relative to roots of the same plant (Bowling et al., 2008; Ghashghaie and Badeck, 2014; Werth and Kuzyakov, 2010). Due to vertical soil mixing, e.g. through bioturbation,  $^{13}\text{C}$ -depleted topsoil is mixed with  $^{13}\text{C}$ -enriched subsoil organic carbon, causing an increase in the  $\delta^{13}\text{C}$  value of soil organic carbon with depth.
- b) The  $^{13}\text{C}$  – Suess effect, which has led to a relative  $^{13}\text{C}$  depletion of atmospheric  $\text{CO}_2$  over the past ca. 250 years (Keeling, 1979) (Figure 1-7), as described in the previous section. As topsoil organic carbon is assumed to cycle faster compared to subsoil organic carbon, topsoil organic carbon is assumed to be more influenced by the incorporation of additional  $^{12}\text{C}$  isotopes, leading to an increase in the total  $\delta^{13}\text{C}$  value of soil organic carbon with depth.
- c) Two different microbial effects on isotopic discrimination have been proposed: (i) the preferential uptake of  $^{13}\text{C}$  compared to  $^{12}\text{C}$  and (ii) the preferential respiration of  $^{12}\text{C}$  during metabolism, with the former being proposed to be more important compared to the latter (Werth and Kuzyakov, 2010). The first mechanisms can be caused by the preferential utilization of specific organic compounds by microorganisms, as it has been shown that these can differ substantially in their isotopic composition (Bowling et al., 2008). For example, sugars are generally enriched in  $^{13}\text{C}$  compared to bulk plant leave material, while lignin is generally relatively depleted in  $^{13}\text{C}$ . The second mechanism is related to the effect of the metabolism of microorganisms on the isotopic composition of their own biomass and the  $\text{CO}_2$  that they respire. Although the mechanisms leading to this effect are currently not clear, it is generally accepted that microorganisms are slightly enriched in  $^{13}\text{C}$  compared to the substrate they consume (Dijkstra et al., 2006; Werth and Kuzyakov, 2010).
- d) Another effect of microbial metabolism was proposed by Ehleringer et al. (2000) and is related to the presence of atmospheric  $\text{CO}_2$  in the soil atmosphere. As atmospheric  $\text{CO}_2$  is relatively enriched in  $^{13}\text{C}$  compared to  $\text{CO}_2$  respired by roots and heterotrophic microorganisms in soils, the use of this heavier  $\text{CO}_2$  in carboxylation reactions during catabolism would lead to an additional uptake of  $^{13}\text{C}$  by soil microorganisms. Although this is an interesting hypothesis which would additionally explain why the  $^{13}\text{C}$  enrichment of soil organic carbon with depth is less pronounced with depth under C4 type vegetation (as this implies that  $^{13}\text{C}$  enrichment is related to the difference between the  $\delta^{13}\text{C}$  value of soil organic carbon and atmospheric  $\text{CO}_2$ ), this hypothesis seems, however, not to have been further explored in literature.
- e) A new mechanism was recently proposed by Kohl et al. (2015) and involves observations by the authors that, based on  $\delta^{13}\text{C}$  analyses of phospholipid fatty acids of soil microorganisms, fungi were relatively depleted in  $^{13}\text{C}$  compared to total soil organic carbon, while bacteria were relative enriched in this heavy isotope. As the relative abundance of fungi decreases with depth in the studied soil, while the relative abundance of bacteria increased, the authors argued that the generally observed increase in  $\delta^{13}\text{C}$

value can at least partly be explained by this mechanisms. This mechanisms thus implies that the relative importance of microbial necromass (which is generally enriched in  $^{13}\text{C}$ ) to the total soil organic carbon increases with depth would at least partly explain the generally observed increase in  $\delta^{13}\text{C}$  with depth. A mechanism based on an increase in the relative contribution of microbes to total soil organic carbon was earlier proposed by Ehleringer et al. (2000) and Boström et al. (2007).

- f) A last group of proposed mechanisms are related to observed interactions between dissolved organic carbon (DOC) and soil minerals. A first mechanisms was proposed by Kaiser et al. (2001). Based on field measurement of depth profiles of the  $\delta^{13}\text{C}$  value to DOC, these authors concluded that ( $^{13}\text{C}$ -depleted) hydrophobic DOC is preferentially adsorbed to soil minerals in topsoil, while the relative proportion of ( $^{13}\text{C}$ -enriched) hydrophilic DOC that is adsorbed to minerals increases with soil depth. Secondly, Nakanishi et al. (2012) analyzed water-extractable organic matter from soil minerals (down to a depth of 0.15 m) and found that the relative fraction of hydrophilic organic matter (which is enriched in  $^{13}\text{C}$ ) increased with depth, relative to the hydrophobic fraction (which is depleted in  $^{13}\text{C}$ ). They similarly argued that the generally observed increase in the  $\delta^{13}\text{C}$  value of organic carbon with depth can at least partly be explained by an increasing contribution of hydrophilic OC to total OC with soil depth.

Mechanisms a and b (isotopic differences between aboveground biomass and roots and the  $^{13}\text{C}$  – Suess effect) are based on many observations and do undoubtedly play a role in the observed increasing  $\delta^{13}\text{C}$  value of soil organic carbon with depth. As a consequence, they have been put forward to explain this pattern at least to some extent by multiple studies (e.g. Acton et al., 2013; Boström et al., 2007; Powers and Schlesinger, 2002). However, it is noted here that the role of the  $^{13}\text{C}$  – Suess effect might be overstated, as the  $^{14}\text{C}$  analyses of soils have shown that substantial amounts of ‘bomb carbon’ are generally only present in the upper 10 – 20 cm of soils (see section 1.3.2). As the majority of the  $^{13}\text{C}$  – Suess effect took place since 1950, the period when ‘bomb carbon’ was introduced to the atmosphere, it is unlikely that a substantial amount of ‘Suess carbon’ has been included in deeper soil layers (> 0.2 m). As a consequence, the  $^{13}\text{C}$  – Suess effect cannot explain the generally observed increase in  $\delta^{13}\text{C}$  values down to deep soil layers (> 0.5 m).

The proposed mechanisms related to interactions between DOC and soil minerals (mechanism f) do also provide no conclusive evidence on the mechanisms causing the observed depth patterns in  $\delta^{13}\text{C}$ . Kaiser et al. (2001) observed that ( $^{13}\text{C}$ -depleted) hydrophobic DOC is preferentially adsorbed to soil minerals in topsoil layers while ( $^{13}\text{C}$ -enriched) hydrophilic DOC is preferentially adsorbed in subsoil layers. It is, however, not clear if the observed increase in  $\delta^{13}\text{C}$  of DOC with depth is driving the  $^{13}\text{C}$  enrichment of total SOC with soil depth or the other way around, that an increasing contribution of  $^{13}\text{C}$ -enriched SOC is causing the increase in the  $\delta^{13}\text{C}$  value of DOC by intense interactions with SOC, as proposed by Kaiser and Kalbitz (2012). In addition, the sorption experiments by Kaiser et al. (2001) were performed using litter-derived DOC, which does not account for observations that a large portion of mineral-associated OC can be microbial-derived OC (Liang et al., 2017; Miltner et al., 2012). This is further discussed in chapter 7. In addition, although the experiments by

Nakanishi et al. (2012) clearly show that the proportion of hydrophilic organic carbon (enriched in  $^{13}\text{C}$ ) that is desorbed from minerals increases with depth, this provides no direct evidence of the mechanisms controlling the sorption of organic carbon on minerals, and the source of the organic carbon that is adsorbed (although they state that the hydrophilic fraction of water-extractable organic carbon can contain carbohydrates and microbial necromass).

The last group of mechanisms relate to the effect of microbial processing of organic carbon. The first mechanism (under mechanism c), preferential uptake of molecules enriched in  $^{13}\text{C}$  by soil microorganisms (Werth and Kuzyakov, 2010), is unlikely to play a substantial role in soils, as it has been recently shown that, given the right conditions and enough time, all plant inputs to soils are decomposed by the microbial community, ruling out the possibility of a consistent preferential uptake of certain plant compounds by soil microbes (Lehmann and Kleber, 2015). The second mechanism (under mechanism c), the preferential respiration of  $^{12}\text{C}$  compared to  $^{13}\text{C}$ , has also been disputed in literature based on contrasting results of  $\text{CO}_2$  respired during incubation studies (Boström et al., 2007). However, multiple studies using pure fungal or bacterial cultures have shown that microorganisms are generally  $^{13}\text{C}$ -enriched compared to the substrate on which they feed, while respiring  $^{13}\text{C}$ -depleted  $\text{CO}_2$  (as summarized by Lerch et al. (2011)). This has been attributed to a kinetic isotopic effect during metabolism, during the decarboxylation of pyruvate to form acetyl coenzyme A (as summarized by Ghashghaie et al. (2003)), which is subsequently used in the Krebs cycle by aerobic organisms. An isotopic enrichment of the microbial biomass has also been reported for incubation studies on soil samples (Lerch et al., 2011) or from samples collected in natural soils (Kohl et al., 2015). The mechanism of an increase in the relative proportion of microbial-derived organic carbon to the total soil organic carbon with depth, mechanism e, (Ehleringer et al., 2000; Kohl et al., 2015) is in line with the emerging view on soil organic carbon cycling, which shows substantial evidence that most stabilized soil organic carbon in soils (e.g. on soil minerals) has a microbial origin (Cotrufo et al., 2013; Lehmann and Kleber, 2015; Miltner et al., 2012; Schmidt et al., 2011). Indeed, the combination of observations that soil microbes are isotopically enriched compared to substrate on which they feed and observations that the majority of soil organic carbon stabilized on minerals has a microbial origin is able to explain why soil organic carbon is enriched in  $^{13}\text{C}$  compared to the biomass from which it is derived. Furthermore, it has recently been suggested that organic carbon that is adsorbed onto minerals can be desorbed to serve as a source of organic carbon for soil microbes (Miltner et al., 2012), while it has been proposed that recycling and re-stabilization of soil organic carbon that was previously been stabilized in soils, can be responsible for the generally observed old age (multiple thousands of years) of soil organic carbon (Ahrens et al., 2015). This means that soil organic carbon that is present in deep soil layers has potentially been processed by soil microbes multiple times and, consequentially, is more enriched in  $^{13}\text{C}$  compared to organic carbon in more shallow soil layers. Thus, a scenario in which microbial processing of soil organic carbon is the only source of relative  $^{13}\text{C}$  enrichment (in addition to the  $^{13}\text{C}$  – Suess effect and isotopic differences between litter and roots) is able to explain both (i) the less negative  $\delta^{13}\text{C}$  value of soil organic carbon compared to plant biomass and (ii) the increasing

$\delta^{13}\text{C}$  value of soil organic carbon with depth. This hypothesis is explored in a model exercise in chapter 7.

In conclusion, it is argued here that research on the reasons as to why  $^{13}\text{C}$  enrichment of soil organic carbon with depth takes place has focused too much on formulating hypotheses on why the 'remaining soil organic carbon' is enriched in  $^{13}\text{C}$  compared to initial inputs. For example, although Ehleringer et al. (2000) argue that the observed patterns are a result of a larger contribution of microbial-derived organic carbon to total soil organic carbon, they suggest that microbes constitute a larger portion of the 'residual' carbon, i.e. organic carbon that has not been decomposed. Furthermore, the widely applied approach of Rayleigh distillation as a method to model depth profiles of  $\delta^{13}\text{C}$  (e.g. Acton et al., 2013; Diochon and Kellman, 2008; Garten, 2006; Wynn et al., 2005) assumes that the  $\delta^{13}\text{C}$  value of soil organic carbon increases as a function of the fraction of organic carbon that has not been decomposed. This approach thus explicitly assumes that a portion of soil organic carbon will not be decomposed by soil microorganisms. Other authors have attributed the relative  $^{13}\text{C}$  enrichment with depth to increasing rates of humification (Ladyman and Harkness, 1980). These lines of reasoning are based on the 'traditional view' on soil organic carbon cycling, which assumes that a portion of OM inputs is recalcitrant and will remain in the soil for a long time (Lehmann and Kleber, 2015; Schmidt et al., 2011). Although it cannot be excluded that a limited fraction of organic matter will indeed be preserved in soils as a consequence of its chemical structure or the absence of microorganisms specialized in decomposing these compounds, it is argued here that focus must shift towards assessing why microbial biomass is enriched in  $^{13}\text{C}$  compared to other SOM compounds, which factors control this and how this carbon is preserved on the long-term. As an increasing amount of studies argue that microbial-derived organic carbon is the main precursor of stabilized organic carbon (Cotrufo et al., 2013; Lehmann and Kleber, 2015; Miltner et al., 2012), these microbes are argued to be responsible for the increasing  $^{13}\text{C}$  enrichment with depth that is commonly observed in soils.

### 1.3.2 Radioactive isotopes ( $^{14}\text{C}$ )

The only naturally occurring radioisotope of C,  $^{14}\text{C}$ , is used in this thesis as a proxy of organic carbon (chapter 3) and as a tool to assess the accuracy of soil organic carbon models (chapter 6 and 7).  $^{14}\text{C}$  is a cosmogenic radionuclide, which means it is continuously being created in the stratosphere by interaction between cosmic rays and the  $^{14}\text{N}$  in the atmosphere, after which it is incorporated in the global C cycle as  $^{14}\text{CO}_2$  (Schoor et al., 2016).  $^{14}\text{C}$  has a half-life of 5732 years, making the isotope very useful and widely used for dating organic materials, as  $^{14}\text{C}$  uptake by heterotrophic organisms ceases after it has died. In addition,  $^{14}\text{C}$  has been widely applied in soil sciences as a proxy for the age of soil organic carbon (e.g. Pessenda et al., 1998; Rumpel et al., 2002; Schrumpp et al., 2013; Trumbore, 2000), for the assessment of soil organic carbon turnover rates (e.g. Gaudinski et al., 2000; He et al., 2016; Schrumpp and Kaiser, 2015) and to constrain model parameter values (e.g. Ahrens et al., 2015; Braakhekke et al., 2013; Jenkinson and Coleman, 2008).

The  $^{14}\text{C}$  content of a substance is often expressed as  $\Delta^{14}\text{C}$ , which is defined as:

$$\Delta^{14}\text{C} = \left[ \frac{\left[ \frac{^{14}\text{C}}{^{12}\text{C}} \right]_{\text{Sample}, -25}}{\left[ \frac{^{14}\text{C}}{^{12}\text{C}} \right]_{\text{OX1}, -19} \exp\left(\frac{y-1950}{8267}\right)} - 1 \right] \times 1000 \quad (1.2)$$

With  $\left[ \frac{^{14}\text{C}}{^{12}\text{C}} \right]_{\text{Sample}, -25}$  being the ratio of  $^{14}\text{C}/^{12}\text{C}$  normalized to a  $\delta^{13}\text{C}$  value of -25 ‰ (to remove the effect of mass-dependent isotopic discrimination during the photosynthetic assimilation of organic carbon),  $\left[ \frac{^{14}\text{C}}{^{12}\text{C}} \right]_{\text{OX1}, -19}$  being the  $^{14}\text{C}/^{12}\text{C}$  of the OX-I (Oxalic acid I) standard measured at the same time (with a  $\delta^{13}\text{C}$  of -19 ‰), corrected for radioactive decay of this standard between 1950 and year  $y$ .

Over the past centuries, the  $^{14}\text{C}$  content of the atmosphere has been modified by two processes. The first process which has significantly altered the  $^{14}\text{C}$  content of the atmosphere is the  $^{14}\text{C}$  – Suess effect (similar to the  $^{13}\text{C}$  – Suess effect, as described in the previous section). As a consequence of the burning of fossil fuels, which contain mainly ‘old C’, depleted in  $^{14}\text{C}$  as this has nearly all decayed, atmospheric  $\text{CO}_2$  became depleted in  $^{14}\text{C}$ . This is clear from Figure 1-9, which shows a negative  $\Delta^{14}\text{C}$  for the first part of the 20<sup>th</sup> century, indicating that the atmospheric  $^{14}\text{C}$  content was lower compared to pre-industrial levels due to the addition of  $^{14}\text{C}$ -depleted  $\text{CO}_2$ . In addition, aboveground nuclear weapon testing in the 1950’s and the beginning of the 1960’s caused the addition of a large amount of  $^{14}\text{C}$  isotopes to the atmosphere (Figure 1-9). This resulted in a doubling of the atmospheric  $^{14}\text{C}$  content (a  $\Delta^{14}\text{C}$  of ca. 1000 ‰) just before the international ban on aboveground nuclear weapon testing in 1963. The addition of this ‘bomb carbon’ to the atmosphere made  $^{14}\text{C}$  a useful tool to study carbon dynamics over timescales ranging from millennia to years (Schrumppf and Kaiser, 2015; Schuur et al., 2016; Trumbore, 2009). In soils, the content of  $^{14}\text{C}$  of soil organic carbon generally decreases substantially with depth, as shown in Figure 1-3c. In that figure, the  $^{14}\text{C}$  content is expressed as the fraction modern  $^{14}\text{C}$ , with values < 1 indicating that the C has been predominantly fixed before 1950. This depth profile thus indicates that only soil layers above 0.3 m depth have received a substantial input of C since 1950.

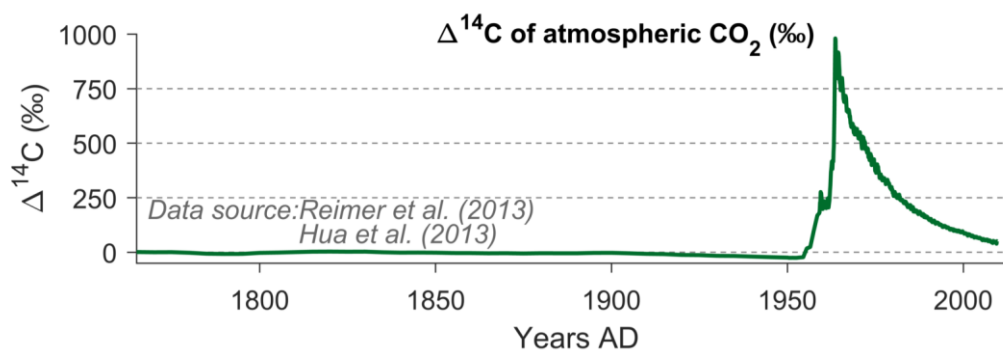


**Figure 1-9** Record of historical  $\Delta^{14}\text{C}$  values of atmospheric  $\text{CO}_2$  (data sources: Hua et al., 2013; Reimer et al., 2013)

## 1.4 Environments in which soil organic carbon is studied

### 1.4.1 Tidal marshes

The first environment in which soil organic carbon dynamics are studied in this dissertation are tidal marshes. These constitute the vegetated portion of the intertidal zone along coastlines (the area on which tidal water progresses during high tide (flood) and on which the water retreats during low tide (ebb)) and in estuaries (the portion of rivers which are affected by the tidal wave entering from the coast). A picture of a tidal marsh in the Scheldt estuary (Belgium – The Netherlands), which is the estuary in which tidal marshes are studied in this research, is shown in Figure 1-10.

Tidal marshes have received a considerable amount of research attention over the past years, mainly because of the recognition that while these ecosystems globally only cover a limited surface area (substantially less than 1 % of the global land surface), they store a disproportionately large amount of soil organic carbon (Duarte et al., 2013, 2005). In addition, tidal marshes are thought to sequester organic carbon (storing it over the long term) at rates higher than in most other terrestrial ecosystems (Mcleod et al., 2011). This notion has fueled hundreds of research projects, resulting in a manifold of publications, concerning organic carbon storage in tidal marshes over the past decades. Despite this large research effort, many knowledge gaps concerning the controls on soil organic carbon storage in tidal marsh sediments still exist today. These range from uncertainties which are related to the total global area covered by tidal marshes (Mcowen et al., 2017) to more specific questions about the effect of rising sea level on tidal marsh vegetation (Kirwan and Guntenspergen, 2012), sedimentation rates at the tidal marsh surface (Kirwan et al., 2016, 2010) and the amount of organic carbon stored in tidal marsh sediments (Kirwan and Mudd, 2012). Concerning tidal marshes in estuaries, another important issue causing uncertainties is the effect of the intrusion of saltwater further into estuaries as a consequence of rising sea level (Weston et al., 2011).



**Figure 1-10** View on a tidal marsh in the salt portion of the Scheldt estuary ('Paulina marsh'). The picture is taken from an embankment, with the tidal marsh fringed between this dike and the Scheldt river (in the upper right corner of the picture). During spring tide and storm events, the vegetated tidal marsh is flooded and sediments are deposited, which causes the marsh platform to grow vertically. © Marijn Van de Broek (May 2016)

One of the main characteristics of the estuarine portion of a river is that water comes from two distinct sources: freshwater is delivered from upstream areas, while saltwater enters the estuary from the coast. As a consequence, estuaries are characterized by a salinity range from saltwater (salinity > 18), over brackish water (salinity between 5 and 18) to oligohaline (salinity between 0.5 and 5) and freshwater (salinity < 0.5). For practical purposes, these last two categories are combined in this study and referred to as freshwater (salinity 0 – 5). As a consequence, tidal marshes located along estuaries are flooded with water having different salinities, influencing the characteristics of vegetation (Hansen et al., 2016; Wieski et al., 2010) and soil chemical properties (Craft, 2007; Dausse et al., 2012). In addition, despite similar morphological processes controlling the formation of tidal marshes along an estuary (although sedimentation rates at tidal marshes generally decline towards the coast (Temmerman et al., 2004)), decreasing sedimentary organic carbon stocks with increasing salinity have been reported (Hansen et al., 2016; Weston et al., 2014; Williams and Rosenheim, 2015).

The large sedimentary organic carbon stocks of tidal marsh sediments have generally been explained by high levels of organic carbon inputs through local vegetation (Duarte et al., 2013) and sources from outside these ecosystems (Mcleod et al., 2011), combined with limited decomposition due to high salinity levels (Hemminga et al., 1991) and the chemical composition of macrophytes (Hemminga and Buth, 1991), while the increase in the volume of sediments due to sediment deposition continuously increases the carbon sink capacity of these ecosystems (Duarte et al., 2013; Mcleod et al., 2011). Along estuaries, higher sedimentary organic carbon stocks in freshwater marshes compared to saltmarshes have been attributed to multiple factors, such as higher rate of primary production (Hansen et al., 2016), higher sedimentation rates and/or higher organic carbon concentrations associated with deposited sediments (Hansen et al., 2016; Hayes et al., 2017) and lower decomposition rates of organic matter (Craft, 2007).

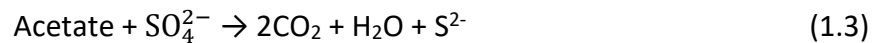
In addition, tidal marsh platforms are often water saturated as a consequence of regular flooding events by tidal water. The consequent absence of oxygen (O<sub>2</sub>) prevents the decomposition of organic carbon in these sediments, although it has been shown that anaerobic decomposition (in the absence of O<sub>2</sub>) can be as efficient as aerobic decomposition (in the presence of O<sub>2</sub>) (Bianchi, 2007). Microorganisms in soils or sediments derive energy by transferring electrons from an electron source (often organic molecules) to an electron sink (generally termed 'terminal electron acceptor') (Megonigal et al., 2004). In the presence of O<sub>2</sub>, this molecule is generally used as terminal electron acceptor, for example during the oxidation of glucose (C<sub>6</sub>H<sub>12</sub>O<sub>6</sub>):



In freshwater wetlands, such as freshwater tidal marshes, the breakdown of organic molecules by specialized anaerobic microorganisms generally ends with a process called methanogenesis, whereby e.g. H<sub>2</sub> (which is produced during earlier steps of the degradation of organic compounds) is oxidized and has methane (CH<sub>4</sub>) as an end product (Megonigal et al., 2004):



In saltmarshes, in contrast, the production of CH<sub>4</sub> through methanogenesis is generally more limited because of the presence of alternative terminal electron acceptors which can be used by microorganisms. For example, due to the presence of sulfate (SO<sub>4</sub><sup>2-</sup>) in sea water, sulfate reduction is often the final step in the anaerobic decomposition of organic molecules. For example, complete organic carbon (here in the form of acetate (C<sub>2</sub>H<sub>3</sub>O<sub>2</sub><sup>-</sup>)) oxidation can be performed by anaerobic sulfate reducers (Megonigal et al., 2004):



It is important to note that the end products of these different anaerobic decomposition pathways are different: methanogenesis has methane (CH<sub>4</sub>) as an end product (although this can be oxidized in tidal marsh sediments (Van Der Nat and Middelburg, 2000)), while sulfate reduction eventually leads to CO<sub>2</sub> production. This is important, as the global warming potential (i.e. the potential of a molecule to warm the atmosphere) of CH<sub>4</sub> is 25 times that of CO<sub>2</sub> on a time horizon of 100 years (IPCC, 2013). Despite the importance of the emission of different greenhouse gases from tidal wetlands at different salinities, this is not further considered in this dissertation. More information about anaerobic metabolism can be found in Megonigal et al. (2004), while additional information about biogeochemistry of estuaries is provided in (Bianchi, 2007).

Considerable knowledge gaps still exist concerning the mechanisms controlling long-term organic carbon preservation in these coastal sediments, and how these vary along estuaries. Moreover, current estimates of the rate of organic carbon sequestration are calculated by combining (i) measurements of the organic carbon concentration in the upper centimeters of the sediments with (ii) sediment deposition rates. This approach potentially greatly overestimates calculated rates of long-term atmospheric CO<sub>2</sub> removal in these sediments by not accounting for losses of organic carbon after burial and the fact that a substantial portion of organic carbon in these sediments may be imported from other ecosystems during sediment deposition, thereby not actively contributing to in-situ CO<sub>2</sub> removal from the atmosphere. In order to reduce these knowledge gaps, the controls on sedimentary organic carbon stocks in tidal marsh sediments along the Scheldt estuary (Belgium and The Netherlands) were studied in this dissertation (chapters 2 and 3).

In a first study (chapter 2), the factors controlling soil organic carbon stocks were assessed for three tidal marshes in the Scheldt estuary, one in every salinity zone (fresh, brackish and salt). Therefore, depth profiles of organic carbon concentration and δ<sup>13</sup>C were used to gain insights in the mechanisms preserving organic carbon with depth. In addition, the δ<sup>13</sup>C value of aboveground vegetation and roots was compared to δ<sup>13</sup>C values of sedimentary organic carbon to gain insight into the source of organic carbon, which can originate from local vegetation (aboveground litter and roots, referred to as autochthonous organic carbon) and carbon associated with deposited sediments (referred to as allochthonous organic carbon), although for the latter no direct measurements were available at the time this study was

performed. These data were subsequently used to formulate hypotheses about the factors controlling organic carbon preservation in these tidal marsh sediments.

These hypotheses were subsequently tested in a follow-up study, which is presented in the third chapter of this dissertation. To assess if the observed patterns and the proposed hypotheses hold for tidal marshes along the entire estuary, additional data were collected, resulting in measurement for a total of 18 sampling locations on 10 tidal marshes. In addition, sediments that were deposited during inundation events in winter and summer were collected to characterize the allochthonous inputs of organic carbon to these systems. In order to improve our understanding on the origin of organic carbon that is preserved in these sediments (autochthonous versus allochthonous), soil samples collected at different depths in tidal marshes in different salinity zones were fractionated to isolate organic carbon protected by different mechanisms, while the  $^{14}\text{C}$  content was determined for topsoil and subsoil sediments and deposited sediments at tidal marshes in different salinity zones. These data have led to novel insights about the mechanisms controlling the long-term storage of organic carbon in the sediments of these coastal ecosystems.

#### **1.4.2 Polders**

The second environment in which soil organic carbon dynamics were studied in this PhD thesis are polders. 'Polder' is the Dutch word for an area that has been reclaimed from uninhabitable land, often a lake, a peatland or a tidal marsh. In this thesis, the word polder is used to refer to land created by the embankment of a tidal marsh, for it to be used for mainly agricultural purposes. An example of a marsh embankment as evident from historical maps is shown in Figure 1-11, while a picture of a polder landscape in the southern Netherlands is shown in Figure 1-12. In order to create a polder, an embankment is constructed at the seaward side of a tidal marsh, with a portion of the sandflat in front of the marsh sometimes being embanked as well (Jongepier et al., 2015). The reclaimed land is subsequently drained through deep ditches and by mechanical drainage (Hoeksema, 2007). As a consequence of this drainage land subsidence occurs, which has caused a major part of polder regions in The Netherlands to be located below sea level (Verhoeven and Setter, 2010). At the seaward side of the constructed embankment, often a new tidal marsh is initiated. The process of stepwise tidal marsh embankment results in a dynamic landscape in which the area covered by polders increases through time, while the spatial distribution of tidal marshes changes continuously (see [www.topotijdreis.nl](http://www.topotijdreis.nl) for a series of historical maps which show these dynamics for the polder series studied in chapter 4 of this thesis).

While tidal marshes store a large amount of organic carbon in their sediments, a large portion of this organic carbon is lost upon embankment (Bai et al., 2013; Bu et al., 2015). Given the high rates of tidal marsh embankment in the past (An et al., 2007; Duarte et al., 2013; Ma et al., 2014; Verhoeven and Setter, 2010), it has been calculated that losses of soil organic carbon as a consequence of this type of land use change are in the order of ca. 3 – 19 % of total  $\text{CO}_2$ -equivalent emissions caused by global deforestation (Pendleton et al., 2012). Although the process of tidal marsh conversion is currently very limited in economically developed countries, many more projects are planned in southeast Asia in the near future



**Figure 1-11** Historical topographic maps (the left map is from 1898, the right map from 1910) showing how the embankment of a tidal marsh (1 on the left map) leads to the creation of a polder (2 on the right map) and the initiation of a new tidal marsh (3 on the right map) in the southern Netherlands. Source: [www.topotijdreis.nl](http://www.topotijdreis.nl)

(Wang et al., 2014), potentially releasing vast quantities of previously stored organic carbon in tidal marsh sediments. Although rates at which sedimentary organic carbon is lost from tidal marshes upon their embankment have been studied in the past, large uncertainties still exist with respect to the magnitude of these losses and the timescale at which they occur (Pendleton et al., 2012). Moreover, these losses are generally studied along chronosequences of embanked tidal marshes (thus by sampling polders which have been embanked at different moments in the past) without accounting for spatial differences. Indeed, as it is clear from historical maps that after the creation of a polder generally a new tidal marsh is initiated at the sea-ward side of the embankment, the organic carbon that is stored in these newly formed marshes could at



**Figure 1-12** Picture of a polder landscape in the Kreekrak area (Völckerpolder, embanked in 1904), taken from an embankment which was constructed to separate the previous tidal marsh from the estuary. © Marijn Van de Broek (August 2015)

least partly offset CO<sub>2</sub> losses from the created polder. This process has up till now, however, not been accounted for.

It should be noted that the construction of an embankment to prevent further tidal flooding of a tidal marshes does not always trigger the formation of a new tidal marsh at the seaward side of the embankment. As discussed in chapter 4, this has likely been the case for the studied polder regions since the former tidal marshes were located in 'sub-basins' of the Scheldt estuary. The construction of an embankment in these sub-basins reduced the area over which tidal inundations took place and therefore potentially reduced water velocities of the inundating tidal water. As a consequence, sediment deposition and the formation of new tidal marshes was promoted against the constructed embankments. However, in situations where this is not the case, e.g. because of a strong water current at the seaward side of the constructed embankment, it is unlikely that a new tidal marsh is initiated against the embankment as the strong currents would inhibit sediment deposition. This is likely to be the case along a large portion of the main channel of the Scheldt river, as there are large stretches of embankments against which only very small or no tidal marshes are present. This is discussed in more detail in chapter 4 of this dissertation.

Organic carbon dynamics in polders of the Scheldt estuary (Belgium – The Netherlands) were studied in this dissertation. The aims of this study were to quantify (1) to total amount organic carbon lost from tidal marsh sediments upon their embankment and (2) the rates at which this occurs. In addition, as polders are present along the entire salt and brackish part of the estuary, a third aim was to (3) assess if the observed losses and rates at which they occur differ between polders originating from salt and brackish marshes. In order to account for the spatial dynamics of this landscape during the stepwise embankment of tidal marshes, a numerical landscape model was constructed to answer a fourth research question: (4) how do landscape-scale soil organic carbon dynamics vary through time in a landscape affected by stepwise tidal marsh embankments. The results of this work are present in chapter 4 of this dissertation.

## **1.5 Current gaps in soil organic carbon research**

The most important current knowledge gaps that are addressed in this dissertation are listed per topic that is being addressed:

### **Organic carbon dynamics in tidal marsh sediments**

- There is a very limited knowledge on the organic carbon stabilization mechanisms in tidal marsh sediments, e.g. protection by chemical interactions with soil minerals, incorporated in aggregates or the presence of organic matter as unprocessed plant remains.
- Knowledge on the rate of atmospheric CO<sub>2</sub> sequestration in tidal marsh sediments is very limited, as current estimates of organic carbon burial in tidal marsh sediments include both locally-produced organic matter (originating from in-situ CO<sub>2</sub> uptake) and deposited organic carbon (which is mobilized from another location, thereby not leading to in-situ CO<sub>2</sub> sequestration).

- Knowledge on the controls on often observed decreasing soil organic carbon stocks in tidal marsh sediments with increasing salinity in estuaries is limited, but is necessary to assess how future environmental changes will affect the amount organic carbon stored in tidal marsh sediments along a salinity gradient.
- Mid-infrared spectroscopy is a tool that is being increasingly used to predict soil organic carbon concentrations of sediment samples from tidal marshes (and other ecosystems). However, while uncertainties on predicted organic carbon concentrations have been assessed in the past (but are often not reported in studies utilizing this technique), there is almost no knowledge on the potential error associated with organic carbon stocks that are calculated using mid-infrared spectroscopy predictions of soil organic carbon concentrations. *Note:* the technique of mid-infrared spectroscopy as a tool for the prediction of organic carbon concentrations is not discussed in this introduction. More information about this technique can be found in the introduction of chapter 5.

### **Organic carbon dynamics in polder soils**

- The magnitude of losses of sedimentary organic carbon in tidal marshes as a consequence of tidal marsh embankment are poorly constrained, while knowledge on the rate at which these losses occur is very limited.
- Spatial processes in intertidal landscapes affected by tidal marsh embankments have up till now not been taken into account when assessing the effect of tidal marsh embankments on soil organic carbon losses. This is a major limitation, and should be accounted for to accurately calculate net organic carbon losses as a consequence of this practice.

### **Numerical modelling of soil organic carbon**

- Traditional soil organic carbon models have been attributed to rely on 'outdated concepts' related to soil organic carbon cycling (e.g. Bradford et al., 2016). This limits the ability of these models to reliably predict future soil organic carbon stocks.
- The resulting trend in increasing complexity of soil organic carbon models, which has been observed over the past years, increases the difficulty to calibrate the parameters used by these models. This is a major limitation which hampers accurate and reliable predictions of future changes in soil organic carbon stocks. New approaches and data are thus needed to fill this gap.
- While deep soil organic carbon (> 0.3 m depth) has been recognized to constitute an important part of the global carbon cycle, this is often not taken into account in soil organic carbon models (although exceptions exist). A better representation of subsoil organic carbon would therefore lead to more reliable predictions of future soil organic carbon stocks.

## **1.6 Research questions**

These research gaps can subsequently be translated into the main **research questions** which will be addressed in this dissertation:

**RQ 1: How do organic carbon stocks vary in tidal marsh sediments along the salinity gradient of a temperate estuary and which factors control the observed variations?** Knowledge on the mechanisms controlling the generally observed large soil organic carbon stocks in tidal marsh sediments is limited. Insights in the patterns of soil organic carbon stocks in tidal marshes along the salinity gradient of the Scheldt estuary (Belgium and The Netherlands) and the factors controlling the observed pattern can lead to more general insights in how organic carbon cycling is controlled in the sediments of these coastal vegetated ecosystems.

**RQ 2: At which rate is organic carbon lost from tidal marsh sediments after these are embanked and how do spatial variations in the area of tidal marshes and polders affect regional soil organic carbon stocks?** As it has been shown that the embankment and subsequent drainage and cultivation of tidal marshes leads to a large loss of previously stored organic carbon (Pendleton et al., 2012), gaining knowledge on the magnitude of these losses and the rate at which they occur will allow to better predict how this land use change contributes to the loss of previously stored soil organic carbon and the consequent emissions of greenhouse gases (e.g. CO<sub>2</sub>).

**RQ 3: Can mid-infrared spectroscopy be used to accurately predict organic carbon stocks of tidal marsh sediments?** As the organic carbon concentration of tidal marsh sediments varies considerable both spatially and temporally, a large number of sediment samples needs to be analyzed for organic carbon concentration to calculate accurate sedimentary organic carbon stocks for these ecosystems. Mid-infrared spectroscopy has been shown to accurately predict the organic carbon concentration of sediment samples, but knowledge on the uncertainty associated with calculated soil organic carbon stocks when using this technique is currently very limited.

**RQ 4: Can realistic depth profiles of stable carbon isotopes ( $\delta^{13}\text{C}$ ) be modelled using two soil organic carbon models build on different principles?** Modelled stable carbon isotopes ( $\delta^{13}\text{C}$ ) have a large potential to serve as an effective additional constraint on model parameters if  $\delta^{13}\text{C}$  can be realistically modelled. Therefore, two established soil organic carbon models, (1) a cascade model using first order kinetics and predefined turnover rates (ICMB; Andr en and K atterer, 1997) and (2) a process-based model simulating soil microbes and mineral protection of organic carbon (COMISSION; Ahrens et al., 2015) were adapted to simulate depth profiles of stable carbon isotopes, in order to assess the extent to which both models are able to simulate reliable  $\delta^{13}\text{C}$  depth profiles.

**RQ 5: Can insights gained from the incorporation of stable carbon isotopes in established models be used to construct a soil organic carbon model that simulates realistic depth profiles of total soil organic carbon,  $\delta^{13}\text{C}$  and  $^{14}\text{C}$ ?** The results from the exercise previous exercise, where stable carbon isotopes were simulated using established models, will be used to construct a soil organic carbon model that simulates realistic depth profiles of total organic carbon,  $\delta^{13}\text{C}$  and  $^{14}\text{C}$ .

## 1.7 Dissertation outline

The structure of this dissertation is shown in Figure 1-13. In chapters 2 and 3, the results of the studies concerning the controls on soil organic carbon stocks along the salinity gradient of the Scheldt estuary (Belgium and The Netherlands) are presented. In chapter 2, depth profiles of organic carbon concentration and  $\delta^{13}\text{C}$  from one tidal marsh in every salinity zone (fresh – brackish – salt) are combined with measurements of biomass and the  $\delta^{13}\text{C}$  value of aboveground biomass and roots to gain first insights into the controls on (i) total soil organic carbon stocks, (ii) the fate of organic carbon in these sediments and (iii) how allochthonous (deposited organic carbon) and autochthonous (locally-produced organic carbon) sources of organic carbon contribute to the total sedimentary organic carbon stock. Based on these insights, a more extensive field campaign was organized to collect depth profiles of soil organic carbon and  $\delta^{13}\text{C}$  from 7 additional tidal marshes along the estuary, together with deposited sediments during flooding events in winter and summer. Data obtained from these soil samples, including measurements of the  $^{14}\text{C}$  content and carbon fractionation, are presented in chapter 3 and conclusions are derived about the mechanisms controlling organic carbon storage in tidal marsh sediments along a temperate estuary.

Chapter 4 is centered on organic carbon dynamics in embanked tidal marsh sediments, referred to as polders. This was done for two polder chronosequences (polders embanked at different moment in the past) along the Scheldt estuary, one in the salt part and another in the brackish part. Based on measured depth profiles of soil organic carbon and  $\delta^{13}\text{C}$  in polders embanked at different times in the past, the rate at which soil organic carbon stocks decline upon embankment were determined. In addition, insights were gained in the rate at which the original tidal marsh organic carbon was replaced with organic carbon from agricultural inputs at different depths along the soil profiles. In addition, a numerical landscape model was constructed to assess the effect of spatial and temporal variations in the spatial coverage of tidal marshes and polders on landscape-scale organic carbon stocks.

The fifth chapter is methodologically-oriented and is focused on the accuracy with which soil organic carbon stocks in tidal marshes can be calculated using predicted organic carbon concentration obtained through mid-infrared spectroscopy. It was assessed how differences in the characteristics of organic matter in tidal marsh sediments along the Scheldt estuary, as presented in chapters 2 and 3, affect predictions of the organic carbon concentration of these intertidal sediments.

The topic of the last two chapters of this dissertation differs from the previous chapters and is focused on the capacity of numerical models to predict depth profiles of stable carbon isotopes ( $\delta^{13}\text{C}$ ). In chapter 6, two established soil organic carbon models were adapted to simulate depth profiles of  $\delta^{13}\text{C}$ : a cascade model using first order kinetics and predefined turnover rates (ICMB; Andr en and K atterer, 1997) and a process-based model simulating soil microbes and mineral protection of organic carbon (COMISSION; Ahrens et al., 2015). The results derived from this model assessment were subsequently used in chapter 7 to develop a new mechanistic soil organic carbon model. This model explicitly simulates microbial

dynamics and the stabilization of organic carbon on soil minerals and simulates realistic depth profiles of total organic carbon,  $\delta^{13}\text{C}$  and the  $^{14}\text{C}$  content of soil organic matter.

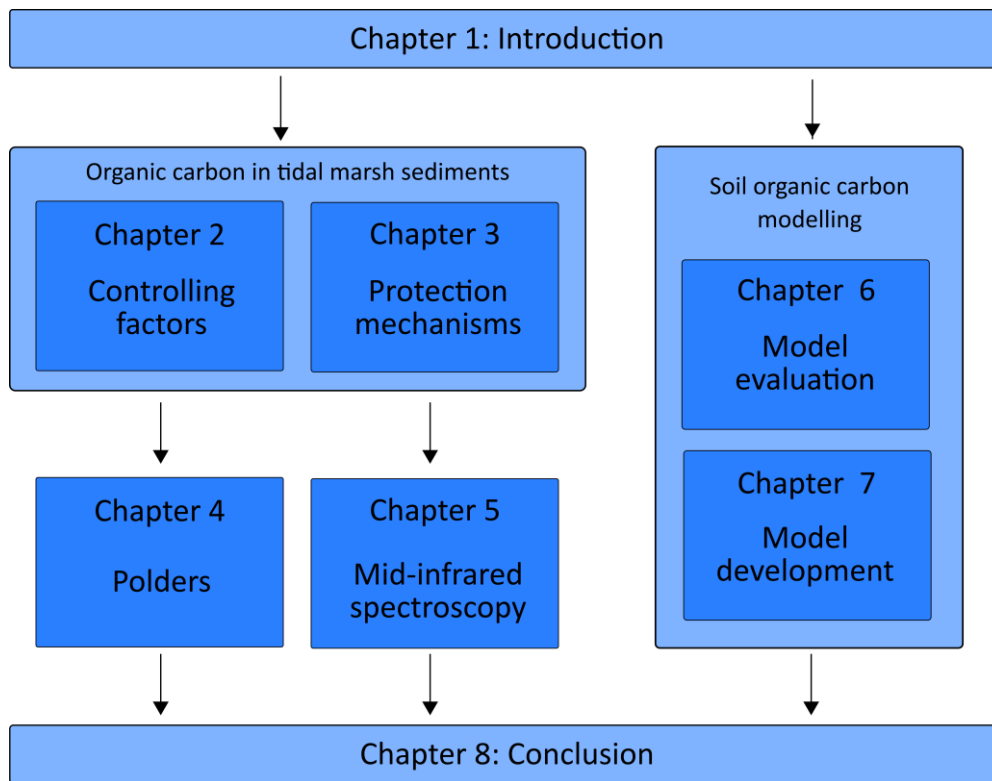


Figure 1-13 Flowchart of the outline of the dissertation



## Chapter 2 Controls on soil organic carbon stocks in tidal marshes along an estuarine salinity gradient<sup>1</sup>

---

**Abstract.** Tidal marshes are sedimentary environments and are among the most productive ecosystems on Earth. As a consequence they have the potential to reduce atmospheric greenhouse gas concentrations by sequestering organic carbon (OC). In the past decades, most research on soil organic carbon (SOC) storage in tidal marsh environments has focused on salt marshes, leaving carbon dynamics in brackish and freshwater marshes largely understudied and neglecting the diversity among tidal marshes. We therefore conducted an extensive sampling campaign to quantify and characterize SOC stocks in marshes along a salinity gradient in the Scheldt estuary (Belgium and The Netherlands). We find that SOC stocks vary significantly along the estuary, from 46 kg OC m<sup>-2</sup> in freshwater marshes to 10 kg OC m<sup>-2</sup> in salt marshes. Our data also show that most existing studies underestimate total SOC stocks due to shallow soil sampling, which also influences reported patterns in OC storage along estuaries. In all sampled tidal marsh sediments the SOC concentration is more or less constant from a certain depth downward. However, this concentration decreases with increasing salinity, indicating that the amount of stable SOC decreases from the upper estuary towards the coast. Although the net primary production of macrophytes differs along the estuary, our data suggest that the differences in OC storage are caused mainly by variations in suspended sediment concentration and stable particulate OC (POC) content in the water along the estuary. The fraction of terrestrial suspended sediments and POC that is transported downstream of the maximum turbidity zone is very limited, contributing to smaller amounts of long-term OC sequestration in brackish and salt marsh sediments. In addition, high rates of sediment deposition on freshwater tidal marshes in the maximum turbidity zone promote efficient burial of OC in these marsh sediments.

---

<sup>1</sup>This chapter is published as Van de Broek, M., Temmerman, S., Merckx, R. and Govers, G.: Controls on soil organic carbon stocks in tidal marshes along an estuarine salinity gradient, *Biogeosciences*, 13, 6611–6624, doi:10.5194/bg-13-6611-2016, 2016. The supplementary data associated with this paper, to which is referred in this chapter, can be found on <http://dx.doi.org/10.5194/bg-13-6611-2016-supplement>.

## 2.1 Introduction

As a consequence of increasing atmospheric greenhouse gas concentrations and the recognition that soils have the potential to store vast amounts of organic carbon (OC), there is large interest in the OC storage potential of soils in different ecosystems (Duarte et al., 2013; Govers et al., 2013; Scharlemann et al., 2014). Although coastal vegetated habitats occupy only 0.2 % of the ocean surface, it has been estimated that they account for approximately 50 % of carbon burial in marine sediments, referred to as blue carbon (Donato et al., 2011; Duarte et al., 2013; Mcleod et al., 2011; Nelleman et al., 2009). It has recently been shown that the OC sequestration potential of these ecosystems will depend to a large extent on future climatic changes and sea level rise (Cherry et al., 2009; Kirwan and Blum, 2011; Kirwan and Mudd, 2012; Weston et al., 2011). Moreover, changing carbon storage in these ecosystems can potentially cause important feedbacks to atmospheric concentrations of carbon dioxide (CO<sub>2</sub>) and methane (CH<sub>4</sub>) (Duarte et al., 2013; Pendleton et al., 2012; Poffenbarger et al., 2011). Constraining the amount of OC that is sequestered in these ecosystems and understanding the processes controlling the size of this pool are of major importance for understand the global carbon cycle.

A significant fraction of coastal wetlands is occupied by tidal marshes. These are vegetated intertidal areas located along coastlines and estuaries in sub-Arctic to tropical climates (although they occur mostly in temperate zones) and are among the most productive ecosystems on Earth (Rocha and Goulden, 2009; Whigham, 2009). Their elevation increases as a consequence of the deposition of both mineral sediments and allochthonous organic matter (OM) during flooding events on the one hand and the incorporation of in situ produced biomass (both above and below ground) on the other hand (Fagherazzi et al., 2012; Neubauer, 2008). Recently formed young tidal marshes, with a low elevation, receive more mineral sediments than their higher counterparts, with sedimentation rates decreasing through time until the marsh platform elevation is in equilibrium with the local mean high water level (Temmerman et al., 2003).

Despite the fact that the importance of vegetated coastal ecosystems and tidal marshes is now widely recognized, estimates of the total amount of OC stored in tidal marshes are subject to a large uncertainty. Estimates of soil organic carbon (SOC) stocks in salt marshes (i.e. tidal marshes bordering saltwater bodies) range between 0.4 and 6.5 Pg (Bridgham et al., 2006; Chmura et al., 2003; Duarte et al., 2013). To the best of our knowledge, no global estimates are available for brackish and freshwater marshes.

There are multiple reasons for the large uncertainty in estimates of the global OC storage in tidal marsh soils. Firstly, the total area of global salt marshes currently used to estimate global stocks is poorly constrained, with estimates between 22 000 and 400 000 km<sup>2</sup> (Chmura et al., 2003; Woodwell et al., 1973), while a global inventory for freshwater marshes is lacking (Barendregt and Swarth, 2013). Secondly, the available data set on SOC stocks is limited, both in terms of the number of samples analysed and the geographical scope: hitherto, most studies were carried out in a limited number of estuaries, mostly located on the southern and eastern coasts of North America. Differences in sampling procedure and depth beneath the

soil surface also contribute to uncertainty. Very often only topsoil samples are analysed, with a limited number of studies considering carbon storage in deeper horizons, although it has been recognized that these also store a significant amount of OC (Elschot et al., 2015; Wang et al., 2011). An additional factor complicating the extrapolation of data to tidal marshes for which no data are available, is the wide range of reported OC contents for tidal marsh soils (Bouillon and Boschker, 2006; Middelburg et al., 1997). A third important reason for the uncertainties mentioned above is that tidal marshes in estuaries are characterized by steep gradients of multiple environmental and ecological factors (Craft, 2007). A sharp increase in salinity towards the coast is present, resulting in a longitudinal estuarine gradient from salt marshes in the most seaward part over brackish marshes to freshwater tidal marshes. As a consequence of this salinity gradient a vegetation gradient develops, with macrophyte biomass generally being higher on freshwater and brackish marshes compared to salt marshes (Dausse et al., 2012; Hansen et al., 2016; Weston et al., 2014; Wieski et al., 2010). In addition, the OC input in tidal marsh soils is a mixture of upland, riverine, estuarine and marine sources and the relative contribution of these sources to the total OC pool varies significantly along the estuary (Middelburg and Nieuwenhuize, 1998).

Currently available data suggest that these environmental gradients along estuaries generally result in decreasing SOC stocks with increasing salinity (Craft, 2007; Hansen et al., 2016; Hatton et al., 1983; Wieski et al., 2010). However, our knowledge on how location along the estuary affects total SOC stocks and which processes control the magnitude of these stocks is, at present, still very limited, mainly because most studies only consider SOC storage down to a depth of 0.3m and generally the reasons for the observed variability are not identified. Nevertheless, understanding the effect of environmental gradients on SOC dynamics in tidal marshes is important. Such understanding may not only help to improve our estimates of current SOC storage but will also be of great help in assessing the effects of sea level rise on these SOC stocks (Morrissey et al., 2014; Poffenbarger et al., 2011; Weston et al., 2011). Here, we study the variation in SOC inventories in tidal marshes along a salinity gradient in the Scheldt estuary, located in Belgium and the Netherlands. This estuary is characterized by strong gradients in salinity and sediment concentration, making it a suitable location to investigate the impact of these gradients on OC stocks in tidal marsh sediments. The aims of this study are therefore 1) to determine the SOC stocks of tidal marsh soils along the salinity gradient of a temperate estuary, 2) to determine the main controls on SOC stocks along this gradient and 3) to use this knowledge to assess how future environmental changes may influence SOC stocks in estuarine tidal marsh soils.

## **2.2 Materials and methods**

### **2.2.1 Study sites**

The Scheldt river is located in western Europe and flows into the North Sea in the southern Netherlands (Figure 2-1). The estuary of the river extends from its mouth up to 160 km upstream where the tide is stopped by sluices near the city of Ghent (Belgium). The estuary is influenced by a semi-diurnal meso- to macrotidal regime, with mean tidal ranges between 3.8 m at the mouth and 5.2 m in the inner estuary (Meire et al., 2005). The estuary has a total length of about 235 km (including tributary tidal rivers) and comprises a salt or polyhaline



**Figure 2-1** Map of the Scheldt estuary showing the salinity zones and the location of the sampled tidal marshes in a western European context. Intertidal sand flats are depicted in light grey.

zone (salinity > 18), brackish or mesohaline zone (salinity 5 – 18) and freshwater/oligohaline zone (salinity 0 – 5) (Figure 2-1). The Scheldt estuary is described in detail in Van Damme et al. (2005) and Meire et al. (2005).

Tidal marshes are present along the entire length of the estuary and tributary tidal rivers, resulting in approximately 518 ha of freshwater marshes, 3035 ha of brackish marshes and 652 ha of salt marshes (Tolman and Pranger, 2012; Van Braeckel et al., 2012). We sampled a salt, brackish and freshwater tidal marsh, and within each marsh we sampled two locations with different but known rates of historical sediment accretion (Figure 2-2 and Table 2.1). The first location, referred to as high marsh, has an elevation of 0.1 to 0.3 m above mean high water level (MHWL), and has been accreting during the past decades at a rate that is in equilibrium with the rise of MHWL. At the second location, referred to as low marsh, marsh formation started during the past decades at heights well below MHWL. Average accretion rates at these locations were therefore significantly higher than sea level rise. However, the accretion rate at these locations can currently be similar to the high marsh if sediment deposition on the low marsh was sufficient for the marsh platform to accrete in equilibrium with sea level rise at present, causing high and low marshes to have a similar elevation (Figure 2-2). For the period 1955 – 2002, the average accretion rates at low and high marshes were 0.5 and 0.75 cm yr<sup>-1</sup> for the salt marshes 1–2 and 0.5–1 cm yr<sup>-1</sup> for the brackish marshes and 1–2 and 1 cm yr<sup>-1</sup> for the freshwater marshes (Temmerman et al., 2004). The vegetation history for the different sites is shown in Figure 2-3. The locations of the sampled tidal marshes are indicated in Figure 2-1 and GPS coordinates of the sampling locations are provided in Table S1.

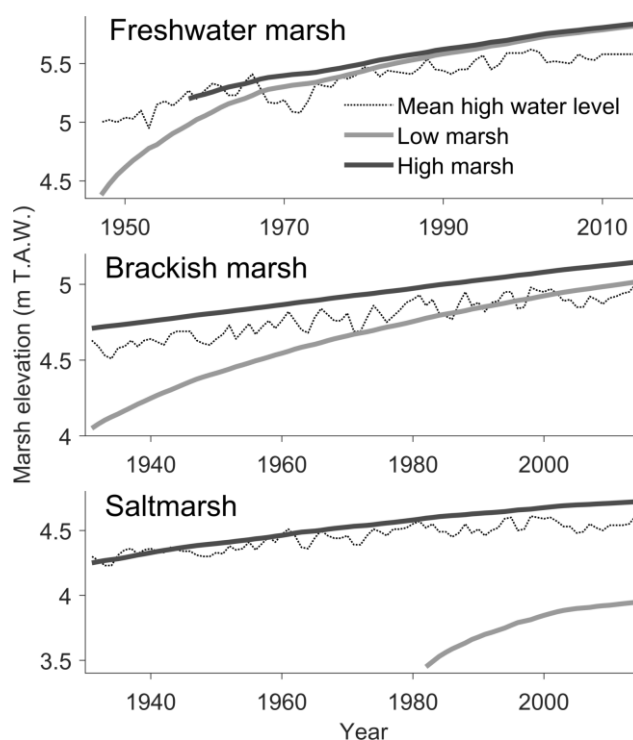


**Figure 2-2** Evolution of marsh surface elevation and mean high water level (relative to Belgian ordnance level, m T.A.W.) at the sampled locations (based on Temmerman et al. (2004)).

**Table 2.1** Main properties of the sampled tidal marshes

Name	Name in this study	Vegetation	Tidal range (m) <sup>A</sup>	Elevation relative to local MHWL (m)	POC% of suspended sediment <sup>B</sup>	Marsh sediment depth (m) <sup>C</sup>
Notelaar marsh	Freshwater low	<i>Phragmites australis</i>	5.14	+0.24	6 - 10	1.2
	Freshwater high	<i>Salix sp + Urtica dioica</i>	5.14	+0.25	6 - 10	> 1.4
Waarde marsh	Brackish water low	<i>Elymus athericus</i>	4.85	+0.01	4 - 5	0.8
	Brackish water high	<i>Elymus athericus</i>	4.85	+0.14	4 - 5	> 1.4
Paulina marsh	Saltwater low	<i>Spartina anglica</i>	4.19	-0.66	3 - 4	0.2
	Saltwater high	Mixed vegetation <sup>D</sup>	4.19	+0.11	3 - 4	0.6

Notes: <sup>A</sup>from Meire et al. (2005), <sup>B</sup>from Abril et al. (2002), <sup>C</sup>based on depth profiles of grain size and OC concentration, <sup>D</sup>*Atriplex portulacoides*, *Limonium vulgare*, *Triglochin maritima*, *Elymus athericus*, *Puccinellia maritima*.

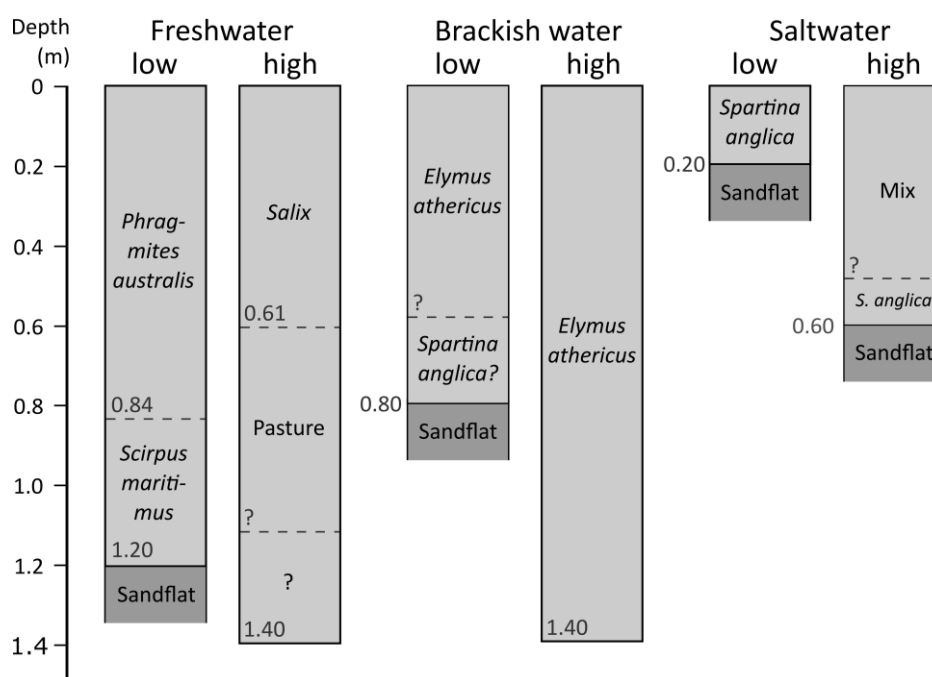


**Figure 2-3** Depth profiles of the sampled tidal marshes showing the vegetation history at each location. At locations where the sand flat was reached this is indicated, at the other locations the marsh sediments extended below 1.4m depth. The vegetation history is based on Temmerman et al. (2003) and information from the  $\delta^{13}\text{C}$  profiles of this study, in combination with information from Boschker et al. (1999) and Middelburg et al. (1997). Mix denotes mixed vegetation which includes *Atriplex portulacoides*, *Limonium vulgare*, *Triglochin maritima*, *Elymus athericus* and *Puccinellia maritima*. A '?' near a dashed line indicates that the exact depth of this line is uncertain, a '?' after species names indicates that the presence of this species was hypothesized.

### 2.2.2 Sample collection

Depth profiles were collected in November 2014 using a manual gouge auger (0.06 m diameter) down to a maximum depth of 1.4 m. Three replicate soil cores were collected with a maximum distance of 3 m in between the coring locations. The cores were divided into 0.03 m sections and every soil sample was stored in a resealable bag in the field before transport to the lab. Samples for soil bulk density and root density measurements were collected using a Kopecky ring sampler or with the gouge auger if soil wetness prevented the use of Kopecky rings. These samples were collected at the soil surface and at depth increments of 0.1 m up to 0.5 m, then in 0.2 m increments down to the maximum depth of 1.4 m. Above-ground biomass was collected on a surface area of 0.25 m<sup>2</sup> (five replicates) at the end of August 2015 at each coring location. The difference in timing between soil and biomass collections is due to the fact that standing biomass is maximum in August in estern European tidal marshes (De Leeuw et al., 1990; Groenendijk, 1984).

### 2.2.3 Soil and biomass analysis

Before analysis of the soil samples, macroscopic vegetation residues were removed manually using tweezers. The soil samples were oven-dried at 35°C for 48 hours and crushed until they passed through a 2mm sieve. After carbonates were removed with a 10% HCl solution, the

samples were analysed for OC,  $\delta^{13}\text{C}$  and C:N ratio using an Elemental Analyser (FlashEA 1112 HT, Thermo Scientific). Soil texture was determined using a laser diffraction particle size analyser (LSTM 13 320, Beckman Coulter) after the destruction of organic matter using hydrogen peroxide (35 %) and aggregates were destroyed using ultrasonic dispersion. Grain size was classified into clay (<2  $\mu\text{m}$ ), silt (2–63  $\mu\text{m}$ ) and sand (>63  $\mu\text{m}$ ) fractions. Soil pH was determined after diluting 5 g of soil in 25 ml of a 0.01M  $\text{CaCl}_2$  solution and electrical conductivity was measured after diluting 5 g of soil in 25 ml of deionized water. The collected biomass was dried at 60°C for 48 hours after sediments were removed and weighed in order to calculate the total dry weight of the biomass. The total above-ground biomass of one of the replicates collected on a 0.25 m<sup>2</sup> surface area was shredded and repeatedly divided into equal parts until only a small portion was left. This was further grinded and analysed for OC content,  $\delta^{13}\text{C}$  and C:N ratio using the Elemental Analyser (FlashEA 1112 HT, Thermo Scientific). Soil bulk density samples were dried at 105°C for 24 hours. After soil bulk densities were calculated, the samples were washed over a 0.5 mm sieve using deionized water and all roots were collected. The roots were cleaned using deionized water, dried at 60°C and weighed.

#### 2.2.4 Data analysis

At every location one soil profile was analysed in detail (every other depth sample, i.e. 0–0.03, 0.06–0.09m, ...). For all three replicate profiles every third sample was analysed (i.e. 0–0.03, 0.09–0.12m, ...) to a depth of 0.72m. Below this depth, samples were analysed every 0.18 m. Continuous depth profiles of OC percentage for layers of 0.01 m were obtained by linear interpolation, using the average OC percentage at the depths at which three replicates were analysed (i.e. every 0.09 m). Continuous depth profiles for bulk density were obtained in an identical way. These continuous depth profiles were then used to calculate total SOC stocks for a volume of soil with a surface area of 1 m<sup>2</sup> and a depth equal to the total sampling depth of the marsh sediments. Root biomass was measured at discrete depths as explained above. For every layer the total root biomass for a surface area of 1 m<sup>2</sup> was calculated by rescaling the average root biomass for the three replicates to the total volume of that soil layer. Linear interpolation between measurements at different depth intervals was used to calculate the total root density per surface area of 1 m<sup>2</sup>. To test whether annual above-ground biomass production was significantly different between the sites a one-way analysis of variance was used in Matlab<sup>®</sup>, after checking for normality (Anderson–Darling test) and homogeneity of variances (Levene’s test) with a level of significance of  $p < 0.05$ . For the other variables only three replicates were available so no reliable significance test could be performed.

### 2.3 Results

#### 2.3.1 Soil characteristics

The studied tidal marsh soils are classified as tidalic Fluvisols with a silt loam grain size (detailed grain size data are provided in the Supplementary data). The maximum depth of marsh sediments at the different study sites varies between 0.2 and > 1.4 m (Table 2.1). The average bulk density ranges from 0.40 to 0.99 g cm<sup>-3</sup> (detailed bulk density data are provided in the Supplementary data), and both the topsoil pH and electrical conductivity increase in the downstream direction, from freshwater to salt marshes (Table 2.2).

**Table 2.2** General characteristics of the soil profiles at the studied sites. Bulk density values are averages for the upper meter of soil, while soil pH and electrical conductivity were measured in the topsoil only.

	Bulk density (g cm <sup>-3</sup> )	Soil pH	Electrical conductivity (dS cm <sup>-1</sup> )
Freshwater low	0.40 ± 0.07	7.47 ± 0.02	0.0271 ± 0.0009
Freshwater high	0.54 ± 0.04	7.35 ± 0.10	0.0262 ± 0.0007
Brackish water low	0.89 ± 0.06 <sup>A</sup>	7.70 ± 0.06	0.0389 ± 0.0048
Brackish water high	0.99 ± 0.06	7.49 ± 0.09	0.0365 ± 0.0023
Saltwater low	0.63 ± 0.07 <sup>B</sup>	7.93 ± 0.02	0.0959 ± 0.0021
Saltwater high	0.96 ± 0.11	7.87 ± 0.03	0.1131 ± 0.0006

Notes: <sup>A</sup>Down to 0.7m depth, <sup>B</sup>Down to 0.2m depth

### 2.3.2 Vegetation biomass production

Based on the measured total annual biomass (Figure S2-1, Table S2-2) and reported values of both above- and below-ground annual turnover rates (Table S2-3), annual biomass production for the different sites was calculated, as shown in Figure 2-4. In this figure, sample locations that do not share a letter have significantly different annual biomass production rates. The average annual above-ground biomass production is the highest for the brackish marshes, followed by the low freshwater marsh and both saltwater marshes.

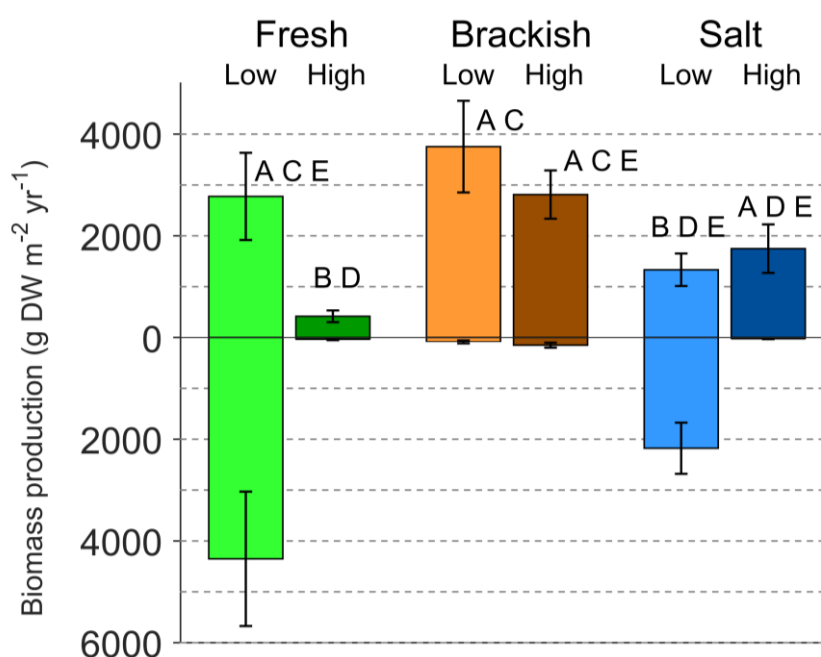


**Figure 2-4** Annual biomass production (g dry weight m<sup>-2</sup> yr<sup>-1</sup>), with upward pointing bars representing above-ground biomass production and downward pointing bars representing below-ground production (data are provided in Table S2-2). Standard deviations for above-ground biomass are calculated based on five replicates, for below-ground biomass on three replicas. Sample locations that do not share a letter have significantly ( $p < 0.05$ ) different annual above-ground biomass production rates

The high freshwater marsh has an above-ground biomass production that deviates from this pattern as a consequence of the fact that only fallen leaves of the willow trees were taken into account at this site, while standing willow vegetation could not be collected, so we underestimate total biomass production in this case. Upper limits for biomass production on this marsh may be deduced from other studies, which typically result in production rates of 500 - 1000 g dry weight  $\text{m}^{-2} \text{y}^{-1}$  (Kopp et al., 2001). Although no clear pattern in the annual production of below-ground biomass along the estuary is observed, large differences between the sites are present (Figure 2-4). Below-ground biomass production on the low freshwater marsh and the low salt marsh are 2 orders of magnitude larger compared to the other tidal marsh sites. At the former locations, most biomass is located below-ground, while at the latter locations the majority of the vegetation biomass is located above ground.

### 2.3.3 Soil organic carbon depth profiles

The depth profiles of SOC show that the depth-averaged concentration decreases from fresh water to salt marshes, although the highest topsoil OC concentration is observed on the brackish marshes (Figure 2-5), data on OC and C:N ratio are provided in the supplementary data). In contrast to the freshwater soils, which show a gradual but limited decrease in OC concentration with depth, the brackish and salt marshes show a sharp decrease in OC concentration in the upper 0.25 m.

### 2.3.4 Soil organic carbon inventories

The highest total SOC stocks are found in the freshwater marshes, followed by the brackish and salt marshes (Table 2.3). For every marsh, SOC stocks are greater for the high marsh compared to the low marsh, as a consequence of both deeper marsh soils and higher SOC

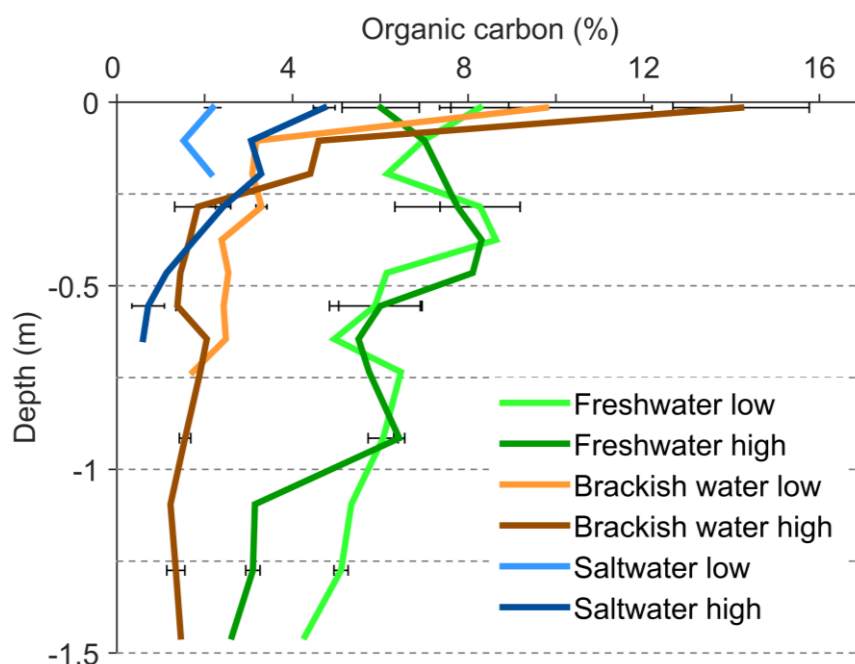


**Figure 2-5** Depth profiles of organic carbon concentration for all study sites. Data points show the average of three replicate soil samples. Error bars for specific depths represent the standard deviation

**Table 2.3** Total organic carbon (OC) stock (kg OC m<sup>-2</sup>) and standard deviations calculated for the full vertical sampling profiles (depths used for calculations are given in brackets) and the upper 0.6m.

	OC stock (kg OC m <sup>-2</sup> )	
	Low marsh	High marsh
<u>For the entire marsh profile</u>		
Freshwater	32.35 ± 0.65 (1.2m)	46.44 ± 0.80 (1.4m)
Brackish water	20.50 ± 0.72 (0.75m)	32.23 ± 0.31 (1.4m)
Saltwater	2.84 ± 0.10 (0.2m)	9.93 ± 0.34 (0.6m)
<u>Down to 0.6m depth</u>		
Freshwater	16.38 ± 0.54	21.66 ± 0.71
Brackish water	18.63 ± 0.71	19.63 ± 0.27
Saltwater	-	9.93 ± 0.34

concentrations. In order to compare the marshes directly to each other the stocks down to the largest common depth have been calculated (Table 2.3). Using this approach, freshwater and brackish marshes have comparable SOC stocks, while both locations on the salt marsh have significantly lower stocks. Depth profiles of cumulative SOC stocks per 0.01 m layer, after interpolation as explained in section 2.2.4, are shown in Figure S2-2.

### 2.3.5 Stable carbon isotopes

The depth profiles of stable OC isotopes ( $\delta^{13}\text{C}$ ) are shown in Figure 2-6, together with the  $\delta^{13}\text{C}$  signal of above- and below-ground vegetation (data on  $\delta^{13}\text{C}$  is provided in the supplementary Information). In general an increase in  $\delta^{13}\text{C}$  values with depth is observed, although deviations from this pattern occur along the profiles. For all sites except the low salt marsh, which is characterized by *Spartina anglica* vegetation (C4 type), the  $\delta^{13}\text{C}$  signal of SOC in the topsoil layer is similar to the  $\delta^{13}\text{C}$  signal of standing vegetation. However, a close inspection shows differences. On the high freshwater marsh the topsoil  $\delta^{13}\text{C}$  signal is higher than the signal for both above- and below-ground vegetation, while on the low freshwater marsh the topsoil  $\delta^{13}\text{C}$  signal is lower than the above- and below-ground vegetation signal. On both the low and high brackish marshes, the topsoil  $\delta^{13}\text{C}$  is very similar to the  $\delta^{13}\text{C}$  signal of roots, while it is about 1‰ lower compared to the  $\delta^{13}\text{C}$  signal of above-ground vegetation. On the high saltmarsh, the topsoil  $\delta^{13}\text{C}$  signal has a value in between the  $\delta^{13}\text{C}$  signals of above- and below-ground vegetation, while on the low salt marsh the topsoil  $\delta^{13}\text{C}$  signal is significantly lower compared to the signal of both above- and below-ground vegetation.

## 2.4 Discussion

### 2.4.1 Observed patterns in SOC storage

While our data do not allow for a full statistical or mechanistic analysis of the mechanisms controlling the long-term storage of SOC in the studied tidal marshes, some important observations can be made. A first observation is that low SOC stocks are not systematically related to low biomass production, as no statistical relationship between total annual biomass production (above and below ground) and SOC stocks is found ( $R^2 = 0.01$ , Figure S2-3). For example, the annual biomass production on the low saltwater marsh (*Spartina anglica*) is

relatively high (Figure 2-4), while this site is characterized by the lowest SOC stocks. In addition, there is no relationship between annual root carbon production and SOC stocks ( $R^2 = 0.004$ , data not shown). This is rather surprising, as it has been proposed that roots contribute significantly to the subsoil OC pool in tidal marshes (Craft, 2007; Saintilan et al., 2013).

A second important observation is the very rapid decrease of SOC with depth at the brackish sites. This decrease is accompanied by a shift in  $\delta^{13}\text{C}$  to less negative values with depth in the topsoil of these marshes, suggesting that on the brackish marshes a significant fraction of OC is rapidly decomposed after burial (Figure 2-6). On the high brackish marsh the decline in SOC and the shift in  $\delta^{13}\text{C}$  show the same tendency down to a depth of 0.3 m, while deeper along the profile, both variables remain approximately constant with depth. This indicates that a significant fraction (approx. 87 %) of deposited OC is decomposed in this top layer. In the low brackish marsh sediments the situation is different. Here the SOC concentration only decreases from the top of the profile down to a depth of 0.15 m, while the  $\delta^{13}\text{C}$  signal increases throughout the profile. At this location *Spartina anglica* (a C4 plant) was possibly present during early marsh development, resulting in a more positive  $\delta^{13}\text{C}$  signal (Boschker et al., 1999; Middelburg et al., 1997). Currently *Elymus athericus*, a C3 plant, is dominating the marsh vegetation. This implies that the shift in  $\delta^{13}\text{C}$  with depth on the low brackish marsh could partly be the result of a shift from a C4 to C3 type vegetation, rather than resulting from the decomposition of SOC alone. This is very likely, as shifts in  $\delta^{13}\text{C}$  as a consequence of kinetic fractionation during decomposition are generally of the order of 1 – 3 ‰ (Choi et al., 2001), while the shift we observe is much larger (ca. 5.7 ‰). However, the decrease in SOC together with the shift in  $\delta^{13}\text{C}$  in the top 0.15 m suggests that also on this marsh significant decomposition of deposited OC (approx. 68%) took place after burial. It should be noted that the  $\delta^{13}\text{C}$  signal of the most recent sediments found on the intertidal areas can vary throughout

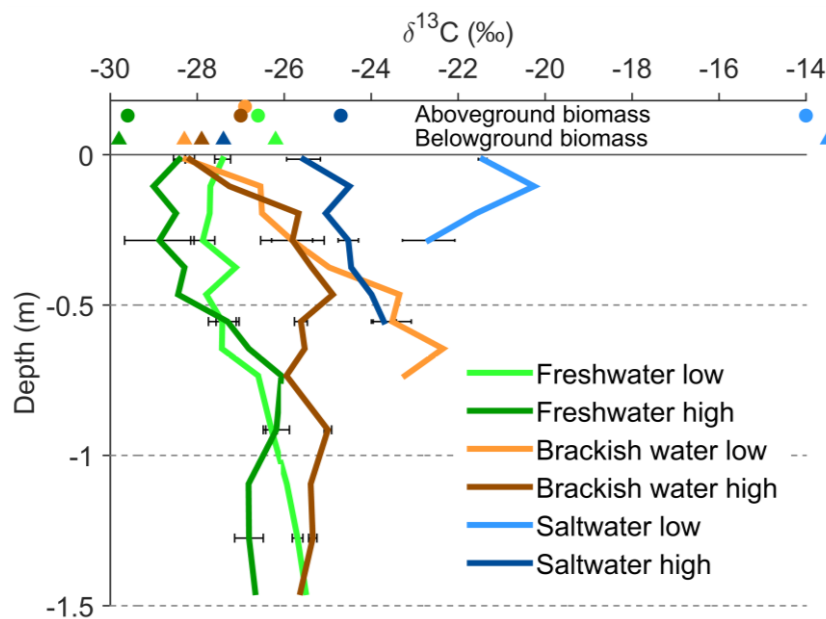


**Figure 2-6** Depth profiles of  $\delta^{13}\text{C}$ , together with the  $\delta^{13}\text{C}$  signal of above-ground (circles) and below-ground (triangles) biomass (values are provided in table S2-2). Error bars represent the standard deviation

the year (Zetsche et al., 2011). However, the  $\delta^{13}\text{C}$  depth profiles we observe are an integration of these annual cycles, limiting the effect of the timing of sample collection on the observed depth profiles of  $\delta^{13}\text{C}$ .

On the high salt marsh a significant decrease of SOC concentration with depth also occurs. This is again accompanied by a shift in  $\delta^{13}\text{C}$  towards more positive values with depth. This location is currently characterized by a mixture of C3 type vegetation. It is uncertain, however, whether the isotopic shift with depth can entirely be attributed to kinetic fractionation caused by OC decay. It is likely that at the beginning of marsh growth *Spartina anglica* was also present at this location, as it is currently present on the low part of this marsh. This would imply that also at this location the shift in  $\delta^{13}\text{C}$  with depth is the result of a combination of decomposition of OC and a shift in vegetation from C4 to C3 type.

Our observations indicate that on both the salt and brackish marshes a significant fraction of OC is lost after burial. Although in the brackish marsh sediments a larger fraction of OC is lost after burial compared to salt marshes, total SOC stocks in the brackish marsh sediments are significantly higher compared to the salt marshes.

On the freshwater marshes the situation is different. In both the low and high freshwater marsh sediments the decline in OC concentration with depth is very limited. In addition, the  $\delta^{13}\text{C}$  signal does not show a significant shift in the top 0.5 m of the soil profile. Below this depth there is a limited shift in  $\delta^{13}\text{C}$  toward more positive values, but the interpretation of this pattern is complicated by the effect of previous land uses on the marsh (Figure 2-3). These observations indicate that at both locations on the freshwater marsh there is limited decomposition of OC after burial.

### **2.4.2 Explanations for the observed patterns in soil organic carbon stocks**

An explanation for the variation in SOC stocks between salt and brackish marshes on the one hand and freshwater marshes on the other hand needs to account for the differences in depth gradients in both SOC and  $\delta^{13}\text{C}$ . Several factors may contribute to these differences and their possible role is discussed below.

#### **2.4.2.1 Salinity**

Although the Scheldt estuary is characterized by a strong salinity gradient (Van Damme et al., 2005), it is unlikely that salinity as such is a direct factor controlling the difference in decomposition of OC that we observed. If salinity directly controlled OC decomposition, this would necessitate a positive relationship between decomposition rate and salinity. However, litterbag experiments with *Elymus athericus* on a tidal marsh in the Scheldt estuary showed that there was an inverse relationship between soil salinity and decomposition (Hemminga et al. 1991b). In addition, Hemminga et al. (1991b) concluded that there is no significant variation in cellulose decomposition in tidal marsh sediments along the brackish and saltwater portion of the Scheldt estuary.

#### 2.4.2.2 Vegetation type

The type of vegetation present on the different marshes is another possible controlling factor, as it has been shown that the residues of different macrophytes have a different resistance against decomposition (Buth and de Wolf, 1985; Hemminga and Buth, 1991; Valery et al., 2004). One of the factors that determines the decomposition rate of plant material is the nitrogen content, whereby plant material with a higher C:N ratio is generally more resistant to decomposition (Hemminga and Buth, 1991; Jones et al., 2016; Webster and Benfield, 1986). The C:N ratio of the vegetation present on the salt marsh (values between 27 and 30) is substantially lower compared to the vegetation present on the brackish and freshwater marshes (values between 33 and 55) (Table S2-2). However, our OC and  $\delta^{13}\text{C}$  profiles suggest that decomposition rates are highest on the brackish marshes and lowest on the freshwater marshes, while the vegetation present at these locations has comparable C:N ratios. Thus, there does not appear to be a direct relationship between the C:N ratio of the biomass and SOC decomposition.

Although our data do not allow us to isolate the effect of vegetation type on SOC stocks along the estuary, some important observations can be made. Firstly, the low and high freshwater marsh have different vegetation types (*P. australis* and *Salix* resp.). However, both soils show a similar SOC profile. In addition, the high freshwater marsh, where annual biomass production is significantly lower, has the largest SOC stock. This indicates that the effect of local biomass production on SOC stock is limited in the freshwater marshes. Secondly, both brackish marshes have the same vegetation type (*E. athericus*), while topsoil OC concentrations and total SOC stocks on the high marsh are larger compared to the low marsh. In addition, the high marsh is characterized by a somewhat lower annual biomass production (although the difference is not statistically significant). Thus, variations in local biomass production do not explain the differences in SOC stock between young and old brackish marshes either. The presence of *Spartina anglica* on the low salt marsh is indeed likely to be responsible for the low SOC stocks. While *Spartina anglica* is characterized by a high net primary productivity, the organic material produced is known to be very labile (Boschker et al., 1999; Bouillon and Boschker, 2006; Middelburg et al., 1997). Taken together, these observations indicate that local biomass production is not likely to be a dominant factor controlling overall variations in SOC stocks along the estuary as variations in OC stocks both along the salinity gradient of the estuary and between old and young marshes at a given salinity level cannot be explained by variations in biomass production. The effect of *Spartina anglica* on the SOC stock of the lower salt marsh shows, however, that in some cases the presence of a certain vegetation type may be a dominant factor.

#### 2.4.2.3 Allochthonous organic carbon inputs along the estuary

The OC that is present in tidal marsh sediments is not only derived from autochthonous biomass. Estuaries are often characterized by relatively high concentrations of suspended sediment to which a significant amount of particulate organic carbon (POC) is associated (Abril et al., 2002). Due to the long residence time of water in the Scheldt estuary (2-3 months, Soetaert and Herman, 1995), organic matter is intensively processed as it moves through the

estuary (Abril et al., 2002; Middelburg and Herman, 2007). In addition, mixing between fluvial and marine particles takes place (Nolting et al., 1999; Regnier and Wollast, 1993). Overall, this leads to significant variations in both the quantity and the quality of the POC that is present in the water and deposited on the marshes. Clearly, this variation may not only affect the magnitude of the OC inputs but also the decomposability of the OC that is deposited.

The freshwater marshes are located near the upstream border of the Scheldt estuary close to the maximum turbidity zone (MTZ), with average suspended sediment concentrations of ca.  $0.15 \text{ g l}^{-1}$  (Temmerman et al., 2004; Van Damme et al., 2001). The suspended sediments in this zone contain 7-10% POC (Abril et al., 2002). The higher values are observed in summer, when phytoplankton growth is important, while the lower values are reported in winter. The POC that is present in winter may be assumed to be processed POC of terrestrial origin (Hellings et al., 1999). In addition, during the past decades a large fraction of OC that has entered the freshwater portion of the estuary originated from untreated wastewater from the city of Brussels (Abril et al., 2002; Billen et al., 2005). It has, however, been shown that this OC is mineralized on a timescale of weeks, possibly even before it enters the estuary (Muylaert et al., 2005; Servais et al., 1987).

Sediment concentrations strongly decline downstream of the MTZ (Abril et al., 2002; Van Damme et al., 2005). At the location of the brackish and salt marshes (ca. 20 km and ca. 50 km from the mouth) sediment concentrations are about  $0.05 \text{ g l}^{-1}$  (Temmerman et al., 2004; Van Damme et al., 2001). Furthermore, the POC content of these sediments decreases systematically in the downstream direction, except during the spring season when local production of OC due to phytoplankton is important in the marine part of the estuary (Muylaert et al., 2005). As a result, average POC concentrations vary between 4 and 6 % in the brackish water zone and between 2 and 5 % in the saltwater zone (Abril et al., 2002). The overall decline in POC content is not only explained by the progressive downstream mineralization of OC but also by the upstream transport of marine sediments that carry less POC.

The variations in both suspended sediment concentration and POC content have important consequences for the relative importance of allochthonous OC input on the marshes. On the freshwater marshes, both the high suspended sediment concentration and high POC loadings lead to a combination of high sedimentation rates ( $10\text{-}20 \text{ mm yr}^{-1}$ , with the highest sedimentation rates on the young marshes (Temmerman et al., 2004)) and high inputs of allochthonous POC. On the saltwater marshes, sedimentation rates are much lower ( $5\text{-}10 \text{ mm yr}^{-1}$  (Temmerman et al., 2004)) and the deposited sediments contain 50 – 70 % less OC than the sediments deposited on the freshwater marsh (Abril et al., 2002). Evidently, these differences may have important effects on OC storage in tidal marsh sediments (Figure 2-7). It can reasonably be assumed that the allochthonous POC that is deposited with the sediments on the freshwater marsh consists of a large fraction of terrestrial, recalcitrant POC. This POC may be expected to have a high burial efficiency (i.e. it will decompose relatively slowly after burial) and will remain in the sediments for a considerable time. The local, autochthonous POC is fresh and will therefore be less recalcitrant. As a consequence, it may be expected to decompose much more rapidly with time and contribute much less to long-

term OC storage. The latter explains why variations in biomass production and vegetation type on the marshes (both now and in the past, Figure 2-3) do not explain variations in SOC storage in different marsh environments. Furthermore, the decomposition rate of both autochthonous and allochthonous POC can be expected to be inversely related to the burial rate as rapid sedimentation will protect OC from decomposition (Hartnett et al., 1998; Wang et al., 2015b). Thus, OC will be better preserved when sedimentation rates are high.

Figure 2-7 illustrates how these factors combine. One may indeed expect to find a much less steep decline of the OC content with depth on the freshwater marsh (Figure 2-7a) due to (1) the dominance of allochthonous, recalcitrant OC and (2) the rapid burial of OC. Furthermore, a relatively large fraction of labile autochthonous OC may be preserved, as it is advected rapidly to deep sediment layers. On the salt and brackish marshes a low sedimentation rate combines with low OC contents of the deposited sediments (Figure 2-7b). As a consequence, autochthonous OC is a dominant input, but this OC decomposes rapidly with depth. This results in a significant decline of OC content with depth, combined with a significant increase in  $\delta^{13}\text{C}$  due to kinetic isotopic fractionation. In a recent study, Hansen et al. (2016) also attributed decreasing SOC stocks with increasing salinity in the Elbe estuary (Germany) to a decreasing OC content of suspended sediments and decreasing macrophyte biomass with increasing salinity.

Thus, both sedimentation rate as well as the rate of allochthonous OC input to the marsh system appear to place important controls on OC preservation in marsh sediments. While other factors such as local biomass production and salinity gradients may also be locally important, they do not appear to be key controls in the Scheldt estuary as most autochthonous POC appears to decompose rapidly, independent of the specific environmental conditions. This finding is similar to the observations of Omengo et al. (2016),

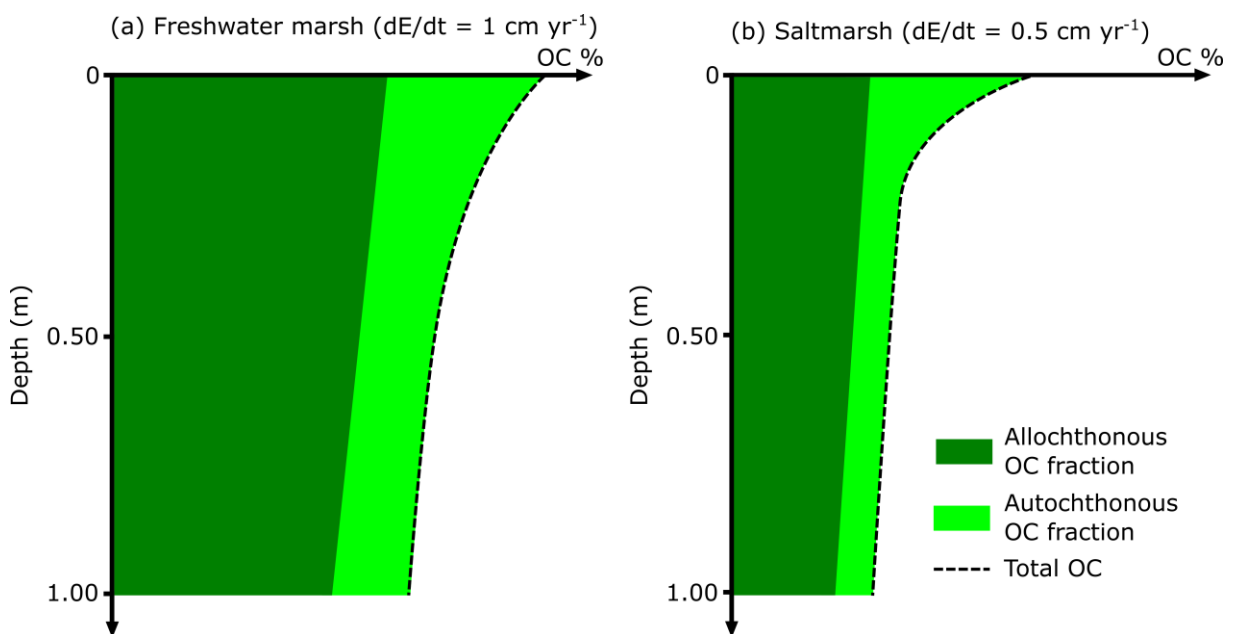


**Figure 2-7** Conceptual diagram of the effect of both sediment deposition rate ( $dE/dt$ ,  $E$  = elevation) and the relative inputs of recalcitrant allochthonous organic carbon and labile autochthonous organic carbon on the fate of buried OC in a tidal freshwater marsh (a) and salt marsh (b)

who found that the OC preserved at depth in floodplain sediments of the Tana River in Kenya consisted dominantly of processed OC that was deposited by the river, while locally produced OC contributed little to long-term OC preservation.

### 2.4.3 Effect of sampling procedure on reported estuarine OC stocks

The results of this study show that both SOC concentrations and stocks of tidal marshes vary significantly along a temperate estuary, with freshwater marshes having the highest stocks, followed by brackish and salt marshes (Figure 2-5 and Table 2.3). This tendency is in agreement with observations in other studies (Table 2.4). However, the differences reported in previous studies are almost always much smaller than the differences we find. As the estuaries reported in Table 2.4 cover a large geographical range, differences in environmental conditions will have an influence on the reported SOC stocks. For example, the estuaries

**Table 2.4** Reported SOC stocks (kg OC m<sup>-2</sup>) of tidal marsh soils along estuarine salinity gradients

Estuary	Sampling depth (m)	Freshwater	Oligohaline	Mesohaline	Polyhaline	Reference
Delaware (U.S.A.)	0.16	3.136	2.41	3.528	-	Weston et al. (2014)
Sapelo Doboy, Altamaha (Georgia, U.S.A.)	0.30	8.379	10.692	4.626	5.932	Craft (2007)
Dovey (Wales)	0.10	-	2.8	1.8	2.4 (low), 1.4 (high)	Dausse et al. (2012)
Barataria (Louisiana, U.S.A.)	0.38	10.3	24.1	12.9	12.8	Hatton et al. (1983)
Satilla Altamaha Ogeechee (Georgia, U.S.A.)	0.30	8.096 ± 1.245	-	6.816 ± 0.997	6.069 ± 0.482	Wieski et al. (2010)
Barataria basin (Louisiana, U.S.A.)	0.50	5.37	-	4.38	2.90	Williams and Rosenheim (2015)
San Francisco Bay (California, U.S.A.)	0.20	-	-	7.82	5.33	Callaway et al. (2012) <sup>A</sup>
Louisiana (USA)	1.5	65.76	-	-	56.65	Wang et al. (2011)
Elbe (Germany)	1.0	-	27.05	16.04	11.31	Hansen et al. (2016) <sup>B</sup>
Scheldt (Belgium, The Netherlands)	0.6	-	21.66 ± 0.71	19.63 ± 0.27	9.93 ± 0.34	This study <sup>A</sup>

Notes: <sup>A</sup>Data for high marshes only, <sup>B</sup>Average for all unmanaged sites

reported in Table 2.4 that are located along the southern coast of the U.S.A. experience significantly higher average temperatures compared to the Scheldt estuary. In addition, the vegetation species present on the tidal marshes, as well as differences in regional geology and estuarine morphology, will play a role. However, as the studies listed in Table 2.4 report SOC stocks in tidal marsh sediments along a salinity gradient, similarities in the factors controlling these stocks are also present. For example, the freshwater marshes will receive considerably more OC from terrestrial sources, while the influence of OC inputs from marine sources will be the largest in the salt marshes. Moreover, macrophyte production is generally considerably higher at freshwater marshes compared to salt marshes (e.g. Dausse et al. (2012) and Hansen et al. (2016)).

In addition to these factors, differences in sampling procedures can also explain some discrepancies. In most studies, marshes were sampled to a limited depth (Table 2.4). Generally, the differences in SOC content between different marshes reported in Table 2.4 are smallest for the top layers and increase with depth. As a consequence, the difference in SOC inventory will increase if a larger sampling depth is considered. Evidently, considering a larger sampling depth will also lead to higher estimates of SOC stocks. This is one of the factors explaining why our stock estimates are generally much higher than those reported in the other studies in Table 2.4, especially for the freshwater marshes, and why we find larger differences in total SOC stocks between different marshes.

It is important to know whether carbon stocks should be compared by considering stocks down to a certain depth or whether the total stock present in the marsh sediments should be taken into account. While it is simpler and more transparent to consider a certain depth, this approach does not account for the differences in dynamics between marshes. As Figure 2-2 shows, marsh accumulation rates are significantly higher for the freshwater marshes. This automatically implies that, when different marshes are sampled to a common depth, the time frame that is accounted for will be shorter for those marshes that have the highest accumulation rates (Elschot et al., 2015). We suggest that the establishment of a correct time frame, from which sedimentation rates and their variations over time can be deduced, is indispensable for a correct interpretation of differences in SOC stocks (as well as C sequestration rates) between marshes.

#### **2.4.4 Implications of sea level rise for estuarine soil organic carbon stocks**

As global sea level is predicted to continue to rise during the next centuries, progressive intrusion of saltwater further into estuaries may be expected (Robins et al., 2016; Ross et al., 2015). As it is shown that freshwater and brackish tidal marshes store more SOC compared to salt marshes (Table 2.3), one may expect that this will lead to a decrease in OC sequestration at locations where brackish marshes are replaced by salt marshes. Furthermore, the MTZ is predicted to shift more inland (Robins et al., 2016). Because the Scheldt estuary is completely embanked and the tidal wave is stopped by sluices near the city of Ghent, the total area of freshwater marshes is likely to decline after sea level rise (Barendregt and Swarth, 2013). As we have shown that SOC sequestration rates are the largest in the freshwater portion of the estuary, the amount of OC sequestration in the estuary is therefore likely to decline with sea

level rise. Moreover, as a consequence of the upstream migration of the MTZ, terrestrial organic matter is less able to travel downstream in the estuary. Therefore, tidal marshes which are now located at the downstream end of the MTZ will receive less stable terrestrial OC in the future. On the other hand, overall sedimentation rates are expected to increase with a rising sea level, which will automatically lead to an increase in the rate of OC deposition as well as of OC burial rates, resulting in an increase of the OC sequestration rate per unit surface area.

Saltwater intrusion can also influence the decomposition of previously sequestered OC, with some studies concluding that saltwater intrusion will enhance decomposition of organic matter (Craft, 2007; Morrissey et al., 2014; Weston et al., 2011, 2006), while others find that decomposition rates will decrease (Hemminga et al., 1991a; Weston et al., 2011). From these studies and from the analysis by Chambers *et al.* (2011), it is clear that this effect is highly dependent on local factors, such as the concentration of elements in the sea water that intrudes the estuary. Therefore, no reliable estimation of the impact of saltwater intrusion on OC mineralization in the Scheldt estuary can be made.

The above illustrates that our current understanding of the future evolution of the Scheldt estuary is still insufficient to make a quantitative assessment of how SOC stocks in the tidal marsh environment may change in the future.

### **2.5 Conclusion**

As reported data on estuarine gradients of SOC are very scarce and, more importantly, often based on shallow soil sampling, additional research is needed to better constrain estimates of global estuarine OC stocks. This study shows that the quantification of SOC stocks in tidal marsh sediments critically depends on the sampling depth. Gradients in SOC concentrations with depth strongly vary between marsh types, so a full inventory can only be made if sampling is carried out over the entire depth of the marsh sediments. Even if such data are available, interpretation has to be done with care, as sedimentation rates may vary considerably within a single estuary, making it complex to convert inventories to sedimentation or preservation rates. In the Scheldt estuary, total SOC stocks are largest in a freshwater and brackish tidal marsh and significantly lower in a saltwater marsh. These variations are to some extent controlled by variations in autochthonous biomass production, but our data strongly suggest that the key control on long-term OC preservation is the relative contribution of terrestrial, allochthonous OC to the total OC input, while OC burial rate may also be important. The impact of future sea level rise on OC stocks in tidal marsh sediments will be determined by an interplay of different factors, including the evolution of the spatial extent of marshes in different salinity zones and sediment and OC deposition rates. Our study allowed us to identify the factors that are important controls on OC storage but further research may be needed to resolve this issue.

#### **Data availability**

The following data are provided in the supplementary information: depth profiles of (i) bulk density, (ii) OC,  $\delta^{13}\text{C}$  and CN values and (iii) grain size in Excel format and (iv) data on

vegetation characteristics and sample locations in pdf format (available at <http://dx.doi.org/10.5194/bg-13-6611-2016-supplement>).

### **Acknowledgements**

We would like to thank Lore Fondu and Jianlin Zhao for their much-appreciated help during fieldwork and lab analysis. We are also grateful to Natuurpunt, Staatsbosbeheer Zeeland and Stichting het Zeeuwse Landschap for providing us with the opportunity to sample the tidal marshes.



## Chapter 3 Long-term organic carbon sequestration in tidal marsh sediments is dominated by old-aged allochthonous inputs in a macro-tidal estuary<sup>1</sup>

---

**Abstract.** Tidal marshes are vegetated coastal ecosystems that are often considered as hotspots of atmospheric CO<sub>2</sub> sequestration. Although large amounts of organic carbon (OC) are indeed being deposited on tidal marshes, there is no direct link between high OC deposition rates and high OC sequestration rates due to two main reasons. First, the deposited OC may become rapidly decomposed once it is buried and, second, a significant part of preserved OC may be allochthonous OC that has been sequestered elsewhere. In this study we aimed to identify the mechanisms controlling long-term OC sequestration in tidal marsh sediments along an estuarine salinity gradient (Scheldt estuary, Belgium and The Netherlands). Analyses of deposited sediments have shown that OC deposited during tidal inundations is up to millennia old. This allochthonous OC is the main component of OC that is effectively preserved in these sediments, as indicated by the low radiocarbon content of buried OC. Furthermore, OC fractionation showed that autochthonous OC is decomposed on a decadal timescale in saltmarsh sediments, while in freshwater marsh sediments locally-produced biomass is more efficiently preserved after burial. Our results show that long-term OC sequestration is decoupled from local biomass production in the studied tidal marsh sediments. This implies that OC sequestration rates are greatly overestimated when they are calculated based on short-term OC deposition rates, which are controlled by labile autochthonous OC inputs. Moreover, as allochthonous OC is not sequestered in-situ, it does not contribute to active atmospheric CO<sub>2</sub> sequestration in these ecosystems. A correct assessment of the contribution of allochthonous OC to the total sedimentary OC stock in tidal marsh sediments as well as a correct understanding of the long-term fate of locally-produced OC are both necessary to avoid overestimations of the rate of in-situ atmospheric CO<sub>2</sub> sequestration in tidal marsh sediments.

---

<sup>1</sup>This chapter is published as: Van de Broek, M., Vandendriessche, C., Poppelmonde, D., Merckx, R., Temmerman, S. and Govers, G.: Long-term organic carbon sequestration in tidal marsh sediments is dominated by old-aged allochthonous inputs in a macro-tidal estuary, *Global Change Biology*, doi:10.1111/gcb.14089, 2018. Additional figures and tables can be found in the online version of this paper, on <https://onlinelibrary.wiley.com/doi/abs/10.1111/gcb.14089>

### 3.1 Introduction

Tidal marshes are vegetated coastal ecosystems that can efficiently adapt to rising sea level by vertical accretion of organic and mineral material and burial of locally produced biomass (Kirwan et al., 2016; Kirwan and Mudd, 2012; Neubauer, 2008). Over the past decades, organic carbon (OC) dynamics in tidal marsh ecosystems have been studied intensively as these coastal zones have been recognized as potential hotspots for atmospheric CO<sub>2</sub> sequestration, often termed 'blue carbon' (Duarte et al., 2013; Mcleod et al., 2011; Nelleman et al., 2009). As a consequence of their location at the interface between terrestrial, riverine, estuarine and marine ecosystems, tidal marshes do indeed receive considerable OC inputs from different sources. These inputs can be subdivided into (i) OC that is locally produced by macrophytes (autochthonous OC) and (ii) OC that is produced elsewhere, e.g. in terrestrial or marine ecosystems, and subsequently supplied by tidal inundation and deposition at the marsh surface (allochthonous OC).

The contribution of autochthonous and allochthonous sources to the total OC stock in tidal marsh sediments can differ greatly between marshes at different locations. In organogenic tidal marshes, where vertical accretion is dominated by the accumulation of organic material, OC is mostly derived from local biomass, while minerogenic marshes, dominated by mineral sediment accretion, receive a considerable input of sediment-associated OC (Allen, 1990; Bouillon and Boschker, 2006; Middelburg et al., 1997). However, the relative contribution of autochthonous and allochthonous sources varies strongly among minerogenic marsh sites whereby in some cases autochthonous sources dominate (Chen et al., 2016; Saintilan et al., 2013; Tanner et al., 2010), while the origin of OC is mainly allochthonous in other cases (Boschker et al., 1999; Bouillon and Boschker, 2006; Middelburg et al., 1997).

The rates and mechanisms of OC sequestration do not only vary among saltmarshes, but also along estuarine salinity gradients where marshes vary from salt over brackish to freshwater tidal marshes. Although soil organic carbon (SOC) stocks are generally higher in freshwater tidal marshes as compared to saltmarshes (Craft, 2007; Loomis and Craft, 2010; Van de Broek et al., 2016), knowledge on OC sequestration mechanisms in brackish and freshwater tidal marshes is currently limited. Higher SOC stocks in freshwater tidal marsh sediments, compared to saltmarshes, have been attributed to multiple factors, such as higher rates of primary production of macrophytes (Hansen et al., 2016), higher OC concentrations and/or higher sedimentation rates associated with deposited terrestrial sediments (Hansen et al., 2016; Hayes et al., 2017; Van de Broek et al., 2016), lower extracellular enzyme activity and microbial activity (Morrissey et al., 2014) and lower overall decomposition rates of organic matter (Craft, 2007; Loomis and Craft, 2010). Systematic studies of the controls on SOC stocks in tidal marsh sediments along the full salinity gradient of estuaries, including differences in characteristics of OC inputs and preservation mechanisms of OC upon burial, are scarce (Hansen et al., 2016). This lack of information limits our understanding of the mechanisms controlling SOC storage in these ecosystems and hampers constructing reliable projections of the potential of these ecosystems to sequester CO<sub>2</sub> under future climatic and environmental changes.

When considering the potential of tidal marsh sediments to act as a carbon sink on a decadal to centennial timescale, it is important to make a distinction between the terms 'OC accumulation or deposition' and 'OC sequestration'. Organic carbon accumulation or deposition refers to the magnitude of OC inputs to the system, while OC sequestration refers to the long-term removal of carbon from the atmosphere. These terms are, however, often confused, which can lead to misinterpretations of reported data on both variables. For example, reported rates of globally-averaged annual OC accumulation in saltmarsh sediments are 210 - 250 g C m<sup>-2</sup> yr<sup>-1</sup> (Chmura et al., 2003; Duarte et al., 2013; Ouyang and Lee, 2014), which considerably exceed rates at which OC is sequestered in most terrestrial ecosystems per unit area (Mcleod et al., 2011). These OC accumulation rates are calculated by combining sediment deposition rates with topsoil OC densities, thereby neglecting longer-term (decadal – centennial) OC losses through mineralization after burial of organic matter. In these studies, the OC accumulation rates are often equated to the capacity of the tidal marshes for long-term removal of carbon from the atmosphere (the OC sequestration rate). This potentially leads to a substantial overestimation of the long-term OC sink of tidal marsh sediments as (i) substantial losses of OC from the marsh sediments may occur at decadal or centennial timescales and (ii) a significant fraction of the OC that is buried in the marsh sediments may be allochthonous OC that is recycled from other long-term stores and therefore does not contribute to in-situ OC sequestration.

The aim of our study is to assess the controls on OC sequestration in tidal marsh sediments along a temperate, macro-tidal estuary (Scheldt estuary, Belgium and the Netherlands) in order to (i) understand how OC inputs to tidal marshes vary along the full salinity gradient of the estuary and (ii) which factors control OC accumulation as well as long-term sequestration. We performed a systematic analysis of (i) the different inputs of OC to these sediments, both from locally produced biomass and deposited sediments, and (ii) the importance of different physical stabilization mechanisms of OC along a gradient from freshwater- to saltmarsh sediments. Moreover, using the characteristics (OC concentration,  $\delta^{13}\text{C}$  and radiocarbon content) of OC from different input sources and the OC preserved in sediments we determined the extent to which OC from different sources contributes to long-term preservation of OC in these sediments and how this varies along the temperate Scheldt estuary.

## **3.2 Materials and Methods**

### **3.2.1 Study site**

The estuary of the Scheldt river is located in northern Belgium and the southwest Netherlands, where it flows into the North Sea (Figure 3-1). It has a semi-diurnal meso- to macro-tidal regime with a tidal range between 3.8 m at the mouth and 5.2 m upstream of the city of Antwerp (Meire et al., 2005). Tidal marshes are present along the full salinity gradient of the estuary and can be divided into saltmarshes (salinity > 18), brackish marshes (salinity 5 – 18) and oligohaline/freshwater tidal marshes (salinity 0 – 5), hereafter called freshwater marshes (Figure 3-1).

For this study, 18 locations on a total of 10 tidal marshes were sampled for the construction of depth profiles of OC characteristics (Figure 3-1, Table 3.1). Where possible, both a high-lying and a low-lying area of the tidal marshes were sampled. The high marshes are located at an elevation of about 0.1 – 0.3 m above local mean high water level (MHWL) and are accreting at a rate in equilibrium with local sea level rise (see Temmerman *et al.* (2003, 2004) for detailed studies of the sediment accretion rates at the sampled tidal marshes). The low marshes were located well below local MHWL during the past decades, and have consequently experienced a higher inundation frequency and higher sediment accretion rates compared to the high portions of the same marsh (Temmerman *et al.*, 2004, 2003). As sediment deposition rates at the high portion of the studied tidal marshes are in the order of magnitude of 0.004 – 0.017 m year<sup>-1</sup> (Temmerman *et al.*, 2004) and the formation of the low marshes generally started less than a century ago, the time since deposition of the upper meter of the studied sediments is generally less than 100 years (Temmerman *et al.*, 2004, 2003). The collected data was further complemented with similar data from 3 tidal marshes in the Scheldt estuary from which data on OC dynamics is presented in Van de Broek *et al.* (2016). General information about the tidal marshes used in this study is provided in Table 3.1 and Table S3-1. The numbers in Figure 3-1 are used to refer to the tidal marshes throughout this paper, in combination with the salinity (s) at which the marshes are located. The salinities were obtained from published measurements and interpolation between locations for which measurements were available (Middelburg *et al.*, 1996; Middelburg and Herman, 2007). The description of sample collection and processing applies to all samples

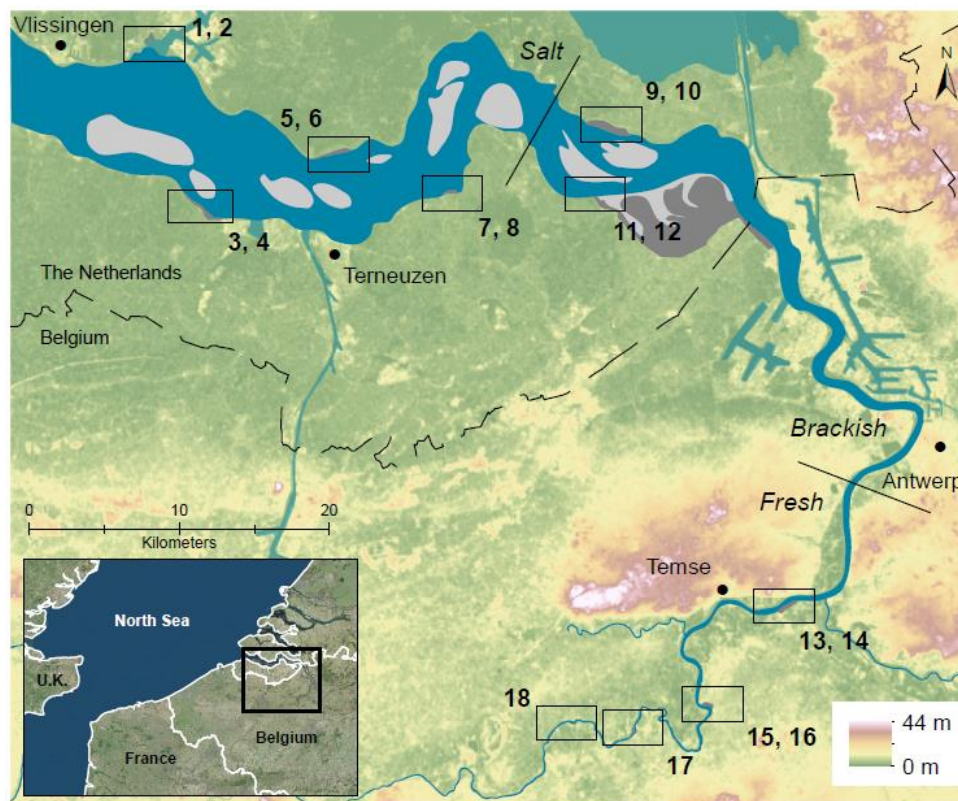


**Figure 3-1** Map of the Scheldt estuary. Black rectangles indicate the locations of the sampled tidal marshes, the numbers refer to the sampling locations as listed in Table 3.1

collected for this study (Table 3.1). The SOC depth profiles used from Van de Broek *et al.* (2016) were obtained and processed using identical methods, but one year prior to the samples collected for the present study.

### 3.2.2 Biomass

The total amount of aboveground biomass was collected at every sampling location for a surface area of 0.25 m<sup>2</sup> in five replicates. This was done towards the end of August and the beginning of September 2016, when biomass is at its maximum on tidal marshes in western Europe (De Leeuw *et al.*, 1990; Groenendijk, 1984). Biomass of *Salix* trees could not be sampled. At locations where *Salix* was present, the mass of *Salix* litter measured at the high marsh at salinity 1.5 (215 g dry weight (DW) m<sup>-2</sup>, Van de Broek *et al.* (2016)) was added to the measured biomass from the local vegetation species. Depth profiles of the total root biomass were measured by washing the soil samples collected for bulk density measurements, after determination of bulk density, over a 0.7 mm sieve using deionized water and collecting all roots (see next section for depth intervals). Aboveground and belowground biomass was

**Table 3.1** General characteristics of the sampled tidal marshes and indication of the locations where different analyses are performed (s = summer, w = winter).

Name	Number	Average salinity	Distance from mouth (km)	OC fractionation	Sediment traps	<sup>14</sup> C measurements
<b>Saltmarshes</b>						
Sloehaven low	1	30	6			
Sloehaven high	2	30	6	✓		
Paulina low*	3	27	15			
Paulina high*	4	27	15	✓	✓ (s+w)	✓
Zuidgors low	5	24	24			
Zuidgors high	6	24	24	✓		
Hellegat low	7	22	28			
Hellegat high	8	22	28		✓ (w)	
<b>Brackish marshes</b>						
Waarde low*	9	17	44			✓
Waarde high*	10	17	44	✓	✓ (s+w)	
Kruispolder low	11	15	46			
Kruispolder high	12	15	46			
<b>Freshwater tidal marshes</b>						
Notelaar low*	13	1.5	97			✓
Notelaar high*	14	1.5	97	✓	✓ (s+w)	
Mariekerke low	15	0.5	110			
Mariekerke high	16	0.5	110	✓		
Grembergen high	17	0.4	120	✓		
Appels low	18	0.3	127		✓ (w)	

\* Data and methods for these tidal marshes are presented in Van de Broek *et al.* (2016).

dried at 60 °C before weighing. Weights of aboveground and belowground biomass are reported for a surface area of 1 m<sup>2</sup>.

### 3.2.3 Soil samples

Undisturbed soil profiles and soil samples for bulk density analyses were collected between July and September 2016 in three replicates at each sampling location using a gouge auger (0.06 m diameter). The undisturbed soil cores were divided into subsamples with 0.03 m depth intervals in the field and transported to the lab in closed ziploc bags. Before analysis, the soil samples were dried at a maximum temperature of 50 °C for 48 hours, crushed to a grainsize < 2 mm and macroscopic vegetation residues were removed manually using tweezers. Samples for bulk density analyses were collected separately by cutting exactly 0.05 m of sediment out of the gouge auger, at depth increments of 0.1 m down to a depth of 0.5 m (0 – 0.05 m; 0.10 – 0.15m etc.) and deeper down the profile at depth increments of 0.2 m (0.50 – 0.55 m; 0.70 – 0.75 m etc.).

Samples for soil bulk density were dried at 105 °C for 24 hours before weighing and calculating the soil bulk density, using the inside volume of the gouge auger (17.02 cm<sup>2</sup> cross section). Sediment grain size was analyzed on the samples collected for general soil analyses using a laser diffraction particle size analyzer (LTSM 13 320, Beckman Coulter) and classified into clay (< 2 µm), silt (2 – 63 µm) and sand (> 63 µm), after organic matter was removed using hydrogen peroxide (35 %) and aggregates were destroyed using ultrasonic dispersion.

Before analysis of OC characteristics, the soil samples of one of the replicate soil cores at every sampled location were weighed into pre-combusted silver cups and carbonates were removed in situ using a 10 % HCl solution. Organic carbon concentration and stable carbon isotopes ( $\delta^{13}\text{C}$ ) measurements were performed using an Elemental Analyser – isotope ratio mass spectrometer (FlashEA 1112 HT, Thermo Scientific – DELTA V Advantage). The OC concentration of soil samples from the second and third replicate soil cores were determined using mid-infrared (m-IR) spectroscopy, using a calibration dataset which was created by relating the measured OC concentrations of samples from the first replicate soil core to the measured m-IR spectra of these soil samples. The spectra were obtained over a spectral range of 400 to 4000 cm<sup>-1</sup> at a resolution of 4 cm<sup>-1</sup>, using a PerkinElmer® Fourier FT-IR spectrometer which was coupled to a PIKE® XY autosampler. Before the OC concentration was estimated using partial least squares regression (PLSR) with 4 latent variables, the soil spectra were pre-processed using the standard normal variate procedure (SNV, see e.g. Igne et al., 2010; Viscarra Rossel, McBratney, & Minasny, 2010). Total SOC stocks were calculated down to a depth of 0.6 m for each site by combining depth profiles of OC concentration and soil bulk density. This depth was chosen as tidal marsh sediments were present down to this depth at every sampling location, with the exception of the low marshes at salinity 27 and 30.

Soil samples for radiocarbon measurements were prepared the same way as for OC analysis and combusted at 900 °C for 1 hour, after which the produced CO<sub>2</sub> was cryogenically trapped on a vacuum line. Graphitization of CO<sub>2</sub> and <sup>14</sup>C measurements were performed at the Royal Institute for Cultural Heritage in Brussels (Belgium) using a MICADAS (mini carbon dating system). The concentration of <sup>14</sup>C was calculated using the measured <sup>14</sup>C/<sup>12</sup>C ratio relative to

95 % of the oxalic acid standard and corrected for isotopic fractionation using the  $^{13}\text{C}/^{12}\text{C}$  ratio (Stuiver and Polach, 1977). Results are expressed as the fraction modern  $^{14}\text{C}$  ( $F^{14}\text{C}$ ), with values  $> 1 F^{14}\text{C}$  indicating the presence of (modern) bomb  $^{14}\text{C}$ , while values  $< 1 F^{14}\text{C}$  indicate that the OC has been formed from atmospheric  $\text{CO}_2$  before 1950 (IAEA, 2001). The tidal marsh sediments for which radiocarbon analysis was performed are marshes no. 4 ( $s = 27$ ), 9 ( $s = 17$ ) and 13 ( $s = 1.5$ ), which are described in detail in Van de Broek et al. (2016), in addition to both summer and winter deposits at these marshes.

### 3.2.4 Collection of deposited sediments

In order to determine the characteristics of OC associated with allochthonous inputs, sediments deposited at the surface of tidal marshes along the estuary were collected using sediment traps. These sediment traps consisted of a plastic dish which was fixed at the marsh surface, in which settled suspended sediment was trapped during inundation events. The dishes were covered with a lid which floated on top of the inundation water, allowing sediments to be deposited in the dish, and dropped after the flooding water has receded in order to protect deposited sediments against contamination (Figure S3-2). As characteristics of OC in the Scheldt estuary are different between summer and winter as a consequence of e.g. phytoplankton growth in summer months (Muylaert et al., 2000), sediment traps were installed at three tidal marsh locations in summer 2016 (3 replicates per location), and at 5 locations in winter 2017 (5 replicates per location), as indicated in Table 3.1, Table S3-2 and Figure S3-1. The sediment traps were installed at the high portion of marshes, thus only collecting sediments during spring-tide events. After each spring tide event (4 in summer 2016, 3 in winter 2017), the sediments and water present in the dishes were collected from the traps and the traps were thoroughly cleaned using demineralized water.

In the lab, the collected sediments and water were poured through a 0.7 mm sieve, in order to remove vegetation residues that were present in the dishes. Next, the sediments were rinsed multiple times using demineralized water, in order to remove salt from the solution, and dried at 50 °C. Subsequently, OC concentration and  $\delta^{13}\text{C}$  values were measured for all sediment samples according to the procedures explained in the previous section. Radiocarbon contents were determined for one summer and one winter deposit for the tidal marshes at which sediment traps were present during summer 2016. These are the same marshes for which radiocarbon contents were determined for OC present in subsoil sediments.

### 3.2.5 Physical fractionation of organic carbon

Soil samples for physical OC fractionation were collected at three freshwater tidal marshes, one brackish marsh and three saltmarshes (Table 3.1 and Figure S3-1). At every location, both topsoil (0 – 0.05 m) and subsoil sediments were collected using a gouge auger (0.06 m diameter), in order to analyse SOC fractions of freshly deposited OC ( $< 5$  years old, considering a mean sediment accretion rate of ca.  $0.01 \text{ m yr}^{-1}$  (Temmerman et al., 2004)) on the one hand and OC that has been buried for several decades on the other hand (Figure S3-3). Tidal marsh soils typically exhibit a sharp boundary from silt-size (tidal marsh sediments) to sand-size

(former sandflat) sediments with depth. The subsoil samples for OC fractionation were collected as close as possible to the lower boundary of the silt-size sediments. However, if the depth of this boundary was located at  $> 1$  m depth, subsoil sediments were collected between 0.8 – 1 m depth (Figure S3-3). In total, 27 soil samples were fractionated. When necessary, e.g. in the case of very low bulk density of topsoil sediments, soil material from different soil cores collected next to each other was mixed to obtain enough sediment to perform the fractionation analyses. For three tidal marshes, no. 4 ( $s = 27$ ), 10 ( $s = 17$ ) and 14 ( $s = 1.5$ ), samples from three different locations a couple of meters from each other were analysed to calculate standard deviations on the results (see supplementary data). For the other locations, topsoil and subsoil samples were analysed for only one location.

Soil samples for OC fractionation were dried at  $50\text{ }^{\circ}\text{C}$  for 48 hours after sample collection in order to preserve them until fractionation analyses took place. A total of three fractionation steps were performed (Figure 3-2). Before the first fractionation step the soil samples were re-wetted by putting them in a glass beaker which was subsequently filled with demineralized water, to allow slaking of aggregates. In the first fractionation step the soil samples were separated in three size classes by wet sieving: (i) silt and clay ( $sc$ ,  $< 53\text{ }\mu\text{m}$ ), (ii) microaggregates, sand and particulate organic matter (POM) ( $m$ ,  $53 - 250\text{ }\mu\text{m}$ ) and (iii) macroaggregates and POM ( $M$ ,  $> 250\text{ }\mu\text{m}$ ). If roots were present, these were removed, oven-dried and weighed. The OC concentration of these root fragments was determined using the elemental analyser as described above. In the second step the  $M$  fraction was dispersed using ultrasonic dispersion. Thirty gram of this fraction was suspended in 150 ml demineralised water and subjected to an output energy of  $22\text{ J ml}^{-1}$  (Zimmermann et al., 2007) and output power of 25 W. The time over which dispersion was performed was calculated at 2 minutes and 18 seconds, based on Poeplau and Don (2014). If less than 30 g of material was available for ultrasonic dispersion, the amount of demineralised water and the output energy were adjusted to achieve the same output energy per unit volume. After ultrasonic dispersion, the material was transferred onto a  $53\text{ }\mu\text{m}$  sieve in order to separate the silt and clay fraction ( $scM$ ,  $< 53\text{ }\mu\text{m}$ ) from the microaggregates sand and POM fraction ( $mM$ ,  $> 53\text{ }\mu\text{m}$ ). In the last fractionation step, a density separation was applied to the microaggregates, sand and POM fractions obtained after both fractionation step one and two ( $m$  and  $mM$ ) combined, according to De Clercq et al. (2015). These fractions were separated in a sodium polytungstate (Sometu, Berlin, Germany) solution with a density of  $1.8\text{ g cm}^{-3}$ . The solution containing the sediments was stirred using a spatula after which the heavy fraction was allowed to settle. This resulted in a light fraction (POM) and a heavy fraction (microaggregates and sand,  $m+S$ ).

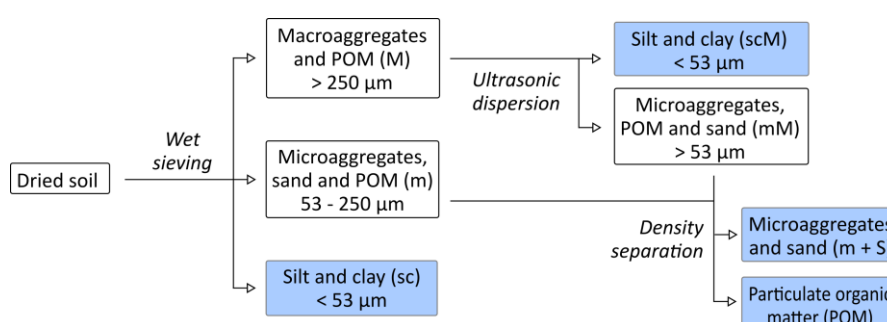


**Figure 3-2** Organic carbon fractionation scheme, with final derived fractions highlighted in blue

The fractionation scheme was constructed so that the final fractions can be linked to the different physical mechanisms through which OC is stabilized in the studied sediments: (i) sc and scM is OC that is associated with minerals, (ii) m + S is OC protected mainly by microaggregates and (iii) POM is interpreted as locally produced autochthonous OC that is not fully decomposed. The weight and OC concentration were determined for the soil fractions obtained after each fractionation step. By combining these data, the contribution of each fraction to the total amount of OC in each soil sample was calculated.

### 3.2.6 Statistical analysis

Differences in average values of OC stocks down to 0.6 m depth, biomass and deposited OC concentration for the different salinity zones were tested for significance using a one-way analysis of variance (ANOVA) or Kruskal-Wallis test (for non-normal distributed data) using Matlab® software. Homogeneity of variances (Levene’s test for normally distributed data, Brown-Forsythe test for non-normal distributed data) and normality (Shapiro-Wilk test) of the data were assessed using Matlab®, at a confidence level of 0.05.

## 3.3 Results

### 3.3.1 Grain size

The grain size distribution of disaggregated topsoil sediments (0 – 0.03 m depth) of the tidal marshes is dominated by the silt-size fraction and shows no systematic variation along the estuary (Figure 3-3). The sampled tidal marshes show a limited variation of grain size with depth, with the exception of a sharp increase in sand size particles and a decrease in silt size particles at the boundary between the silt size marsh sediments and sand size former sandflat sediments (supplementary data). Grain size distributions of the soil samples used for fractionation are shown in Figure S3-4.

### 3.3.2 Biomass

There is no clear gradient in the amount of both aboveground and root biomass present at the tidal marshes along the estuary (Figure 3-4). When disregarding the exceptionally large biomass of reed vegetation at marsh no. 13 ( $s = 1.5$ ), the average amount of total biomass

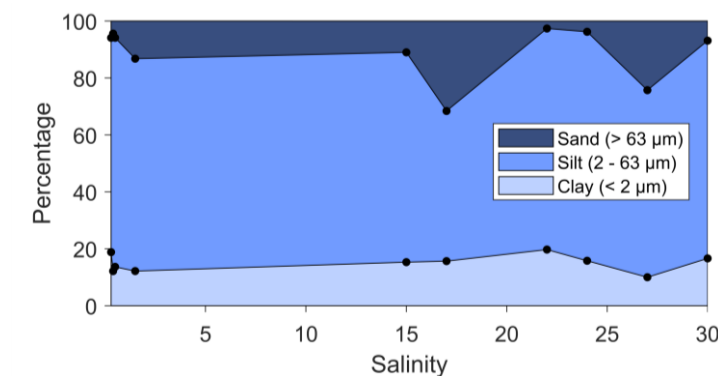


**Figure 3-3** Grain size distribution of disaggregated topsoil sediments of tidal marshes along the Scheldt estuary

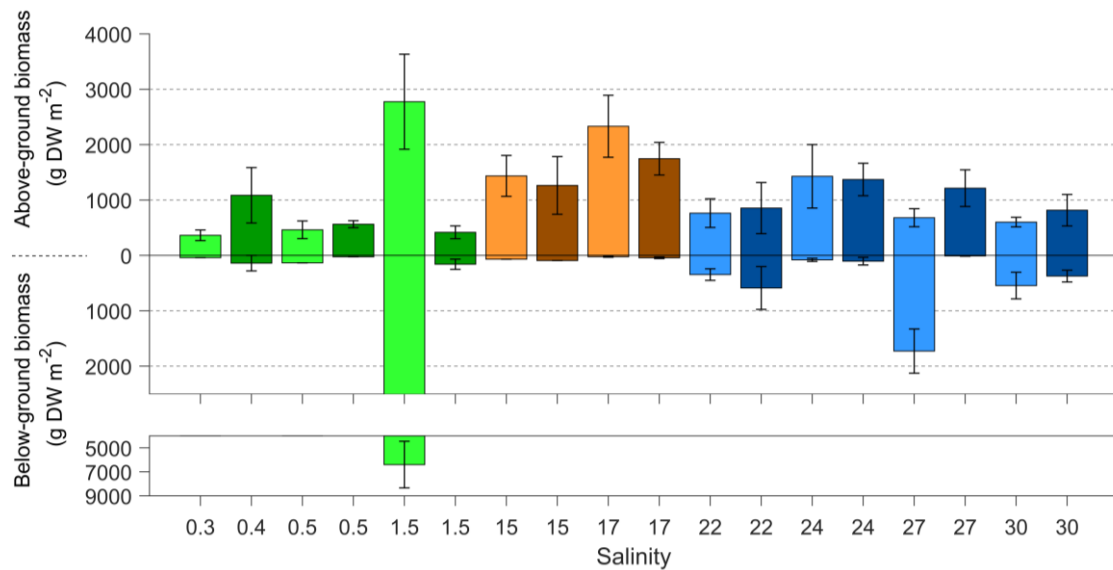


**Figure 3-4** Total biomass (g DW m<sup>-2</sup>) present at the sampled freshwater (green), brackish (brown) and saltmarshes (blue). Upward pointing bars represent above-ground biomass and downward pointing bars represent belowground biomass, while light colors indicate low marshes and dark colors indicate high marshes. Error bars represent the standard deviation around the average (based on 5 replicate measurements).

was only significantly different between freshwater ( $679 \pm 257$  g DW m<sup>-2</sup>) and brackish marshes ( $1751 \pm 449$  g DW m<sup>-2</sup>), while biomass at the saltmarshes ( $1438 \pm 405$  g DW m<sup>-2</sup>) was not significantly different from the freshwater- and brackish marshes. A complete description of statistical tests applied to biomass measurement is provided in the supplementary information. Clearly, local variations in vegetation composition have an important effect on local biomass production. The amount of aboveground biomass exceeds root biomass at all tidal marshes except for marshes no. 13 ( $s = 1.5$ ) and no. 3 ( $s = 27$ ), where respectively *Phragmites australis* and *Spartina anglica* vegetation are present.

### 3.3.3 Organic carbon characteristics of deposited sediments

Organic carbon concentrations of surface deposits at the sampled tidal marshes differ both temporally, between different seasons, and spatially, along the salinity gradient (Figure 3-5a). First, sediments deposited during winter consistently contain less OC compared to sediments deposited at the same location in summer. This difference is about 1 – 2 % for the freshwater and saltmarshes and about 7 % for the brackish marsh. Second, the OC concentration of deposited sediments decreases towards the coast, from 4 – 6 % OC at the freshwater tidal marshes to 2 – 4 % at the saltmarshes, with the exception of summer deposits on the brackish marsh. A description of statistical tests applied to the OC concentration of deposited sediments is provided in the supplementary information.

Also the  $\delta^{13}\text{C}$  values of the OC in the deposited sediments show a clear pattern along the estuary. Deposits on freshwater and brackish marshes have a  $\delta^{13}\text{C}$  value closely related to that of terrestrial vegetation ( $-28$  ‰), while this value consistently increases from the brackish

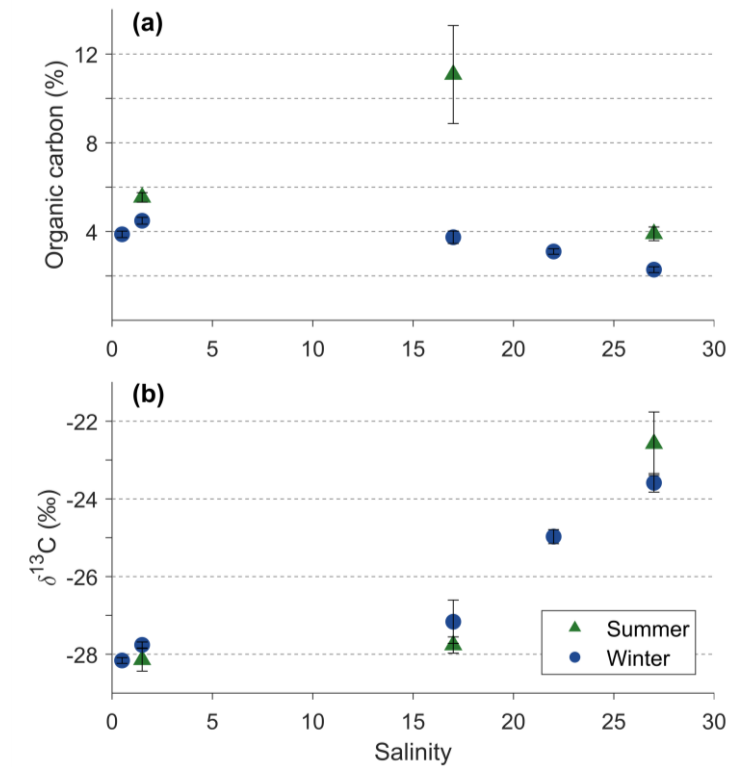


**Figure 3-5** Organic carbon concentration and  $\delta^{13}\text{C}$  values of sediments deposited at the tidal marsh surface during flooding events. Points represent the average of 4 flooding events in summer (2016) and 3 events in winter (2017), error bars represent the standard deviations.

portion of the estuary towards the coast, with  $\delta^{13}\text{C}$  values of about  $-23\text{‰}$ . The variation in  $\delta^{13}\text{C}$  values between summer and winter deposits at the same location is limited to  $1\text{‰}$ .

### 3.3.4 Soil organic carbon stocks

Combining data on detailed depth profiles of both OC concentration and bulk density (provided in the supplementary data), total OC stocks for the sampled tidal marshes were calculated (Figure 3-6). There is a clear pattern of decreasing SOC stocks in tidal marsh sediments with increasing salinity. Average OC stocks in the top 0.6 m are  $19.4 \pm 1.2 \text{ kg OC m}^{-2}$  in freshwater marsh sediments,  $17.3 \pm 0.9 \text{ kg OC m}^{-2}$  in brackish marsh sediments and  $12.63 \pm 0.8 \text{ kg OC m}^{-2}$  in saltmarsh sediments. Organic carbon stocks were not significantly different between freshwater- and brackish marshes, but were significantly different between (i) freshwater- and saltmarshes and (ii) brackish- and saltmarshes (see supplementary information). Furthermore, SOC stocks are generally larger for the high marsh locations as compared to low-lying locations of the same tidal marsh.

### 3.3.5 Radiocarbon content of deposits and SOC

Radiocarbon contents were determined for OC in (i) subsoil sediments in different tidal marshes and (ii) sediments deposited in summer and winter along the estuary (Figure 3-7). These data show that OC ages were substantially older for winter deposits compared to summer deposits for tidal marshes in all salinity zones, as shown by the lower fraction modern

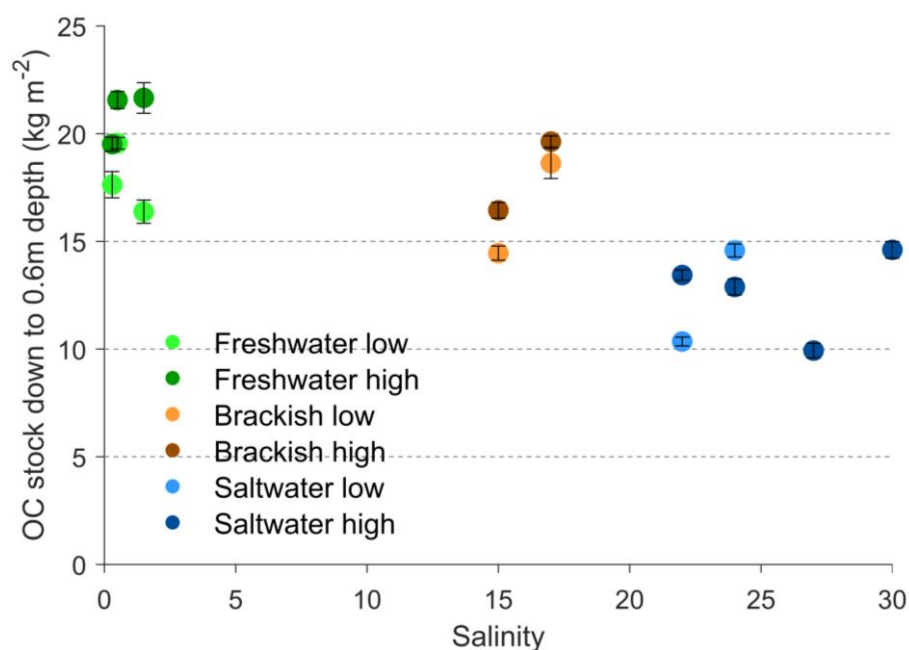


**Figure 3-6** Total organic carbon stock ( $\text{kg OC m}^{-2}$ ) in the top 0.6 m of tidal marsh sediments along the Scheldt estuary. The dots represent the average values calculated based on three replicate soil cores, error bars represent standard deviations.

$^{14}\text{C}$  ( $F^{14}\text{C}$ ) in winter deposits compared to summer deposits. The  $F^{14}\text{C}$  was  $< 1$  for both summer and winter deposits, indicating that the contribution of carbon fixed from atmospheric  $\text{CO}_2$  after 1950 is very low. Furthermore, the  $F^{14}\text{C}$  in tidal marsh sediments decreases substantially with depth. As there is a continuous exchange of carbon atoms between SOC and its environment, SOC cannot be regarded as a closed system. It is therefore not straightforward to convert  $^{14}\text{C}$  data measured for SOC to calendar years (IAEA, 2001). However, for comparison, according to the IntCal13 calibration curve (Reimer et al., 2013),  $F^{14}\text{C}$  values of 0.51 and 0.91, which are the lowest and highest values we obtained for OC in subsoil sediments, correspond to calibrated ages of  $6230 \pm 57$  and  $694 \pm 31$  years BP respectively, indicating that a substantial portion of the OC that is preserved at the studied tidal marshes has been fixed from atmospheric  $\text{CO}_2$  centuries up to millennia ago. Importantly, this is significantly older than the time since sediment deposition, which is less than a century for the sampled tidal marshes (Temmerman et al., 2004). Furthermore, the  $F^{14}\text{C}$  value of topsoil sediments is higher than for subsoil sediments, with the highest and lowest values resulting in radiocarbon ages of  $694 \pm 31$  and  $962 \pm 41$  calibrated years BP respectively (IntCal13, Reimer et al. (2013)), indicating that a substantial portion of fresh OC that is present in topsoil sediments is decomposed after burial.

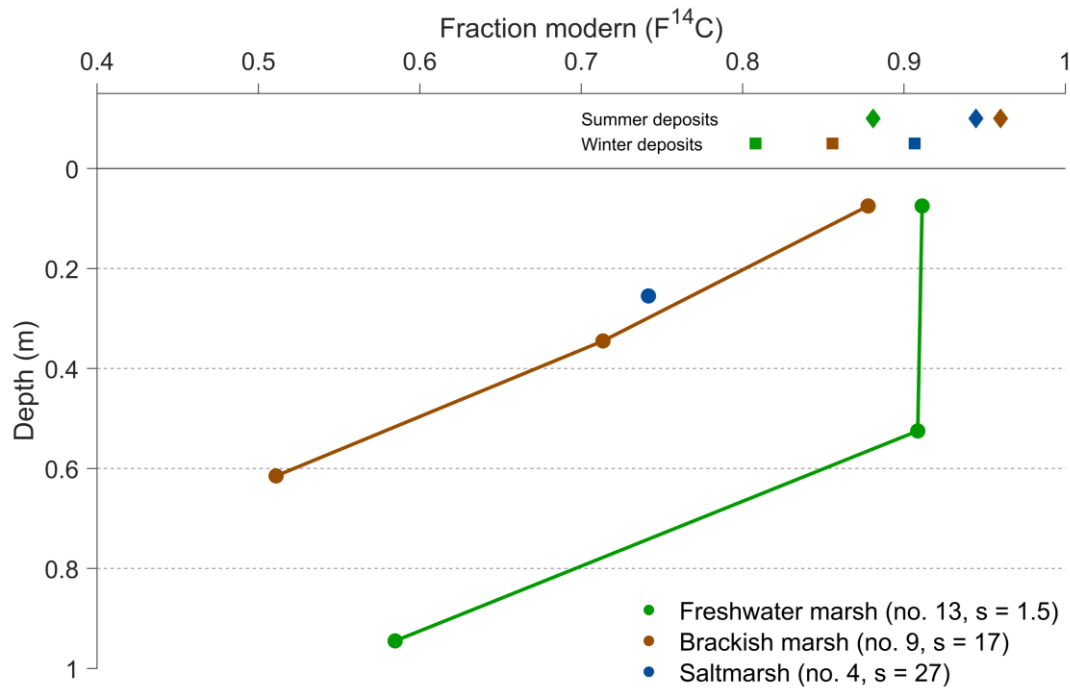


**Figure 3-7** Fraction modern  $^{14}C$  ( $F^{14}C$ ) of deposited sediments at the surface of tidal marshes in summer and winter, and sediments at different depths ('s' in the legend refers to salinity).

### 3.3.6 Organic carbon fractionation

After initial drying of the sediments for OC fractionation, the majority of soil particles was present in macroaggregates ( $> 250 \mu m$ ) for both topsoil and subsoil sediments (Figure S3-5). Aggregation was less pronounced for subsoil sediments from saltmarshes, where only about 50% of the soil particles was incorporated in macroaggregates. As macroaggregates were not observed in the field, this suggests that the process of initial sample drying had an effect on the results from the first fractionation step (wet sieving). Therefore, the results from the first fractionation step are not used to derive conclusions about OC stabilization mechanisms in tidal marsh sediments.

During sonication of the macroaggregates (M), this fraction was broken up into silt and clay (scM) on the one hand and microaggregates and POM (mM) on the other hand. The results of this intermediate fractionation step are not described in detailed here but are shown in figure S3-6. During the last fractionation step, the m and mM fraction were separated into (i) microaggregates and sand (m+S) and (ii) POM (Figure 3-8, Figure S3-7). The OC concentration was the largest for the POM fraction and the smallest for the silt and clay fractions (sc and scM) (Figure 3-8b, d). The microaggregates had an intermediate OC concentration. Roots contained between 4 – 9% of the total amount of OC in the topsoil samples (Figure S3-8 and supplementary data). In the subsoil samples, a substantial amount of roots was only present in the freshwater marsh no. 14 (s = 1.5) (11 % of total OC), while in the other subsoil sediments roots were nearly absent ( $< 1.1$  % of total OC, Figure S3-9 and supplementary data).

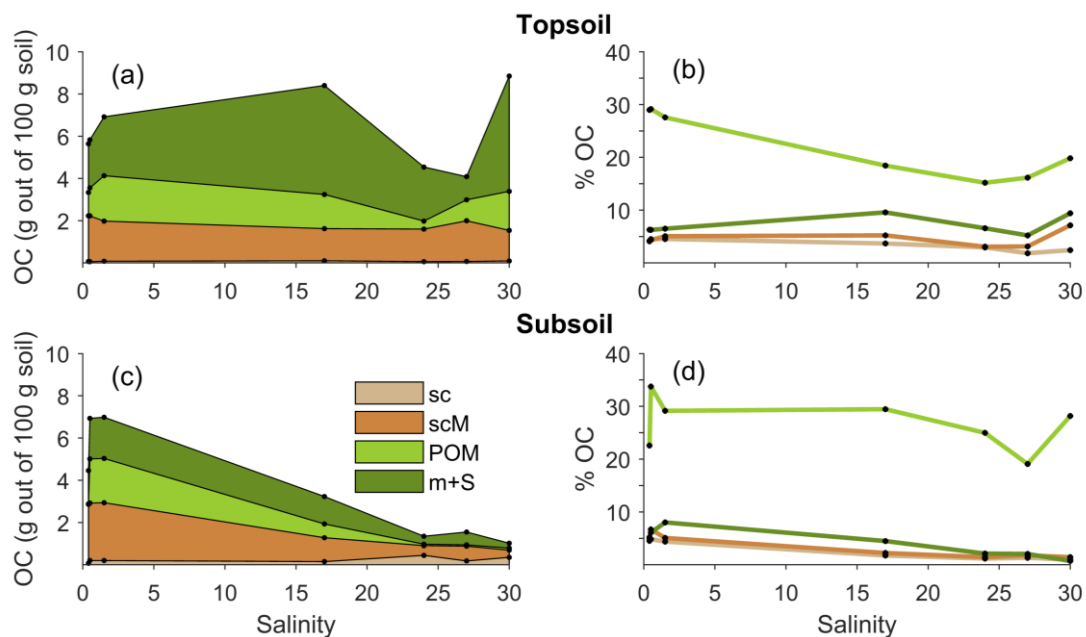


**Figure 3-8** Final OC fractions of topsoil (a, b) and subsoil (c, d) tidal marsh sediments along the estuary (see Figure S3-3 for depths of subsoil samples). a) and c) show the contribution of OC in each fraction to a total soil mass of 100 g, b) and d) show the OC concentration of the different fractions. sc = free silt and clay, scM = silt and clay in macroaggregates, POM = particulate organic matter, m+S = microaggregates and sand.

For topsoil sediments, the amount of OC present in the m+S fraction was generally larger in freshwater marshes compared to saltmarshes, with the exception of saltmarsh no. 2 ( $s = 30$ ) (Figure 3-8a). With the exception of the marsh no. 6 ( $s = 24$ ), the amount of POM was relatively constant in topsoils along the estuary. In subsoil sediments, clear patterns could be observed (Figure 3-8c). First, while in freshwater marsh subsoils about one third of the total OC was present as free POM after the disruption of macroaggregates, POM was nearly absent in the subsoil of saltmarshes ( $< 0.1$  g POM out of 100 g sediments) (Figure 3-8c and Figure S3-7). Second, the subsoil m+S fraction stored less OC compared to topsoil samples and showed a strong decrease towards the coast (Figure 3-8c). As sand generally does not stabilize significant amounts of OC, it can be assumed that the majority of OC in this fraction was stabilized in microaggregates. In the freshwater subsoils, the OC concentration of the m+S fraction was higher (5.0 – 8.0 %) compared to the sc fraction (4.4 – 4.9 %, Figure 3-8d), suggesting that these aggregates contained a substantial amount of POM. Hence, microaggregates have the potential to protect POM from decomposition in freshwater subsoils (Figure 3-8d). At the saltmarshes, however, the difference in OC concentration between microaggregates (0.7 – 2.1 %) and the sc fraction (1.0 – 1.3 %) was much smaller, suggesting that the majority of OC in this fraction was associated with silt and clay particles while the amount of POM in these microaggregates was very limited. Third, the OC concentration of the subsoil sc fraction (from 4.4 – 4.9 % at the freshwater marshes to 1.0 – 1.3 % at the saltmarshes) was similar to the OC concentrations of deposited sediments in winter (Figure 3-5), from  $4.5 \pm 0.2$  % at the freshwater marshes to  $2.3 \pm 0.1$  % at the saltmarshes.

### 3.4 Discussion

#### 3.4.1 Autochthonous organic carbon inputs along the estuary

Locally produced (autochthonous) biomass is generally considered to contribute significantly to the total OC pool in tidal marsh sediments (Ouyang et al., 2017), as tidal marshes are among the most productive ecosystems in the world (Rocha and Goulden, 2009). Along estuaries, biomass is generally larger on freshwater and brackish marshes than on saltmarshes (Dausse et al., 2012; Hansen et al., 2016; Wieski et al., 2010). This is a consequence of the generally larger nutrient availability and lower salinity levels in the former portions of estuaries, in addition to species differences (Whigham, 2009). This pattern is, however, not found in the Scheldt estuary (Figure 3-4). Moreover, there was no relationship between the SOC stocks down to a depth of 0.6 m and the amount of aboveground-, belowground- and total biomass at the studied tidal marshes, ( $r^2 < 0.02$ ,  $n = 16$ ) (Figure S3-10). There was, however, a weak relationship between topsoil OC stocks (down to 0.05 m depth) and aboveground biomass ( $r^2 = 0.31$ ), which suggests that local biomass production might have an influence on the amount of topsoil OC and partially controls the spatial pattern of OC deposition along the estuary (Figure S3-11). The lack of a strong relationship between biomass and OC stocks suggests, however, that factors other than local biomass control the long-term sequestration of OC in the studied tidal marsh sediments.

The analysis above only considers macrophyte biomass and does not take into account the potential contribution of edaphic algae to the OC pool of the marsh sediments. The OC produced by algae is generally considered to be very labile and may therefore be expected to be rapidly mineralized in a tidal marsh environment (Chmura and Aharon, 1995). This appears also the case in the Scheldt estuary: Boschker et al. (1999) showed that algal-derived OC was rapidly mineralized on the brackish marsh at salinity 17 as it was the primary source for bacterial growth (Boschker et al., 1999). However, some microbial-derived DOC can potentially be stabilized on mineral surfaces (Ahrens et al., 2015).

#### 3.4.2 Allochthonous organic carbon deposits along the estuary

The low radiocarbon contents of deposited OC show that this OC in winter is very old, indicating that a significant fraction of this OC has been fixed from atmospheric CO<sub>2</sub> up to millennia ago (Figure 3-7). Summer deposits are systematically younger as indicated by a higher F<sup>14</sup>C, suggesting a contribution of fresh carbon to deposited OC. This contribution is, however, limited: the F<sup>14</sup>C of summer deposits is still well below 1. Several earlier studies have already shown that the organic matter that is transported within an estuary consists for a substantial fraction of highly processed, stable organic matter (Klap et al., 1996; Raymond and Bauer, 2001), which is being enriched with fresh, more labile organic matter in summer (De Brabandere et al., 2002; Mariotti et al., 1984; Muylaert et al., 2000).

As the production of riverine and estuarine phytoplankton is generally absent during winter (Hellings et al., 1999; Muylaert et al., 2000), deposited sediments at tidal marshes during this season contain mainly old OC. Also in terrestrial soils, average SOC ages of up to millennia old are regularly reported (He et al., 2016; Martinelli et al., 1996; Rumpel et al., 2002). However,

the old SOC in these ecosystems is not necessarily stable, as environmental disturbances can result in a rapid decomposition of old SOC (e.g. Hobbey et al. (2017)). The old OC that is deposited at tidal marshes is, in contrast, likely to be quite stable as it has first been sequestered in terrestrial ecosystems, was then eroded and has travelled through the river system until it was finally deposited on the marsh. The fact that this old OC is not being mineralised is likely to be also related to the fact that suspended sediment in the Scheldt estuary is mainly transported as cohesive organo-mineral aggregates (Chen et al., 2005), thereby physically protecting the OC.

The concentration of this stable OC in deposited sediments decreases towards the mouth of the estuary, with winter deposits containing 4 – 5 % OC in the freshwater section and 2 – 3 % in the saltwater section (Figure 3-5). There is also a clear gradient in the source of this stable OC along the estuary. The  $\delta^{13}\text{C}$  signal of OC deposited at freshwater marshes, on average  $-28 \pm 0.48 \text{ ‰}$  (Figure 3-5) strongly suggests that this OC has a terrestrial origin (Kohn, 2010). Middelburg and Nieuwenhuize (1998) calculated a value of  $-26 \text{ ‰}$  for the terrestrial OC present in the estuary. The  $\delta^{13}\text{C}$  of the deposited sediment is on average slightly lower than this value, which could indicate that relatively small amounts of fresh material with a lower isotopic signal are also present in the deposits. Winter deposits at saltmarsh no. 4 ( $s = 27$ ) have an average  $\delta^{13}\text{C}$  value of  $-23.6 \pm 0.46 \text{ ‰}$ , which is very similar to  $\delta^{13}\text{C}$  values reported for marine sediments in the North Sea in front of the mouth of the Scheldt river ( $-23.2$  to  $-23.8 \text{ ‰}$ , Salomons and Mook, 1981). This indicates a marine origin of the stable OC that is deposited at the saltmarshes. This is not surprising, as it has been shown that marine sediments are able to efficiently stabilize OC (Keil et al., 1994; Mayer, 1994). The origin of the OC deposited on brackish marshes is a mixture between these terrestrial and marine end-members (Figure 3-5).

In summer, old OC in deposited sediments is mixed with a substantial amount of fresh, young OC, as indicated by the higher  $F^{14}\text{C}$  of summer versus winter deposits (Figure 3-7). Assuming that the concentration of old, stabilized OC in the deposited sediments is constant throughout the year, the importance of labile OC that is deposited in summer can be assessed from the isotopic shift that is observed. At the freshwater marshes, the contribution of labile phytoplankton-derived OC to summer deposits is very limited. Reported  $\delta^{13}\text{C}$  values for phytoplankton in the freshwater portion of the estuary are in the range of  $-29$  to  $-34 \text{ ‰}$  (Hellings et al., 1999; Middelburg and Nieuwenhuize, 1998). A significant contribution of recent OC to summer deposits would therefore result in a significant shift towards lower  $\delta^{13}\text{C}$  values, which is not observed. Moreover, the concentration of suspended particulate OC is up to 10 % in this part of the estuary during summer (Abril et al., 2002), while the OC concentration in deposits is ca. 5.5 %. This suggests that most OC that is produced in the freshwater section of the estuary is not deposited on the freshwater marshes. At the saltmarsh, in contrast, there is a clear contribution of marine phytoplankton-derived OC to summer deposits, as indicated by (i) the doubling in OC concentration in the deposited sediments (Figure 3-5a), which is (ii) accompanied by a shift in  $\delta^{13}\text{C}$  values towards marine values ( $-18$  -  $-22 \text{ ‰}$ , Middelburg and Herman, 2007; Middelburg and Nieuwenhuize, 1998) (Figure 3-5b) and (iii) the relatively high  $F^{14}\text{C}$  of summer deposits (Figure 3-7). The large inter-annual variation in OC concentration in deposits at the brackish marsh (between  $3.7 \pm 0.3 \text{ ‰}$

and  $11.1 \pm 2.2$  %) indicates that there is a large amount of labile OC present in summer deposits (Figure 3-5a), which is confirmed by the higher  $F^{14}C$  in summer deposits (Figure 3-7). It is not clear why deposition of labile OC is so substantial in this section of the estuary in comparison to the salt and freshwater sections, as phytoplankton blooms are present along the entire estuary (Gypens et al., 2013; Muylaert et al., 2009). This additional labile OC is, however, only present in the topsoil layers, below which there is a steep decline in OC concentration with depth (ca. 10 % OC in the topsoil compared to ca. 3 % OC below 0.10 m depth) as well as a clear decrease of  $F^{14}C$  (see supplementary data for depth profiles of OC concentration). Thus, the relatively large input of labile OC in summer has little effect on the long-term SOC storage in these sediments.

### 3.4.3 Preservation mechanisms of organic carbon in tidal marsh sediments

The  $F^{14}C$  in subsoil tidal marsh sediments suggests that this OC is up to millennia old, while the upper meter of sediments in all studied tidal marshes has been deposited within less than a century (Temmerman et al., 2004, 2003). This can only be explained by the fact that the OC in the studied sediments consists for a significant fraction of old, allochthonous OC. In topsoil sediments of marshes for which the radiocarbon content has been determined, OC is a mixture between this old OC and locally produced biomass, as indicated by the higher  $F^{14}C$  of topsoil sediments.

Depth patterns of the  $F^{14}C$  vary along the estuary. The lack of a decrease in  $F^{14}C$  with depth in the top 0.5 m of freshwater sediments suggests that the contribution of locally produced OC is relatively stable with depth (Figure 3-7). At the brackish and saltmarsh, in contrast, the steep decrease in OC concentration with depth (see supplementary data) is accompanied by a steep decrease in the  $F^{14}C$ , indicating that the majority of fresh OC is rapidly decomposed after burial. Thus, in freshwater sediments a substantial portion of locally produced OC is preserved after burial, while the majority of the fresh OC is rapidly mineralized in brackish and saltmarsh sediments.

Although OC associated with deposited sediments is considered to be an important source of OC for minerogenic tidal marshes (Bouillon and Boschker, 2006; Craft, 2007; Middelburg et al., 1997), stabilization mechanisms of OC in tidal marsh sediments are rarely identified (with the exception of Spohn et al., 2013). From our results it is clear that there are substantial gradients along the estuary with regard to (i) the mechanisms of OC stabilization and (ii) the relative contribution of allochthonous versus autochthonous sources to long-term preserved OC. In our analyses, we interpreted POM as originating from locally produced biomass, a hypothesis which is supported by the fact that the deposited sediment samples did not contain any visible particulate organic fragments apart from parts of locally produced vegetation, which can be redistributed at the surface of tidal marshes during storm events. While systematic variations of the relative importance of OC fractions in topsoil sediments are limited (Figure 3-8a), clear patterns along the estuary are present for subsoil sediments (Figure 3-8c). On the one hand, freshwater marsh sediments preserve a significant amount of locally produced OC (POM) after burial (Figure S3-7), both as free POM and as POM protected inside microaggregates. The latter is suggested by the observation that the OC concentration

of the m + S fraction in freshwater marsh subsoils is substantially larger compared to the silt and clay (sc) fraction, indicating the presence of POM in the microaggregates (Figure 3-8d). On the other hand, in saltmarsh sediments nearly all POM is decomposed upon burial. These data provide evidence that locally produced biomass is decomposed on a decadal timescale in saltmarsh sediments, while being better preserved and contributing to long-term OC storage in freshwater marsh sediments. Furthermore, the results confirm that the decomposition of OC associated with minerals (sc and scM) upon burial is very limited, as the amount of OC stored in this fraction does not decrease substantially with depth in most tidal marsh sediments (Figure S3-7). It can be assumed that the majority of OC associated with minerals is allochthonous OC, as all minerals in these tidal marshes have been deposited during inundation events. However, there is a potential exchange of mineral-associated OC through desorption of allochthonous, old OC and adsorption of locally-produced OC (Schrumpf and Kaiser, 2015). This exchange is however likely to be minimal, as suggested by the low  $F^{14}C$  values of bulk OC found in the studied sediments.

Based on our data it is not possible to derive an explanation for the rapid decomposition of OC in saltmarsh sediments. Research on the effect of location along an estuary on decomposition of organic matter in tidal marsh sediments has suggested both a positive (Loomis and Craft, 2010) and negative (Mendelssohn et al., 1999) correlation between decomposition and salinity. Experimental studies on the effect of saltwater addition on the decomposition of organic matter formed in freshwater marshes have shown that an increase in salinity generally results in an increase in the decomposition of organic matter (Morrissey et al., 2014; Weston et al., 2011, 2006). Results from these studies suggest that sulphate reduction is the preferential decomposition pathway and an increasing availability of extracellular enzymes might be responsible for higher decomposition rates in saltmarsh sediments. However, more research is needed to confirm if these mechanisms can also explain the higher in situ OC loss rates we found in saltmarsh sediments. Another important factor is that rates of mineral sediment deposition at the freshwater marshes are higher compared to the saltmarshes (Temmerman et al., 2004) leading to more rapid advection of deposited OC to deeper soil layers which results in more efficient preservation of OC (Kirwan and Mudd, 2012), as proposed by Van de Broek et al. (2016).

In the freshwater subsoils, stable microaggregates store a substantial fraction of total OC, while aggregates in saltwater subsoils were almost completely broken up after sonication (Figure S3-6). This suggests that aggregates which are formed in freshwater marshes are more stable and thus more effective at preserving organic matter compared to saltmarshes. To our best knowledge, there are no earlier studies on aggregate stability in tidal marsh sediments along a salinity gradient. The effectiveness of soil aggregates to stabilize organic matter in tidal marsh sediments thus requires further research attention.

The combined results from radiocarbon analysis and OC fractionation quantitatively support the hypothesis that preservation of autochthonous OC is more important in freshwater compared to saltmarsh sediments, while characteristics of OC associated with deposited sediments are a major control on OC stocks along the estuary (Van de Broek et al., 2016). In addition, our results suggest that in minerogenic saltmarshes long-term OC sequestration is

decoupled from local primary production, implying that these sediments do not serve as an atmospheric CO<sub>2</sub> sink on a decadal timescale. In contrast, freshwater marsh sediments efficiently store a substantial amount of locally produced OC, thereby actively sequestering atmospheric CO<sub>2</sub> on a decadal to centennial timescale. It should be noted that the assessment of the potential of tidal marsh sediments to serve as an effective OC sink depends on the spatial and temporal scale in which these results are framed. In our analysis, allochthonous OC is not assumed to contribute to atmospheric CO<sub>2</sub> sequestration at the scale of the tidal marsh profile, as this OC has not been fixed in-situ. However, at the spatial scale of the entire basin of the Scheldt river, tidal marshes can be considered as an effective sink for OC that has been eroded in the upper catchment and is transported through the river system into the estuary. This interpretation, however, depends on the alternative fate of this allochthonous OC if it would not be deposited on these tidal marshes, which is highly uncertain.

These findings have important implications for the assessment of the response of the tidal marsh OC pool to future environmental changes. Studies on the effect of sea level rise on the tidal marsh OC pool generally only consider short-term changes observed in a controlled lab environment (Chambers et al., 2011; Morrissey et al., 2014; Weston et al., 2011, 2006). However, our results show that the response to environmental changes such as a sea level rise over decennial/centennial time scales will be mainly controlled by the supply of allochthonous OC, while the characteristics of in-situ produced biomass and its decomposition are less relevant at this timescale. This stresses the importance of studying OC dynamics in tidal marsh sediments over a period of time (or sediment depth) that is relevant for the change in environmental conditions that is considered.

#### **3.4.4 Consequences for calculated CO<sub>2</sub> sequestration rates**

The magnitude of short-term contemporary OC deposition at the studied tidal marshes is controlled by the accumulation of relatively labile OC originating from locally produced biomass, while long-term OC sequestration depends on the supply of stable allochthonous OC from terrestrial and marine origin. This has important consequences for the calculation of OC sequestration rates in coastal sediments, which is generally performed using one of the following methods: (i) using short-term sediment deposition rates in combination with topsoil OC densities (e.g. Chmura, Anisfeld, Cahoon, & Lynch, 2003; Ouyang & Lee, 2014) or (ii) by relating decreasing OC concentrations with depth to time since sediment deposition (e.g. Artigas *et al.*, 2015). However, both approaches generally result in an overestimation of the rate of atmospheric CO<sub>2</sub> sequestration for two reasons, as illustrated in Figure 3-9.

First, using topsoil OC densities to calculate long-term OC sequestration rates neglects potentially large losses of OC upon burial (Figure 3-9b, c); the calculated rates should therefore be interpreted as short-term carbon deposition rates. Second, while methods which relate decreasing OC concentrations with depth to the time since sediment deposition account for OC losses through time, they do not account for the fact that a substantial fraction of the OC in coastal sediments can have an allochthonous origin and has not been sequestered at the tidal marsh. As a consequence, this old-aged allochthonous OC does not

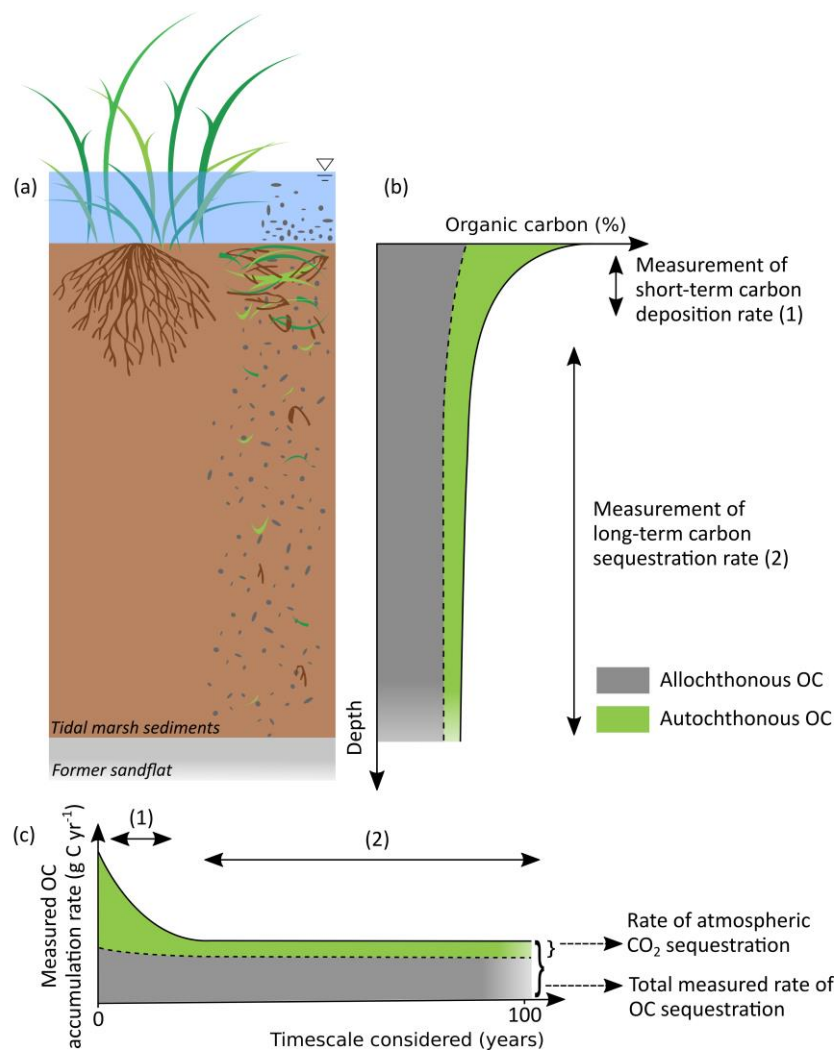


**Figure 3-9** Conceptual framework of OC dynamics in tidal saltmarsh sediments and measurements of OC accumulation rates. (a) Topsoil sediments contain large amounts of OC from allochthonous sediments (grey shapes) and both aboveground- and belowground-produced autochthonous biomass (brown and green). Upon burial, however, mainly autochthonous OC is being mineralized. (b) The associated OC depth profile, subdivided into autochthonous- and allochthonous-derived OC. (c) Measured rates of OC accumulation in saltmarsh sediments depend on the timescale considered.

contribute to active removal of atmospheric CO<sub>2</sub> by tidal marsh ecosystems (Figure 3-9c). These considerations are up till now not accounted for in the assessment of rates of blue carbon sequestration in these ecosystems (Chmura et al., 2003; Duarte et al., 2013; Ouyang and Lee, 2014). In order to obtain more reliable estimates of the potential of tidal marsh ecosystems to store atmospheric CO<sub>2</sub>, future studies should (i) sample marsh sediments to a sufficient depth so that OC decomposition within the marsh sediments can be accounted for and (ii) identify the contribution of autochthonous and allochthonous OC to total OC storage in marsh sediments.

The results of this study show that the majority of preserved OC in tidal marsh sediments along a temperate estuary is old, allochthonous OC which has not been sequestered in-situ but has a terrestrial or marine origin at freshwater- and saltmarshes respectively. Furthermore, the concentration of stable OC in deposits is substantially higher in freshwater

compared to saltwater reaches, contributing to decreasing OC stocks with increasing salinity. Radiocarbon analysis and OC fractionation showed that freshwater tidal marsh sediments effectively preserve locally produced OC, while this is decomposed on a timescale of decades in saltmarsh sediments. As the majority of preserved OC in saltmarsh sediments has not been sequestered in-situ, the contribution of these sediments to atmospheric CO<sub>2</sub> sequestration is very limited on a decadal to centennial timescale. In contrast, freshwater marsh sediments preserve a substantial amount of in-situ produced biomass, thereby actively sequestering atmospheric CO<sub>2</sub>.

### **Acknowledgements**

The authors would like to thank Lore Fondu, Taciana Gomes, Lotte Baert, Maarten Vanopstal, Jarne Buttiens, Amber Bruynseels, Britta Lahaye and Maarten Parent for their help during sample collection. Furthermore, we are grateful to Lore Fondu and Tim De Clercq for their much-appreciated help with analyses of the samples in the lab. Staatsbosbeheer, Natuurpunt, Rijkswaterstaat, Zeeland seaports, Waterwegen en zeekanal and Natuurmonumenten are being thanked for granting access to the tidal marshes for sample collection.

### **Data availability**

The data associated with the published paper is available at <http://dx.doi.org/10.17632/2nnv9bw3hh.2>, supplementary figures and tables at <https://onlinelibrary.wiley.com/doi/abs/10.1111/gcb.14089>



## Chapter 4 Soil organic carbon stocks in a tidal marsh landscape are largely affected by human marsh embankment and subsequent marsh progradation<sup>1</sup>

---

**Abstract.** Tidal marshes are coastal and estuarine ecosystems that store large amounts of organic carbon (OC) in their sediments. Despite their valuable ecosystem services, tidal marshes have been converted to human land use at high rates over the past centuries and this is still going on in many parts of the world. Previous studies have reported large decreases in soil organic carbon (SOC) stocks after the embankment and subsequent drainage of tidal marshes for conversion to agricultural land use. However, studies on the effect of marsh embankment on changes in SOC stocks have up till now only focused on SOC losses locally within the embanked marshes, thereby neglecting that the construction of embankments can stimulate the development of new tidal marshes in front of the embankment and additional SOC storage can take place in these newly created tidal marshes. To bridge this gap, we studied the effect of stepwise embankments and subsequent progradation of brackish and salt marshes on SOC stocks in the Scheldt estuary (The Netherlands) since the 16<sup>th</sup> century. We used a combined field and modelling approach to show that despite substantial SOC losses from embanked brackish (-8.66 kg OC m<sup>-2</sup>) and salt marsh sediments (-6.77 kg OC m<sup>-2</sup>), regional average SOC stocks in the brackish and salt polder regions increased with ca. 2 and 1.1 kg OC m<sup>-2</sup> respectively as a consequence of marsh progradation, compared to the initial situation when only sandflats were present. Our results show the importance of accounting for both losses and gains of SOC in order to avoid overestimations of the amount of SOC lost during the process of embankment and subsequent progradation of tidal marshes.

---

<sup>1</sup>This work is the result from a collaboration with prof. dr. Stijn Temmerman (Universiteit Antwerpen) and Lotte Baert (MSc, KU Leuven).

## 4.1 Introduction

Tidal marshes are highly productive ecosystems located along coastlines and in estuaries. These ecosystems deliver a wide range of important ecosystem services, such as mitigation of coastal flood risks and shoreline erosion risks, providing breeding grounds for fish and regulation of water quality (Barbier et al., 2011). Furthermore, it has been well-established that vegetated coastal ecosystems, including tidal marshes, mangroves and seagrass beds, store large amounts of organic carbon (OC) in their sediments (Duarte et al., 2013).

Despite the high social, economic and environmental importance of vegetated coastal ecosystems, they are under immense pressure (Halpern et al., 2008; Lotze, 2006). Apart from sea level rise, which can cause tidal marsh loss due to marsh drowning and erosion, the most imminent threat to vegetated coastal wetlands is by direct human transformations (Kirwan and Megonigal, 2013). Globally, up to half of the area covered by vegetated coastal ecosystems has been lost over the past century (An et al., 2007; Huang et al., 2010; Mcleod et al., 2011) due to the anthropogenic conversion of these ecosystems for mainly agricultural, aquaculture, industrial and residential purposes. This process is referred to in literature by several terms, such as 'conversion' or 'reclamation' of coastal ecosystems. Here we use the term 'marsh embankment', referring to the construction of flood protecting structures (embankments, dikes, levees, ...) and subsequent soil drainage, in order to convert marshes into agricultural land. The embanked agricultural land is addressed after the Dutch word 'polder'. Over the past centuries, tidal marsh embankment was an active process in countries which were economically developing, such as The Netherlands (Dijkema, 1987; Hoeksema, 2007; Verhoeven and Setter, 2010), Germany (Goeldner, 1999) and the United Kingdom and Ireland (Ellis and Atherton, 2003; Healy and Hickey, 2002). In some of the countries with historic marsh embankments, there is currently a tendency to re-convert polders again to natural ecosystems by subjecting them back to tidal flooding (Eertman et al., 2002; Goeldner, 1999). In contrast, the practice of conversion of coastal wetlands has over the past decades shifted to economically developing countries. In east Asia, for example, large areas of intertidal wetlands have been embanked and used for agricultural, aquaculture and industrial purposes since the 1950's, e.g. in China (Huang et al., 2010; Ma et al., 2014), the Korean Peninsula (Choi, 2014; Murray et al., 2014; Williams et al., 2014) and Japan (Suzuki, 2003), mainly as a consequence of strong economic development (He et al., 2015). Moreover, many more embankments of intertidal wetlands are planned in east Asia for the years to come (Wang et al., 2014).

The destruction of natural coastal wetlands has some important consequences for the health of coastal ecosystems (Hood, 2004; Jin et al., 2016; Ma et al., 2014), in addition to great economic losses for affected regions (Wang et al., 2010; Zhu et al., 2017). This, combined with the high rates at which the area of coastal wetlands has been reduced over the past decades globally (0.7 - 3 % yr<sup>-1</sup>) (Duarte et al., 2013; Pendleton et al., 2012), stresses the great importance to correctly assess how this practice affects the properties and services of these ecosystems. For example, the embankment of coastal vegetated ecosystems results in the development of soil horizons in these sediments, increases in soil bulk density, a decrease in soil pH and carbonate content, and it changes cation concentrations (Beke, 1990; Cui et al.,

2012; Ellis and Atherton, 2003; Fernández et al., 2010; Iost et al., 2007; Li et al., 2014; Yin et al., 2016). Moreover, multiple studies have shown that the embankment and drainage of OC-rich coastal sediments leads to a loss of previously stored OC (Bai et al., 2013; Bu et al., 2015; Deng et al., 2016). In a study summarizing available data on this process, Pendleton et al. (2012) calculated that the conversion and degradation of vegetated coastal ecosystems results in an average annual emission of 0.45 Pg CO<sub>2</sub>, equivalent to 3 – 19 % of annual CO<sub>2</sub> emission due to global deforestation. In contrast, multiple studies have reported increases in soil organic carbon (SOC) stocks upon conversion of intertidal wetlands in east Asia (Fu et al., 2014; Li et al., 2014; Zhang et al., 2016). These studies generally concern embankments of bare intertidal flats, having very low OC concentrations (< 0.5 %) which are likely to increase due to additional OC inputs following cultivation.

Despite the acknowledgement that the embankment and subsequent drainage of vegetated coastal ecosystems affects regional and global OC budgets, research concerning this topic has been very limited up till now. Although research efforts have increased recently, SOC dynamics in converted vegetated coastal ecosystems and the timescale over which these changes occur remains greatly understudied (Pendleton et al., 2012). Moreover, these processes are generally studied using a space-for-time conversion approach along chronosequences of embanked marshes, by linking measured SOC stocks to the time since embankment. Although this approach allows to calculate SOC losses from embanked sediments, it neglects the fact that at the seaward side of the embankment a new tidal marsh is often initiated (Jongepier et al., 2015), which can store additional OC. Although research on the effect constructed embankments on sediment dynamics on tidal sandflats at the seaward side of embankments is very limited, some studies have suggested that the consequential reduction of the tidal prism (the volume of ebb or flood water) results in reduced water velocities and higher rates of sediment deposition (Cuvilliez et al., 2009; Hood, 2004; Xie et al., 2017). This can promote the initiation and growth of a new tidal marsh against the newly constructed dike and consequentially an increase in SOC storage in these tidal marsh sediments. To the best of our knowledge, this has up till now not been included in assessments of the effect of tidal marsh reclamation on regional SOC budgets and may lead to an overestimation of SOC losses.

To address this issue, we studied temporal changes in regional SOC budgets in landscapes created through stepwise embankment of tidal marshes in the Scheldt estuary (The Netherlands). We aim to answer the following research questions: (1) How much and at which time scales do OC stocks in tidal marsh sediments change after the conversion to an agricultural land use? and (2) How are landscape-scale SOC stocks affected by the stepwise embankment and subsequent progradation of tidal marshes? As the OC content of tidal marsh sediments varies substantially along the salinity gradient in the Scheldt estuary (as shown in chapter 3), a third research question was formulated: (3) How do post-embankment changes in SOC stocks differ between brackish and salt marshes?

## 4.2 Material and methods

### 4.2.1 Study area

The polder regions included in this study are located in the salt- (salinity > 18) and brackish (salinity ca. 17) portion of the Scheldt estuary (southern Netherlands) (Figure 4-1). The studied regions have been created by the embankment and subsequent drainage of tidal marshes for agricultural purposes since the 16<sup>th</sup> century. The embankment of tidal marshes typically initiated the formation of new tidal marsh on initially bare tidal flats at the seaward side of the embankment, and after a period of time this new tidal marsh was in its turn embanked (Jongepier et al., 2015). This process, called stepwise embankment, results in a landscape consisting of a chronosequence of embanked tidal marshes.

The sampled polder landscape in the brackish part of the Scheldt estuary (region 1, Figure 4-1) initially formed the connection between the Eastern and Western Scheldt (nowadays there form two separated estuaries) and consisted of extensive intertidal sandflats on which brackish marshes have established (van der Spek, 1997). In this region, 10 polders which have been reclaimed between 1571 and 1973 have been sampled. These are referred to as brackish polders. The sampled polder landscapes in the salt portion of the Scheldt estuary are located in four distinct regions (Figure 4-1). Here, 15 polders with reclamation ages between 1542 and 1952 have been sampled. These will be referred to as salt polders. A detailed description of the embankment history of the brackish and salt polder regions is provided in

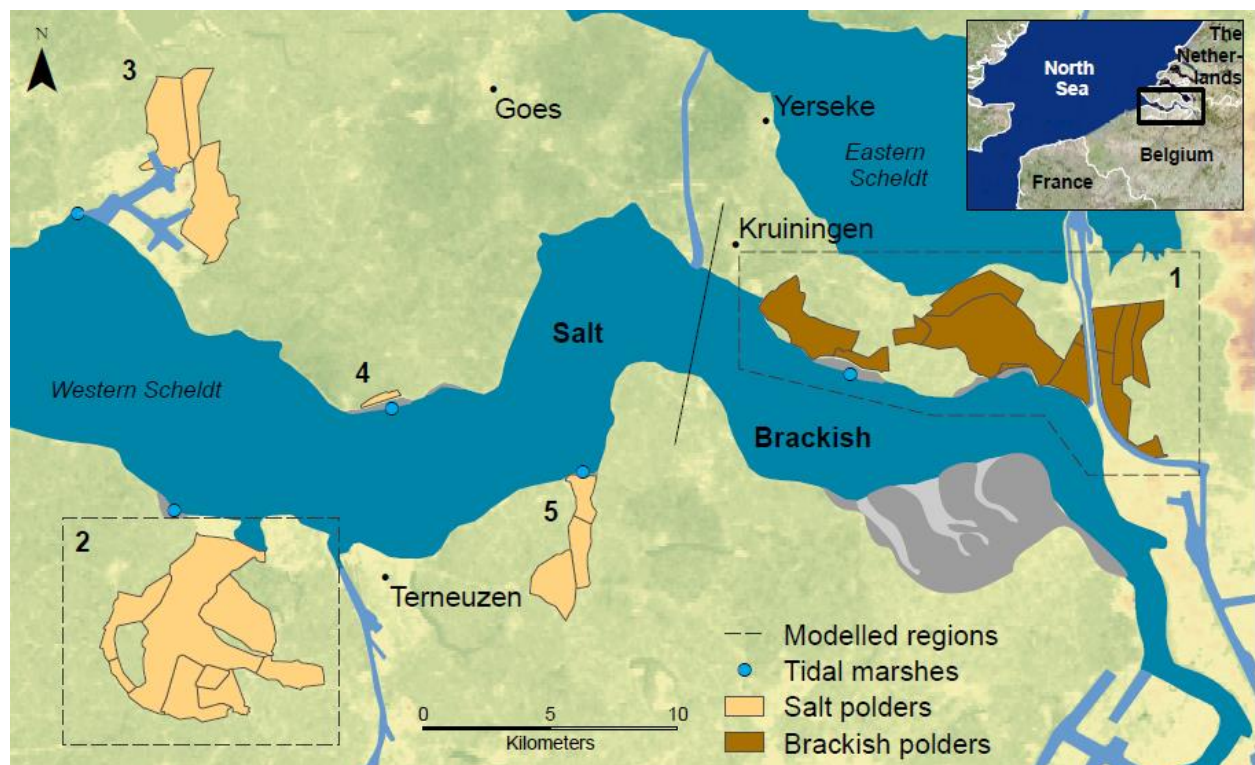


**Figure 4-1** Map of the sampled salt and brackish polders along the Scheldt estuary and associated tidal marshes (dark grey) and sandflats (light grey). Polder regions in dashed polygons have been used for modelling. The numbers refer to the different polder regions (Table 4.1). Detailed maps of the different regions are provided in the online supplementary information. Source background DEM: EU-DEM.

Wilderom (1968) and Wilderom (1973) respectively (in Dutch). To complement the polder chronosequences with the situation before embankment (i.e. the tidal marsh situation), SOC data presented in chapter 3 on both a low- and high-lying location on a present-day tidal marsh in each sampled polder region was used (Figure 4-1). The tidal marshes used in this study are the marsh near Waarde (at salinity ( $s$ ) = 17, region 1), Paulina marsh ( $s$  = 27, region 2), Sloehaven marsh ( $s$  = 30, region 3), Zuidgors marsh ( $s$  = 24, region 4) and Hellegat marsh ( $s$  = 22). A detailed overview of the SOC characteristics in these tidal marshes is presented in chapter 2 and 3. An overview of the sampled locations is provided in Table 4.1. Detailed maps of the sampled polders landscapes can be found in the online supplementary information and coordinates of sampling locations are provided in Table S4-3.

#### 4.2.2 Field sampling

Soil samples were collected in August 2015 in the brackish polders and in August and September 2016 in the salt polders. As our aim was to study SOC dynamics in embanked tidal marsh sediments, which are typically dominated by a silt grain size in the Scheldt estuary (see chapter 2 and 3), sampling locations were chosen carefully to make sure to be located in former tidal marsh sediments in the sampled polders. This is important, as embanked tidal creeks have a sand-dominated grain-size (Jongepier et al., 2015). The sampling locations were chosen i) using historical topographic maps, ii) using soil grain size maps and iii) by visual assessment of the grain size during sample collection.

**Table 4.1** Characteristics of the sampled polders per region ( $s$  denotes the present-day average salinity of the estuarine water at the respective locations). \*Depth of former tidal marsh sediments at the sampling location.

Name and embankment year	Sediment depth (m)*	Name and embankment year	Sediment depth (m)*
<i>Region 1 (brackish, <math>s</math> = 17)</i>		Van Dunnépolder (1907)	1.8
Waardepolder (1571)	0.3	Van Wuijckhuisepolder (1912)	0.55
Mairepolder (1694)	0.4	Dijckmeesterpolder (1920)	0.6
Reigersbergsche polder (1773)	0.7	Braakmanpolder (1952)	0.55
Tweede Bathpolder (1862)	0.5		
Emmanuëlpolder (1864)	> 0.9	<i>Region 3 (salt, <math>s</math> = 30)</i>	
Damespolder (1884)	0.4	Nieuwe West-Kraaijertpolder (1676)	0.5
Völckerpolder (1904)	0.5	Jacobpolder (1856)	0.55
Kreekrakpolder (1923)	0.35	Quarlespolder (1949)	1.05
Unknown (1953)	> 0.9		
Paviljoenpolder (1973)	> 0.7	<i>Region 4 (salt, <math>s</math> = 24)</i>	
		Hattumpolder (1957)	0.45
<i>Region 2 (salt, <math>s</math> = 27)</i>		<i>Region 5 (salt, <math>s</math> = 22)</i>	
Koudenpolder (1542)	0.75	Aan- en Genderdijkepolder (1600)	1.1
Kleine Stelpolder (1866)	0.55	Van Lijndenpolder (1877)	0.55
Koninginnepolder (1893)	0.35	Hellegatpolder (1926)	0.55
Mosselpolder (1900)	0.55		

At every sampled location in the polders, three undisturbed soil profiles were collected using a gouge auger (0.06 m diameter) at a distance of a couple of meters from each other. When the boundary between silty (former tidal marsh sediments) and sandy (former tidal sandflat below the marsh) sediments was encountered in the upper meter, a continuous depth profile down to the upper sand layers was collected. If this boundary was situated deeper than one meter, sample collection was generally limited to the upper meter (Table 4.1). The collected profiles were divided in depth intervals of 0.03 m in the field and transported to the lab in closed bags, where they were stored at 4 °C until analysis. To construct depth profiles of soil bulk density, three additional depth profiles were collected at the same location using a gouge auger (0.06 m diameter) at 0.05 m depth intervals (0 – 0.05 m; 0.05 – 0.10 m; 0.10 – 0.15 m; 0.20 – 0.25 m etc.). The tidal marshes from which data is used in this study were sampled using identical procedures as described in chapter 2 and 3.

### 4.2.3 Lab analyses

Before analyses, the samples for analyses of general soil characteristics were oven-dried at 50 °C, crushed until they passed through a 2 mm sieve and macro-vegetation residues and roots were removed manually using tweezers. Grain size was determined using a laser diffraction particle size analyzer (LTSM 13 320, Beckman Coulter) for one replicate soil core at every location at 0.18 m depth intervals, and classified into clay (< 2 µm), silt (2 – 63 µm) and sand (> 63 µm) size fractions. Before grain size analysis, organic matter was removed using hydrogen peroxide (35 %) and aggregates were destroyed using ultrasonic dispersion. The pH of selected soil samples was determined in the lab after diluting 5 g of soil into 25 ml of a 0.01 M CaCl<sub>2</sub> solution. The bulk density was determined after drying the soil samples collected for this purpose at 105 °C for 24 hours. The weight of these samples was combined with the calculated inside volume of the gouge auger for a depth section of 0.05 m to calculate the bulk density. The inorganic carbon concentration of soil samples collected in the brackish region was analyzed using the pressured calcimeter principle (Horváth et al., 2005).

Organic carbon concentrations and  $\delta^{13}\text{C}$  values were analyzed for soil samples from one of the replicate soil profiles at every location at 0.06 m depth intervals (0.00 – 0.03 m; 0.06 – 0.09 m etc.) using an elemental analyzer – isotope ratio mass spectrometer (FlashEA 1112 HT, Thermo Scientific – DELTA V Advantage). Before analyses, soil samples were weighed in pre-combusted silver cups and carbonates were removed using a 10 % HCl solution. For soil samples from the other two replicate profiles, OC concentrations were calculated using mid-infrared (m-IR) spectroscopy. Soil samples for m-IR spectroscopy analyses were finely ground and five replicates of each soil sample were scanned at wavenumbers between 400 and 4000 cm<sup>-1</sup> at a spectral resolution of 4 cm<sup>-1</sup> using a PerkinElmer® FT-IR spectrometer which was coupled to a PIKE® XY Autosampler. In addition, five replicates of a dried and finely ground KBr powder were scanned to serve as a background. After analyses, the ratio of the average energy spectrum of five replicates over the average spectrum of the five KBr energy spectra was calculated to obtain the reflectance spectrum and subsequently converted to an absorbance spectrum for further analyses by calculating the logarithm of the inverse of the reflectance spectrum.

Organic carbon concentrations were subsequently calculated using partial least squares regression (PLSR) separately for the salt- and brackish polders in R, to minimize variability within the datasets. The applied procedures are described in detail in the online supplementary information, while brief overview is presented here. For both datasets, the calibration of PLSR was done using soil samples with known OC concentrations ( $n = 102$  for the brackish polders,  $n = 171$  for the salt polders) to calculate the OC concentration of the samples for which only m-IR spectra were available ( $n = 201$  for the brackish polders,  $n = 200$  for the salt polders). Before analyses of the m-IR spectra, they were smoothed using Savitsky-Golay filtering (3<sup>rd</sup> polynomial,  $9\text{ cm}^{-1}$  moving window, no derivative) according to Vasques et al. (2008). PLSR using the optimal pre-treatment method (Standard Normal Variate) and number of PLS components (5) yielded an  $R^2$  of 0.91 for the brackish polders and  $R^2 = 0.87$  for the salt polders. The average absolute deviation between measured and predicted OC concentration was 0.15 % OC for the brackish polders and 0.12 % OC for the salt polders.

#### **4.2.4 Data analyses**

After the embankment and drainage of tidal marshes, substantial soil compaction and mineralization of soil organic matter occurs. Therefore, care has to be taken when comparing SOC stocks between existing tidal marshes and a chronosequence of embanked marshes. For example, a compaction factor of 2 implies that the sediment present in the upper meter of a tidal marsh is, after compaction, located in the upper 0.5 m of soil in a polder. When the amount of OC present in the upper meter of the soil would be directly compared between these two sites, the potential decline in SOC after embankment would be severely underestimated. Therefore, in the analyses below, OC and inorganic carbon stocks are calculated for a constant mass of bulk soil (top 400 kg) for a surface area of  $1\text{ m}^2$ . The  $\delta^{13}\text{C}$  value of these sediments is calculated by weighting the  $\delta^{13}\text{C}$  value of each soil layer by the amount of OC present in that layer. Bulk density is reported as the average bulk density in the top 0.3 m.

#### **4.2.5 Landscape-scale soil organic carbon model**

The impact of stepwise embankments of tidal marshes on regional SOC stocks was assessed using a 2D landscape model. The processes simulated in the model are (1) the progradation of tidal marshes, this means both vertical and lateral sediment accretion, and the accumulation of OC in these sediments, (2) the embankment of tidal marshes and potentially a part of the sandflat in front of the marsh, depending on the rate of lateral marsh progradation and (3) the resulting soil compaction and loss of OC from the embanked sediments. It is noted that we do not aim to accurately reconstruct historical changes in SOC stocks, as data for model calibration and validation are lacking for this purpose. The aim of this modeling exercise was to assess how embankments of tidal marshes affect the spatial distribution of SOC stocks, as affected by the area covered by tidal marshes and polder soils in the modelled regions and the spatial distribution in the thickness of tidal marsh sediments. A detailed description of the model, together with parameter values, is provided in the online supplementary information, a summary is presented here.

Model simulations were performed for the brackish polder region 1 and the salt polder region 2 (Figure 4-1) at a spatial resolution of 10 m. The model assumes an initial situation in which only sandflats are present (Coen, 1988; van der Spek, 1997) on which tidal marshes are subsequently developing at the seaward side of constructed embankments. The timing of embankment constructions was based on historical data, and the model was ran until the average landscape-scale SOC stocks had reached an equilibrium. For the brackish region, simulations are performed for the period 1500 – 2100 AD, for the salt region from 1700 to 2100 AD. These starting dates were chosen as the first embankments in the respective regions occurred a couple of decades later, therefore first allowing for the growth of a tidal marsh. The model simulates vertical tidal marsh accretion for every tidal marsh cell, and keeps track of the OC in the simulated cells down to a depth of 3 m at a vertical resolution of 0.01 m. This depth was chosen to allow for sufficient deposition of tidal marsh sediments, which are generally less thick in the Scheldt estuary, as shown in chapters 2 and 3.

The thickness of OC-rich tidal marsh sediments on top of OC-poor former sandflat sediments is calculated for every grid cell to calculate total SOC stocks. The simulated accumulation of OC in tidal marsh sediments is based on measured depth profiles of OC in a tidal marsh in the simulated polder regions (Figure 4-1). The rates of decreasing SOC stocks and increasing bulk densities upon embankment are calculated based on the measured values of SOC stock and bulk density as a function of time since embankment (see results, section 4.3). By tracking the amount of OC present in every simulated grid cell for every time step, both the spatial variation in OC stocks as well as the total amount of SOC present in the simulated region are calculated for every simulated time step. The model results are presented as the SOC stock for the upper 400 kg m<sup>-2</sup> of sediments (kg OC m<sup>-2</sup>) (i) for every grid cell and (ii) as the average landscape-scale SOC stock for the simulated regions. This average landscape-scale OC stock is calculated by dividing the total amount of OC present in the upper 400 kg m<sup>-2</sup> of sediment of all grid cells of the simulated region (irrespective of the land use) by the total area of the simulated region.

### **4.3 Results**

#### **4.3.1 Grain size, pH and inorganic carbon content**

An overview of the average general soil characteristics per study site are provided in Table S4-2. In general, sediment grain size is very similar between polders and tidal marshes located in the same region. Depth variations in the average clay-, silt-, and sand grain size fractions are very limited in the former marsh sediments, with average fractions being  $16.6 \pm 4.0$  % clay,  $61.5 \pm 9.3$  % silt and  $21.6 \pm 12.5$  % sand for the brackish polders and  $9.2 \pm 2.7$  % clay,  $58.5 \pm 12.4$  % silt and  $32.2 \pm 14.7$  % sand for the salt polders. The content of inorganic carbon (IOC) was calculated for the upper 400 kg m<sup>-2</sup> of sediments for the brackish chronosequence and shows lower IOC contents for some polders (4.1 – 2.9 kg IOC m<sup>-2</sup>) compared to the present-day tidal marsh (4.4 – 4.9 kg IOC m<sup>-2</sup>), while other polders contain similar amounts of IOC as the active marshes. In the brackish region, pH values decrease after reclamation from 7.5 – 7.7 in an active tidal marsh to steady-state values of ca. 7.1 in the polder soils. In the salt

region, in contrast, pH values show no decrease after conversion of tidal marshes, and have values in the range between 7.4 and 7.9.

#### 4.3.2 Organic carbon and $\delta^{13}\text{C}$ depth profiles

Depth profiles of OC concentration for selected polder soils and associated tidal marshes in the brackish (region 1) and salt polder region (region 2 in Figure 4-1) are shown in Figure 4-2 (a) and (c) respectively. Depth profiles of all sampled locations are provided in Figure S4-2 – S4-6. Concerning the initial situation before embankment, it should be noted that OC depth profiles of the tidal marshes in the brackish and salt region of the estuary are different: brackish marshes have higher OC concentrations and stocks compared to salt marshes, as shown in chapter 3.

In both the brackish and salt polder regions, SOC concentrations decline after the embankment of tidal marshes. In the brackish region, OC concentrations in the tidal marshes range from 14 % OC in the topsoil to ca. 2 % OC below 0.4 m depth. The polder which was embanked 41 years before sample collection has intermediate OC concentrations (ca. 3 % OC), while OC concentrations are lowest and OC depth profiles are similar for polders which have been embanked for more than 60 years (ca. 1.4 % OC in the top 0.4 m). This suggests that new equilibrium OC concentrations are reached ca. 60 years after the reclamation of brackish marshes. The depth profiles of OC concentration of the youngest polders in the salt portion of the estuary, embanked ca. 60 years prior to sampling, do not show substantial differences with older polders (ca. 1.1 % OC), indicating that here new equilibrium topsoil OC concentrations are reached < 60 years after reclamation.

The depth profiles of  $\delta^{13}\text{C}$  of the same marshes and polders are shown in Figure 4-2 b and d. For the polders in both the brackish and salt regions, variability in  $\delta^{13}\text{C}$  depth profiles among polders is larger compared to the variability in profiles of OC concentration. In the brackish polders,  $\delta^{13}\text{C}$  values decrease consistently with polder age in the top 0.4 m, from ca. -25.3 ‰ for the polder embanked 62 years prior to sampling to ca. -26.7 ‰ for the polder embanked 111 years prior to sampling. This pattern of decreasing  $\delta^{13}\text{C}$  values over time is however not consistent with the  $\delta^{13}\text{C}$  depth profile at the brackish marsh, which has a value of -28.1 ‰ at the soil surface and increased to -25.5 ‰ from a depth of 0.3 m downwards (Figure 4-2 b). For the polders in the salt region (region 2), there is a consistent pattern in  $\delta^{13}\text{C}$  values along the soil profile for the salt marsh – polders chronosequence. The  $\delta^{13}\text{C}$  values for the salt marsh vary between -21 - -22 ‰ in the top 0.5 m and are on average -26.3 and -27.1 ‰ in the plough layer of the 64 and 116 years old polders, respectively. Moreover, the decrease in  $\delta^{13}\text{C}$  values through time occurs at a faster rate in the plough layer compared to the subsoil.

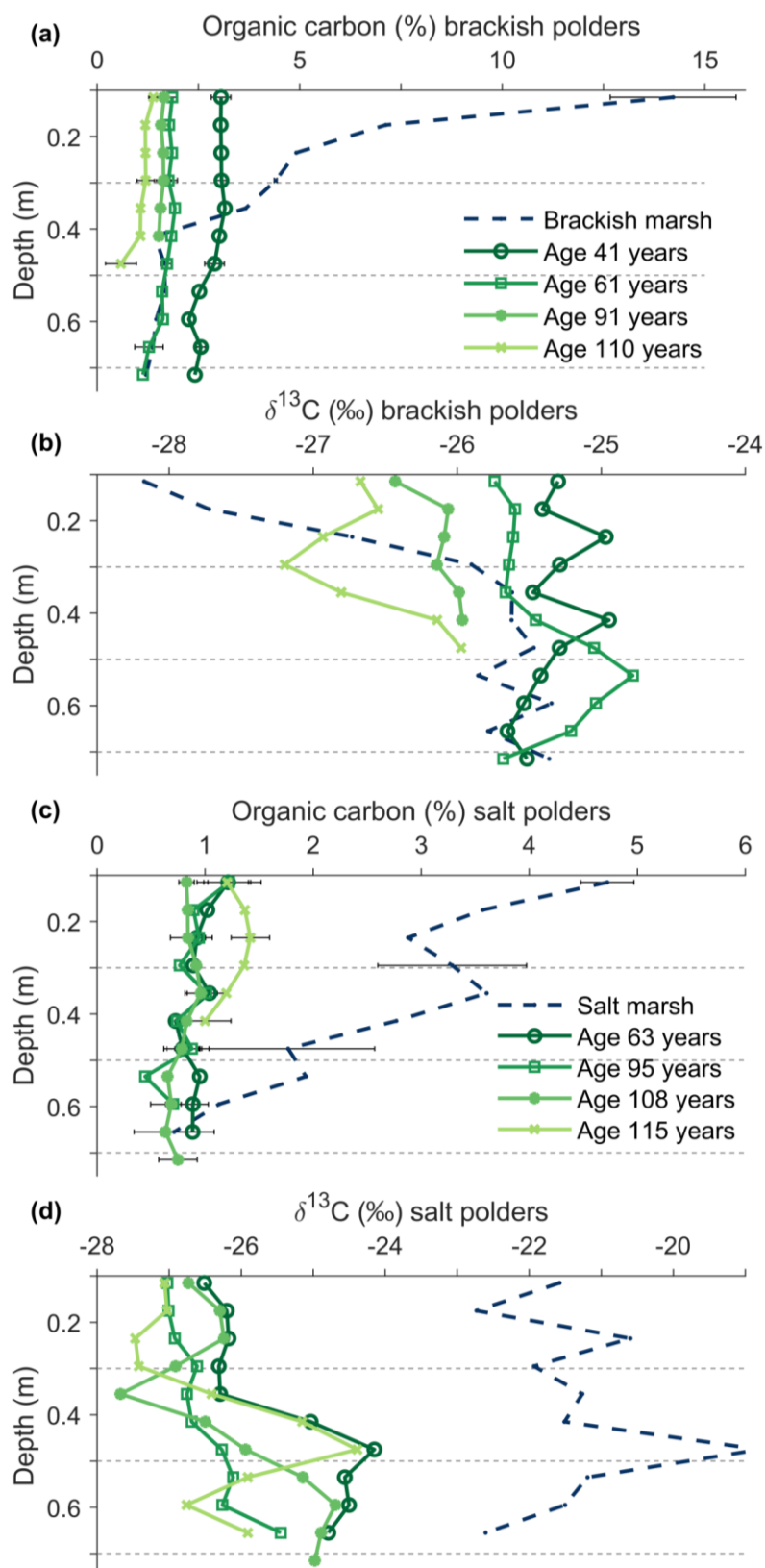


**Figure 4-2** Depth profiles of organic carbon concentration (%) (A, C) and  $\delta^{13}\text{C}$  values (‰) (B, D) of selected polder soils in the brackish (A, B) and salt (C, D) region (regions 1 and 2 in Figure 4-1 resp.) with a different time since embankment (age). The blue dashed lines represent a tidal marsh in the same region. The legend of B is similar to A, while the legend of D is similar to C. Error bars represent the standard deviation based on 3 replicates where available.

### 4.3.3 Changes in soil bulk density

The average soil bulk density in the top 0.3 m increases substantially after the embankment and drainage of tidal marshes (Figure 4-3). The average bulk density in the topsoil of the brackish marshes and polders is  $0.81 \pm 0.11 \text{ g cm}^{-3}$  and  $1.25 \pm 0.25 \text{ g cm}^{-3}$  respectively. In the salt region of the estuary, the average topsoil bulk densities for the tidal marshes and polders are  $0.61 \pm 0.18 \text{ g cm}^{-3}$  and  $1.35 \pm 0.26 \text{ g cm}^{-3}$  respectively.

### 4.3.4 Changes in organic carbon stocks and $\delta^{13}\text{C}$ values

The soil mass for which OC stocks are calculated is determined at  $400 \text{ kg m}^{-2}$  (see section 2.4), as this mass of former tidal marsh sediments is present below a surface area of  $1 \text{ m}^2$  in all but one of the studied polders. The average depths down to which this amount of sediment is present in the tidal marshes ranges from 0.52 and 0.63 m, and for the polder soils between 0.28 and 0.35 m (Table 4.2).

The calculated SOC stocks as a function of time since marsh embankment are shown in Figure 4-4 for all studied locations. The studied soil chronosequences allow to determine the time it takes for the OC stocks in these sediments to reach a new equilibrium after an initial decrease. For the brackish polders this equilibrium time is determined to be ca. 100 years, while for the polders in the salt region the maximum equilibrium time is determined at 64 years, due to the lack of polders which were converted < 64 years prior to sampling. As a consequence, the new equilibrium SOC stocks is likely to be reached in a shorter period of time.

The average amount of OC present in the soils for the different regions is shown in Table 4.2. For the brackish region, average OC stocks in tidal marsh sediments is  $14.76 \pm 0.46 \text{ kg OC m}^{-2}$  and decreases to an average equilibrium stock of  $6.10 \pm 0.22 \text{ kg OC m}^{-2}$  in embanked polders. For the salt regions, the average amount of OC present in the salt marsh sediments shows a considerable variation (between  $16.06 \pm 0.11$  and  $9.01 \pm 0.13 \text{ kg OC m}^{-2}$ ) with an average of

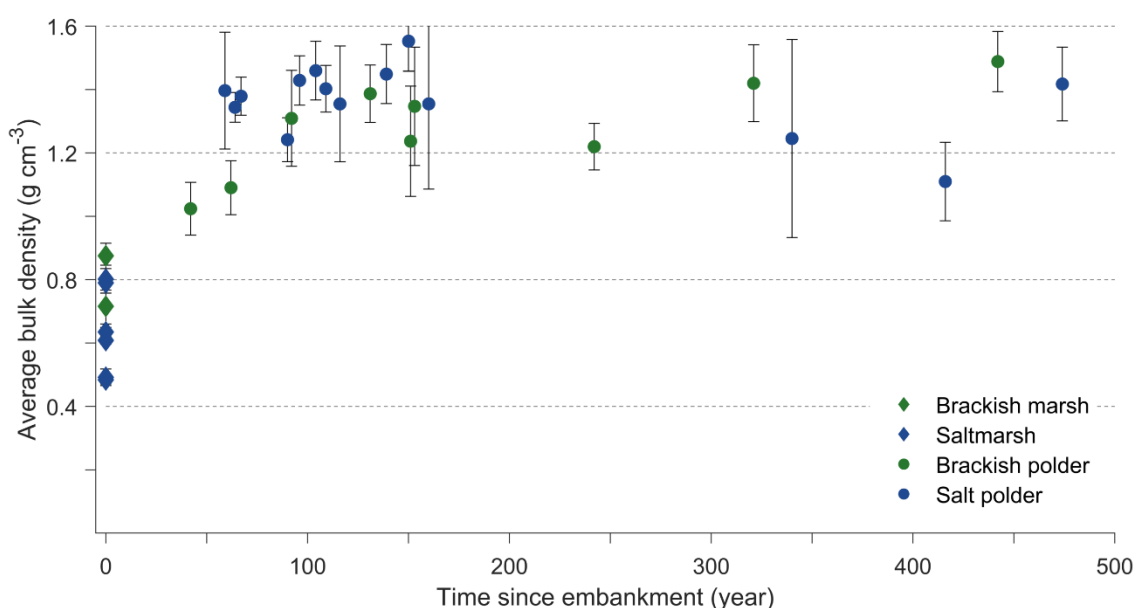


**Figure 4-3** Average bulk density in the top 0.3 m of present-day tidal marsh sediments and embanked polders ( $\text{g cm}^{-3}$ ). Error bars represent the standard deviation calculated based on three replicates.

$11.82 \pm 0.22$  kg OC  $m^{-2}$ . Along all studied chronosequences in the salt regions combined, OC stocks decrease to an average of  $5.05 \pm 0.19$  kg OC  $m^{-2}$ . Calculated rates of absolute OC losses over the time periods that losses are observed (100 and 60 years for the brackish and salt polders respectively) show that on average, embanked brackish marshes release OC at a lower rate ( $86.6$  g OC  $m^{-2} yr^{-1}$ ) compared to embanked salt marshes ( $112.8$  g OC  $m^{-2} yr^{-1}$ ). The relative loss of OC after conversion is, however, similar between polders in both regions (58 and 57 % for brackish and salt polders respectively). Along the chronosequences for both the brackish and salt regions, an increase in OC stocks after ca. 200 years is observed (Figure 4-4). However, the oldest polders in both the salt and brackish region have OC stocks which are comparable to the stocks found in polder soils which are about a century old.

The average  $\delta^{13}C$  values of SOC in the top 400 kg  $m^{-2}$  of sediments is shown in Figure 4-5. For the brackish region, on the one hand, an initial increase in  $\delta^{13}C$  values is observed along the chronosequence, as the  $\delta^{13}C$  value of currently active tidal marshes ( $-26.7$  ‰) is more negative compared to the youngest polder soils ( $-25.2$  –  $-26.1$  ‰) (Figure 4-2). The  $\delta^{13}C$  values of older polder soils range between  $-25.5$  and  $-28.11$  ‰. For the salt region, on the other hand, a consistent decline in  $\delta^{13}C$  values is observed in the first decades after marsh conversion, with active tidal marsh sediment having  $\delta^{13}C$  values between  $-22.1$  and  $-25.8$  ‰, and polder soils showing  $\delta^{13}C$  values between  $-25.6$  and  $-27.7$  ‰.

**Table 4.2** Depths down to which SOC stocks are calculated (for a mass of 400 kg  $m^{-2}$  of bulk soil) and the average SOC stocks of soils in the different regions. Standard deviations represent the spatial variation within the sampled polders based on 3 replicate soil profiles. The rate of OC loss for the brackish polders was calculated for a time span of 100 years, for the salt polders a time span of 60 years was used. The time to OC equilibrium was determined based on the results for each individual chronosequence, which are shown together in Figure 4-4.

	<i>Average marsh sediment depth (m)</i>	<i>Average polder soil depth (m)</i>	<i>Time to OC equilibrium (years)</i>	<i>Average marsh OC (kg <math>m^{-2}</math>)</i>	<i>Average polder equilibrium OC (kg <math>m^{-2}</math>)</i>	<i>Absolute average OC loss (g OC <math>m^{-2} yr^{-1}</math>)</i>	<i>Relative OC loss (%)</i>
Region 1	0.56	0.35	Ca. 100	$14.76 \pm 0.46$	$6.10 \pm 0.22$	$86.6 \pm 5.1$	$59 \pm 19$ %
Region 2	0.52	0.28	< 64	$9.23 \pm 0.31$	$4.41 \pm 0.13$	$80.5 \pm 5.6$	$52 \pm 16$ %
Region 3	0.59	0.29	< 66	$14.41 \pm 0.29$	$5.45 \pm 0.28$	$149.3 \pm 6.7$	$62 \pm 16$ %
Region 5	0.63	0.32	< 89	$12.54 \pm 0.12$	$6.34 \pm 0.20$	$103.3 \pm 3.9$	$49 \pm 9$ %
Total salt	0.59	0.29	< 64	$11.82 \pm 0.22$	$5.05 \pm 0.19$	$112.8 \pm 4.8$	$57 \pm 12$ %

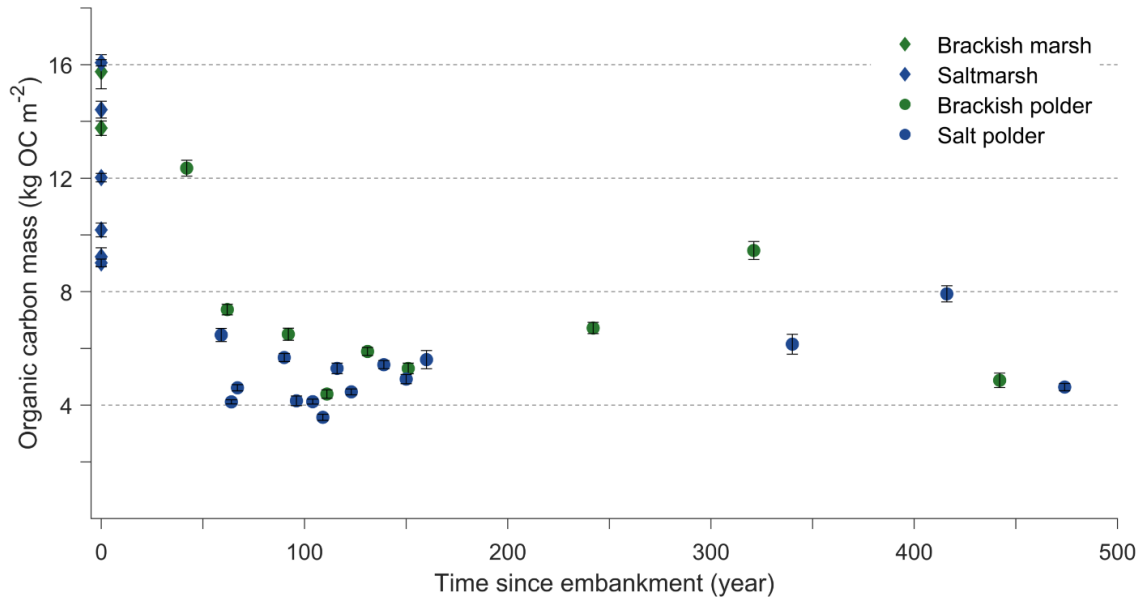


**Figure 4-4** Mass of organic carbon ( $\text{kg OC m}^{-2}$ ) in the uppermost  $400 \text{ kg m}^{-2}$  of sediments in both present-day tidal marsh sediments and embanked polder soils.

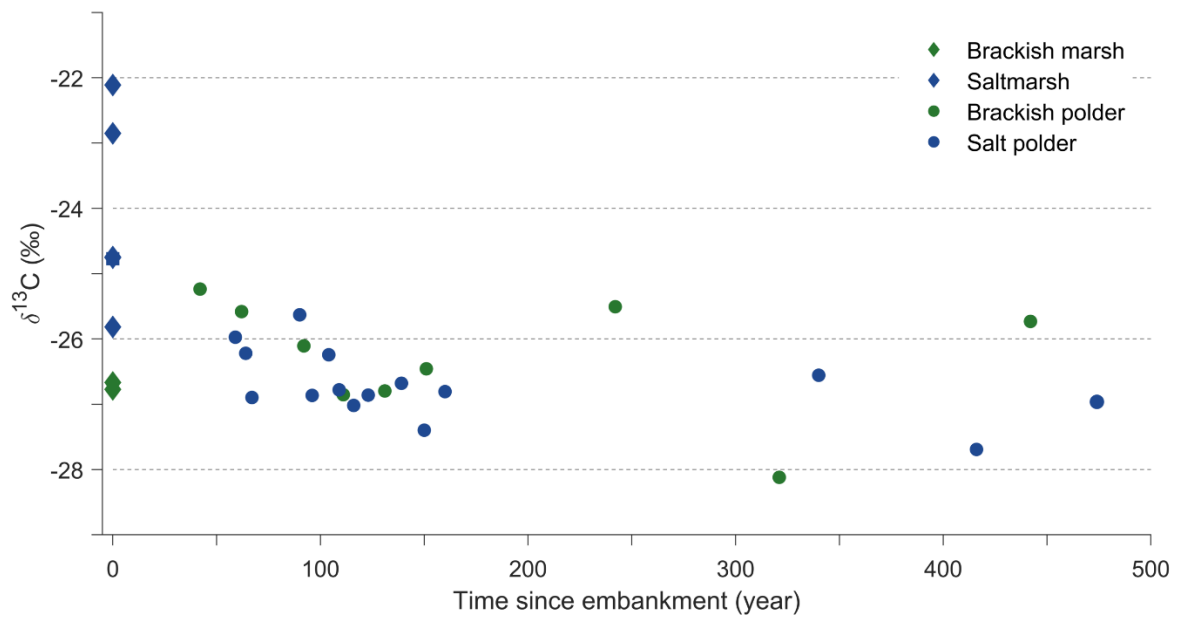


**Figure 4-5**  $\delta^{13}\text{C}$  values (‰) of OC in the uppermost  $400 \text{ kg m}^{-2}$  of sediments in both present-day tidal marsh sediments and embanked polder soils.

#### 4.3.5 Temporal changes in landscape-scale organic carbon stocks

The results of the 2D landscape simulations for regions 1 (brackish) and 2 (salt) are shown in Figure 4-6 - Figure 4-8. In the brackish region, the regions fringing the polder landscape containing the highest estimated SOC stocks (calculated for the upper  $400 \text{ kg m}^{-2}$  of sediments) are currently active tidal marshes (Figure 4-7). Moreover, in both simulated regions, spatial variations in estimated SOC stocks within and between the polders are observed, as a consequence of differences in (i) time since embankment and (ii) spatial variations in the thickness of deposited tidal marsh sediments.

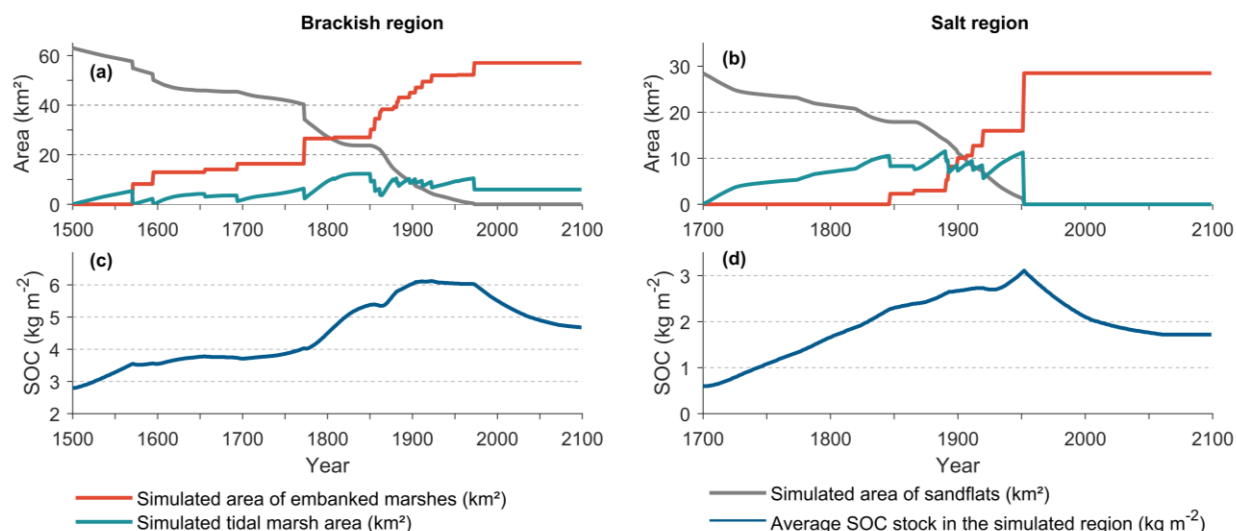


**Figure 4-6** Results of the landscape-scale OC model for the brackish (a, c) and salt (b, d) polders. The upper graphs (a, b) show the change in the simulated area covered by sandflats, tidal marshes and polders, while the lower graphs (b, d) show the simulated change in the average landscape-scale SOC stock for the upper 400 kg m<sup>-2</sup> of sediments, calculated for the entire simulated region (Figure 4-7 - Figure 4-8).

In the brackish region (Figure 4-6 (a) and (c)), the initial estimated average SOC stock, when the landscape consisted solely of tidal sandflats, was 2.80 kg OC m<sup>-2</sup>. Until 1773, the rate at which embankments took place was low and resulted in an approximately equal ratio between the area covered by tidal marshes and polders. Afterwards, the increasing area covered by tidal marshes led to a substantial increase in the average estimated OC stock to ca. 5.37 kg OC m<sup>-2</sup>. During the following period, 1862 – 1923, a substantial number of embankments led to a decrease in the average OC stock, after the maximum average estimated OC stock was reached (6.10 kg OC m<sup>-2</sup>). The last embankment in the region took place in 1973, after which the average estimated OC stock declined to reach an equilibrium of 4.70 kg OC m<sup>-2</sup> around the year 2100.

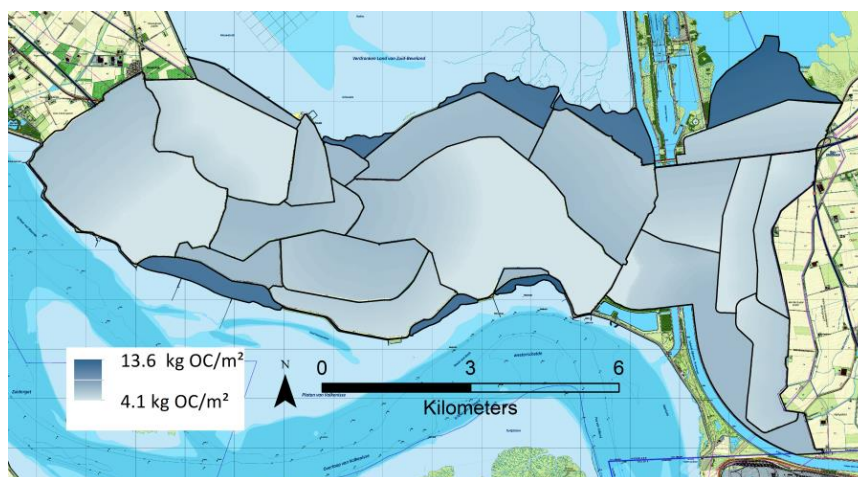


**Figure 4-7** Results of the landscape-scale SOC model for the brackish polder region (region 1), showing the estimated spatial distribution of SOC stocks in the upper 400 kg m<sup>-2</sup> of sediments (kg OC m<sup>-2</sup>) for the year 2100.

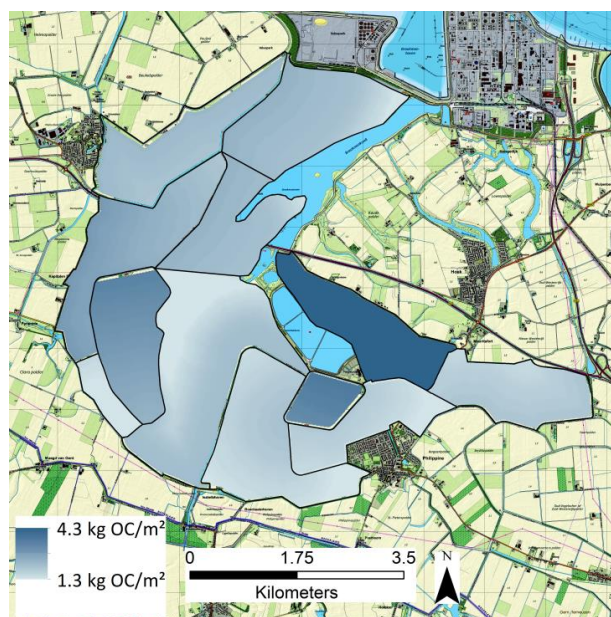


**Figure 4-8** Results of the landscape-scale SOC model for the salt polder region (region 2), showing the estimated spatial distribution of SOC stocks in the upper 400 kg m<sup>-2</sup> of sediments (kg OC m<sup>-2</sup>) for the year 2100.

For the salt polder region, the estimated average initial SOC stock was 0.59 kg OC m<sup>-2</sup> (Figure 4-6 (b) and (d)). During the first 150 simulation years no embankments took place, which resulted in a sharp increase in the average estimated SOC stock to 2.30 kg OC m<sup>-2</sup>. The subsequent embankments over the next century resulted in limited variations in the total area of tidal marshes and a small increase in the average estimated SOC stock to 3.11 kg OC m<sup>-2</sup>. After the last embankment in 1952 no new tidal marshes were initiated in this region, leading to a steep decline in the average estimated OC stock to a new equilibrium stock of 1.72 kg OC m<sup>-2</sup>.

#### 4.4 Discussion

##### 4.4.1 Organic carbon losses from embanked coastal marsh sediments

###### 4.4.1.1 Changes in soil organic carbon stocks

Tidal marshes located at different salinities along an estuary have been shown to differ substantially with regard to (i) the amount of OC that is present in their sediments and (ii) the sources from which this OC originates, as shown in chapter 2 and 3. In general, salt marshes trap OC from mainly marine sources and contain less SOC compared to brackish marshes, which trap a mixture of OC originating from marine and terrestrial sources. The higher SOC stocks in brackish marshes compared to salt marshes result in larger OC losses in the former (8.7 kg OC m<sup>-2</sup>; 86.6 g OC m<sup>-2</sup> yr<sup>-1</sup>) compared to the latter (6.8 kg OC m<sup>-2</sup>; 67.6 g OC m<sup>-2</sup> yr<sup>-1</sup>). These results thus suggest that the embankment of brackish marshes potentially results in more emission of CO<sub>2</sub>. The lower equilibrium SOC stock in polders originating from salt marshes results in similar relative OC losses in both systems (ca. 58 % of the initial SOC stock is lost after embankment in both regions).

Comparing these results with previously reported rates of SOC losses after the embankment of tidal marshes is not straightforward as most studies only report changes in OC concentrations while not converting these concentrations to changes in OC stocks (Cui et al., 2012; Ellis and Atherton, 2003; Iost et al., 2007). Studies reporting SOC stocks, however, usually do so by comparing SOC stocks down to a common depth between different sites. For example, Bu et al. (2015) report a loss of 21 % of the OC stock in the top meter after conversion, while Bai et al. (2013) and Deng et al. (2016) report declines in SOC stocks of 44 % (0 - 0.2 m depth) and 30 % (0 – 0.5 m depth) respectively. These studies, however, do not account for soil compaction after the embankment and subsequent drainage of coastal wetlands. This process has been shown to be very important, as relative increases in bulk density in the range of 25 – 50 % are generally reported for embanked tidal marsh sediments (Bai et al., 2013; Cui et al., 2014; Ellis and Atherton, 2003). This is also clear from our study sites, where relative increases in bulk density of 54 and 121 % were found in the brackish and salt polders respectively. Neglecting soil compaction when reporting changes in SOC stocks along a chronosequence can lead to a substantial underestimation of OC losses, as has been shown for terrestrial ecosystems (Don et al., 2011). Therefore, we strongly suggest that future studies explicitly account for changes in soil bulk density when calculating SOC losses along chronosequences.

The relative decline in OC stocks along the studied tidal marsh – polder chronosequences (-58 %) is substantially larger than reported declines in SOC stock after the conversion of forest to cropland in temperate (-32 ± 20 %) (Poeplau et al., 2011) and tropical ecosystems (-25 %) (Don et al., 2011). This is not surprising, as tidal marsh sediments generally contain more SOC compared to terrestrial forests (De Vos et al., 2015; Duarte et al., 2013), while OC stocks in the studied polder soils reach an equilibrium which is comparable to values found in the top 0.3 m of non-polder croplands in western Europe (Lettens et al., 2004).

#### 4.4.1.2 *Changes in organic carbon characteristics along the depth profile*

More insight in the dynamics of SOC cycling in converted tidal marsh soils is obtained by combining the observed depth profiles of SOC concentration and  $\delta^{13}\text{C}$  values. This is possible because the  $\delta^{13}\text{C}$  value of allochthonous OC inputs to the salt marshes (between -23 and -24 ‰, see chapter 3) is significantly different from the  $\delta^{13}\text{C}$  value of terrestrial vegetation (-25 - -30 ‰, with an average of -27 ‰ (Kohn, 2010)). This is reflected in the  $\delta^{13}\text{C}$  depth profiles of the salt polders (Figure 4-2d), where the  $\delta^{13}\text{C}$  value of SOC increases after conversion, from marine values in the salt marsh (ca. -21 ‰) to values associated with agricultural OC (-26 - -27 ‰ in the top 0.4 m).

On the brackish marshes the situation is different. Here, the  $\delta^{13}\text{C}$  values of deposited OC are between -27 and -28 ‰ (see chapter 3), while subsoil  $\delta^{13}\text{C}$  values in the active marsh are on average -25 - -26 ‰. Similar values are also found in the subsoil of the 41 years old polder (Figure 4-2b). Therefore, we hypothesize that after 1970, a substantial shift in the  $\delta^{13}\text{C}$  values of deposited OC on these marshes has taken place towards the more negative values that are currently observed. The timing of this proposed shift coincides with a significant intensification of dredging and sediment dumping activities in the beginning of the 1970's in

this portion of the estuary (Anon, 2010), which have a large effect on the sediment dynamics in the estuary (Jeuken et al., 2003; van Kessel et al., 2015). Despite these uncertainties on historical  $\delta^{13}\text{C}$  values of OC inputs to the brackish marshes, it is observed that the  $\delta^{13}\text{C}$  value of SOC in the brackish polder soils increases after reclamation, from values similar to the subsoil of the active tidal marsh (-25 - -26 ‰) to values closely related to terrestrial values (ca. -27 ‰ in the top 0.4 m) (Figure 4-2b).

The rate at which tidal marsh OC is replaced by OC originating from agricultural practices is substantially different between the top 0.4 m and deeper soil layers (Figure 4-2). In the top 0.4 m, which is intensively affected by ploughing and rooting, the  $\delta^{13}\text{C}$  values shift to terrestrial values (-27 ‰) on a timescale of ca. a century in all sampled chronosequences (see Figure S4-2 - S4-6 for all depth profiles). In addition, there is a clear difference in the time it takes for topsoil OC concentrations and  $\delta^{13}\text{C}$  values to reach equilibrium, indicating that although no major changes in the amount of OC occur ca. 60 years after conversion, there is still a substantial replacement of OC in these polder soils up till about a century after conversion.

In subsoils (> 0.4 m depth), the time over which  $\delta^{13}\text{C}$  values shift towards terrestrial values is substantially longer compared to the topsoils. Brackish polders up to ages of ca. 250 years have subsoil  $\delta^{13}\text{C}$  values between -25 and -26 ‰, indicating the presence of a substantial fraction of tidal marsh OC, while it takes ca. 320 years for subsoil OC to reach values of -27 ‰ (Figure S4-2). In the salt region, polders reclaimed < 167 years ago show subsoil  $\delta^{13}\text{C}$  values between -26 and -24 ‰. Only for the oldest polder, with an age of 415 years, subsoil  $\delta^{13}\text{C}$  values reach ca. 27 ‰ at a depth of 0.6 m (Figure S4-6). Although the lack of older polders in our analysis, our data shows that the time needed for the complete removal of tidal marsh OC and replacement with OC originating from agricultural crops is in the order of centuries for deeper soil layers.

The different rates of OC replacement in top- and subsoils is unlikely to be a consequence of differences in the intrinsic stability of SOC along these soil profiles. Organic carbon in tidal marsh sediments originates from locally produced biomass (both above- and belowground) and allochthonous OC deposits during inundation events. Although topsoil sediments (0 – 0.2 m) in tidal marshes generally contain a substantial amount of locally produced and relatively labile OC, the amount of allochthonous OC is relatively stable along the soil depth profiles, as shown in chapter 3. Therefore, it is unlikely that the intrinsic stability of OC along the soil profile of tidal marsh sediments is substantially different. In contrast, it is more likely that differences in mechanisms of OC inputs and soil disturbance along the soil profile of polder soils control the rates of OC replacement. In the topsoil, on the one hand, soil drainage and aeration (through ploughing) is expected to stimulate the decomposition of marsh OC and direct inputs of OC from crop residues and roots are likely to drive the rapid replacement of OC. In subsoils, on the other hand, leaching of DOC originating from the topsoil layers and subsequent interactions with the mineral phase of the soil is likely to control SOC replacement (Kaiser and Kalbitz, 2012; Schrumpf et al., 2013). These different mechanisms are hypothesized to result in lower rates of SOC replacement in the subsoil as compared to the topsoils.

#### 4.4.2 Additional organic carbon storage during stepwise embankments

Our data show that brackish and salt marsh sediments experience a reduction in SOC content of ca. 60 % upon embankment for agricultural purposes. This is in agreement with previous research, which has similarly reported large SOC losses upon the conversion of coastal wetlands (Pendleton et al., 2012). However, these analyses only consider SOC losses without considering additional SOC storage in newly created wetlands during stepwise embankment. To account for these geographical variations in losses and gains in SOC, a 2D model was created to simulate land use changes (from tidal sandflat to tidal marsh and subsequently to a polder) and to keep track of depth-dependent SOC stocks over time. It is noted that the aim of this modelling exercise was to assess the effect of stepwise embankments on regional-scale SOC stocks and not to accurately reconstruct historical SOC stocks, due to data limitations.

The model results (Figure 4-6 - Figure 4-8) show that in the polder landscapes, stepwise embankments of tidal marshes led to an increase in the average estimated landscape SOC stock of ca. 2 and 1.1 kg OC m<sup>-2</sup> in brackish and salt polders respectively, in the top 400 kg<sup>-2</sup> of sediments, compared to the initial sandflat situation. The initial estimated SOC stock for sandflats in the salt region (0.59 kg OC m<sup>-2</sup>) was substantially lower compared to the brackish region (2.80 kg OC m<sup>-2</sup>), as a consequence of the lower OC concentration of sandflat sediments in the former (0.06 – 0.51 % OC (Moens et al., 2005, 2002)) compared to the latter (0.67 – 1.4 % OC (Boschker et al., 1999; Middelburg et al., 1996)).

It is noted that the OC concentration of sandflat sediments is substantially lower compared to tidal marsh sediments, which have an organic carbon concentrations of ca. 2 % in the subsoil of brackish marshes. As both sandflat and tidal marsh sediments have an allochthonous origin (these are imported from both terrestrial and marine ecosystems), the lower OC concentration of sandflat sediments contrasts the finding that the high concentration of stable OC associated with allochthonous sediments is one of the main drivers of high OC stocks of tidal marsh sediments (see chapter 3). The contrasting grain size between sediments on sandflats (sand grain size) and in tidal marshes (clay-silt grain size) is likely to explain the main difference in the OC content of these sediments, as sand-sized sediments generally stabilize substantially less OC compared to silt- and clay-sized sediments (see e.g. Hansen et al. (2016) for an example of sediments in the Elbe estuary, Germany). This was also clear from the sampled brackish polders soils, where it was found that the sandflat remains found below the silt-sized former tidal marsh sediments contained substantially less OC (ca. 0.3 % OC) compared to the former silt-sized tidal marsh sediments (> 1.3 % OC) (data not shown).

The simulated equilibrium SOC stocks in the year 2100 are also significantly higher for the brackish polders (4.70 kg OC m<sup>-2</sup>) compared to the salt polders (1.72 kg OC m<sup>-2</sup>). This is a consequence of (i) the fact that sedimentation rates at the surface of brackish marshes are larger compared to salt marshes and consequently more OC-rich sediments are being deposited (Temmerman et al., 2004), (ii) higher equilibrium SOC stocks in the brackish polders (Table 4.2) and (iii) the fact that in the brackish region currently a substantial number of tidal marshes are present which store large amounts of SOC, which is not the case in the salt region.

The latter is also clear from the model results, which show that simulated landscape-scale SOC stocks are the largest at times the area covered by tidal marshes is the largest. This shows that a management strategy which aims to increase SOC storage in intertidal landscapes should be to minimize the area covered by polders and to maximize the area covered by tidal marshes, which additionally provide a wide range of beneficial ecosystem services (Barbier et al., 2011).

To the best of our knowledge, this is the first study that accounts for additional SOC storage during stepwise embankment of coastal wetlands. However, Bai et al. (2013) reported increasing regional SOC stocks after the conversion of tidal marshes due to additional OC storage in ditches in the reclaimed region. In addition, Huang et al. (2010) found that the conversion of terrestrial marshland to cropland in a large region in northeast China (Sanjiang plain, 11 Mha) resulted in reduced regional greenhouse gas emissions, despite large losses of SOC upon the conversion of the marshes. The observed reduction in greenhouse gas emissions was mainly a consequence of reduced methane (CH<sub>4</sub>) emissions due to a reduction in the area occupied by marshland, a large CH<sub>4</sub> source. It is noted that these authors only studied freshwater systems, which hampers a direct comparison with the results presented here.

It should be noted that the model results indicating increasing regional SOC stocks as a consequence of the stepwise embankment of tidal marshes is only valid when the embankment process is triggering the growth of a new tidal marsh at the seaward side of the embankment. If this would not be the case, it can be hypothesized that the entire initial sandflat would be covered by tidal marshes as a consequence of natural marsh progradation. In this case, these regions would of course store more OC than in the current situation. Previous studies in other estuaries have found that the constructions of embankments led to a reduction of the tidal prism, i.e. the volume of ebb discharge during a tidal cycle, and therefore lower water velocities and increasing rates of sediment deposition after embankment construction (Cuvilliez et al., 2009; Gregory Hood, 2004; Xie et al., 2017). In the Scheldt estuary, in contrast, no reduction in the volume of the tidal prism was observed over the past centuries, as the reduction in the size of intertidal surface area was compensated by an increase in the celerity and amplitude of the tidal wave (Van den Berg et al., 1996). As the modelled polder regions were located in small 'intertidal basins' fringing the estuary (Figure 4-1) it is, however, possible that the volume of the local tidal prism in these basins was reduced after the construction of each embankment, therefore promoting sediment deposition. In addition, there has been a net import of sand into the estuary over the past centuries (Van den Berg et al., 1996). As a consequence of the reduction in intertidal area in the intertidal basins due to embankments of tidal marshes, this sediment has been deposited on a smaller surface area over time, which also potentially led to increasing sedimentation rates as a consequence of tidal marsh embankments. Moreover, based on a reconstruction of an intertidal landscape in the Scheldt estuary, Jongepier et al. (2015) have shown that marshes growing against an embankment expand rapid laterally in the first decade after embankment construction (40 – 200 m year<sup>-1</sup>). The average rate of lateral expansion for marshes older than ca. 20 years is much lower (< 10 m year<sup>-1</sup>). This suggests that the rate at which a tidal marsh expands can be affected by the construction of embankments. Although

no direct evidence is present, these hypotheses suggest that the process of stepwise embankments has positively affected marsh progradation in the studied regions over the past centuries.

#### **4.4.3 Limitations and opportunities**

There are some limitations associated with the empirical approach applied in this study. First, our approach neglects (i) spatial variations in SOC concentrations in the sampled polders and (ii) variations in the thickness of former tidal marsh sediments in the polders. Both are expected, as Jongepier et al. (2015) have shown that spatial variations in soil grain size and the depth of former marsh sediments varies in polders within the Scheldt estuary. Therefore, care has to be taken when extrapolating reported losses in SOC stock to the total polder area, as regions with less thick former marsh sediments potentially lose less OC compared to locations where these sediments are thicker.

Although novel, our approach of applying a 2D landscape model to reconstruct land use changes in polder landscapes is affected by uncertainties. A first set of uncertainties is associated with the input parameters used to run the model, such as (i) the OC concentration of former tidal flats, (ii) depth profiles of tidal marsh OC concentration, (iii) the assumption that this has remained constant through time and (iv) historical rates of sea level rise which drive the rate of sediment deposition on the tidal marshes. Despite the lack of detailed data for some variables, it should be noted that the geomorphology of and SOC dynamics in tidal marshes and polders have been studied extensively in the Scheldt estuary (e.g. Van de Broek et al., 2016, 2018; Jongepier et al., 2015; Temmerman et al., 2003, 2004), rendering this a unique study area to assess the effect of tidal marsh embankment on SOC stocks. Secondly, uncertainty on the model results arises from the fact that the model could not be validated due to a lack of data on spatial pattern of both SOC stocks and the thickness of former tidal marsh sediments in the studied regions.

In spite of these shortcomings, the presented study has offered novel insights in SOC dynamics in converted intertidal landscapes and offers multiple opportunities for future work. First, it provides a framework to assess the effect of future embankments of intertidal regions. This is important in countries like China, where many projects to convert coastal wetlands are planned in the near future (Ma et al., 2014; Wang et al., 2014). Secondly, the current study does not consider regional scale changes in emissions of carbon dioxide (CO<sub>2</sub>), methane (CH<sub>4</sub>) and nitrous oxide (N<sub>2</sub>O), which differ between tidal marshes and polders (Huang et al., 2010). As SOC dynamics are well constrained in both tidal marsh (see chapters 2 and 3) and polder soils of the Scheldt estuary, this is an ideal study area to study the effect of embankments of tidal marshes on emissions of these potent greenhouse gases. Last, this study has shown that OC stored in tidal marshes is lost from these sediments rapidly after the conversion to cropland. This contrasts with earlier findings that an important fraction of OC in the studied tidal marsh sediments has been deposited as allochthonous OC during tidal inundations, which is up to millennia old and was not mineralized during transport from upland areas, through rivers to the estuary, and is therefore presumable very stable as shown in chapter 3. Draining these soils, however, causes the release of the majority of this millennia old OC on a

timescale of ca. a century. These tidal marsh – polder chronosequences thus offer a natural laboratory to study protection mechanisms of SOC, in addition to the dynamic replacements of OC from different sources.

#### **4.5 Conclusion**

In this study, we assessed the effect of the stepwise embankment of tidal marshes on SOC stocks in the Scheldt estuary (The Netherlands). Our results show that upon embankment, the absolute amount of SOC lost from brackish marsh sediments ( $8.7 \pm 0.5 \text{ kg OC m}^{-2}$  at a rate of  $86.6 \pm 5.1 \text{ g OC m}^{-2} \text{ yr}^{-1}$ ) is larger than SOC losses from salt marsh sediments ( $6.8 \pm 0.3 \text{ kg OC m}^{-2}$  at a rate of  $112.8 \pm 4.8 \text{ g OC m}^{-2} \text{ yr}^{-1}$ ), while the time to reach a new equilibrium SOC stock is considerably shorter in polders originating from salt marsh sediments (< 60 years) compared to polder soils originating from brackish marsh sediments (ca. 100 years). Moreover,  $\delta^{13}\text{C}$  depth profiles showed that the time over which tidal marsh OC is replaced by terrestrial OC can be substantially longer compared to the time needed for total OC stocks to reach equilibrium. In addition, a 2D landscape model was constructed to simulate how the average landscape-scale SOC stock changes during the stepwise embankment and subsequent progradation of tidal marshes. Model results showed that despite large losses of SOC locally within the embanked marshes, the average landscape-scale OC stock increased with ca. 2 and 1.1  $\text{kg OC m}^{-2}$  in brackish and salt polders respectively, compared to the initial situation when only tidal sandflats were present. This additional OC storage is a consequence of marsh progradation after embankment construction in both the brackish and salt marsh regions. These results emphasize that accounting for additional OC storage during the reclamation of coastal wetlands is necessary to correctly assess the effect of these management practices on changes in regional SOC stocks.



## Chapter 5 Assessing the uncertainty on predictions of soil organic carbon stocks in tidal marsh sediments using mid-infrared spectroscopy

---

**Abstract.** Tidal marshes are coastal ecosystems which store large amounts of organic carbon (OC). Reducing the current uncertainty on the total amount of OC stored in tidal marsh sediments requires the analyses of a large number of sediment samples. Soil sensing techniques, using m-IR spectroscopy combined with partial least squares regression (PLSR), have been proven to be a valid alternative for standard OC measurements in a wide range of terrestrial ecosystems. However, the application of m-IR spectroscopy/PLSR to tidal marsh sediments has been very limited and the error associated with calculated sedimentary OC stocks using m-IR spectroscopy/PLSR data has up till now not been assessed. Therefore, we used m-IR spectroscopy/PLSR to predict the total OC stock and associated errors of tidal marsh sediments in a temperate estuary (Scheldt estuary, Belgium and The Netherlands). Our results show that m-IR spectroscopy/PLSR predicts the OC concentration of tidal marsh sediments along the entire estuary with a high accuracy ( $R^2 = 0.94$ , RMSE = 0.56 % OC) while an optimal PLSR model can be obtained using only 70 samples with a known OC concentration. Moreover, combining depth profiles of predicted OC concentrations with measured bulk densities resulted in predictions of total OC stocks with a relative error < 3 % for freshwater and brackish marshes while errors for saltmarshes were up to 40 %. As m-IR spectroscopy/PLSR is not able to accurately predict bulk density or OC density, standard field measurements of bulk density remain currently necessary to reliably predict sedimentary OC stocks in tidal marshes using this technique. This study shows the potential of m-IR spectroscopy/PLSR to predict OC stocks of tidal marsh sediments characterized by a large variety in quantity and quality of OC, although the spatial scale at which the model is applied is an important factor controlling the accuracy of OC concentration predictions.

## 5.1 Introduction

Tidal marshes are highly productive vegetated coastal ecosystems storing large amounts of sedimentary organic carbon (OC) (Duarte et al., 2013; Mcleod et al., 2011). Because of their presence in climatologically and geomorphologically diverse settings (Mcowen et al., 2017), large variations in the characteristics of OC stored in tidal marsh sediments exist, while OC concentrations vary substantially with depth (Hayes et al., 2017; Kelleway et al., 2016; Van de Broek et al., 2016) as well as in space (Chen et al., 2016; Choi et al., 2001; Elschot et al., 2015). As a result, total OC stocks in tidal marsh sediments show large variations (Duarte et al., 2013; Ewers Lewis et al., 2017; Schile et al., 2017) and data on the OC concentration of a large number of soil samples are required to accurately estimate the amount of SOC stored in these sediments.

Multiple studies have shown the potential of diffuse reflectance spectroscopy in the visible and near (vis-NIR) or the mid infrared (m-IR) domain, also referred to as soil sensing, as a fast and cost-efficient method for the prediction of multiple physical and chemical soil properties (Baldock et al., 2013; Bellon-Maurel and McBratney, 2011; Minasny et al., 2008; Reeves et al., 1999; Reeves III, 2010; Viscarra Rossel and Bouma, 2016; Viscarra Rossel et al., 2006). Soil sensing involves the acquisition of a soil spectrum, which is a measure for the amount of reflected radiation in a part of the electromagnetic spectrum. These spectra are subsequently processed using linear regression methods (e.g. principal component regression (PCR) or partial least squares regression (PLSR)) or machine learning techniques (e.g. support vector machines (SVM) or artificial neural networks (ANN)) to predict soil properties based on a calibration dataset for which measured data is available (Dotto et al., 2018; Igne et al., 2010; Kang et al., 2017; Vasques et al., 2008). These methods have been applied at a wide range of spatial scales, from regional (Bornemann et al., 2010; Jia et al., 2017) to continental (Baldock et al., 2013; Reeves and Smith, 2009; Stevens et al., 2013), to successfully predict soil properties. In addition, the construction of large libraries of soil spectra (e.g. Stevens et al., 2013; Viscarra Rossel et al., 2016), combined with the development of methods to efficiently sample these libraries (e.g. Lobsey et al., 2017) significantly contributes to the potential of soil sensing as a valuable alternative for standard methods for the analysis of soil properties.

Despite the fact that soil sensing techniques have been shown to provide reliable estimates of soil organic carbon (SOC) concentrations in terrestrial ecosystems, their application to intertidal sediments has been limited to Australian tidal marshes, where the methods developed by Baldock et al. (2013) are generally applied (e.g. Ewers Lewis et al., 2017; Hayes et al., 2017; Macreadie et al., 2017). Moreover, the potential error associated with m-IR predictions of the OC concentration of tidal marsh sediments, and how this error affects calculated SOC stocks, has to date not been investigated. Although the accuracy of m-IR predictions has been assessed for terrestrial soils (see many of the references in the previous paragraph) these findings cannot be directly transferred to tidal marsh environments for two main reasons. First, OC concentrations found in tidal marsh sediments exhibit a range which is substantially larger compared to most terrestrial soils (Bouillon and Boschker, 2006). Second, and more important, the quality of OC in tidal marsh sediments is substantially different from terrestrial soils. Tidal marsh OC is a mixture of terrestrial, marine and estuarine

OC, which are found in different ratios in tidal marsh sediments depending on their location along an estuary (see chapters 2 and 3). In addition, the physical mechanisms stabilizing OC in tidal marsh sediments vary, as freshwater marsh sediments can contain a substantial amount of locally produced plant material and aggregation can efficiently preserve SOC. In saltmarshes, in contrast, fresh plant material can be rapidly mineralized upon burial and aggregates have a low capacity to protect OC from mineralization, as shown in chapter 3. Therefore, calibration models developed from terrestrial soil may not be directly transferable to intertidal sediments. It is also unclear whether a single calibration model can be used to predict the variation of OC concentrations within a whole estuary, or if multiple models are necessary for regions with distinct SOC characteristics.

In this study we made an assessment of the potential of m-IR spectroscopy to provide reliable estimates of the OC stocks of tidal marsh sediments along a temperate macro-tidal estuary. More specifically, our aims were to (i) find the optimal spatial scale in the estuary to obtain the best PLSR model to predict SOC concentrations, (ii) assess the accuracy of predictions of SOC concentrations using m-IR spectroscopy, (iii) determine the minimum size of the calibration dataset needed to obtain an optimal PLSR model and (iv) assess the error associated with SOC stocks calculated using m-IR spectroscopy/PLSR.

## 5.2 Material and methods

### 5.2.1 Study site and sample processing

Soil depth profiles from 10 tidal marshes along the Scheldt estuary (Belgium and The Netherlands, salinity 0.3 – 30) were used for this study (Figure S5-1). The dataset included a total of 325 soil samples from 4 freshwater marshes (salinity 0 – 5, n = 141, 6 depth profiles), 2 brackish marshes (salinity 5 – 18, n = 84, 4 depth profiles) and 4 saltmarshes (salinity > 18, n = 100, 8 depth profiles). For all but two tidal marshes, both (i) a location located above the local mean high water level (MHWL) and (ii) a location which is nowadays located below MHWL, or was located below this level during most of the past decades, were sampled. The study sites and the sample collection methodology are described in detail in chapter 2 and 3. In short, at every sampling location soil cores were collected using a gouge auger for the analyses of (i) bulk density (3 replicate depth profiles) and (ii) general soil properties (3 replicate depth profiles). These replicates were collected a couple of meters apart from each other, to represent small-scale spatial differences in these variables. Samples for general soil properties were collected at a depth resolution of 0.03 m while soil samples for bulk density were collected at depth increments of 0.05 m (0 - 0.05 m, 0.10- 0.15 m etc.). The maximum sampling depth ranged from 0.2 to 1.8 m, depending on the thickness of the tidal marsh sediments.

Soil samples for bulk density were dried at 105 °C for 24 hours. The soil samples for the determination of other soil properties were dried at 50 °C and crushed to < 2 mm using a mortar and pestle, after which macrovegetation residues and roots were removed manually using tweezers. At every sampling site, samples from one of the three replicate soil profiles were analyzed for OC using an Elemental Analyzer (FlashEA 1112 HT, Thermo Scientific), after the removal of carbonates using a 10 % HCl solution. This data will be referred to as OC%<sub>meas</sub>.

For 2 locations in each salinity zone, samples from the other two replicate soil cores were also analyzed for OC concentration using the Elemental Analyzer (Figure S5-1). In the analyses below, it was assumed that measurements of  $OC\%_{meas}$  and bulk density were free from errors.

### 5.2.2 Spectroscopy measurements

For each soil sample, soil spectra were obtained for five subsamples for wavenumbers between 4000 and 400  $cm^{-2}$  at a resolution of 4  $cm^{-2}$ , using a PerkinElmer® Frontier FT-IR spectrometer which was coupled to a PIKE® XY autosampler. Before scanning, the soil samples were ground to a powder and transferred to a well plate with 96 wells without pressing or flattening the surface. The average reflectance spectrum of the 5 replicates of each soil sample was then combined with the average reflectance spectrum of 5 replicates of a KBr powder, which served as a background, to calculate the absorbance spectrum for further analyses (absorbance =  $\log(R^{-1})$ , R being the ratio of the soil reflectance over the KBr reflectance). Predicted OC concentrations using m-IR spectroscopy/PLSR are referred to as  $OC\%_{m-IR}$ .

### 5.2.3 Data analyses

We used Partial Least Squares Regression (PLSR) to predict the OC concentration from the spectral information. PLSR analyses were performed in R (R Core Team, 2017) using the *prospectr* package (Stevens and Ramirez Lopez, 2014). Before analyses, the soil spectra were smoothed using Savitsky-Golay filtering (3<sup>rd</sup> order polynomial, 9  $cm^{-1}$  moving window, no derivative), according to Vasques et al. (2008). Principal Component Analysis (PCA) was applied to the measured spectra to assess differences in spectral characteristics between samples from different salinity zones.

#### 5.2.3.1 Finding the optimal PLSR model

Several approaches were tested to obtain the optimal PLSR model. First, the analyses using  $OC\%_{meas}$  as the dependent variable were complemented with analyses using a square root- and a logarithmic transformation of  $OC\%_{meas}$ , as proposed by Baldock et al. (2013). Second, analyses were performed using different spectral pre-processing methods: (i) no pre-processing, (ii) a scatter-corrective pre-processing (Standard Normal Variate; SNV) and (iii) a spectral-derivative pre-processing (Savitsky Golay Filtering, 1<sup>st</sup> derivative, 1<sup>st</sup> order polynomial; SG). We justify the comparison of only three methods based on the fact that multiple studies have shown that the effect of pre-processing on the accuracy of OC concentration predictions is limited (Baldock et al., 2013; Dotto et al., 2018; Igne et al., 2010). Third, the number of latent variables included in the PLSR model was varied from 1 to 20. The choice of the optimal number of latent variables was based on a visual analysis of the goodness of fit (GOF) measures (see below) in function of the number of latent variables included in the model. It was made sure that the optimal number of latent variables resulted in good GOF values, while not unnecessarily including more latent variables than needed to avoid overfitting. Finally, as the source of OC in tidal marsh sediments in the Scheldt estuary shows a clear gradient from mainly terrestrial-derived OC in freshwater marshes to mainly

marine OC in saltmarshes (as shown in chapter 3), separate analyses were performed for samples from (i) the freshwater marshes, (ii) the brackish marshes, (iii) the saltmarshes (referred to as 'local models') and (iv) all tidal marshes combined (referred to as 'general model'). The GOF measures used to quantify the performance of each combination of parameters are the Pearson  $R^2$ , the root mean square error of prediction (RMSE), ratio of performance to interquartile distance (RPIQ, Bellon-Maurel et al., 2010), the percentage of variance explained by the PLSR model ( $\%var_{exp}$ ) and the average absolute and relative deviation between measured and predicted values ( $e_{abs}$  and  $e_{rel}$  respectively). For every combination of model parameters as described above, 100 runs were performed with randomly chosen calibration (2/3 of the dataset) and validation samples (1/3 of the dataset). The resulting GOF measures are expressed as the mean  $\pm$  standard deviation ( $\sigma$ ) based on the results from these 100 runs. Transformed values of OC were re-transformed to OC concentration before calculation of the GOF measures.

### 5.2.3.2 Finding the optimal number of calibration samples

Next, the minimum number of soil samples with measured OC concentrations necessary to construct the optimal PLSR model was determined. Therefore the optimal general model, as determined in the first part of this study, was ran using an increasing number of calibration samples (from  $n+1$  to 100, with  $n$  being the number of PLSR latent variables). The calibration samples were determined using the Kennard-Stone algorithm with mahalanobis distances (Kennard and Stone, 1969) to include the maximum amount of variance in the calibration dataset. To create a representative validation dataset for the entire estuary, an equal number of validation samples were chosen from the freshwater, brackish and salt marshes ( $n=40$  for each salinity zone).

### 5.2.3.3 Assessing the error of predicted soil organic carbon stocks

In a final step, the accuracy of predicted OC stocks using m-IR spectroscopy/PLSR was determined. Three different strategies involving m-IR spectroscopy/PLSR were applied to calculate total sedimentary OC stocks:

1. Combining depth profiles of  $OC\%_{m-IR}$  with measured bulk density data, referred to as  $OC_{m-IR}$
2. Combining depth profiles of  $OC\%_{m-IR}$  with m-IR spectroscopy/PLSR predictions of bulk density ( $BD_{m-IR}$ ) values, referred to as  $OC-BD_{m-IR}$
3. m-IR spectroscopy/PLSR predictions of the OC density, the known value of which is calculated by multiplying the measured BD data [ $kg\ m^{-3}$ ] with measured OC concentrations, referred to as  $OCdens_{m-IR}$  [ $kg\ OC\ cm^{-3}$ ]

Total SOC stocks were calculated for both the low- and high portion of one tidal marsh in every salinity zone (Figure S5-1), for which measured depth profiles of OC concentration and bulk density were available in three replicates. The PLSR model for the prediction of the OC concentrations was constructed using the global model with the minimum number of necessary calibration samples. The procedures applied for the prediction of  $OC-BD_{m-IR}$  and  $OCdens_{m-IR}$  were identical to the above described methods for  $OC_{m-IR}$ . However, the selection

of the samples using the Kennard-Stone algorithm was done separately for each variable. Prior to the construction of the PLSR model, the soil samples that were being predicted were removed from the calibration dataset. The propagation of uncertainty associated with PLSR predictions to the uncertainty of the calculated SOC stock was calculated as follows:

$$\sigma_{tot} = \sqrt{(\sigma_{spat}^2 + \sigma_{m-IR}^2)}$$

Where  $\sigma_{tot}$  is the calculated standard deviation of the total SOC stock,  $\sigma_{spat}$  is the standard deviation associated with spatial differences based on the three replicate soil cores and  $\sigma_{m-IR}$  is the calculated standard deviation associated with the uncertainty on the PLSR predictions. As the aim of this exercise was to assess the difference between SOC stocks calculated using standard methodologies (bulk density determination and OC analyses using an Elemental Analyzer) and m-IR spectroscopy/PLSR, it was assumed that SOC stocks calculated using standard procedures (measured OC % and bulk density) were free from errors. The extent to which the measured and predicted SOC stocks were significantly different was assessed using an ANOVA for summary data at a confidence level of 0.05 in R (*ind.oneway.second* function, *rpsychi* package (Okumura, 2015)).

The uncertainty of predicted OC concentrations using m-IR spectroscopy/PLSR ( $\sigma_{m-IR}$ ) was calculated using the residuals of the OC concentrations predicted with the global model for all available soil samples, after doing 100 runs with randomly chosen calibration (2/3 of total samples) and validation samples (1/3 of total samples). First, the residuals (measured - predicted OC concentration) were sorted according to increasing predicted OC concentration. Next, the standard deviation of the residuals was calculated for neighboring samples using a moving average (window size = 21), as a measure of the spread of the measured values around the predictions. Subsequently, a linear relationship between the modelled OC concentrations and these standard deviations was constructed to report the error on predicted OC concentration as a standard deviation around the predicted value (Figure S5-5).

## 5.3 Results and discussion

### 5.3.1 Characterization of the dataset

The average ( $\pm \sigma$ ) OC concentration of the freshwater, brackish and salt marsh samples were  $6.09 \pm 1.96$ ,  $3.77 \pm 2.42$  and  $2.88 \pm 1.6$  % OC respectively (Figure S5-2). The freshwater data was left-skewed (Skewness = -0.41), while the brackish- and saltmarsh data were right-skewed (Skewness = 2.63 and 1.99 respectively). More characteristics of the dataset can be found in Figure S2. The PCA scores of the soil spectra on the first two components showed a limited overlap between the freshwater and salt marshes, while brackish marshes are located at their interface (Figure S5-3). This is in line with reported differences in OC quality and protection mechanisms between freshwater marshes (mainly terrestrial OC), salt marshes (mainly marine OC) and brackish marshes (a mixture of both sources) (see chapter 3).

### 5.3.2 Determination of the optimal PLSR model

The optimal predictions of OC concentration were obtained when no pre-processing was applied to the spectra, although differences with SNV pre-processing were minimal. SG pre-processing resulted in unsatisfactory models in all cases (results not shown). For all models, a square root transformation of the OC data lead to optimal results, although the differences with a logarithmic transformation and no transformation of the data were minimal. Furthermore, the performance of the general model ( $R^2 = 0.96$ , RMSE = 0.48 % OC) was similar to the performance of the local models ( $R^2 = 0.87 - 0.97$ ; RMSE = 0.28 – 0.68 % OC). This shows that a model calibrated on sediment samples along the entire estuary results on average in accurate predictions of OC concentration. In contrast, the accuracy of both bulk density and OC density predictions was substantially lower, with optimal RMSE values of  $0.64 \pm 0.09 \text{ g cm}^{-3}$  and  $8.28 \pm 3.41 \text{ kg OC m}^{-3}$  respectively (Table 5.1).

The optimal models (in bold in Table 5.1) were subsequently used to assess the accuracy of predictions of OC concentration. The results confirm the good fit between  $\text{OC}\%_{\text{m-IR}}$  and  $\text{OC}\%_{\text{meas}}$  for both the local (Figure 5-1a,b and c) and general models (Figure 5-1d), with an absolute average error ( $e_{\text{abs}}$ ) of 0.4 % OC for the general model. The  $e_{\text{abs}}$  of OC prediction for samples from the freshwater and brackish marshes was similar when using the local and general models, while the  $e_{\text{abs}}$  for saltmarshes was substantially higher when using the general model (0.22 vs 0.30 % OC, Figure 5-1d). Analyses of the residuals of the results of the global model showed a linear relationship between  $\text{OC}\%_{\text{m-IR}}$  and the uncertainty, expressed as the standard deviation of measured values around  $\text{OC}\%_{\text{m-IR}}$ , of the form  $\sigma_{\text{m-IR}} = 0.067 + \text{OC}\%_{\text{m-IR}} \times 0.097$  (section 5.2.3.3, Figure S5-5). The RMSE (0.56 % OC) and  $R^2$  (0.94) of the optimal general model are very similar to characteristics obtained for m-IR spectroscopy/PLSR predictions of SOC concentrations in terrestrial ecosystems. Baldock et al. (2013) reported an  $R^2$  of 0.92 based on a dataset spanning a large portion of Australia, Jia et al. (2017) obtained a  $R^2$  and RMSE of 0.82 and 0.92 % OC respectively in an alpine landscape, Stevens et al. (2013) found RMSE values between 0.4 and 1.5 % OC for a dataset covering 23 European countries and Dotto et al. (2018) found an  $R^2$  and RMSE of 0.81 and 0.49 % OC respectively for a large region in southern Brazil (ca. 1800 km<sup>2</sup>). Moreover, these results are in line with  $R^2$  measures of models developed for Australian tidal marshes, which are in the range of 0.91 – 0.95 (Hayes et al., 2017; Macreadie et al., 2017).

The accuracy of predicted bulk density and OC density values is lower, with absolute average errors of  $0.1 \text{ g cm}^{-3}$  and  $5.15 \text{ kg OC m}^{-3}$  (Figure 5-1e). Similar difficulties in predicting soil bulk density were encountered in terrestrial environments using both NIR (Cambou et al., 2016; Moreira et al., 2009) and m-IR spectroscopy (Minasny et al., 2008). This low accuracy was expected as soil spectra were obtained from dried and ground soil samples. Alternatively, Lobsey and Viscarra Rossel (2016) have shown that a combination of gamma-ray attenuation and vis-NIR spectroscopy allows to accurately predict bulk density values of both wet and dried soil cores. Also the predicted OC densities showed a weak relationship with modelled values (Figure 5-1f,  $R^2 = 0.45$ , RMSE = 7.05 kg OC m<sup>-3</sup>). A relatively low accuracy of predicted OC densities has also been reported by Cambou et al. (2016) ( $R^2 = 0.70$ ) while

**Table 5.1** Results of the determination of the optimal PLSR model, shown for the different salinity zones (fresh – brackish – salt) and all data combined - the general model - (all), for OC concentration (OC), bulk density (BD) and OC density (OCdens). ‘sqrt’ and ‘log’ refer to the transformation of the data, ‘No’ indicates the set-up using no spectral pre-treatment. GOF measures show the average  $\pm$  standard deviation for 100 runs with randomly chosen calibration and validation samples. The model with the best performance per salinity zone is indicated in bold.

	Pre-processing method	# of latent variables	R <sup>2</sup>	RMSE	RPIQ	% var <sub>exp</sub>
Fresh OC	No	7	0.86 $\pm$ 0.04	0.71 $\pm$ 0.10	2.45 $\pm$ 0.65	97.11 $\pm$ 0.29
<b>Fresh OC – sqrt</b>	<b>No</b>	<b>6</b>	<b>0.87 <math>\pm</math> 0.04</b>	<b>0.68 <math>\pm</math> 0.10</b>	<b>2.57 <math>\pm</math> 0.70</b>	<b>96.44 <math>\pm</math> 0.19</b>
Fresh OC – log	No	6	0.86 $\pm$ 0.04	0.69 $\pm$ 0.09	2.53 $\pm$ 0.64	96.45 $\pm$ 0.24
Brackish OC	No	8	0.94 $\pm$ 0.03	0.46 $\pm$ 0.09	4.00 $\pm$ 1.25	98.50 $\pm$ 0.15
<b>Brackish OC – sqrt</b>	<b>No</b>	<b>5</b>	<b>0.97 <math>\pm</math> 0.02</b>	<b>0.41 <math>\pm</math> 0.12</b>	<b>4.30 <math>\pm</math> 1.48</b>	<b>97.07 <math>\pm</math> 0.42</b>
Brackish OC – log	No	6	0.95 $\pm$ 0.03	0.48 $\pm$ 0.28	4.71 $\pm$ 2.38	97.5 $\pm$ 0.29
Salt OC	No	9	0.94 $\pm$ 0.04	0.34 $\pm$ 0.06	4.44 $\pm$ 1.00	98.07 $\pm$ 0.17
<b>Salt OC – sqrt</b>	<b>No</b>	<b>9</b>	<b>0.96 <math>\pm</math> 0.02</b>	<b>0.28 <math>\pm</math> 0.06</b>	<b>5.65 <math>\pm</math> 1.17</b>	<b>98.06 <math>\pm</math> 0.18</b>
Salt OC – log	No	9	0.95 $\pm$ 0.03	0.33 $\pm$ 0.07	4.80 $\pm$ 0.99	98.02 $\pm$ 0.21
All OC	No	10	0.95 $\pm$ 0.01	0.54 $\pm$ 0.09	7.25 $\pm$ 1.29	98.15 $\pm$ 0.12
<b>All OC – sqrt</b>	<b>No</b>	<b>10</b>	<b>0.96 <math>\pm</math> 0.01</b>	<b>0.48 <math>\pm</math> 0.07</b>	<b>8.00 <math>\pm</math> 1.18</b>	<b>98.14 <math>\pm</math> 0.15</b>
All OC – log	No	10	0.95 $\pm$ 0.02	0.55 $\pm$ 0.09	6.93 $\pm$ 1.19	96.18 $\pm$ 0.14
<b>BD</b>	<b>No</b>	<b>4</b>	<b>0.64 <math>\pm</math> 0.09</b>	<b>0.13 <math>\pm</math> 0.02</b>	<b>2.45 <math>\pm</math> 0.41</b>	<b>88.4 <math>\pm</math> 1.72</b>
BD – sqrt	No	4	0.64 $\pm$ 0.08	0.13 $\pm$ 0.01	2.45 $\pm$ 0.41	87.7 $\pm$ 2.15
BD – log	No	4	0.66 $\pm$ 0.08	0.13 $\pm$ 0.02	2.50 $\pm$ 0.37	87.6 $\pm$ 1.95
<b>OCdens</b>	<b>No</b>	<b>5</b>	<b>0.51 <math>\pm</math> 0.12</b>	<b>8.28 <math>\pm</math> 3.41</b>	<b>1.86 <math>\pm</math> 0.59</b>	<b>91.5 <math>\pm</math> 1.31</b>
OCdens – sqrt	No	5	0.53 $\pm$ 0.15	8.74 $\pm$ 3.97	1.85 $\pm$ 0.76	91.76 $\pm$ 1.58
OCdens – log	No	5	0.53 $\pm$ 0.19	8.94 $\pm$ 4.31	1.85 $\pm$ 0.84	91.64 $\pm$ 2.11

Vågen and Winowiecki (2013) used m-IR spectroscopy to predict SOC densities but did not report accuracy measures.

### 5.3.3 Minimal size of the calibration dataset

The relationship between the number of samples included in the calibration dataset, identified using the Kennard-Stone algorithm, and the model fit shows a decreasing model error when the size of the calibration set is increased up to 70 samples, while including more samples does not improve the PLSR model (Figure 5-2). This contrasts the commonly applied practice whereby ca. 2/3 of the total dataset is used for calibration while the remaining samples are used for validation, independent of the number of samples that is available (e.g. Dotto et al., 2018; Jia et al., 2017; Kuang and Mouazen, 2011). These results show that an optimal PLSR model can be constructed using a lower number of samples, thereby increasing the efficiency and even further reducing the cost of soil sensing techniques. A similar approach showed that the optimal number of calibration samples for the prediction of bulk density and OC density values were 70 and 80 samples respectively (data not shown).

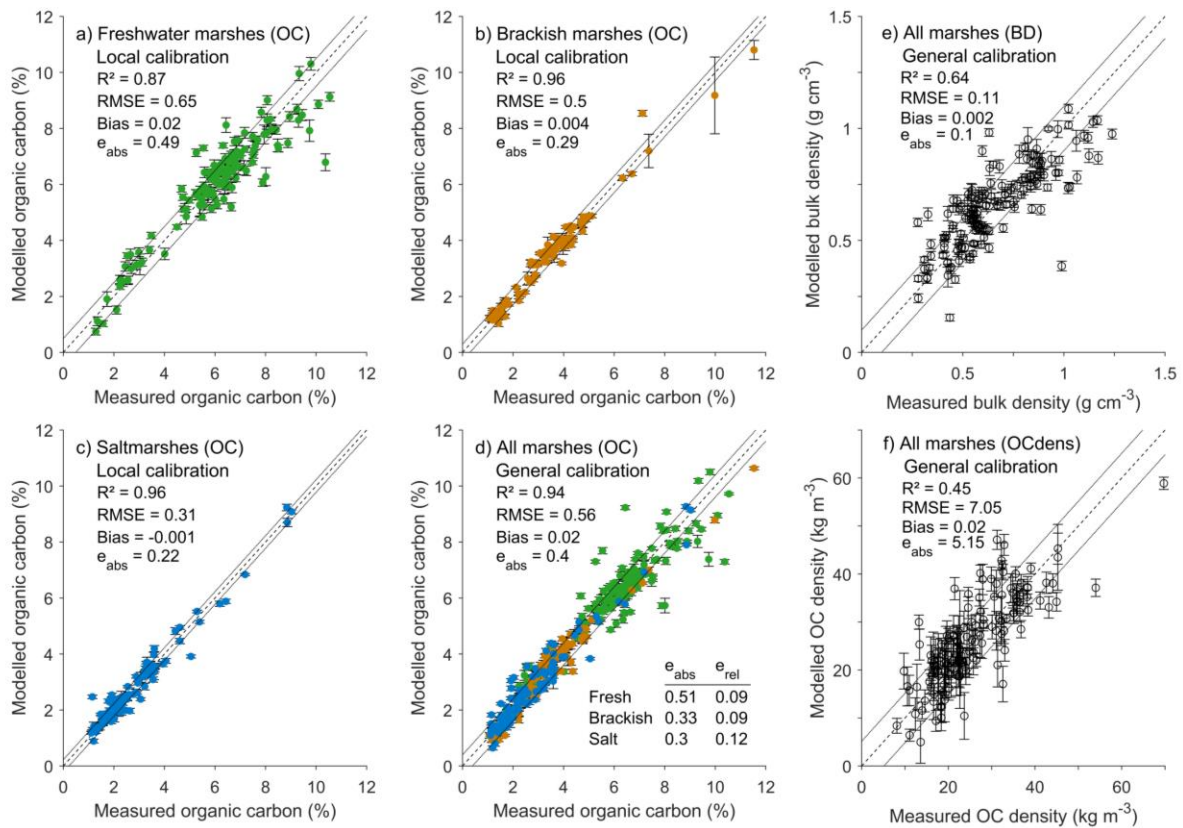


**Figure 5-1** Modelled versus the measured OC concentrations, based on the optimal PLSR models (Table 5.1). Plots a), b) and c) show the results for different salinity zones using the local models. Plot d), e) and f) show the validation results for OC concentrations, bulk density and OC stock respectively, using the general model. ‘ $e_{abs}$ ’ and ‘ $e_{rel}$ ’ are the average absolute and relative differences between modelled and measured values. Error bars show the standard deviation based on results with 100 randomly chosen calibration (2/3) and validation (1/3) datasets.

### 5.3.4 Errors associated with predicted organic carbon stocks

In the final step, OC concentrations were calculated for soil samples from a low- and high-lying location on 3 tidal marshes with the global model, after removing these samples from the calibration dataset. The measured ( $OC\%_{meas}$ ) and modelled ( $OC\%_{m-IR}$ ) depth profiles of OC concentration are very similar for the freshwater and brackish marshes, while the fit for the saltmarshes was less good (Figure 5-3). The results for bulk density values were substantially worse, as both depth patterns and absolute values showed a poor match (Figure S5-4).

The calculated total OC stocks differ significantly in their accuracy for the different methods (see section 5.2.3.3) (Figure 5-4). Organic carbon stocks predicted using  $OC\%_{m-IR}$  and measured bulk density depth profiles ( $OC_{m-IR}$ ) were very similar to the measured OC stocks, with relative errors for the freshwater and brackish marshes < 3 % and none of the predicted stocks being significantly different. For the saltmarshes, in contrast, relative errors were higher (20 – 42 %) and predicted SOC stocks were significantly different from the measured stocks.

The lower accuracy of predicted SOC stocks for saltmarsh sediments is a direct consequence of the lower accuracy of the predictions of OC concentration (Figure 5-3). This is also clear from Figure 5-1d, which shows that the relative error associated with predictions of OC

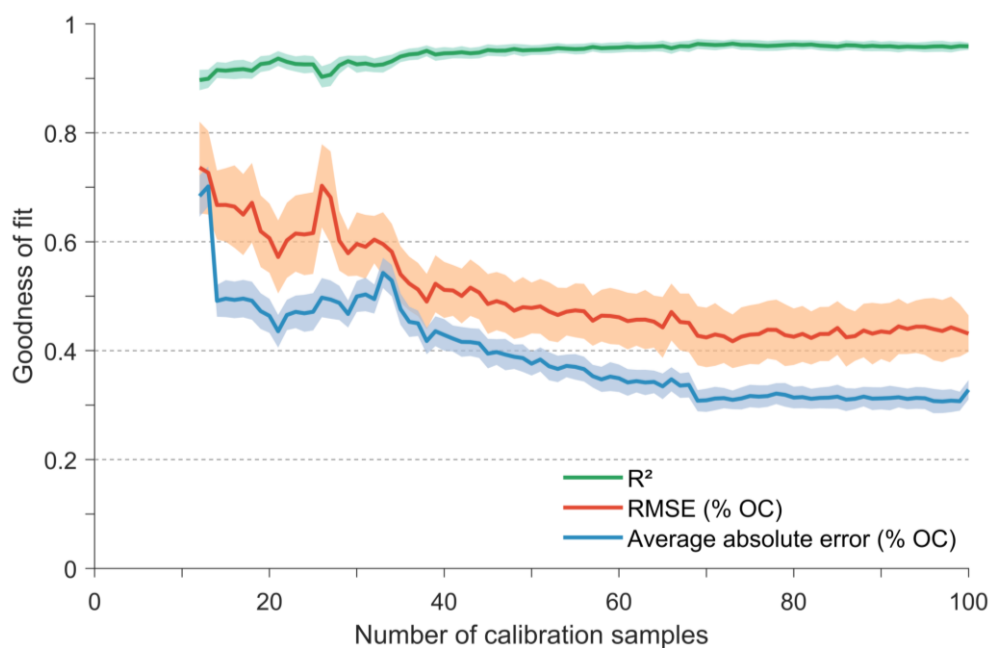


**Figure 5-2** R<sup>2</sup>, root mean square error (RMSE) and the average absolute difference between OC%<sub>meas</sub> and OC%<sub>m-IR</sub> in function of the number of calibration samples used to construct the general PLSR model. Shadings represent the spread around the average (as a standard deviation) based on 100 runs with different randomly chosen validation datasets.

concentration for saltmarsh sediments (0.12) is higher compared to brackish and freshwater marshes (0.09). Moreover, while the absolute error on the prediction of OC concentrations for brackish and freshwater marshes is similar when using the local and global models, this error is about 50 % higher when the OC concentration of saltmarsh sediments is predicted with the global compared to the local model (Figure 5-1d). This shows that despite very good average goodness of fit measures for the global model, OC concentrations from salt marsh sediments are predicted less good compared to samples from brackish and freshwater marshes. These results show that care has to be taken when soil sensing is used to predict OC concentrations from sediment samples with a wide range of OC characteristics. However, the accuracy of predicted OC concentrations can be improved if the optimal spatial scale at which PLSR models are applied can be chosen based on a preliminary analysis.

Organic carbon stocks predicted using (i) predicted bulk density values together with OC%<sub>m-IR</sub> and (ii) predicted OC densities differed substantially from the predicted OC stocks, with relative differences of -16.1 to +67.0 % and -43 to +64 % respectively. This shows that although m-IR spectroscopy/PLSR can reliably predict the OC concentration of tidal marsh sediments, this technique is not able to predict total OC stocks with an acceptable accuracy if supporting data on bulk density are lacking. Although other soil sensing techniques (gamma-ray attenuation combined with vis-NIR spectroscopy) have been shown to hold the potential to reduce the need for standard analyses of bulk density (Lobsey and Viscarra Rossel, 2016), measured bulk density profiles still need to be obtained in order to reliably predict OC stocks using m-IR spectroscopy/PLSR.

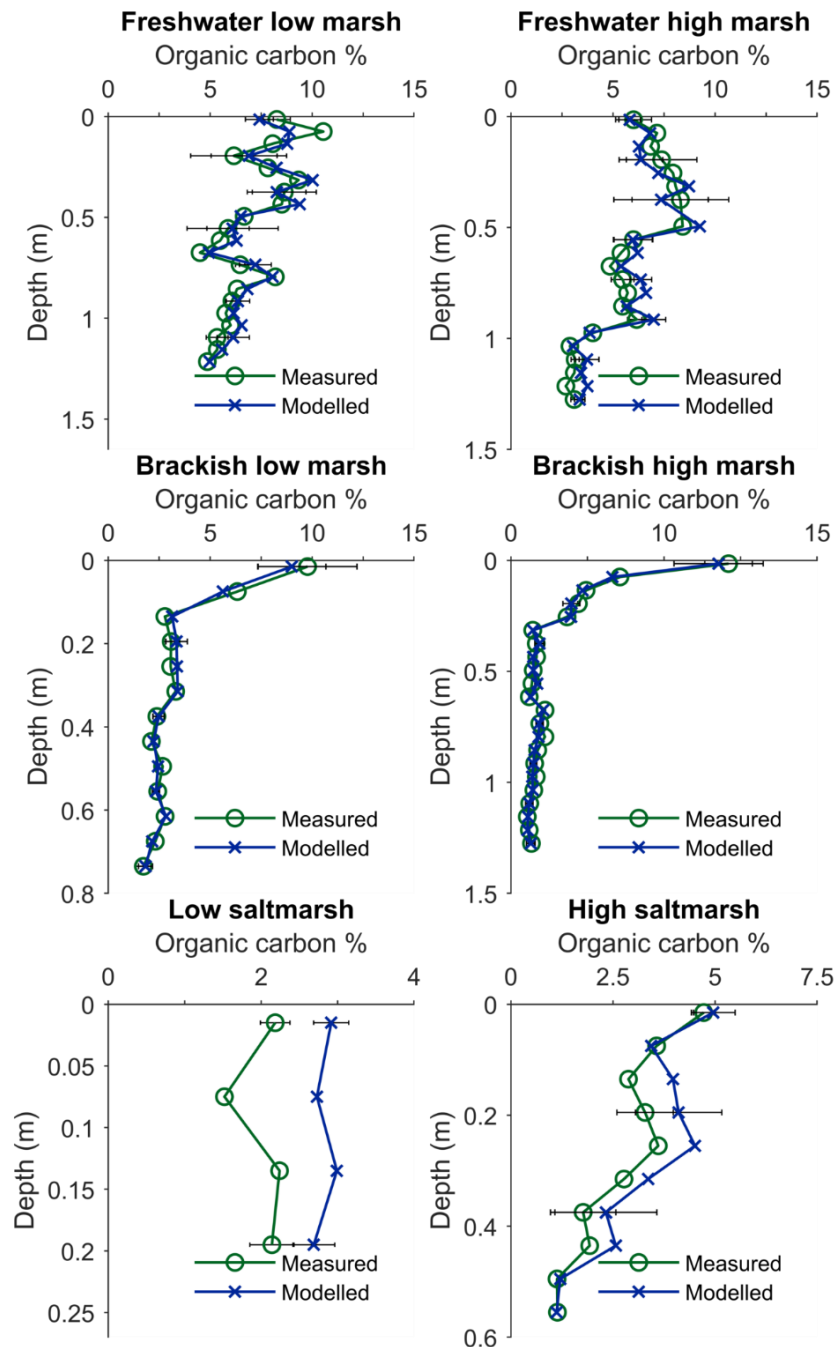


**Figure 5-3** Depth profiles of  $OC\%_{m-IR}$  and  $OC\%_{meas.}$  Error bars for the measured values show the standard deviation representing the spatial variation between 3 replicate soil cores, the error bars for the modelled values show the standard deviation for spatial variations plus the uncertainty associated with the m-IR spectroscopy/PLSR predictions.

The main advantage of using soil sensing techniques compared to standard lab techniques is that multiple soil properties (e.g. grain size, cation exchange capacity and pH) can be derived from the obtained soil spectrum at once, thereby substantially reducing the cost and time required to obtain these data (Minasny et al., 2008; Reeves et al., 1999; Viscarra Rossel et al., 2006). This study, however, only focused on the advantages associated with obtaining SOC concentration from soil samples, so the accuracy with which other soil properties from these tidal marsh sediments can be derived, in order to assess the full potential of this technique in

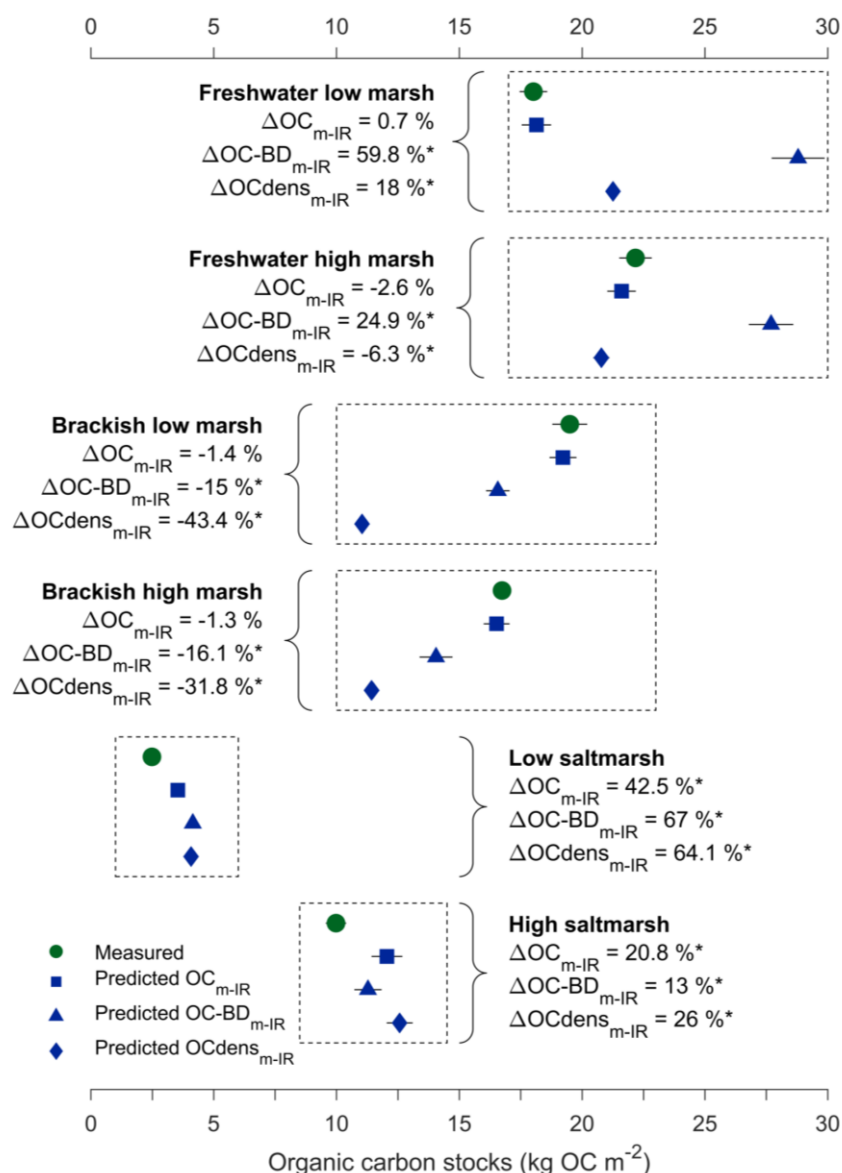


**Figure 5-4** Modelled and measured sedimentary organic carbon stocks using different methods. Error bars for the measured values show the standard deviation ( $\sigma$ ) representing the spatial variation between 3 replica soil cores, the error bars for the modelled values show the  $\sigma$  for spatial variations plus the uncertainty associated with the m-IR predictions.  $\Delta$  is the relative difference between measured and modelled OC stocks, while significantly differences between modelled and measured OC stocks are denoted with an \* ( $p = 0.05$ ).

these environments, is an interesting subject of future research. Our study showed that to calculate soil organic carbon stocks in these environments, field samples need to be obtained for the analysis of both bulk density and SOC concentration, thereby not reducing the time needed for sample collection. When only assessing SOC concentration, there is also no substantial reduction in the time needed to prepare the samples for analyses. This would, however, be the case if also other soil properties are derived from the same soil spectrum. The main advantage of obtaining SOC stocks using soil sensing techniques lies in the reduction of the cost of the analyses. As the results from this chapter have shown that a reliable calibration model can be predicted using the OC concentration of ca. 70 samples, a great

reduction in the cost of the analysis can be obtained when analyzing a large number of samples.

#### **5.4 Conclusion**

Our results show that m-IR spectroscopy/PLSR is a reliable method to predict the OC concentration of tidal marsh sediments at a high accuracy ( $R^2 = 0.94$ , RMSE = 0.56 % OC) using only 70 calibration samples covering a maximum variation in the total dataset. Combining predicted OC concentrations with measured bulk density profiles resulted in accurate predictions of total sedimentary OC stocks in brackish and freshwater marsh sediments (relative errors < 3 %) while predictions were less accurate for salt marsh sediments (relative errors of 20 – 42 %). These results show that care has to be taken when soil sensing techniques are used to predict OC concentrations for soil samples characterized by different OC characteristics and protection mechanisms. If knowledge on SOC characteristics is present, this can be used to construct multiple calibration models for soil samples having distinct OC characteristics in order to obtain optimal predictions of OC concentration.

#### **Acknowledgements**

I would like thank Dries Poppelmonde for his help in obtaining mid-infrared spectra from the soil samples.



## Chapter 6 Assessment of the capacity of soil organic carbon models to simulate depth profiles of stable carbon isotopes ( $\delta^{13}\text{C}$ )

---

**Abstract.** Soils are an important component of the global carbon cycle, as they constitute the largest carbon reservoir of the biosphere and store more carbon compared to the atmosphere. Perturbations to the soil system can therefore affect the global carbon cycle, causing soils to take up additional carbon or to release it to the atmosphere as carbon dioxide or methane. As future atmospheric greenhouse gas concentrations are being predicted using earth system models (ESMs), an accurate representation of soil organic carbon in the soil sub-models of ESMs is a prerequisite to make reliable predictions of future climate change. The soil component is, however, one of the most uncertain components of ESMs. In addition, soil organic carbon models have become more complex over the past years. This calls for additional methods to calibrate soil organic carbon models and to assess their validity. Stable carbon isotopes ( $\delta^{13}\text{C}$ ) can be used for this purpose, but their incorporation in soil organic carbon models has been very limited up till now. Therefore, the aim of this study is to assess the potential of two soil organic carbon models to correctly simulate depth profiles of  $\delta^{13}\text{C}$ . As both models are based on different principles, empirical versus process-based, a second aim of this study is to use simulated  $\delta^{13}\text{C}$  depth profiles to assess the accuracy with which both models represent factors affecting soil organic carbon dynamics. The results show that both models do not realistically include the effect of soil microorganisms on  $\delta^{13}\text{C}$  values, and provide insights into mechanisms that are lacking in the structure of current soil organic carbon models.

## 6.1 Introduction

The amount of organic carbon (OC) stored in soils globally (ca. 3500 Pg C; Ciais et al., 2013; Schuur et al., 2015) is an order of magnitude larger than the OC present in the atmosphere (589 Pg C; Ciais et al., 2013) and global vegetation (550 Pg C; Ciais et al., 2013). Although a substantial amount of soil organic carbon (SOC) has been shown to be relatively stable C, with an average age up to several millennia (Rumpel and Kögel-Knabner, 2010), the OC stored in soils is very sensitive to environmental changes. This can lead to both increases and decreases of the amount of SOC. For example, deforestation and the subsequent adoption of agricultural practices has been shown to lead to substantial losses of SOC in both temperate (Poeplau et al., 2011) and tropical (Don et al., 2011) ecosystems. On the other hand, reforestation of arable land or grassland leads to an increase in the amount of OC stored in soils (Guo and Gifford, 2002; Shi et al., 2013). Moreover, the most vulnerable soils with regards to SOC losses are permafrost soils, mostly located at high latitudes. In these soils, water is frozen throughout most of the year but predicted atmospheric warming over the coming centuries might thaw these soils and cause tremendous emission of mineralized OC, both as CO<sub>2</sub> as CH<sub>4</sub> (Schuur et al., 2015). Soils thus have the potential to cause large feedbacks to climate change and serve as a source or sink of atmospheric CO<sub>2</sub> over the coming centuries (Davidson and Janssens, 2006; Heimann and Reichstein, 2008).

In order to assess how SOC will react to future environmental, management and land use changes, empirically-derived understanding of SOC dynamics is used to construct numerical SOC models. Although a large research effort has been done to predict how global SOC stocks will change over the coming decades using SOC models, large uncertainties still exist on predicted SOC stocks (Friedlingstein et al., 2006; Todd-Brown et al., 2014, 2013). This is a consequence of, among other factors, (1) the complex nature of SOC characteristics and the microbial communities responsible for SOC mineralization, (2) the great spatial heterogeneity of soil characteristics, (3) an incomplete understanding of how SOC dynamics are influenced by environmental factors and (4) uncertainties on how to implement this into numerical models. For example, Falloon et al. (2011) showed that the magnitude and, more importantly, the direction of future changes in the global SOC stocks depend on how the relationship between SOC mineralization and soil moisture is represented in earth system models. Similarly, Wieder et al. (2013) found that the magnitude of simulated changes in global SOC stocks over the coming century depends on the characteristics of the SOC model used, while different assumptions about the response of soil microbes to an increase in temperature yield a different direction of SOC changes (from a moderate sink to a massive source of atmospheric CO<sub>2</sub>). Further model development based on an increasing knowledge on the factors controlling SOC dynamics is thus necessary to improve predictions of future changes in global SOC stocks.

Over the past decades, > 200 SOC models have been developed which differ in complexity, process representation and the spatial scale at which they can be applied (Manzoni and Porporato, 2009). Most models developed in the 20<sup>th</sup> century and the beginning of the 21<sup>st</sup> century (e.g. RothC (Coleman and Jenkinson, 1999) and Century (Parton et al., 2001)) consist of one or more conceptual carbon (C) pools with different pre-defined turnover times.

Subsequently, the beginning of the 21<sup>st</sup> century was accompanied by the advent of SOC models which explicitly represent microbial processes, which are the drivers behind the conversion of SOC to  $\text{CO}_2$ , while being an important precursor of stable SOC (Cotrufo et al., 2013; Miltner et al., 2012; Schmidt et al., 2011). Both types of models thus differ substantially with regard to (1) the processes they represent, (2) their complexity and (3) the amount of data needed to drive and validate these models. Over the past years, the changing paradigm on long term SOC storage (from a view where SOC is stored in soils as a consequence of its complex molecular structure to a view where SOC is preserved due to different ecosystem properties (Lehmann and Kleber, 2015; Schmidt et al., 2011)) has prompted a call for the incorporation of microbial dynamics and different protection mechanisms of SOC in numerical models (Luo et al., 2017; Todd-Brown et al., 2012; Wieder et al., 2014).

Although the explicit simulation of microbial processes and mechanisms leading to long-term SOC storage in models might lead to a more realistic representation of reality, it also substantially increases the complexity of SOC models (Lawrence et al., 2009). Therefore, calibration criteria other than total SOC have been used in the past to constrain parameter values of SOC models. The most common additional constraint is the  $^{14}\text{C}$  content of SOC (Ahrens et al., 2014; Braakhekke et al., 2014; Dwivedi et al., 2017; Elzein and Balesdent, 1995; Jenkinson and Coleman, 2008; Koven et al., 2013), while also  $^{14}\text{C}$  and other characteristics of measured OC fractions have been used (Ahrens et al., 2015) in addition to  $^{210}\text{Pb}$  (Braakhekke et al., 2013). In contrast, the second most abundant C isotope,  $^{13}\text{C}$ , is to date not used as an additional calibration criterion for SOC models. This is surprising, as the cost to measure  $^{13}\text{C}$  is much lower compared to  $^{14}\text{C}$ . As the mechanisms causing the generally observed relative enrichment of  $^{13}\text{C}$  compared to  $^{12}\text{C}$  in soils are to date relatively well constrained (see introduction chapter, section 1.3.1.2), explicitly modelling  $^{13}\text{C}$  in addition to total C and  $^{14}\text{C}$  has the potential to serve as a cheap and readily available constraint on parameter values of SOC models. In addition, a wealth of data on the  $\delta^{13}\text{C}$  values (a measure for the  $^{13}\text{C}/^{12}\text{C}$  ratio, see section 1.3.1) of SOC has been collected over the past decades, which shows that the  $\delta^{13}\text{C}$  values of different SOC fractions reflect mechanisms of SOC cycling in soils. For example, Figure 6-1 shows that the  $\delta^{13}\text{C}$  values of measured SOC fractions in European forest soils are substantially less negative for OC associated with minerals, indicating that this OC is highly processed and potentially has a predominant microbial origin, while the  $\delta^{13}\text{C}$  value of free particulate organic matter is similar to that of litter inputs (Schrumpf et al., 2013). The low  $\delta^{13}\text{C}$  value of mineral-associated OC is generally accompanied by a low  $^{14}\text{C}$  content (and thus high age) of this fraction, indicating that OC in this fraction remains in the soil much longer compared to unprotected particulate organic matter. A general feature of depth profiles of  $\delta^{13}\text{C}$  in forest soils is that it increases with depth (Acton et al., 2013; Schrumpf et al., 2013), as explained in the introduction of this dissertation (section 1.3.1.2).

There are currently no SOC models which reliably simulate depth profiles of the  $\delta^{13}\text{C}$  value of SOC. To the best of my knowledge, up till now only two SOC models incorporated the simulation of  $\delta^{13}\text{C}$  values (Baisden et al., 2002; Van Dam et al., 1997). Both models, however, make unrealistic assumptions in order to simulate  $\delta^{13}\text{C}$  profiles which were in accordance with measurements, as argued in section 6.3.1. Therefore, the aim of this study is to assess the potential of two established SOC models to simulate realistic depth patterns of the  $\delta^{13}\text{C}$  value

of SOC. The first one is a model with conceptual C pools with different turnover rates (ICBM – DE; Andr en and K atterer, 1997; Wang et al., 2015b), the second is a process-based SOC model simulating microbial dynamics and SOC stabilization on minerals (COMISSION; Ahrens et al., 2015).

The specific aims of this study are formulated in the following research questions:

- To which extent is it possible to include empirically-derived mechanisms of  $^{13}\text{C}$  enrichment with depth in (i) an empirical SOC model based on first-order kinetics and (ii) a process-based SOC model?
- To which extent can these models simulate different mechanisms leading to  $^{13}\text{C}$  enrichment with depth?
- Are the simulated  $\delta^{13}\text{C}$  depth profiles realistic enough to be used as an additional constraint of parameter values in the future?

In addition, the simulated depth profiles of  $\delta^{13}\text{C}$  are used to draw conclusion about the validity of the model structure of both models. It is noted that the aim of this study is to assess the potential of both models to simulate realistic depth profiles of  $\delta^{13}\text{C}$ , while model results will not be compared to measured data. A realistic  $\delta^{13}\text{C}$  depth profile is interpreted here as a  $\delta^{13}\text{C}$  profile which increases or remains stable with depth, while a realistic  $F^{14}\text{C}$  depth profile substantially decreases with depth, as is generally observed in undisturbed soils (Accoe et al., 2002; Acton et al., 2013; Powers and Schlesinger, 2002; Schrumpf et al., 2013; Torn et al., 2003; Wynn et al., 2005), and explained in the introduction of this dissertation (section 1.3.1.2).

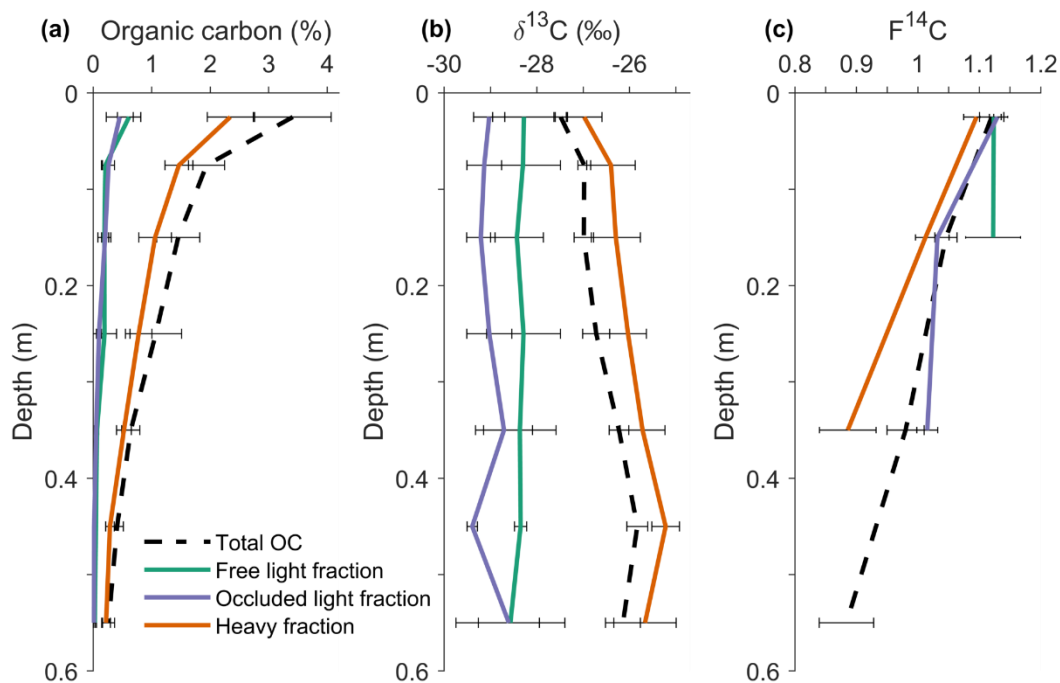


**Figure 6-1** Organic carbon fractionation results from Schrumpf et al. (2013) for the forest site in Hesse (NE France): (a) organic carbon concentration, (b) stable carbon isotope ( $\delta^{13}\text{C}$ ) values and (c) fraction modern carbon ( $F^{14}\text{C}$ ) for the different fractions

## 6.2 Material and methods

### 6.2.1 Model set-up

The tested SOC models were used to simulate depth profiles of OC by dividing the soil profiles in layers of 0.01 m. Although the models were not calibrated, input parameters were chosen to represent an average western European undisturbed forest, to allow a qualitative comparison of the results to the data obtained for a typical European forest (Figure 6-1, Schrumpf et al. (2013)). The total mass of annual litter inputs of C was  $100 \text{ g C m}^{-2}$ , the total amount of annual root inputs was  $200 \text{ g C m}^{-2}$ , based on the data used by Ahrens et al. (2015) for a forest site in NE Bavaria (E-SE Germany). Roots were calculated to decrease exponentially with depth for the application of ICBM – DE and COMMISSION with an e-folding depth of 0.075 m, as was used by Ahrens et al. (2015). All model runs were performed for a period of 10.000 years. The equations of all models presented in this chapter were solved using an explicit finite difference scheme.

To assess the potential of both SOC models to simulate realistic depth profiles of  $\delta^{13}\text{C}$ , each model was used to simulate different mechanisms which are known to lead to  $^{13}\text{C}$  enrichment of SOC. The following model set-ups were simulated:

- A run in which the only mechanism related to  $\delta^{13}\text{C}$  dynamics is a difference in the  $\delta^{13}\text{C}$  value between aboveground litter and roots, with litter ( $-28.5 \text{ ‰}$ ) being assumed to be isotopically lighter compared to root inputs ( $-28 \text{ ‰}$ ) (Bowling et al., 2008; Ghashghaie and Badeck, 2014; Werth and Kuzyakov, 2010).
- A run with the same isotopic difference between aboveground litter and roots, together with the  $^{13}\text{C}$  – Suess effect (see section 6.2.4.3).
- A run with the same isotopic difference between aboveground litter and roots, together with the effect of microbial dynamics on isotopic discrimination. The implementation of this mechanism is specific to each model, as described in sections 6.2.2.3 and 6.2.3.3.
- A run combining all above-described mechanisms, to represent the real-world situation: differences between aboveground litter and roots, the  $^{13}\text{C}$  – Suess effect and microbial mechanisms.

The rationale behind this strategy is that it allows to assess how the models react to different mechanisms affecting the  $\delta^{13}\text{C}$  value of SOC.

### 6.2.2 ICBM-DE model structure

#### 6.2.2.1 General overview of ICBM

ICBM (Introductory Carbon Balance Model), as originally developed by Andrén and Kätterer (1997), is an OC model containing a young and old OC pool in which OC mineralization and fluxes of carbon between the different pools follow first order kinetics. The original version of ICBM was used to simulate OC dynamics on a decadal timescale in topsoils only. To simulate depth profiles of OC using ICBM, Wang et al. (2015b) adapted the model to simulate depth-explicit (DE) profiles of OC (ICBM – DE) in landscape locations where deposition of sediments takes place. In order to simulate decreasing decomposition rates of SOC with depth, the factor in ICBM that regulates the influence of external processes (e.g. soil moisture and

temperature) on SOC decomposition ( $r$ ) was calculated to decrease exponentially with depth. Subsequently, Wang et al. (2015a) and Menichetti et al. (2016) proposed the addition of a third passive pool to the model. The combination of both adaptations is used here to simulate depth profiles of total SOC, and will be referred to as ICBM – DE, according to Wang et al. (2015b). In addition, bioturbation in topsoil layers was added and the model was adapted to simulate dynamics of  $^{13}\text{C}$  and  $^{14}\text{C}$  isotopes as explained in section 6.2.2.3. The model runs with ICBM – DE were performed using a time step of 1 year.

### 6.2.2.2 Organic carbon dynamics in ICBM – DE

The model structure of ICBM – DE is shown in Figure 6-2. Carbon enters the model only in the young pool (Y) after which carbon is transferred subsequently to the old (O) and passive (P) pools. The fluxes are governed by first-order kinetics, while during the transfer of carbon from one pool to the next, a fraction of carbon is lost as  $\text{CO}_2$  (' $1-h$ ', with  $h$  being the humification coefficient). The factors governing the flow of carbon between different pools (the ' $k$ ' factors) are generally defined so that the turnover time of the young pools is  $< 1$  year, while the old and passive pools cycle on decadal and centennial timescales respectively (Juston et al., 2010; Wang et al., 2015a, 2015b). Temporal changes in the size of the different pools are given by the following equations:

$$\frac{\partial Y(t, z)}{\partial t} = i(t, z) - k_Y r(z) Y(t, z) + \frac{\partial}{\partial z} \left( D_b(z) \frac{\partial Y(t, z)}{\partial z} \right) \quad (6.1)$$

$$\frac{\partial O(t, z)}{\partial t} = h_Y k_Y r(z) Y(t, z) - k_O r(z) O(t, z) + \frac{\partial}{\partial z} \left( D_b(z) \frac{\partial O(t, z)}{\partial z} \right) \quad (6.2)$$

$$\frac{\partial P(t, z)}{\partial t} = h_O k_O r(z) O(t, z) - k_P r(z) P(t, z) + \frac{\partial}{\partial z} \left( D_b(z) \frac{\partial P(t, z)}{\partial z} \right) \quad (6.3)$$

With  $z$  being depth below the soil surface (m),  $t$  being time (year),  $i$  being annual OC inputs ( $\text{g C m}^{-2}$ ),  $r$  being the influence of external factors on decomposition (soil moisture and temperature),  $h_Y$  and  $h_O$  the humification coefficients for the carbon flow out of the young and old pool respectively (unitless),  $k_Y$ ,  $k_O$  and  $k_P$  the first-order decay constants of the young, old and passive C pools respectively ( $\text{yr}^{-1}$ ) and  $D_b$  the biodiffusion coefficient ( $\text{m}^{-2} \text{yr}^{-1}$ ). The last term in each equation represents the effect of bioturbation on the vertical movement of OC (see section 6.2.4.1). Note that this is the only mechanism used to vertically redistribute OC along the soil profile, as no DOC pool is defined to be advected together with infiltrating water. The total carbon pool (C) is the sum of Y, O and P.

In order to simulate deteriorating conditions for the processing of OC with depth, the  $r$  parameter is assumed to decrease exponentially with depth (Koven et al., 2013; Wang et al., 2015a, 2015b):

$$r(z) = r_0 e^{-z/z_e r} \quad (6.4)$$

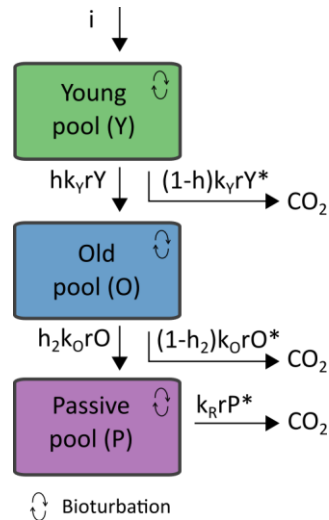


**Figure 6-2** Model structure of ICBM-DE (see main text for explanations of the formulas and parameter names). Fluxes during which isotopic discrimination are simulated are denoted with a '\*’.

With  $z$  being the depth below the soil surface (m),  $z_{e,r}$  being the e-folding depth (m) and  $r_0$  being the value of  $r$  (unitless) at the soil surface. The latter is a function of temperature only, and is calculated based using the formula proposed for the CENTURY model, as proposed by Menichetti et al. (2016):

$$r_0 = 0.56 + 0.465 \arctan(0.097(T - 15.7)) \quad (6.5)$$

With  $T$  being the mean annual temperature ( $^{\circ}\text{C}$ ). A mean annual temperature of  $8^{\circ}\text{C}$  was used, resulting in an  $r_0$  value of 0.26. It is noted that the effect of soil moisture was not included in the calculations of  $r$ . The effect of the magnitude of the exponential decrease of the  $r$  parameter with depth is illustrated in Figure 6-3. It shows that a steep decline with depth of the value of the  $r$  parameter (Figure 6-3a), leads to higher SOC concentrations throughout the soil profile, as would be expected (Figure 6-3b). This has important consequences for the simulated depth profiles of the fraction modern carbon ( $F^{14}\text{C}$ ) (see section 6.2.4.4), with lower values of  $r$  throughout the soil profile leading to lower  $F^{14}\text{C}$  values (and thus older carbon). This is to be expected, as low values of  $r$  prevent OC from flowing from one C pool to another, thereby rendering it ‘immobile’ and thus leading to higher OC ages throughout the soil profile. As a consequence, high SOC ages with depth are generally only obtained when the rate of SOC decomposition decreases significantly with depth in SOC models following first-order kinetics (Koven et al., 2013), although exceptions exist (Baisden et al., 2002; Elzein and Balesdent, 1995) as discussed in section 6.3.1.

Organic carbon dynamics are calculated on a mass basis ( $\text{g OC m}^{-2}$ ). Model results are converted to OC concentration using depth profiles of soil bulk density (assumed here to be  $1.713 \text{ g cm}^{-3}$  for all depth layers), in order to directly compare model results to measured OC concentrations. The parameters used for the ICBM-DE runs are shown in Table 6.1.

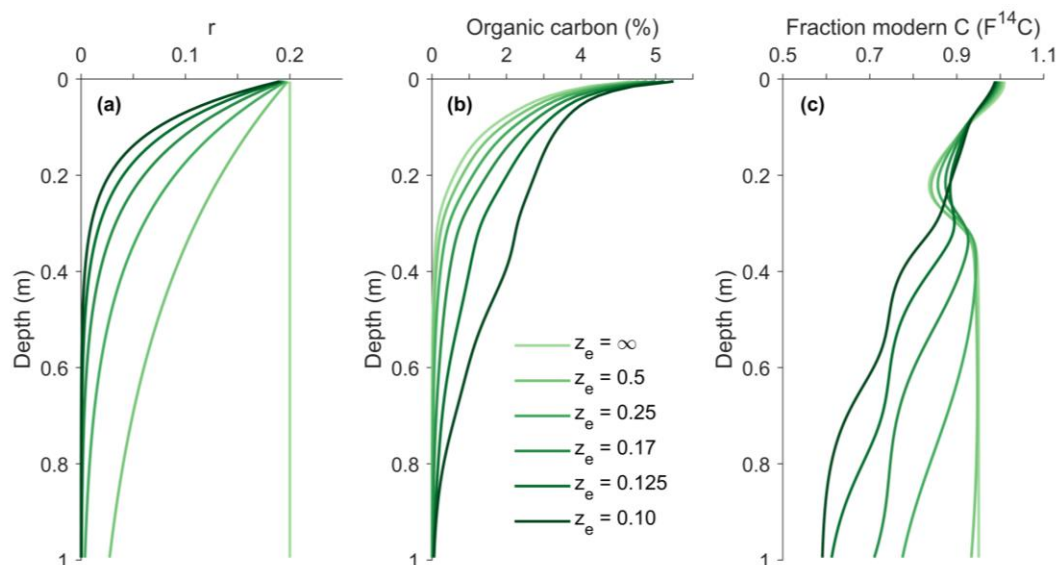


**Figure 6-3** (a) The effect of the  $r$  profile on (b) simulated depth profiles of organic carbon concentration and (c) fraction modern carbon.  $z_e$  is the e-folding depth of  $r$  (in m).

### 6.2.2.3 Simulation of $^{13}\text{C}$ and $^{14}\text{C}$ in ICBM-DE

Dynamics of  $^{13}\text{C}$  and  $^{14}\text{C}$  isotopes were incorporated in ICBM – DE by explicitly simulating the fate of these isotopes using the same equations as for total C (eq. 6.1 – 6.3). The isotopic enrichment of  $^{12}\text{C}$  relative to  $^{13}\text{C}$  of respired  $\text{CO}_2$ , as explained in the introduction of this dissertation (section 1.3.1.2), was simulated using a fractionation factor ( $\alpha$ ):

$$\alpha = \frac{R_{\text{CO}_2}}{R_{\text{OC}}} \quad (6.6)$$

With  $R_{\text{CO}_2}$  being the ratio of  $^{13}\text{C}/^{12}\text{C}$  of respired  $\text{CO}_2$  and  $R_{\text{OC}}$  the  $^{13}\text{C}/^{12}\text{C}$  ratio of OC. For example, if respired  $\text{CO}_2$  is depleted in  $^{13}\text{C}$  by 1 ‰ relative to the OC from which it originates, the fractionation factor will be 0.999. The effect of isotopic discrimination is incorporated in the model by reducing the amount of  $^{13}\text{C}$  isotopes that is being respired, while increasing the amount of  $^{13}\text{C}$  that flows to the next pool accordingly to preserve the mass balance (Figure 6-2).

**Table 6.1** ICBM-DE model parameter values

Parameter	Value	Parameter	Value
$k_Y$	$0.8 \text{ year}^{-1}$	$\delta^{13}\text{C}_{\text{AGveg}}$	$-28.5 \text{ ‰}$
$k_O$	$0.05 \text{ year}^{-1}$	$\delta^{13}\text{C}_{\text{BGveg}}$	$-28 \text{ ‰}$
$k_P$	$0.001 \text{ year}^{-1}$	Aboveground C input	$100 \text{ g C m}^{-2} \text{ year}^{-1}$
$r_0$	0.26	Belowground C input	$200 \text{ g C m}^{-2} \text{ year}^{-1}$
$z_{e_r}$	0.125 m	Root e-folding depth ( $z_{e_r}$ )	0.075 m
$h_Y$	0.125	$\text{Db}_0$	$1 \cdot 10^{-4} \text{ m}^2$
$h_O$	0.0125	$Z_{e\_Db}$	0.2 m
$\alpha$	0.999		

As  $^{14}\text{C}$  decays radioactively, every annual time step the size of the  $^{14}\text{C}$  pools was reduced with the product of the current pool size and the decay constant for  $^{14}\text{C}$ , being  $1.21 \times 10^{-4} \text{ yr}^{-1}$  (Stuiver and Polach, 1977). Annual inputs of  $^{13}\text{C}$  and  $^{14}\text{C}$  were based on measurements of the atmospheric content of both isotopes over the past centuries ( $^{13}\text{C}$ ) and millennia ( $^{14}\text{C}$ ), as explained in more detail in sections 6.2.4.3 and 6.2.4.4.

### 6.2.3 COMISSION model structure

#### 6.2.3.1 General overview of COMISSION

COMISSION (Continuous SOC profile with Microbial Interactions and Sorptive Stabilization) is a process-driven vertically resolved SOC model, developed by Ahrens et al. (2015), simulating SOC dynamics along the soil profile based on microbial interactions, sorption of OC to minerals and vertical DOC transport (Figure 6-4). The main difference between COMISSION and SOC models following first-order kinetics, such as ICBM-DE, is that in the latter there is a unidirectional flow of OC through the different model pools. As a consequence, the oldest OC will be in the last pool of the series, which usually has the longest turnover time. The novelty of COMISSION is that OC ‘loops’ through different pools, so that OC can be up to millennia old, without the assumption that this OC is ‘recalcitrant’ or ‘passive’ (Figure 6-4). Furthermore, mineralization of SOC to  $\text{CO}_2$  is governed by the activity of soil microbes, which are explicitly simulated and treated as a separate OC pool in COMISSION. Therefore, the COMISSION model does not include a factor regulating the rate of decomposition with depth (such as the  $r$  parameter in ICBM – DE). In order to simulate the physico-chemical protection of SOC, COMISSION contains a ‘mineral protected C’ pool. Adsorption and desorption of OC to and from to mineral-associated C pool are controlled by Langmuir sorption. In addition, bioturbation of topsoil SOC is simulated as a diffusion process, while the vertical transport of DOC with infiltrating groundwater is simulated as an advective process. In the next sections, a brief overview of the COMISSION model is presented, based on the description of the model

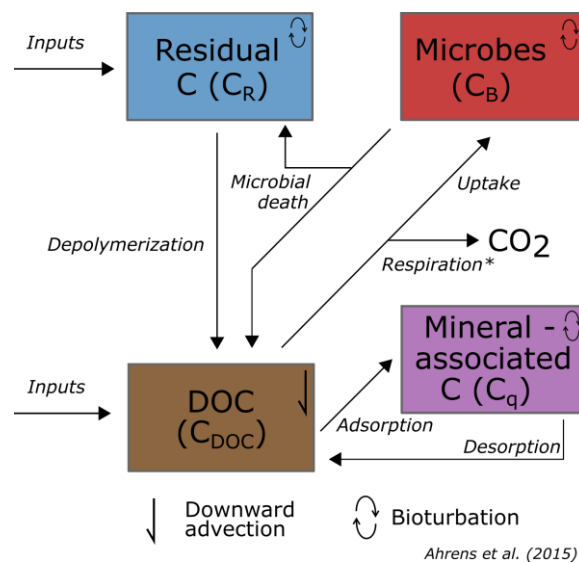


**Figure 6-4** Model structure of the COMISSION model (see main text for explanations of the formulas and parameter names), adapted from Ahrens et al. (2015). Fluxes during which isotopic discrimination are simulated are denoted with a ‘\*’.

in Ahrens et al. (2015). For a complete description of the model, reference is made to this paper. The model runs with COMMISSION were performed using a time step of 1 day, except for bioturbation which was performed on an annual time step (for computational reasons).

### 6.2.3.2 Organic carbon dynamics in COMMISSION

The COMMISSION model comprises four different OC pools: a readily leachable and soluble fraction ( $C_{DOC}$ ), residual C ( $C_R$ ) representing insoluble compounds, microbes ( $C_B$ ) and mineral associated C ( $C_q$ ). The structure of the model and the direction of fluxes between the different pools are shown in Figure 6-4. The  $C_R$  pool represents non-soluble polymeric OC, which has to be depolymerized by extracellular enzymes, produced by the microbial pool ( $C_B$ ), before it can be taken up by soil microbes as a source of energy for growth and maintenance. In the model, extracellular enzymes are not modelled explicitly but are assumed to scale linearly to the size of the microbial biomass pool. Depolimerisation of the  $C_R$  pool is simulated as follows:

$$\text{Depolymerisation} = \underbrace{V_{max,D} \cdot C_R}_{\text{Maximum depolymerisation}} \cdot \underbrace{\frac{C_B}{K_{m,B} + C_B}}_{\text{Rate limitation by microbes}} \quad (6.7)$$

Where  $V_{max,D}$  is the maximum specific depolymerisation rate of  $C_R$  by enzymes produced by soil microbes ( $C_B$ ) ( $\text{day}^{-1}$ ) and  $K_{m,B}$  is the half-saturation constant ( $\text{kg C m}^{-3}$ ). This type of representation is known as ‘reverse Michaelis – Menten’ kinetics (Schimel and Weintraub, 2003). Using this type of equation, high rates of depolymerisation of  $C_R$  by extracellular enzymes are obtained at high levels of  $C_B$ , while depolymerisation will be limited by low levels of  $C_B$ . In ‘traditional Michaelis-Menten’ kinetics, in contrast, the rate of a substrate processes is limited by the amount of available substrate. The half-saturation constant represents the mass of microbes at which the depolymerisation rate is 50 % of the maximum rate. Depolymerized  $C_R$  is transferred to the  $C_{DOC}$  pool, representing potentially available OC for microbial assimilation. Microbes take up DOC according to the following formulation:

$$\text{DOC uptake} = \underbrace{V_{max,U} \cdot C_B}_{\text{Maximum DOC uptake}} \cdot \underbrace{\frac{C_{DOC}}{K_{m,U} + C_{DOC}}}_{\text{Rate limitation by DOC}} \quad (6.8)$$

Where  $V_{max,U}$  is the maximum specific assimilation rate of DOC by microbes ( $\text{day}^{-1}$ ) and  $K_{m,U}$  is the half saturation constant ( $\text{kg C m}^{-3}$ ). This type of equation is known as ‘traditional Michaelis-Menten’ kinetics, as the uptake of DOC is limited by its own availability, while the maximum uptake rate depends on the mass of microbes present. Microbial death is simulated according to first-order kinetics:

$$\text{Microbial death} = \pi \cdot C_b \quad (6.9)$$

Where  $\pi$  is the rate at which microbes die ( $\text{day}^{-1}$ ). In addition to microbial processes, COMMISSION simulates the sorption of SOC on mineral surfaces as a mechanism protecting SOC

from mineralization by microbes. Here, dynamic Langmuir sorption and desorption is used according to the following equations:

$$\text{Adsorption} = \underbrace{K_{ads} \cdot C_{DOC}}_{\text{Maximum Adsorption}} \cdot \underbrace{(q_{max} - C_q)}_{\text{Rate limitation by availability of sorption sites}} \quad (6.10)$$

$$\text{Desorption} = K_{des} \cdot C_q \quad (6.11)$$

Where  $K_{ads}$  is the maximum adsorption rate ( $\text{m}^3 (\text{kg C})^{-1} \text{day}^{-1}$ ),  $q_{max}$  is the maximum sorption capacity ( $\text{kg C m}^{-3}$ ) and  $K_{des}$  is the desorption rate ( $\text{day}^{-1}$ ). In this formulation, the rate at which OC is adsorbed to minerals is directly related to the available sorption sites ( $q_{max} - C_q$ ). It is noted that the value of  $q_{max}$  is kept constant with depth, in contrast to Ahrens et al. (2015) where measured values of decreasing  $q_{max}$  with depth were used as a model input. Organic carbon dynamics are calculated on a mass basis ( $\text{kg OC m}^{-3}$ ). Model results are converted to OC concentration using depth profiles of soil bulk density (assumed here to be  $1.713 \text{ g cm}^{-3}$  for all depth layers), in order to directly compare model results to measured OC concentrations. Temporal changes in the size of the different pools are governed by the differential equations given below, following Ahrens et al. (2015), while the parameter names are provided in Table 6.2 and parameter values used as input for the COMMISSION model are shown in Table 6.3.

$$\frac{\partial}{\partial t} C_{R(t,z)} = \underbrace{(1-L) \cdot i(t,z)}_{\text{Non-leachable inputs}} + \underbrace{(1-p) \cdot \pi \cdot C_B(t,z)}_{\text{Non-soluble microbial remains}} - \underbrace{V_{max,D} \cdot C_{R(t,z)} \cdot \frac{C_B(t,z)}{K_{m,B} + C_B(t,z)}}_{\text{Depolymerisation}} + \underbrace{\frac{\partial}{\partial z} \left( D_b(z) \frac{\partial C_{R(t,z)}}{\partial z} \right)}_{\text{Bioturbation}} \quad (6.12)$$

$$\begin{aligned} \frac{\partial}{\partial t} C_{DOC(t,z)} = & \underbrace{L \cdot i(t,z)}_{\text{DOC inputs}} + \underbrace{p \cdot \pi \cdot C_B(t,z)}_{\text{Soluble microbial remains}} + \underbrace{V_{max,D} \cdot C_{R(t,z)} \cdot \frac{C_B(t,z)}{K_{m,B} + C_B(t,z)}}_{\text{Depolymerisation}} - \underbrace{V_{max,U(t,z)} \cdot C_B(t,z) \cdot \frac{C_{DOC(t,z)}}{K_{m,U} + C_{DOC(t,z)}}}_{\text{DOC uptake by microbes}} \\ & - \underbrace{K_{ads} \cdot C_{DOC(t,z)} \cdot (q_{max} - C_q(t,z))}_{\text{Adsorption}} + \underbrace{K_{des} \cdot C_q(t,z)}_{\text{Desorption}} - \underbrace{v(z) \cdot \frac{\partial(C_{DOC(t,z)})}{\partial z}}_{\text{DOC flux with groundwater}} \end{aligned} \quad (6.13)$$

$$\frac{\partial}{\partial t} C_q(t,z) = \underbrace{K_{ads} \cdot C_{DOC(t,z)} \cdot (q_{max} - C_q(t,z))}_{\text{Adsorption}} + \underbrace{K_{des} \cdot C_q(t,z)}_{\text{Desorption}} + \underbrace{\frac{\partial}{\partial z} \left( D_b(z) \frac{\partial C_q(t,z)}{\partial z} \right)}_{\text{Bioturbation}} \quad (6.14)$$

$$\frac{\partial}{\partial t} C_B(t,z) = \underbrace{CUE \cdot V_{max,U} \cdot C_B(t,z) \cdot \frac{C_{DOC(t,z)}}{K_{m,U} + C_{DOC(t,z)}}}_{\text{Uptake of DOC by microbes used for growth}} - \underbrace{\pi \cdot C_B(t,z)}_{\text{Microbial death}} + \underbrace{\frac{\partial}{\partial z} \left( D_b(z) \frac{\partial C_B(t,z)}{\partial z} \right)}_{\text{Bioturbation}} \quad (6.15)$$

### 6.2.3.3 Simulation of $^{13}\text{C}$ and $^{14}\text{C}$ in COMMISSION

As COMMISSION explicitly simulates microbial dynamics, incorporation of the effect of microbial processes on  $\delta^{13}\text{C}$  dynamics is more straightforward compared to ICBM – DE. The two main processes that have been proposed to affect the  $^{13}\text{C}/^{12}\text{C}$  ratio of SOC are the

**Table 6.2** Overview of the parameters, their names and units of the COMMISSION model

Parameter	Name and units
$C_r$	Residual C [ $\text{kg C m}^{-3}$ ]
$C_{\text{DOC}}$	Dissolved C [ $\text{kg C m}^{-3}$ ]
$C_q$	Mineral-associated C [ $\text{kg C m}^{-3}$ ]
$C_B$	Microbial C [ $\text{kg C m}^{-3}$ ]
$t$	Time [days]
$z$	Depth [m]
$L$	Soluble fraction in C inputs [-]
$i$	C inputs [ $\text{kg C m}^{-2} \text{ day}^{-1}$ ]
$\rho$	Soluble fraction of dead microbes [-]
$\pi$	Mortality rate of microbes [ $\text{day}^{-1}$ ]
$V_{\text{max,D}}$	Maximum specific depolymerisation rate of $C_r$ by extracellular enzymes [ $\text{day}^{-1}$ ]
$K_{\text{m,B}}$	Half-saturation constant for depolymerisation of $C_r$ [ $\text{kg C m}^{-3}$ ]
$D_b$	Biodiffusion coefficient [ $\text{m}^2 \text{ day}^{-1}$ ]
$V_{\text{max,U}}$	Maximum specific uptake rate of $C_{\text{DOC}}$ by $C_B$ [ $\text{day}^{-1}$ ]
$K_{\text{m,U}}$	Half-saturation constant for uptake of $C_{\text{DOC}}$ by $C_B$ [ $\text{kg C m}^{-3}$ ]
$K_{\text{ads}}$	Adsorption rate [ $\text{m}^3 (\text{kg C})^{-1} \text{ day}^{-1}$ ]
$K_{\text{des}}$	Desorption rate [ $\text{day}^{-1}$ ]
$q_{\text{max}}$	Maximum sorption capacity [ $\text{kg C m}^{-3}$ ]
$v$	Pore water velocity [ $\text{m day}^{-1}$ ]
CUE	Carbon use efficiency by microbes [-]

preferential incorporation of molecules enriched in  $^{13}\text{C}$  by soil microbes and the respiration of  $\text{CO}_2$  slightly enriched in  $^{12}\text{C}$  compared to microbial biomass, with the former being more important compared to the latter (Werth and Kuzyakov, 2010). However, this first mechanism is not incorporated in the model, as it has been recently argued that, given the right conditions and sufficient time, all plant-produced organic matter is eventually processed by soil microbes, thereby rejecting the theory of preferential uptake of labile substrates by soil microbes (Lehmann and Kleber, 2015). The module simulating  $^{13}\text{C}$  isotopes was adapted so that microbes ( $C_B$ ) respire  $\text{CO}_2$  which is enriched in  $^{12}\text{C}$  compared to the carbon taken up by microbial biomass. The magnitude of this isotopic discrimination was incorporated in the model using an isotopic fractionation factor,  $\alpha_{\text{respiration}}$ , which is defined as:

$$\alpha_{\text{respiration}} = \frac{R_{\text{CO}_2}}{R_{\text{DOC} \rightarrow \text{microbes}}} \quad (6.16)$$

Where  $R$  is the  $^{13}\text{C}/^{12}\text{C}$  ratio of the different pools and ' $\text{DOC} \rightarrow \text{microbes}$ ' stands for C transferred from the  $C_{\text{DOC}}$  pool to microbes (Figure 6-4). The value of  $\alpha_{\text{respiration}}$  was set to 0.999 (< 1, to ensure preferential  $^{12}\text{C}$  respiration). For the other C fluxes, the magnitude of  $^{13}\text{C}$  was identical to  $^{12}\text{C}$  to assure no isotopic discrimination took place.  $^{14}\text{C}$  isotopes were explicitly modelled, with fluxes of  $^{14}\text{C}$  in the model being proportional to fluxes of  $^{12}\text{C}$  to avoid isotopic discrimination. Radioactive decay of  $^{14}\text{C}$  atoms was simulated identical as for ICBM-DE, as described in section 6.2.2.3.

**Table 6.3** Parameter values for the COMISSION model, based on Ahrens et al. (2015)

Parameter	Value	Parameter	Value
L	0.645	$V_{\max,U}$	$0.3 \text{ day}^{-1}$
$\rho$	0.172	$K_{m,U}$	$5 \cdot 10^{-4} \text{ kg C m}^{-3}$
$\pi$	$5 \cdot 10^{-3} \text{ day}^{-1}$	$K_{\text{ads}}$	$2 \cdot 10^3 \text{ m}^3 (\text{kg C})^{-1} \text{ day}^{-1}$
$V_{\max,D}$	$5 \cdot 10^{-4} \text{ day}^{-1}$	$K_{\text{des}}$	$1 \cdot 10^{-4} \text{ day}^{-1}$
$K_{m,B}$	$0.0101 \text{ kg C m}^{-3}$	$q_{\max}$	$70 \text{ kg C m}^{-3}$
$D_{b0}$	$5 \cdot 10^{-5} \text{ m}^2 \text{ yr}^{-1}$	$v(0)$	$1 \cdot 10^{-3} \text{ m day}^{-1}$
$z_{e,Db}$	0.02 m	CUE	0.392

## 6.2.4 Additional modelled processes

### 6.2.4.1 Bioturbation

To allow for a realistic simulation of OC dynamics in biologically active soils (Nierop and Verstraten, 2004), bioturbation of topsoil OC was simulated as a diffusion process (Cousins et al., 1999; Gerino et al., 1994):

$$\frac{\partial C}{\partial t} = \frac{\partial}{\partial z} \left( D_b(z) \frac{\partial C}{\partial z} \right) \quad (6.17)$$

With  $t$  being time (years),  $z$  being the depth below the surface (m),  $C$  being the OC concentration and  $D_b(z)$  being the biodiffusion coefficient ( $\text{m}^2 \text{ yr}^{-1}$ ) at depth  $z$  below the surface, which is assumed to decrease exponentially with depth (Johnson et al., 2014):

$$D_b = D_{b0} e^{z/z_{e,Db}} \quad (6.18)$$

With  $D_{b0}$  being the biodiffusion coefficient at the soil surface and  $z_e$  the e-folding depth (m). In order to ensure numerical stability of the bioturbation module, the von Neumann stability criterion was used (Anderson, 1995):

$$\frac{D_{b0} \Delta t}{(\Delta z)^2} \leq 0.5 \quad (6.19)$$

The stability criterion was met by reducing the diffusion coefficient whenever necessary and increasing the number of time steps accordingly.

### 6.2.4.2 Advection of dissolved organic carbon

In the COMISSION model, the downward flux of dissolved organic carbon ( $C_{\text{DOC}}$ ) as a consequence of infiltrating groundwater is simulated as an advective process:

$$\frac{\partial C_{\text{DOC}}(z, t)}{\partial t} = -v(z) \frac{\partial (C_{\text{DOC}})}{\partial z} \quad (6.20)$$

With  $z$  being the depth below the soil surface (m) and  $v$  the vertical velocity of infiltrating groundwater along the soil profile ( $\text{m day}^{-1}$ ). This flux was assumed to decrease exponentially with depth to account for e.g. the uptake of soil water by roots, according to:

$$v(z) = v(0) \cdot \exp\left(\frac{-z}{z_{e\_gw}}\right) \quad (6.21)$$

Where  $v(z)$  is the value of  $v$  along the soil profile ( $\text{m day}^{-1}$ ),  $v(0)$  is the value of  $v$  at the soil surface,  $z$  is the depth below the soil surface (m) and  $z_{e\_gw}$  is the e-folding depth (m). The value of  $z_{e\_gw}$  was set to 0.45 m for the model simulations. For ICBM – DE, no advective flux of OC was modelled as no DOC pool is present.

#### 6.2.4.3 The $^{13}\text{C}$ – Suess effect

The  $\delta^{13}\text{C}$  value of atmospheric  $\text{CO}_2$  has changed significantly since the onset of the industrial period as a consequence of the burning of  $^{13}\text{C}$ -depleted fossil fuels. These temporal changes in atmospheric  $\delta^{13}\text{C}$  are generally referred to as the  $^{13}\text{C}$  – Suess effect (Keeling, 1979). The consequence of burning of  $^{13}\text{C}$ -depleted fossil fuels is a decrease in the  $\delta^{13}\text{C}$  value of atmospheric  $\text{CO}_2$  from ca.  $-6.4$  ‰ at the onset of the industrial era to ca.  $-8.4$  ‰ in 2014 (Figure 6-5a). As a consequence of this shift in the  $\delta^{13}\text{C}$  value of atmospheric  $\text{CO}_2$ , also the  $\delta^{13}\text{C}$  value of plant tissue became depleted in  $^{13}\text{C}$  since the onset of the industrial era (Keller et al., 2017). This was included in the model by assuming a constant  $^{13}\text{C}$  discrimination by plants through time. This discrimination was calculated for the year 2014, using the  $\delta^{13}\text{C}$  value of atmospheric  $\text{CO}_2$  for that year ( $-8.4$  ‰) and the  $\delta^{13}\text{C}$  value of a plant with an average aboveground  $\delta^{13}\text{C}$  value of  $-28.5$  ‰ and a  $\delta^{13}\text{C}$  value of roots of  $-28$  ‰. This difference was subsequently used to calculate the  $\delta^{13}\text{C}$  values of plant inputs for all simulation years based on the record of the  $\delta^{13}\text{C}$  value of atmospheric  $\text{CO}_2$  since the onset of the industrial era as compiled by Keller et al. (2017). As this dataset extended only to 1765, it was assumed that

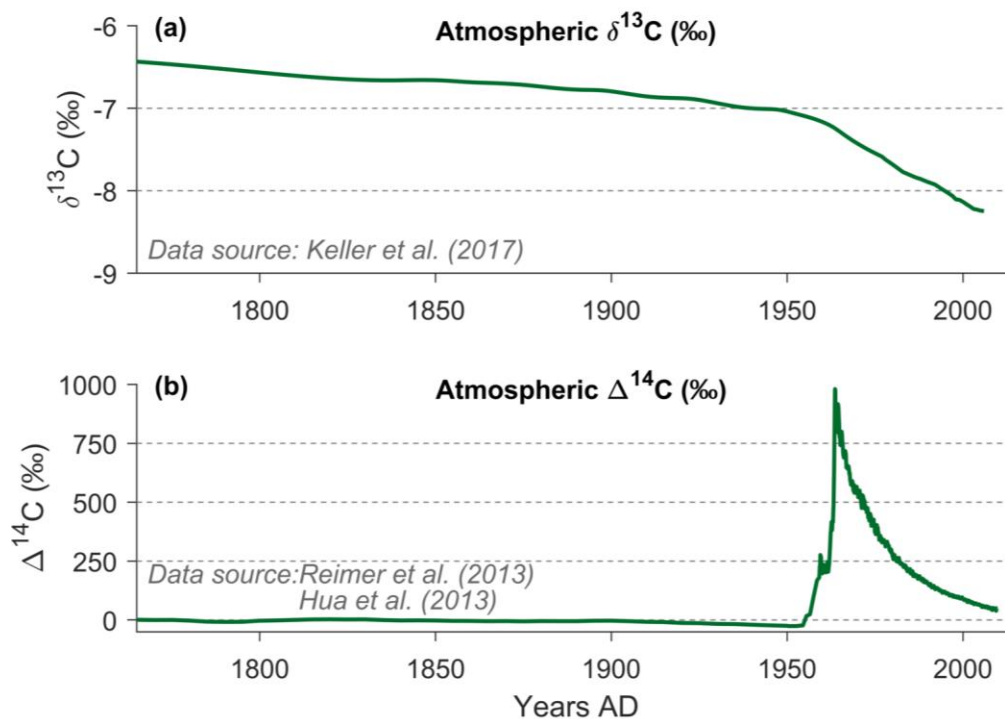


**Figure 6-5** Atmospheric levels of  $\delta^{13}\text{C}$  (a) and  $\Delta^{14}\text{C}$  (b) over the past centuries as used as an input in the model simulations (Hua et al., 2013; Keller et al., 2017; Reimer et al., 2013).

the  $\delta^{13}\text{C}$  value of atmospheric  $\text{CO}_2$  prior to 1765 was constant. In addition to the  $^{13}\text{C}$ -Suess effect, the increasing concentration of atmospheric  $\text{CO}_2$  over the past decades could have influenced the magnitude against which plants discriminate against  $^{13}\text{C}$  and thus the  $\delta^{13}\text{C}$  value of their tissue. The reason behind this is that the higher the atmospheric  $\text{CO}_2$  concentration, the larger the magnitude of isotopic discrimination against  $^{13}\text{C}$  during photosynthetic uptake of  $\text{CO}_2$  (Schubert and Jahren, 2012). The efficiency with which plants can take up  $\text{CO}_2$  also depends on moisture conditions (see Schubert and Jahren (2012) and references therein), with moisture limitations leading to plant stomata being opened for a shorter time, thereby reducing the magnitude of isotopic fractionation against  $^{13}\text{C}$ . This mechanism is, however, not included in the current version of the model.

#### 6.2.4.4 The $^{14}\text{C}$ – Suess effect and ‘Bomb $^{14}\text{C}$ ’

Also the  $\Delta^{14}\text{C}$  value of atmospheric  $\text{CO}_2$  has changed considerable over the past centuries. Here we refer to the atmospheric  $^{14}\text{C}$  content as  $\Delta^{14}\text{C}$ , which is defined as (IAEA, 2001):

$$\Delta^{14}\text{C} = \left[ \frac{\left[ \frac{^{14}\text{C}}{^{12}\text{C}} \right]_{\text{Sample}, -25}}{\left[ \frac{^{14}\text{C}}{^{12}\text{C}} \right]_{\text{OX1}, -19} \exp\left(\frac{y-1950}{8267}\right)} - 1 \right] \times 1000 \quad (6.22)$$

With  $\left[ \frac{^{14}\text{C}}{^{12}\text{C}} \right]_{\text{Sample}, -25}$  being the ratio of  $^{14}\text{C}/^{12}\text{C}$  normalized to a  $\delta^{13}\text{C}$  value of -25 ‰ (to remove the effect of mass-dependent isotopic discrimination during the photosynthetic assimilation of OC),  $\left[ \frac{^{14}\text{C}}{^{12}\text{C}} \right]_{\text{OX1}, -19}$  being the  $^{14}\text{C}/^{12}\text{C}$  of the OX-I (Oxalic acid I) standard measured at the same time (with a  $\delta^{13}\text{C}$  of -19 ‰), corrected for radioactive decay of this standard between 1950 and year  $y$ . This way of reporting expresses the  $^{14}\text{C}/^{12}\text{C}$  ratio relative to an absolute standard that is decay-corrected for changes since the year 1950. Positive  $\Delta^{14}\text{C}$  values indicate that the sample contains more  $^{14}\text{C}$  compared to the preindustrial atmosphere (IAEA, 2001), while a  $\Delta^{14}\text{C}$  value of 1000 ‰ indicates a doubling of the amount of  $^{14}\text{C}$  in the atmosphere compared to 1950. In the modeling exercises, the  $^{14}\text{C}$  content of SOC is reported as the fraction modern carbon ( $F^{14}\text{C}$ ), which is defined as:

$$F^{14}\text{C} = \frac{R_s \left( \frac{0.975}{1 + \delta/1000} \right)^2}{0.95 R_{o,-19}} \quad (6.23)$$

With  $R_s$  being the measured  $^{14}\text{C}/^{12}\text{C}$  ratio of the sample, normalized to a  $\delta^{13}\text{C}$  value of -25 ‰ ( $\delta$  is measured the  $\delta^{13}\text{C}$  value of the sample), and the denominator being 0.95 times the measured ratio of the OX-I standard measured at the same time (with a  $\delta^{13}\text{C}$  value of -19 ‰). The latter is equal to the measured activity of 1890 wood corrected for radioactive decay to 1950, to represent preindustrial atmospheric  $\text{CO}_2$  (IAEA, 2001).  $F^{14}\text{C}$  values  $> 1$  contain indicate the presence of recent, ‘bomb’  $^{14}\text{C}$ , as explained below.

Over the past centuries, the atmospheric  $^{14}\text{C}$  content has changed significantly as a consequence of mainly two processes. First, similar to the  $^{13}\text{C}$  – Suess effect, burning of fossil fuels since the onset of the preindustrial era has led to the addition of ‘old’  $\text{CO}_2$  to the atmosphere, causing a depletion in  $^{14}\text{C}$  and a  $\Delta^{14}\text{C}$  value  $< 0$  in the first part of the 20<sup>th</sup> century, generally referred to as the  $^{14}\text{C}$  – Suess effect (Figure 6-5b). Second, and more importantly, aboveground thermonuclear weapon tests in the 1950’s and the beginning of the 1960’s led to a doubling of the amount of  $^{14}\text{C}$  atoms in the stratosphere, with most intense weapon tests in the early 1960’s leading to the peak in stratospheric  $^{14}\text{C}$  content (Figure 6-5b). After the 1963 ban on aboveground nuclear weapon tests, the addition of  $^{14}\text{C}$  to the atmosphere ceased and its  $^{14}\text{C}$  content decreased due to the absorption of this carbon by other C reservoirs, mainly the ocean and the biosphere (IAEA, 2001).

To reliably simulate dynamics of  $^{14}\text{C}$  in the SOC models, historical records of  $\Delta^{14}\text{C}$  values were used as model inputs. The absolute amount of annually added  $^{14}\text{C}$  to the soil through vegetation was calculated based on equation (6.23), based on the amount of  $^{12}\text{C}$  atoms added annually. For the preindustrial era, data from Reimer et al. (2013) were used, while data from Hua et al. (2013) were used for the post-1950 period. Both datasets were obtained through the soilR package (Sierra et al., 2014) in R and processed to annual average values in Matlab®.

## 6.3 Results and discussion

### 6.3.1 The potential of ICBM-DE to simulate $\delta^{13}\text{C}$ depth profiles

The depth profiles simulated using ICBM – DE are shown in Figure 6-6. The depth profile of OC concentration shows an exponential decrease with depth, with the majority of OC present in the old pool with a decadal turnover time. The young and recalcitrant pools, with approximately annual and millennial turnover times, also store a substantial amount of OC (Figure 6-6a). The depth profile of the fraction modern C ( $F^{14}\text{C}$ ) of total SOC is ca. 1 at the surface, indicating a limited presence of ‘bomb’  $^{14}\text{C}$  (post 1950). The topsoil  $F^{14}\text{C}$  value of the old pool, however, contains ‘bomb’  $^{14}\text{C}$ , while the young pool is characterized by  $F^{14}\text{C}$  values  $> 1$  down to ca. 0.5 m depth, indicating that the majority of OC in this pools is derived from post-1950 inputs.

The scenario in which the only mechanism affecting the  $\delta^{13}\text{C}$  values of SOC was a difference in the  $\delta^{13}\text{C}$  value between aboveground litter and roots shows an increasing  $\delta^{13}\text{C}$  value with depth, from -28.5 ‰ at the soil surface (the litter value) to a value of -28 ‰ in deeper soil layers (the root value) (Figure 6-6c). When the  $^{13}\text{C}$  – Suess effect is added (Figure 6-6d), a substantial increase in the total  $\delta^{13}\text{C}$  value with depth is simulated, with the largest increase occurring in topsoil layers. There is also a general trend in the  $\delta^{13}\text{C}$  value of different pools, with the young pool having a lower value compared to the pools with a slower turnover rate. This is to be expected, as the young pool reacts rapidly to changes in the  $\delta^{13}\text{C}$  value of inputs as a consequence of its fast turnover rate. The effect of the  $^{13}\text{C}$  – Suess effect on the passive pools is, in contrast, very limited, as its value is very similar to the  $\delta^{13}\text{C}$  value of roots before the onset of the  $^{13}\text{C}$  – Suess effect (ca. -26.2 ‰).

When a difference in the  $\delta^{13}\text{C}$  value of litter and roots is combined with microbial effects on isotopic discrimination (Figure 6-6e), the  $\delta^{13}\text{C}$  value of total SOC increases only in the top ca.

0.1 m, and decreases again with depth below ca. 0.2 m. This simulated depth pattern is a direct result from the ICBM – DE model structure (Figure 6-2) and the decreasing value of the  $r$  parameter with depth (regulation the overall decomposition rate). The consequence of the latter is that the rate at which OC moves through the different pools decreases with depth. On the one hand, this is necessary to obtain decreasing  $F^{14}\text{C}$  values (and thus old OC) with depth (Figure 6-3) while, on the other hand, this results in less processed OC with depth. Since the magnitude of isotopic discrimination in the ICBM – DE model depends on the rate of OC mineralization, which is proportional to the rate at which C moves through the different pools (Figure 6-2), this results in decreasing  $\delta^{13}\text{C}$  values of SOC with depth. When all the above-described processes affecting isotopic discrimination are combined, there is only an increase in the  $\delta^{13}\text{C}$  value of total SOC in the top ca. 0.15 m, while the  $\delta^{13}\text{C}$  value decreases with depth in deeper soil layers.

These results show that although ICBM – DE is able to simulate realistic depth profiles of total SOC and  $F^{14}\text{C}$ , the model does not allow to simulate realistic depth profiles of  $\delta^{13}\text{C}$ . The main reason for this is the unidirectional model structure, which assumes that SOC is not processed dynamically, but through time moves to pools with increasing turnover times. Previous applications of these types of models to simulate SOC depth profiles also obtained increasing OC ages with depth because of a decreasing decomposition parameter with depth (Jenkinson and Coleman, 2008; Koven et al., 2013; Van Dam et al., 1997). This approach, however, renders OC in deeper soil layers ‘immobile’, as OC mineralization is very limited in deeper soil horizons while OC is not transferred to other pools. This is clear from Figure 6-6a, as virtually no OC is present in the passive pool beneath a depth of 0.3 and is located in the young and old pools. As a consequence, less processed OC is present in deeper soil layers, causing SOC at depth to be less  $^{13}\text{C}$  enriched compared to SOC in topsoil layers (Figure 6-6f).

To the best of my knowledge, the incorporation of stable C isotopes in a depth-explicit carbon model following first-order kinetics has been limited to only two previous studies. First, Van Dam et al. (1997) were able to simulate increasing  $\delta^{13}\text{C}$  values with depth using a model similar to ICBM – DE. However, in their model set-up the authors had no constraint on the biodiffusion coefficient with depth, resulting in vertical soil mixing over the entire depth of the simulating profile. This should indeed lead to increasing  $\delta^{13}\text{C}$  values with depth, as OC originating from litter is transported downwards through the entire soil profile. As a consequence, the relative contribution of fresh,  $^{13}\text{C}$ - depleted, OC decreases with depth, resulting in a  $^{13}\text{C}$  enrichment with depth. This is however no realistic model set-up, and similar results are obtained with ICBM – DE when the biodiffusion coefficient is assumed to be constant with depth (Figure 6-7). This shows that care has to be taken as realistic results can be obtained based on unrealistic assumptions or model set-ups.

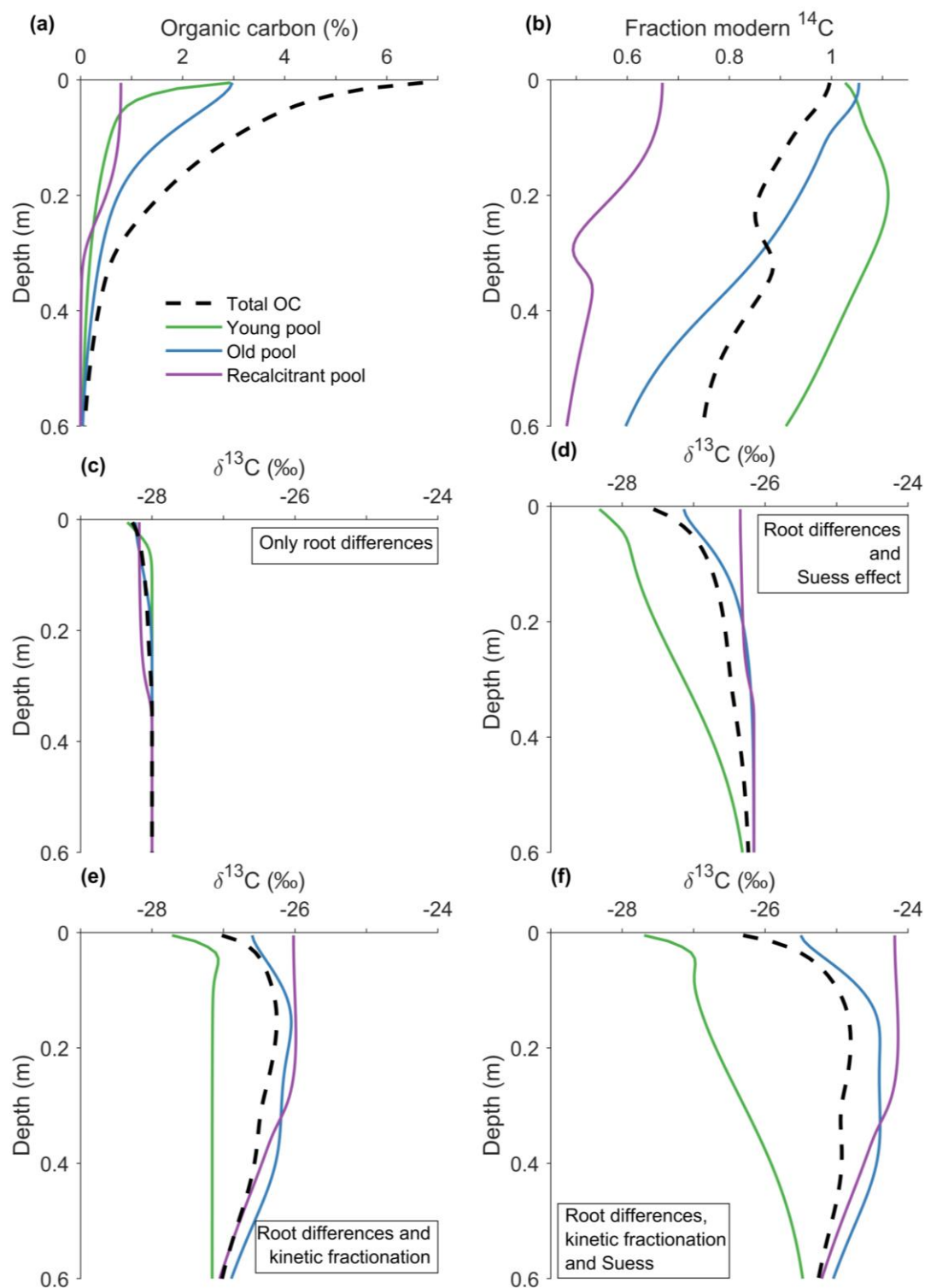


**Figure 6-6** Results of the ICBM simulations of (a) the organic carbon depth profile, (b) the fraction modern  $^{14}\text{C}$ , (c)  $\delta^{13}\text{C}$  assuming only  $^{13}\text{C}$  enrichment of roots, (d) same as (c) but including the Suess effect, (e) same as (c) but including isotopic discrimination during microbial respiration and (f) all processes combined.

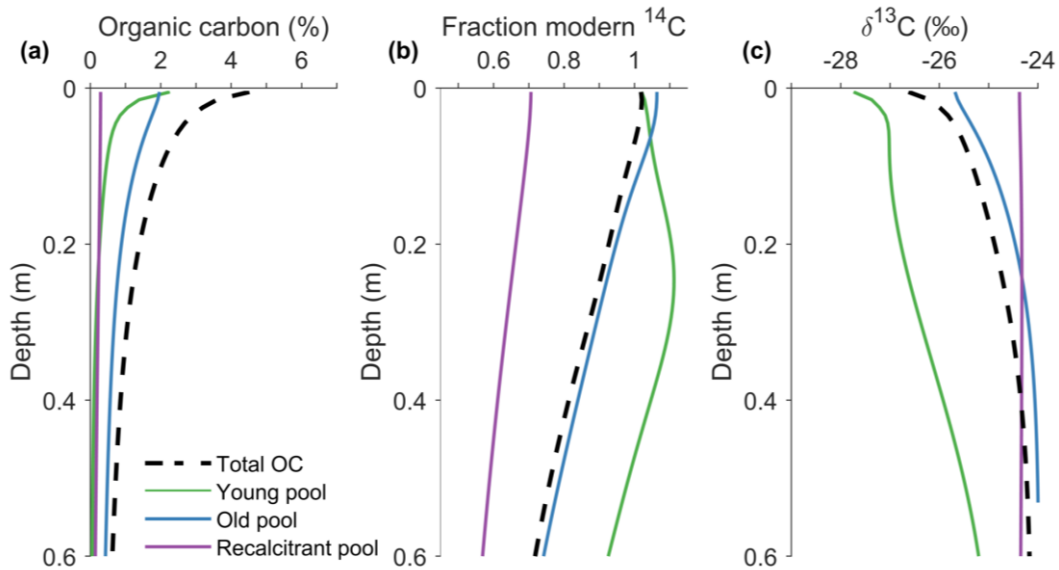


**Figure 6-7** Simulated depth profiles of (a) organic carbon concentration, (b) fraction modern  $^{14}\text{C}$  and (c)  $\delta^{13}\text{C}$  with ICBM - DE, assuming unlimited bioturbation with depth

Second, Baisden et al. (2002) simulated depth profiles of  $\delta^{13}\text{C}$  for a chronosequence of alluvial terraces in the Eastern San Joaquin Valley (California, USA). Their implementation of stable carbon isotopes differed from the methodology used here and in Van Dam et al. (1997) as these authors assumed that isotopic discrimination occurred when OC was transferred from one pool to another, while isotopic discrimination during mineralization was only assumed for the passive pool. This approach yielded a moderately good fit with measured  $\delta^{13}\text{C}$  depth profiles, and resulted in increasing  $\delta^{13}\text{C}$  values with depth in all modelled soils. This is because the authors did not impose decreasing decomposition rates with depth, following Elzein and Balesdent (1995). As a consequence, however, below a depth of 0.2 m nearly all SOC was present in the passive carbon pool (turnover time of 3333 – 5000 years), while very little SOC was present in the active and stabilized C pools (turnover time of ca. 1 and 20 – 40 years respectively). Although Baisden et al. (2002) did not use an arbitrary function causing decreasing decomposition rates with depth, their approach also rendered OC in subsoil ‘immobile’ by assuming C is transferred to the passive C pool on a decadal timescale, to remain in this pool for millennia.

Soil organic carbon models assuming first-order decay kinetics and different SOC pools with increasing turnover rates are built on the assumption that a fraction of OC is recalcitrant based on the average molecular and physical properties of OC (e.g. the chemical structure of OM, the accessibility of OM by microbes and constraints by environmental conditions such as moisture or temperature (Dungait et al., 2012; Ota et al., 2013)). These models thus assume that a portion of SOC is intrinsically recalcitrant. Over approximately the past two decades, however, multiple studies have shown that this intrinsic recalcitrance of SOC is of minor importance with regard to the long-term preservation of SOC in soils (Dungait et al., 2012; Kleber et al., 2011; Lehmann and Kleber, 2015; Schmidt et al., 2011) and that models built around this assumption have a limited capacity to correctly predict SOC dynamics in the light of the current paradigm on the protection mechanisms of SOC, including physico-chemical

protection of OC by interactions with soil minerals and the physical protection of OM in aggregates (Cotrufo et al., 2013; Dungait et al., 2012; Schmidt et al., 2011). In addition, although in the past efforts have been made to link modelled SOC pools to measured SOC fractions (Wang et al., 2015a; Zimmermann et al., 2007), it remains difficult to interpret these pools in terms of processes and protection mechanisms of SOC and to link them to e.g. observed  $\delta^{13}\text{C}$  values of SOC fractions (e.g. as shown in Figure 6-1).

In addition, ICBM – DE (and similar models) does not allow to simulate the downward flux of dissolved organic carbon (DOC), as soluble OC is not explicitly simulated and it is not clear which of the simulated pools could serve this purpose. This is problematic, as it has been shown that a substantial amount of SOC is present in the soil profile below the rooting zone (Jobbágy and Jackson, 2000). Simulating deep OC with these models thus requires the downward extension of the root profile. In an attempt to accommodate this issue, Ota et al. (2013) divided the different modelled pools of the CENTURY model (Parton et al., 2001) (active, slow and passive) into a soluble (DOC) and non-soluble fraction to simulate the downward movement of DOC to the subsoil. Although this model adaptation resulted in SOC being present below the simulated rooting depth, this model still relied on the assumption of empirically-defined C pools, hampering the comparison of the simulated results with observations. In addition to these criticisms, our results show that these types of SOC models are not able to simulate realistic depth profiles of  $\delta^{13}\text{C}$ . Although the results from this study and others (Jenkinson and Coleman, 2008; Van Dam et al., 1997) show that these types of models have the potential to simulate realistic SOC and  $\text{F}^{14}\text{C}$  depth profiles, failure to simulate realistic depth profiles of  $\delta^{13}\text{C}$  suggests that their model structure does not represent SOC dynamics in a correct way along the soil profile.

### **6.3.2 The potential of COMISSION to simulate $\delta^{13}\text{C}$ depth profiles**

The results of the COMISSION model for the simulation of different total OC, fraction modern  $^{14}\text{C}$  and  $\delta^{13}\text{C}$  are shown in Figure 6-8. The OC depth profile decreases exponentially with depth (Figure 6-8a). The majority of OC along the soil profile is associated with minerals, which is in line with empirical observations for European forest soils, as shown in Figure 6-1 (Schrumpf et al., 2013). Also, the presence of a substantial amount of residual OC ( $C_r$ , non-soluble carbon inputs) is limited to the upper ca. 0.2 m, which is in line with the observation that the presence of free particulate organic matter (POM) is limited to the upper ca. 0.1 – 0.2 m in European forest soils (Figure 6-1, Schrumpf et al. (2013)). This suggests that the model is able to reliably simulate the distribution of OC in different operational pools in an undisturbed temperate forest soil. The fraction modern  $^{14}\text{C}$  also decreases with depth (Figure 6-8b) with the presence of ‘bomb  $^{14}\text{C}$ ’ being limited to the upper soil layers, as is generally observed in forest soils of different ecosystems (Pessenda et al., 1996; Rumpel et al., 2002; Trumbore, 2000). The fraction modern  $^{14}\text{C}$  of respired  $\text{CO}_2$ , the dashed grey line in Figure 6-8b, closely resembles the fraction modern  $^{14}\text{C}$  of SOC.

When the COMISSION model is ran with an isotopic difference between aboveground litter and roots as the only mechanisms affecting the  $\delta^{13}\text{C}$  value of SOC, an increase in  $\delta^{13}\text{C}$  with depth is only observed in the top 0.1 m, indicating that the mixing of OC from both sources is

limited to this upper soil layer (Figure 6-8c). This is a direct consequence of the small e-folding depth of the bioturbation coefficient (0.02 m, Table 6.3). When the  $^{13}\text{C}$  – Suess effect is added, a consistent increase in the  $\delta^{13}\text{C}$  value of SOC is observed along the soil profile, from a topsoil value of ca. -28 ‰ to -26.2 ‰ at a depth of 0.5 m (Figure 6-8d). The fact that the increase with depth is most important in the topsoil is related to the isotopic differences between litter and roots, which enforces the effect of the gradual depletion of the atmosphere in  $^{13}\text{C}$  throughout the industrial era. It can also be seen in Figure 6-8d that ‘Suess  $^{13}\text{C}$ ’ (thus carbon fixed after ca. 1800) is incorporated in the soil profile down to a depth of 0.5 m, below which the  $\delta^{13}\text{C}$  value of SOC is similar to assumed pre-industrial value of roots (-26.2 ‰). In addition, the  $\delta^{13}\text{C}$  value of simulated mineral-associated OC is higher compared to the other OC pools, as a consequence of the longer turnover time of OC associated with minerals.

For the run which included isotopic differences between litter and roots and microbial effect on isotopic discrimination, a different pattern is observed (Figure 6-8e). The  $\delta^{13}\text{C}$  value only increases with depth in the top ca. 0.05 m, below which a slight decrease with depth occurs and the  $\delta^{13}\text{C}$  stays constant with depth at 27.5 ‰. As the source of OC that is adsorbed at mineral surfaces in COMMISSION is the  $\text{C}_{\text{DOC}}$  pool, both pools have approximately the same  $\delta^{13}\text{C}$  value. The two most important features of the resulting  $\delta^{13}\text{C}$  depth profile are (i) the isotopic enrichment of residual C ( $\text{C}_{\text{R}}$ ) relative to OC inputs and DOC and (ii) the absence of an increase in  $\delta^{13}\text{C}$  value with depth. The isotopic enrichment (less negative  $\delta^{13}\text{C}$  values) of the  $\text{C}_{\text{R}}$  pool is a consequence of the fact that the majority of dead microbes, which are enriched in  $^{13}\text{C}$ , flow back to this pool (82.8 % of dead microbes flows to the  $\text{C}_{\text{R}}$  pool, Table 6.3 (Ahrens et al., 2015)). As a consequence, C in the DOC pool is a mixture of the  $\text{C}_{\text{R}}$  pool (relatively enriched in  $^{13}\text{C}$ ) and C inputs (relative depleted in  $^{13}\text{C}$ ), thus having a  $\delta^{13}\text{C}$  value more negative compared to the  $\text{C}_{\text{R}}$  pool. This lack of an  $^{13}\text{C}$  enrichment of the DOC pool also results in the absence of an increase in the  $\delta^{13}\text{C}$  value of total simulated SOC with depth.

When all mechanisms affecting the  $\delta^{13}\text{C}$  value of SOC are included, an increasing  $\delta^{13}\text{C}$  signal of the total SOC stock with depth is simulated (Figure 6-8f), as is generally observed in undisturbed soils (Acton et al., 2013). The relative differences between the simulated pools are however not in agreement with observations, e.g. as the residual C pool (representing insoluble inputs and the non-soluble portion of dead microbes) is enriched in  $^{13}\text{C}$  compared to OC inputs, while unprocessed plant material generally has an isotopic signature compared to its source material.

The COMMISSION model represents a significant progress regarding the simulation of depth profiles of SOC. In contrast to SOC models using conceptual pools with different turnover rates, the model incorporates some of the mechanisms that over the past decades have been shown to regulate OC preservation, such as protection of OC from decomposition by organo-mineral interactions (Dungait et al., 2012; Kögel-Knabner et al., 2008; Lehmann and Kleber, 2015; Luo et al., 2017; Schmidt et al., 2011), the vertical mobility of DOC (Kaiser and Kalbitz, 2012) and soil microbes as drivers of SOC mineralization (Allison et al., 2010; Cotrufo et al., 2013; Schimel and Schaeffer, 2012; Todd-Brown et al., 2012; Treseder et al., 2012). Moreover, the modelled pools have a physical basis and can be compared to measured data (Ahrens et al., 2015).

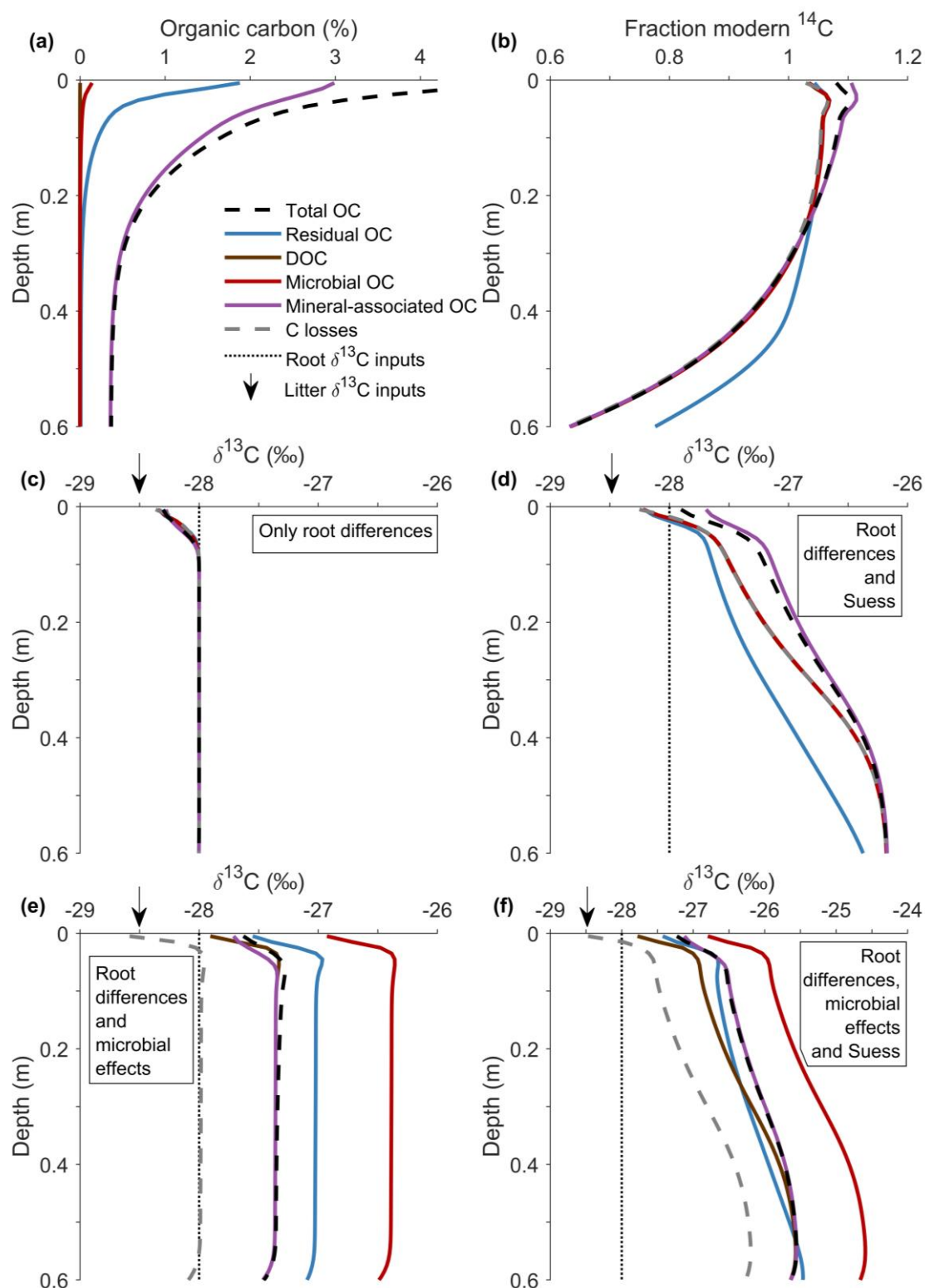


**Figure 6-8** Modelled depth profiles using the COMMISSION model (Ahrens et al., 2015): (a) organic carbon concentration, (b) fraction modern  $^{14}\text{C}$ , (c) - (f)  $\delta^{13}\text{C}$  profiles with different mechanisms leading to  $^{13}\text{C}$  enrichment: (c)  $^{13}\text{C}$  enriched roots, (d)  $^{13}\text{C}$  enriched roots and the Suess effect, (e) same as (c) but including microbial kinetic fractionation and (f)  $^{13}\text{C}$  enriched roots, the Suess effect and microbial kinetic fractionation combined. Note: the value of root inputs refers to the value of the last simulation year, when the Suess effect is simulated these values were higher in the pre-industrial period.

The model structure of COMMISSION is relatively simple and the number of parameters limited (although 11 parameters were optimized by Ahrens et al. (2015)) in comparison to other recently developed depth-explicit SOC models, such as BAMS1 (Dwivedi et al., 2017; Riley et al., 2014). The addition of a microbial biomass pool to the Community Land Model (CLM) by Wieder et al. (2013) is of similar complexity compared to COMMISSION, although this model divides the soil in only topsoil (< 0.3 m depth) and subsoil (0.3 – 1 m depth). As the incorporation of microbial mechanisms into SOC and ecosystem models leads to an increase in the number of parameters which are difficult to constrain (Riley et al., 2014; Treseder et al., 2012) while datasets to validate model results are often not available (Riley et al., 2014; Tang and Riley, 2015), finding the optimal trade-off between process understanding, model complexity and data availability is an important factor to consider when new models are being developed (Oreskes et al., 1994; Schindler and Hilborn, 2015).

The COMMISSION model has been shown to simulate realistic depth profiles of SOC and  $^{14}\text{C}$  (Figure 6-8) and has been successfully validated against field measurements (Ahrens et al., 2015). The model application of COMMISSION here was based on the model formulation in Ahrens et al. (2015) with the only difference that in the original paper a pre-defined depth profile of the  $q_{\text{max}}$  parameter (regulating the rate at which OC is adsorbed to minerals; equation 6.11) was used, while in the present study this parameter was kept constant with depth. For an extensive overview and evaluation of the performance of the COMMISSION model, reference is made to Ahrens et al. (2015).

The simulation of stable carbon isotopes could be included in COMMISSION in a more realistic way compared to ICBM – DE, due to the explicit simulation of soil microbes in COMMISSION. The results showed a realistic response of simulated  $^{13}\text{C}$  isotopes to the  $^{13}\text{C}$  – Suess effect (i.e. an increasing  $\delta^{13}\text{C}$  value with depth, as topsoil OC should be more affected by the gradual  $^{13}\text{C}$  depletion of atmospheric  $\text{CO}_2$  compared to subsoil OC), as shown in Figure 6-8d. When the effect of soil microbes on isotopic discrimination was included (i.e. enrichment of  $^{12}\text{C}$  of respired  $\text{CO}_2$  compared to microbial biomass), in contrast, the simulated  $\delta^{13}\text{C}$  depth profile is not in line with observations as e.g. the  $\delta^{13}\text{C}$  value of the residual C pool (representing mainly unprocessed OC) was substantially different from that of the source material, while an increase of the  $\delta^{13}\text{C}$  with depth was not simulated (Figure 6-8e). It is noted that comparing modelled  $\delta^{13}\text{C}$  depth profiles without including the  $^{13}\text{C}$  – Suess effect is not straightforward, as field measurements of a similar situation are difficult to obtain. An indication of how a  $\delta^{13}\text{C}$  depth profile would look when it's not affected by the  $^{13}\text{C}$  – Suess effect is provided by Torn et al. (2003), who analyzed a soil monolith of a Russian steppe soil which was collected at the end of the 19<sup>th</sup> century (between 1895 - 1903), before the most significant differences in the value of atmospheric  $\delta^{13}\text{C}$  occurred (Figure 6-5). Although no data on the  $\delta^{13}\text{C}$  value of historical litter inputs for that site is provided, correcting the  $\delta^{13}\text{C}$  value of recent litter collected at the same site (ca. -28 ‰) for the  $^{13}\text{C}$  – Suess effect would yield a  $\delta^{13}\text{C}$  value for litter for pre-industrial times of ca. -26.2 ‰. This is lower compared to the  $\delta^{13}\text{C}$  value of SOC in the top 0.5 m of the monolith (-25 – -25.5 ‰), indicating that also in a soil for which the influence of the  $^{13}\text{C}$  – Suess effect was limited the  $\delta^{13}\text{C}$  value of the total SOC is less negative compared to litter inputs. Although this line of evidence is based on many assumptions, it

suggests that even without the  $^{13}\text{C}$  – Suess effect, total SOC would not be depleted in  $^{13}\text{C}$  compared to its inputs.

In conclusion, although COMISSION is able to simulate realistic depth profiles of the total OC and  $^{14}\text{C}$  content of multiple measurable SOC pools, the model structure does not allow to reliably simulate the response of the different simulated pools on isotopic discrimination of stable carbon isotopes by soil microbes. This indicates that a different model structure is needed to correctly simulate depth profiles of  $^{12}\text{C}$ ,  $^{13}\text{C}$  and  $^{14}\text{C}$ .

### 6.4 Conclusion

The aim of this study was to assess the extent to which depth profiles of stable carbon isotopes can be simulated with (i) a SOC model with conceptual pools with different turnover rates (ICBM – DE) and (ii) a process-based SOC model simulating microbial dynamics and OC adsorption to minerals (COMISSION). On the one hand, the results showed that ICBM – DE was not able to simulate realistic depth profiles of  $\delta^{13}\text{C}$  as a consequence of its model structure which assumes OC to be ‘immobilized’ in a passive SOC pool. On the other hand, while the process-based structure of COMISSION allowed to incorporate isotopic processes more realistically compared to ICBM – DE, the model was not able to realistically represent the effect of soil microbes on isotopic discrimination. Therefore, it is concluded that simulated  $\delta^{13}\text{C}$  depth profiles cannot be used as an additional constraint on parameter values in both models. It was shown that the incorporation of stable carbon isotopes in these models allows to identify shortcomings in the structure of both models, which is encouraged to be done for other SOC models in the future. Based on the insights gained in this study, a new process-based SOC model, based on the rationale behind the COMISSION model, is presented in the next chapter.

### Acknowledgements

I would like to thank Marion Schrumpf for sharing her data on organic carbon fractionations in European forest, and for the interesting discussion together with Bernhard Ahrens. I’m also grateful to Kathrin Keller for sharing her dataset on historical atmospheric  $\delta^{13}\text{C}$  values.

## Chapter 7 Development of a soil organic carbon model to simulate depth profiles of stable carbon isotopes ( $\delta^{13}\text{C}$ )

---

**Abstract.** The results from the previous chapter have shown that while two well-established soil organic carbon models (ICBM and COMMISSION) simulate realistic depth profiles of total organic carbon and its  $^{14}\text{C}$  content, these models do not correctly represent the effect of soil microbes on  $\delta^{13}\text{C}$  values of soil organic carbon. The insights gained from this model assessment exercise are used here to construct a new soil organic carbon model to simulate depth profiles of total soil organic carbon, its  $^{14}\text{C}$  content and  $\delta^{13}\text{C}$ : SOILcarb – RM (Simulation of Organic carbon and its Isotopes by Linking carbon in the Rhizosphere and the Mineral soil). This model is based on the rationale behind the COMMISSION models (Ahrens et al., 2015). The novelty of this model is that it separates the rhizosphere (where fast carbon cycling occurs because of rapid uptake of organic carbon inputs by soil microorganisms) from the mineral soils (where slow carbon cycling takes place because organic carbon is stabilized on mineral surfaces). In addition, carbon flows from the rhizosphere to the mineral soil only in the form of dead microbes. This model structure is proposed to account for the generally observed mainly microbial origin of stabilized soil organic carbon and the preferential use of fresh OC by soil microbes as a source of energy. This chapter describes the model structure of SOILcarb – RM, assesses how the model simulates depth profiles of  $\delta^{13}\text{C}$  based on realistic input parameters and discusses the model structure with respect to the current understanding of soil organic carbon cycling. The results show that SOILcarb – RM allows to simulate realistic depth profiles of total OC and both  $^{13}\text{C}$  and  $^{14}\text{C}$  isotopes, while the simulated young age of respired  $\text{CO}_2$  is in line with empirical observations.

## 7.1 Introduction

In this chapter, the results and considerations from the previous chapter are used to construct and introduce a new model to simulate depth profiles of total organic carbon (OC), the fraction modern  $^{14}\text{C}$  and  $\delta^{13}\text{C}$ . However, before doing so, it is useful to reflect on the need of such a model, as a review in 2009 had identified ca. 250 different biogeochemical models (Manzoni and Porporato, 2009) (although some are new models based on previous versions) while over the past years a large number of new models have been developed.

A first reason for the development of a new process-based soil organic carbon (SOC) model is that most widespread models (e.g. RothC (Coleman and Jenkinson, 1999), ICBM (Andr n and K tterer, 1997), Century and Daycent (Parton et al., 2001)) are based on conceptual carbon pools which are difficult to link to measured data, while relating model parameters to environmental variables such as temperature or moisture is not straightforward. Secondly, although over the past years multiple process-based SOC models have been proposed (e.g. DAMM (Davidson et al., 2012); MIMICS (Wieder et al., 2014); CORPSE (Sulman et al., 2014); Allison et al., 2010; Tang and Riley, 2015), one of the most common problems related to these mechanistic models is that they are often too complex to be reliably validated based on measurements (Dwivedi et al., 2017; Riley et al., 2014). Third, only a very limited number of process-based models are able to simulate depth profiles of SOC (e.g. BAMS1 (Dwivedi et al., 2017; Riley et al., 2014); CLM including microbes (Wieder et al., 2013); COMMISSION (Ahrens et al., 2015)). This is noteworthy, as deep (> 0.3 m depth) SOC constitutes an important part of the total global SOC pool (Lal, 2018) and has been shown to be sensitive to environmental and land use changes (Hobley et al., 2017; Shi et al., 2013). Therefore, research concerning the development of models to simulate depth profiles of SOC is necessary and should be focused on (1) the incorporation of processes which have been empirically shown to control the dynamics of SOC and (2) finding an optimal balance between process-representation and the availability of validation data, while (3) providing output data which can be linked to measured SOC pools and characteristics.

The main aim of this study is to construct a process-based depth-explicit SOC model which correctly simulates total SOC, the fraction modern  $^{14}\text{C}$  and  $\delta^{13}\text{C}$ . As multiple studies have already focused on the simulation of  $^{14}\text{C}$  isotopes as an additional constraint on model parameter values (Ahrens et al., 2014; Baisden et al., 2002; Braakhekke et al., 2014), the focus here will be on the incorporation of stable carbon isotopes as this, to the best of my knowledge, has to date not been done for a process-based SOC model. A direct coupling between SOC dynamics and stable carbon isotopes would, however, be very informative for multiple reasons. First, multiple hypotheses concerning the increase of  $\delta^{13}\text{C}$  values with depth have been proposed (Bostr m et al., 2007; Kaiser et al., 2001; Kohl et al., 2015; Nakanishi et al., 2012; Werth and Kuzyakov, 2010; Wynn et al., 2005), but none of these have been tested in a numerical framework. By doing so, the validity of different hypotheses can be tested and can inform future research concerning stable carbon isotopic fractionation in soils. Second, the  $\delta^{13}\text{C}$  value of SOC is to date greatly underused in research concerning SOC dynamics. Currently,  $\delta^{13}\text{C}$  measurements are relatively cheap, have become standard procedure and  $\delta^{13}\text{C}$  data is often available. However, the use of  $\delta^{13}\text{C}$  data is often limited to deriving empirical

relationships between the relative increase in  $\delta^{13}\text{C}$  values with depth and changes in the concentration or calculated turnover time of SOC (Accoe et al., 2002; Acton et al., 2013; Garten, 2006; Powers and Schlesinger, 2002). There is thus a large potential for  $\delta^{13}\text{C}$  data to be used in novel ways to increase our process understanding of SOC cycling. For example, one of the potential applications of  $\delta^{13}\text{C}$  data, as shown in the previous chapter, is that it can provide information about the accuracy of the structure of SOC models. Last, as the complexity of SOC models has substantially increased over the past decades, correctly simulated  $\delta^{13}\text{C}$  data would be a welcome cheap and readily available additional data source for model calibration and validation.

Currently, simulated  $^{14}\text{C}$  values are often used to constrain model parameter values (Ahrens et al., 2014; Braakhekke et al., 2014). Using simulated  $\delta^{13}\text{C}$  values for this purpose would yield an additional value, as the absolute amount of both carbon isotopes in soils is controlled by different mechanisms. On the one hand, the radioactive decay of  $^{14}\text{C}$  removes this isotope from the soil system continuously. As a consequence, simply burying  $^{14}\text{C}$  isotopes and preventing them from taking part in the active C cycle (as is generally done in models containing conceptual C pools with different turnover rates, see previous chapter) while preventing  $^{12}\text{C}$  isotopes to be mineralized at depth will result in a decreasing  $^{14}\text{C}/^{12}\text{C}$  ratio with depth. On the other hand, as  $^{13}\text{C}$  isotopes are not subjected to radioactive decay, their abundance in soils is primarily linked to SOC dynamics and the effect of processes causing isotopic discrimination. It is noted that  $^{14}\text{C}$  are corrected for mass-dependent isotopic fractionation during the calculation of the  $F^{14}\text{C}$  value (see equation 6.23), so this effect is implicitly accounted for.

Based on a literature review of the most important processes governing SOC cycling and the considerations raised in the previous chapter, a new SOC model was constructed based on the following lines of reasoning:

- Soil microbes need to be explicitly simulated, as they regulate SOC mineralization (Schimel and Schaeffer, 2012) and are an important precursor of SOC (Miltner et al., 2012).
- The protection of SOC by interactions with soil minerals has been identified as one of the most important mechanisms responsible for the preservation of SOC (Cotrufo et al., 2013; Lehmann and Kleber, 2015; Schmidt et al., 2011; Six et al., 2002), and should therefore be explicitly simulated. The importance of the protection of SOC inside microaggregates is acknowledged (Six et al., 2000), but due to a lack of models explicitly simulating this mechanism (with the exception of Segoli et al. (2013)) this is currently not incorporated in the model.
- Organic carbon needs to be able to move vertically in the soil profile, both by bioturbation of topsoil sediments and advection of dissolved OC to deep soil layers (Cotrufo et al., 2015; Elzein and Balesdent, 1995; Johnson et al., 2014; Kaiser and Kalbitz, 2012).
- Multiple considerations are related to observed depth profiles of the age of OC:

- Although subsoil OC is generally very old, it cannot be rendered ‘immobile’, as this is in contrast with recently emerged views on SOC dynamics (e.g. Lehmann and Kleber, 2015)
- Although the average age of subsoil OC is old (up to thousands of years) (e.g. Baisden et al., 2002; Rumpel et al., 2002; Schrumpp et al., 2013), this should not restrict direct inputs of C to these deeper soil layers as very old OC ages have been reported for soils with deep rooting profiles in the tropics (Trumbore et al., 1995).
- As a consequence, root carbon cannot be a major direct source of subsoil OC (Kaiser and Kalbitz, 2012)
- The model should include the most important mechanisms that have been identified to lead to increasing  $\delta^{13}\text{C}$  values with depth:
  - Differences in the isotopic signature between aboveground vegetation and roots (Bowling et al., 2008; Ghashghaie and Badeck, 2014; Werth and Kuzyakov, 2010)
  - The terrestrial  $^{13}\text{C}$  – Suess effect (Keeling, 1979)
  - Isotopic discrimination by soil microbes (Werth and Kuzyakov, 2010)

Based on these considerations, the SOILcarb – RM model (Simulation of Organic carbon and its Isotopes by Linking carbon in the Rhizosphere and the Mineral Soil) is proposed in the next sections.

## 7.2 Material and methods

### 7.2.1 General overview of the SOILcarb – RM model

The structure of the SOILcarb - RM model is shown in Figure 7-1. The main difference with existing models simulating depth profiles of SOC is that a distinction is made between OC cycling in the rhizosphere and the mineral soil. In these two model compartments, the rate of SOC cycling is controlled by different processes: in the rhizosphere, OC cycling is controlled by microbial processing of OC inputs while in the mineral soil, OC cycling is controlled by the protection of OC against microbial processing by mineral sorption of OC. The result is that OC cycles more rapidly in the rhizosphere compartment compared to the mineral soil compartment. Carbon cycling in the rhizosphere follows the rationale of the COMMISSION model (Ahrens et al., 2015). Carbon inputs, both through aboveground litter and root inputs, enter the rhizosphere compartment as a soluble (DOC,  $C_{\text{DOC}}$ ) and insoluble fraction (residual carbon,  $C_{\text{R}}$ ). Carbon inputs subsequently need to be depolymerized by extracellular enzymes produced by soil microbes, to become available for uptake by soil microbes (bio-available carbon in the rhizosphere compartment;  $C_{\text{bio-R}}$ ). Extracellular enzymes are not explicitly modelled, but their abundance is assumed to be proportional to the mass of soil microbes present in the rhizosphere compartment ( $C_{\text{B-R}}$ ). Bio-available C is taken up by microbes for growth and maintenance, thereby respiring a portion of this C as  $\text{CO}_2$ . After microbes in the rhizosphere die, a portion of the dead biomass is transferred back to the DOC pool, while the remainder is transferred to the bio-available C pool in the mineral soil ( $C_{\text{BIO-M}}$ ). The rationale for the latter not to flow to a non-depolymerised pool in the mineral soil (similar to  $C_{\text{DOC}}$ ) is based on the assumption that all of this C would be depolymerised to enter a bio-available C

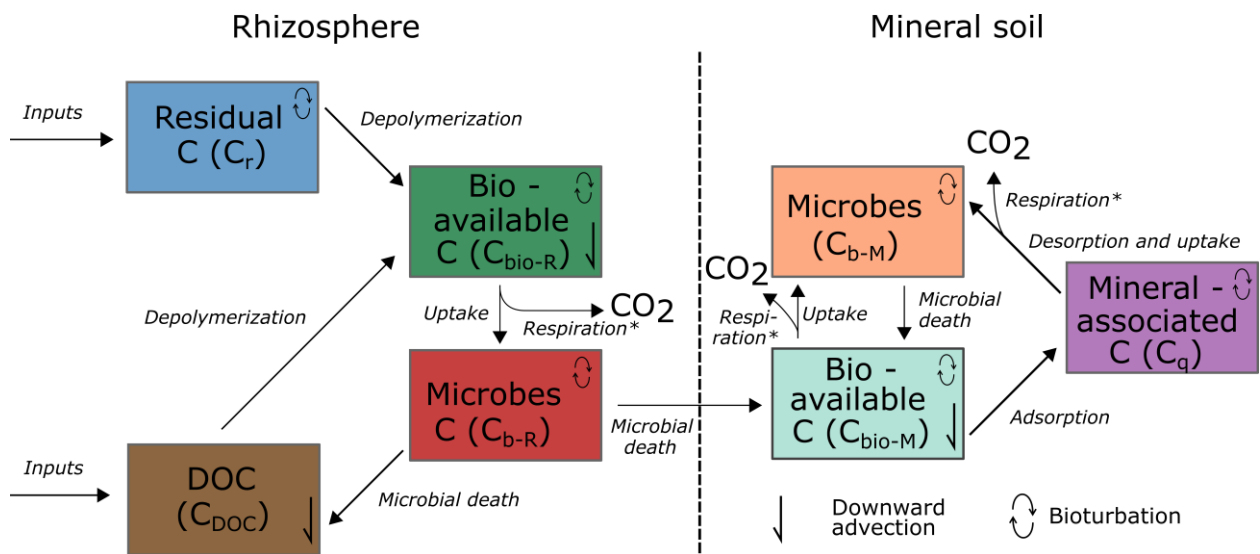


**Figure 7-1** Model structure of the SOILcarb – RM model. Fluxes during which isotopic discrimination are simulated are denoted with a ‘\*’

pool, given the low amount of C available for microbial uptake in the mineral soil. This bio-available C can be either adsorbed to minerals or taken up by the microbial community in the mineral soil compartment. Carbon that is desorbed from minerals is taken up by soil microbes in the mineral soil compartment and a portion of this C is respired as  $\text{CO}_2$ . After microbes in the mineral soil die, their biomass is transferred back to the bio-available C pool in the mineral soil compartment. To account for the vertical mobility of OC as a consequence of the downward flux of infiltrating water, DOC ( $C_{\text{DOC}}$ ) and bio-available OC ( $C_{\text{BIO-R}}$  and  $C_{\text{BIO-M}}$ ) are advected downward. In addition, all modelled pools, except for  $C_{\text{DOC}}$ , are bioturbated using biodiffusion.

The vertical resolution of the simulated soil profile was 0.01 m and the model was run for 10 000 years. The model runs with SOILcarbon – RM were performed using a time step of 1 day, except for bioturbation which was performed on an annual time step (for computational reasons), similar to the runs with COMMISSION in the previous chapter. The mass of annual aboveground litter inputs was  $100 \text{ g C m}^{-2} \text{ year}^{-1}$ , belowground inputs were  $200 \text{ g C m}^{-2} \text{ year}^{-1}$ . Root inputs decreased exponentially with depth using an e-folding depth of 0.2 m (note that this is different from the e-folding depth of 0.075 using in the previous chapter).

## 7.2.2 Carbon dynamics in SOILcarb - RM

The equations governing the size of the different OC pools and the fluxes between these pools are based on the COMMISSION model (Ahrens et al., 2015). The most important characteristics of the equations are presented here, for more detailed information reference is made to the description of COMMISSION in the previous chapter. Carbon inputs to the rhizosphere, both soluble ( $C_{\text{DOC}}$ ) and insoluble ( $C_{\text{R}}$ ), need to be depolymerized before they can be taken up by microbes. This is modelled using ‘reverse Michaelis-Menten’ kinetics, as the rate of depolymerisation is limited by the amount microbial biomass:

$$\text{Depolymerisation} = \underbrace{V_{max,D} \cdot C_{R/DOC}}_{\text{Maximum depolymerisation}} \cdot \underbrace{\frac{C_{B-R}}{K_{m,B} + C_{B-R}}}_{\text{Rate limitation by microbes}} \quad (7.1)$$

Where  $V_{max,D}$  is the maximum specific depolymerisation rate of  $C_R$  and  $C_{DOC}$  ( $C_{R/DOC}$ ) by enzymes produced by soil microbes in the rhizosphere ( $C_{B-R}$ ) ( $\text{day}^{-1}$ ) and  $K_{m,B}$  is the half-saturation constant ( $\text{kg C m}^{-3}$ ). This depolymerised OC is stored in the bio-available C pool in the rhizosphere ( $C_{BIO-R}$ ), representing monomers which can be taken up by soil microbes. This process is simulated using 'traditional Michaelis-Menten' kinetics:

$$C_{BIO-R} \text{ uptake} = \underbrace{V_{max,U} \cdot C_{B-R}}_{\text{Maximum } C_{BIO-R} \text{ uptake}} \cdot \underbrace{\frac{C_{BIO-R}}{K_{m,U} + C_{BIO-R}}}_{\text{Rate limitation by } C_{BIO-R}} \quad (7.2)$$

Where  $V_{max,U}$  is the maximum specific assimilation rate of  $C_{BIO-R}$  by microbes in the rhizosphere ( $\text{day}^{-1}$ ) and  $K_{m,U}$  is the half saturation constant ( $\text{kg C m}^{-3}$ ). A fraction of C taken up by microbes ( $1 - CUE$ ; carbon use efficiency) is lost as  $\text{CO}_2$ . Microbial ( $C_B$ ) death follows first-order kinetics:

$$\text{Microbial death} = \pi \cdot C_B \quad (7.3)$$

Where  $\pi$  is the rate at which microbes die ( $\text{day}^{-1}$ ). The fraction of dead microbes that is transferred to the bio-available C pool in the mineral soil ( $C_{BIO-M}$ ) is denoted with  $F$ , the fraction of dead microbes which is transferred to the DOC pool in the rhizosphere is  $1-F$ . This bio-available C can subsequently be adsorbed minerals ( $C_q$ ) following Langmuir sorption:

$$\text{Adsorption} = \underbrace{K_{ads} \cdot C_{BIO-M}}_{\text{Maximum Adsorption}} \cdot \underbrace{\frac{(q_{max} - C_q)}{q_{max}}}_{\text{Rate limitation by availability of sorption sites}} \quad (7.4)$$

Where  $K_{ads}$  is the maximum adsorption rate ( $\text{m}^3 (\text{kg C})^{-1} \text{day}^{-1}$ ) and  $q_{max}$  is the maximum sorption capacity ( $\text{kg C m}^{-3}$ ). Desorption of OC from minerals is formulated as a first-order process.

$$\text{Desorption} = K_{des} \cdot C_q \quad (7.5)$$

Where  $K_{des}$  is the desorption rate ( $\text{day}^{-1}$ ). In contrast to the formulation of COMMISSION in the previous chapter, where  $K_{des}$  was assumed to be constant with depth, in the SOIL – RM model  $K_{des}$  decreases exponentially with depth:

$$K_{des} = K_{des0} e^{z/z_{e,Kdes}} \quad (7.6)$$

Where  $K_{des0}$  is the value of  $K_{des}$  at the soil surface and  $z_{e,Kdes}$  is the e-folding depth (set to 0.3 m). Carbon that is desorbed is readily taken up by soil microbes in the mineral soil ( $C_{B-M}$ ),

during which a fraction of C ( $1 - CUE$ ; carbon use efficiency) is released as  $\text{CO}_2$ . Dead microbes in the mineral soil are transferred to the bio-available C pool in the mineral soil ( $C_{\text{BIO-M}}$ ), which is in its turn used as substrate by soil microbes in the mineral soil ( $C_{\text{B-M}}$ ) according to ‘traditional Michaelis-Menten’ kinetics (similar to equation 7.2). The full set of differential equations governing the fluxes of C in the SOILcarb – RM is provided below, while parameter names are provided in Table 7.1 and parameter values in Table 7.2.

$$\frac{\partial}{\partial t} C_{\text{R}(t,z)} = \underbrace{(1 - L) \cdot i(t,z)}_{\text{Non-leachable litter input}} - \underbrace{V_{\text{max},D} \cdot C_{\text{R}(t,z)} \cdot \frac{C_{\text{B-R}(t,z)}}{K_{m,B} + C_{\text{B-R}(t,z)}}}_{\text{Depolimerisation of } C_{\text{r}}} + \underbrace{\frac{\partial}{\partial z} \left( D_{b(z)} \frac{\partial C_{\text{R}(t,z)}}{\partial z} \right)}_{\text{Bioturbation}} \quad (7.7)$$

$$\frac{\partial}{\partial t} C_{\text{DOC}(t,z)} = \underbrace{L \cdot i(t,z)}_{\text{DOC input}} + \underbrace{(1 - F) \cdot \pi \cdot C_{\text{B-R}(t,z)}}_{\text{Microbial death}} - \underbrace{V_{\text{max},D} \cdot C_{\text{DOC}(t,z)} \cdot \frac{C_{\text{B-R}(t,z)}}{K_{m,B} + C_{\text{B-R}(t,z)}}}_{\text{Depolimerisation of } C_{\text{doc}}} - \underbrace{v(z) \cdot \frac{\partial(C_{\text{DOC}(t,z)})}{\partial z}}_{\text{DOC flux with groundwater}} \quad (7.8)$$

$$\frac{\partial}{\partial t} C_{\text{BIO-R}(t,z)} = \underbrace{V_{\text{max},D} \cdot C_{\text{R}(t,z)} \cdot \frac{C_{\text{B-R}(t,z)}}{K_{m,B} + C_{\text{B-R}(t,z)}}}_{\text{Depolimerisation of } C_{\text{r}}} + \underbrace{V_{\text{max},D} \cdot C_{\text{DOC}(t,z)} \cdot \frac{C_{\text{B-R}(t,z)}}{K_{m,B} + C_{\text{B-R}(t,z)}}}_{\text{Depolimerisation of } C_{\text{doc}}} - \underbrace{V_{\text{max},U} \cdot C_{\text{B-R}(t,z)} \cdot \frac{C_{\text{BIO-R}(t,z)}}{K_{m,U} + C_{\text{BIO-R}(t,z)}}}_{\text{Bio-available C uptake by microbes in the rhizosphere}} + \underbrace{\frac{\partial}{\partial z} \left( D_{b(z)} \frac{\partial C_{\text{BIO-R}(t,z)}}{\partial z} \right)}_{\text{Bioturbation}} - \underbrace{v(z) \cdot \frac{\partial(C_{\text{DOC}(t,z)})}{\partial z}}_{\text{DOC flux with groundwater}} \quad (7.9)$$

$$\frac{\partial}{\partial t} C_{\text{B-R}(t,z)} = \underbrace{V_{\text{max},U} \cdot C_{\text{B-R}(t,z)} \cdot \frac{C_{\text{BIO-R}(t,z)}}{K_{m,U} + C_{\text{BIO-R}(t,z)}}}_{\text{Bio-available C uptake by microbes in the rhizosphere}} - \underbrace{\pi \cdot C_{\text{B-R}(t,z)}}_{\text{Microbial death}} + \underbrace{\frac{\partial}{\partial z} \left( D_{b(z)} \frac{\partial C_{\text{B-R}(t,z)}}{\partial z} \right)}_{\text{Bioturbation}} \quad (7.10)$$

$$\frac{\partial}{\partial t} C_{\text{BIO-M}(t,z)} = \underbrace{F \cdot \pi \cdot C_{\text{B-R}(t,z)}}_{\text{Microbial death from rhizosphere}} + \underbrace{\pi \cdot C_{\text{B-M}(t,z)}}_{\text{Microbial death from mineral sphere}} - \underbrace{V_{\text{max},U} \cdot C_{\text{B-M}(t,z)} \cdot \frac{C_{\text{BIO-M}(t,z)}}{K_{m,U} + C_{\text{BIO-M}(t,z)}}}_{\text{Bio-available C uptake by microbes in the mineral sphere}} - \underbrace{K_{\text{ads}} \cdot C_{\text{BIO-M}(t,z)} \cdot (q_{\text{max}} - C_{\text{q}(t,z)})}_{\text{Adsorption}} + \underbrace{\frac{\partial}{\partial z} \left( D_{b(z)} \frac{\partial C_{\text{BIO-M}(t,z)}}{\partial z} \right)}_{\text{Bioturbation}} - \underbrace{v(z) \cdot \frac{\partial(C_{\text{DOC}(t,z)})}{\partial z}}_{\text{DOC flux with groundwater}} \quad (7.11)$$

$$\frac{\partial}{\partial t} C_{\text{q}(t,z)} = \underbrace{K_{\text{ads}} \cdot C_{\text{BIO-M}(t,z)} \cdot (q_{\text{max}} - C_{\text{q}(t,z)})}_{\text{Adsorption}} - \underbrace{K_{\text{des}} \cdot C_{\text{q}(t,z)}}_{\text{Desorption}} + \underbrace{\frac{\partial}{\partial z} \left( D_{b(z)} \frac{\partial C_{\text{q}(t,z)}}{\partial z} \right)}_{\text{Bioturbation}} \quad (7.12)$$

$$\frac{\partial}{\partial t} C_{B-M}(t,z) = \underbrace{CUE \cdot K_{des} \cdot C_q(t,z)}_{\text{Desorption}} + \underbrace{V_{max,U} \cdot C_{B-M}(t,z) \cdot \frac{C_{BIO-M}(t,z)}{K_{m,U} + C_{BIO-M}(t,z)}}_{\text{Bio-available C uptake by microbes in the mineral sphere}} - \underbrace{\pi \cdot C_{B-M}(t,z)}_{\text{Microbial death}} \quad (7.13)$$

$$+ \underbrace{\frac{\partial}{\partial z} \left( D_b(z) \frac{\partial C_{B-M}(t,z)}{\partial z} \right)}_{\text{Bioturbation}}$$

**Table 7.1** Overview of the parameters, their names and units of the SOILcarb - RM model

Parameter	Name and units
$C_r$	Residual C [ $\text{kg C m}^{-3}$ ]
$C_{\text{DOC}}$	Dissolved C [ $\text{kg C m}^{-3}$ ]
$C_{\text{BIO-R}}$	Bio-available C in the rhizosphere [ $\text{kg C m}^{-3}$ ]
$C_{\text{B-R}}$	Microbial C in the rhizosphere [ $\text{kg C m}^{-3}$ ]
$C_{\text{BIO-M}}$	Bio-available C in the mineral soil [ $\text{kg C m}^{-3}$ ]
$C_{\text{B-M}}$	Microbial C in the mineral soil [ $\text{kg C m}^{-3}$ ]
$C_q$	Mineral-associated C [ $\text{kg C m}^{-3}$ ]
$t$	Time [days]
$z$	Depth [m]
$L$	Soluble fraction in C inputs [-]
$i$	C inputs [ $\text{kg C m}^{-2} \text{day}^{-1}$ ]
$V_{\text{max,D}}$	Maximum specific depolymerisation rate of $C_r$ by extracellular enzymes [ $\text{day}^{-1}$ ]
$K_{\text{m,B}}$	Half-saturation constant for depolymerisation of $C_r$ [ $\text{kg C m}^{-3}$ ]
$V_{\text{max,U}}$	Maximum specific uptake rate of $C_{\text{DOC}}$ by $C_{\text{B}}$ [ $\text{day}^{-1}$ ]
$K_{\text{m,U}}$	Half-saturation constant for uptake of $C_{\text{DOC}}$ by $C_{\text{B}}$ [ $\text{kg C m}^{-3}$ ]
$F$	Fraction of dead microbes transferred to mineral soil [-]
$\pi$	Mortality rate of microbes [ $\text{day}^{-1}$ ]
$K_{\text{ads}}$	Adsorption rate [ $\text{m}^3 (\text{kg C})^{-1} \text{day}^{-1}$ ]
$K_{\text{des}}$	Desorption rate [ $\text{day}^{-1}$ ]
$q_{\text{max}}$	Maximum sorption capacity [ $\text{kg C m}^{-3}$ ]
$D_b$	Biodiffusion coefficient [ $\text{m}^2 \text{day}^{-1}$ ]
$v$	Pore water velocity [ $\text{m day}^{-1}$ ]
$CUE$	Carbon use efficiency by microbes [-]

### 7.2.3 Simulation of $^{13}\text{C}$ and $^{14}\text{C}$ in SOILcarb – RM

The dynamics of  $^{13}\text{C}$  are explicitly coupled to microbial processes in a similar way as was done for COMMISSION in the previous chapter. In brief, the magnitude of  $^{12}\text{C}$  discrimination, relative to  $^{13}\text{C}$ , was incorporated in SOILcarb – RM using a fractionation factor:

$$\alpha_{\text{respiration}} = \frac{R_{\text{CO}_2}}{R_{\text{BIO} \rightarrow \text{microbes}}} \quad (7.14)$$

Where  $\alpha_{\text{respiration}}$  is the fractionation factors regulating isotopic discrimination during  $\text{CO}_2$  respiration,  $R$  is the  $^{13}\text{C}/^{12}\text{C}$  ratio of the different pools and ' $\text{BIO} \rightarrow \text{microbes}$ ' stands for C transferred from the bio-available C pools to microbes in both the rhizosphere and the mineral soil. Similar to the runs in precious chapter, the value of  $\alpha_{\text{respiration}}$  was set to 0.999 and the  $\delta^{13}\text{C}$  value of aboveground vegetation was -28.5 ‰, the value for belowground C

**Table 7.2** Parameter values for the SOILcarb - RM model

Parameter	Value	Parameter	Value
L	0.9	$K_{\text{ads}}$	$500 \text{ m}^3 (\text{kg C})^{-1} \text{ day}^{-1}$
$V_{\text{max,D}}$	$0.001 \text{ day}^{-1}$	$K_{\text{des}}$	$4 \cdot 10^{-5} \text{ day}^{-1}$
$K_{\text{m,B}}$	$0.01 \text{ kg C m}^{-3}$	$q_{\text{max}}$	$70 \text{ kg C m}^{-3}$
$V_{\text{max,U}}$	$0.1 \text{ day}^{-1}$	$D_{\text{b0}}$	$5 \cdot 10^{-5} \text{ m}^2 \text{ day}^{-1}$
$K_{\text{m,U}}$	$1 \cdot 10^{-5} \text{ kg C m}^{-3}$	$z_{\text{e\_Db}}$	$0.05 \text{ m}^2 \text{ yr}^{-1}$
F	0.5	$v(0)$	$1 \cdot 10^{-3} \text{ m day}^{-1}$
$\pi$	$5 \cdot 10^{-3} \text{ day}^{-1}$	CUE	0.392

inputs was  $-28 \text{ ‰}$ .  $^{13}\text{C}$  fractionation occurs at every location in the model structure where respiration takes place (Figure 7-1). It is noted that the model does not simulate the preferential uptake of  $^{13}\text{C}$  by soil microbes as a consequence of preferential utilization of substrate enriched in  $^{13}\text{C}$ , as proposed by Werth and Kuzyakov (2010) as an additional mechanism leading to  $^{13}\text{C}$  enrichment of soil microbes. The rationale behind this choice is that it has been argued that, given the right conditions and sufficient time, all plant-produced organic matter is eventually processed by soil microbes, thereby rejecting the theory of preferential uptake of labile substrates by soil microbes (Lehmann and Kleber, 2015).  $^{14}\text{C}$  isotopes were explicitly modelled, with fluxes of  $^{14}\text{C}$  in the model being proportional to fluxes of  $^{12}\text{C}$  to avoid isotopic discrimination. Radioactive decay of  $^{14}\text{C}$  atoms performed at every time step, as described in the previous chapter.

### 7.3 Results

#### 7.3.1 The potential of SOILcarb - RM to simulate $\delta^{13}\text{C}$ depth profiles

The results of the simulations performed with the SOILcarb – RM model are shown in Figure 7-2. The depth profile of total OC shows an exponential decrease with depth, from ca. 4 % OC at the soil surface to ca. 0.2 % OC at a depth of 0.6 m (Figure 7-2a). The majority of OC is associated with minerals while significant amounts of unprocessed OC (the  $C_{\text{R}}$  pool) are limited to the upper ca. 0.2 m, which is in accordance with measurements in European forests (Figure 6-1). Also the simulated  $^{14}\text{C}$  depth profile is in line with measurements with only topsoil OC (upper ca. 0.1 m) containing ‘bomb  $^{14}\text{C}$ ’, while deeper down the profile the fraction modern carbon (post 1950) decreases substantially (see Figure 6-1 in the previous chapter for a measured depth profile of  $\delta^{13}\text{C}$  and  $^{14}\text{C}$ , Schrumpf et al. (2013)). It is interesting to note that while substantial root inputs are simulated in the upper 0.5 m (root depth profile not shown, e-folding depth is 0.2 m), OC is present in significant amounts deeper down the soil profile as a consequence of the vertical movement of DOC and subsequent interaction with soil minerals. To show the effect of DOC movement on the simulated total OC and  $^{14}\text{C}$  depth profiles, a run with the same parameter values but without advection of soluble pools was performed (Figure 7-3). This shows that the simulated downward advection of soluble OC pools indeed results in OC storage below the active rooting zone (Figure 7-3a). The depth profile of the fraction modern  $^{14}\text{C}$  shows that when advection of soluble pools is absent, subsoil OC is slightly younger compared to the runs including advection of soluble

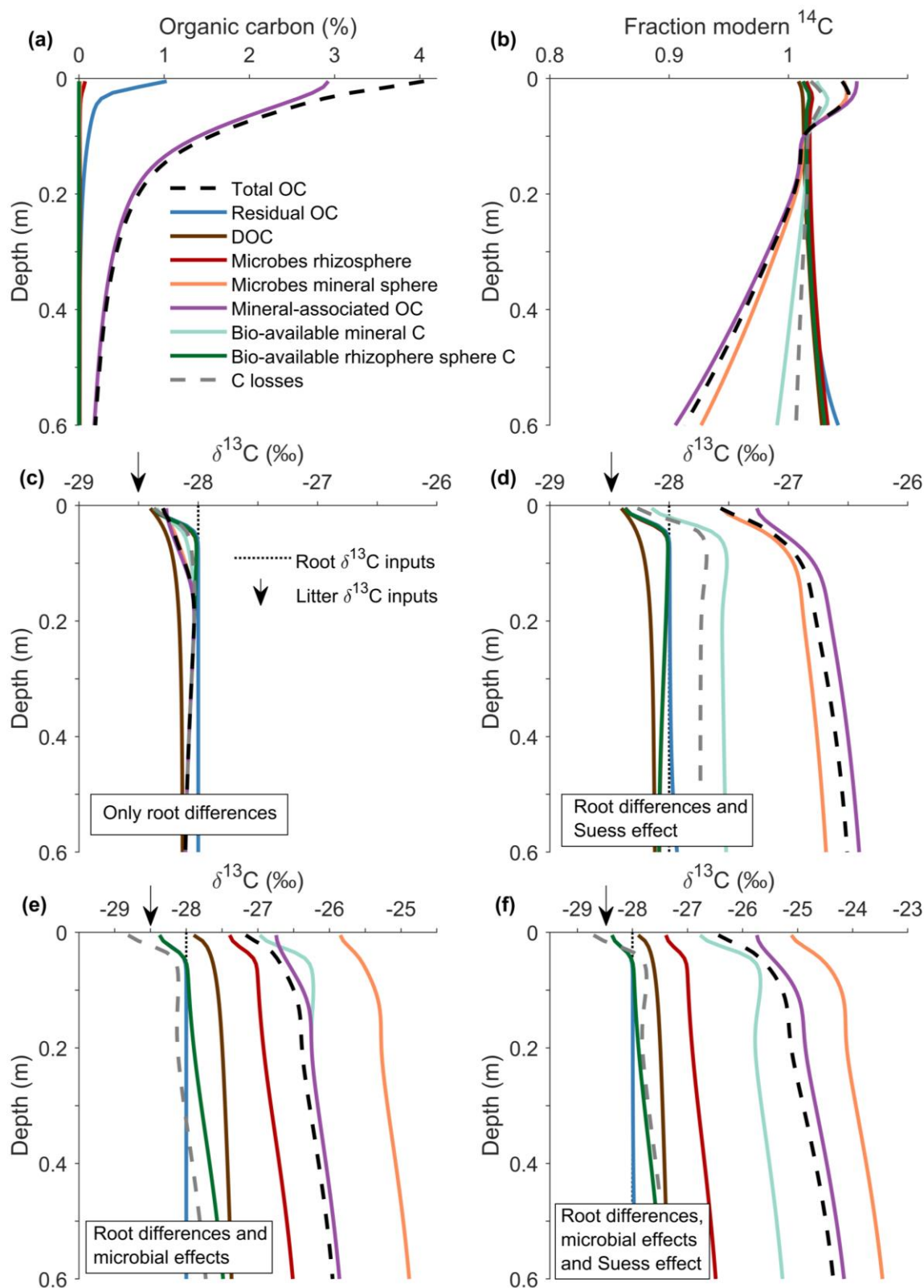


**Figure 7-2** Modelled depth profiles using the SOILcarb - RM model: (a) organic carbon concentration, (b) fraction modern  $^{14}\text{C}$ , (c) - (f)  $\delta^{13}\text{C}$  profiles with different mechanisms leading to  $^{13}\text{C}$  enrichment: (c)  $^{13}\text{C}$  enriched roots, (d)  $^{13}\text{C}$  enriched roots and the Suess effect, (d) same as (c) but including microbial kinetic fractionation and (f)  $^{13}\text{C}$  enriched roots, the  $^{13}\text{C}$  - Suess effect and microbial kinetic fractionation combined. Note: the value of root inputs refers to the value of the last simulation year, when the Suess effect is simulated these values were higher in the pre-industrial period.

pools (Figure 7-3b), as a consequence of a higher relative contribution of fresh C to deeper soil layers (the rooting profile decreases exponentially, thus at a depth of e.g. 0.6 m still a very small amount of C enters the soil through roots) compared to the situation when deeper soil layers receive advected OC which has been in the soil for a longer period of time.

When the SOILcarb – RM model is ran with the isotopic difference between aboveground litter and roots as the only factor affecting the  $\delta^{13}\text{C}$  depth profile, a steep increase in the topsoil  $\delta^{13}\text{C}$  value is observed, from the value of litter at the soil surface (-28.5 ‰) to the value of roots (-28 ‰) at ca. 0.2 m depth (Figure 7-2a). Below this depth, the  $\delta^{13}\text{C}$  value of the total SOC stock (dominated by the  $\delta^{13}\text{C}$  value of mineral-associated OC) decreases again with depth. This is a consequence of the isotopically lighter signature of DOC, which originates partly from isotopically lighter litter (compared to roots). As the majority of mineral-associated OC below ca. 0.4 m originates from vertically leached DOC (Figure 7-3a and Figure 7-2a), the value of mineral-associated OC resembles the isotopic signature of DOC below the rooting zone for this scenario.

When the  $^{13}\text{C}$  – Suess effect is added to this set-up, the  $\delta^{13}\text{C}$  value of total OC shows an increase with depth (Figure 7-2d). There is, however, a clear difference in the  $\delta^{13}\text{C}$  value of the simulated SOC pools, as mineral-associated OC and microbes in the mineral soil have a substantially heavier isotopic signal ( $^{13}\text{C}$ -enriched) compared to the other pools. This is a consequence of the slower cycling rate of OC in the mineral soil compartment compared to the rhizosphere compartment. This causes the mineral soil compartment to contain a substantial amount of pre-industrial (and thus isotopically heavier) OC, while the OC pools in the rhizosphere compartment react faster to changes in the  $\delta^{13}\text{C}$  of C inputs.

Next, the SOILcarb – RM model was ran with the isotopic difference between aboveground litter and roots combined with microbial effects on isotopic fractionation (Figure 7-2e). The  $\delta^{13}\text{C}$  value of total OC, which is similar to the  $\delta^{13}\text{C}$  value of mineral-associated OC, is larger (less negative) compared to OC inputs and increases with depth throughout the soil profile. The fact that the isotopic signature of the mineral-associated OC pool is heavier compared to

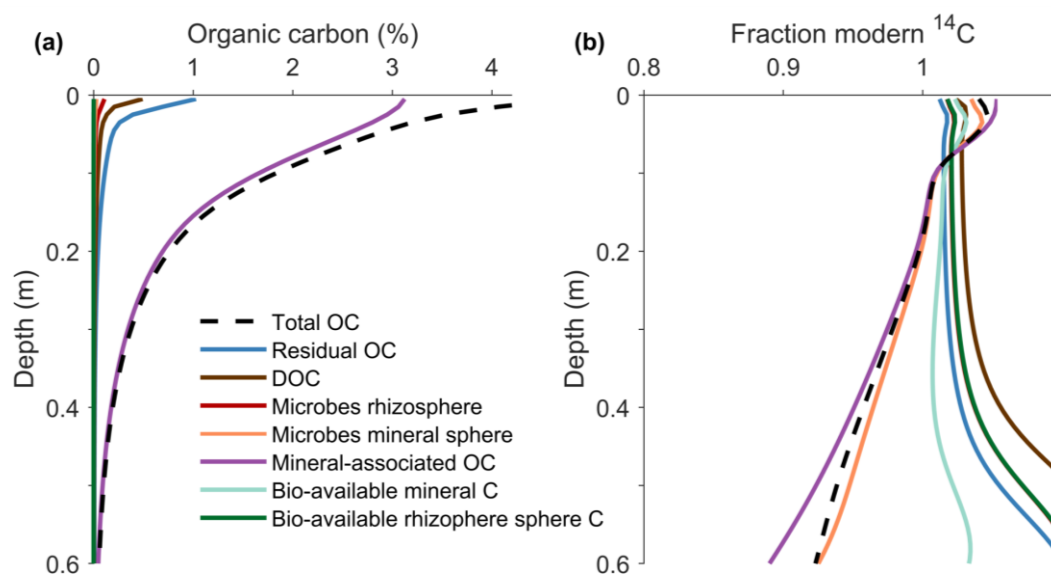


**Figure 7-3** Simulation of the SOILcarb - RM model without advection of DOC

the signature of C inputs is a consequence of the model structure of SOILcarb – RM, as the C that enters the mineral soil has already been processed by soil microbes in the rhizosphere and is therefore isotopically enriched in  $^{13}\text{C}$ . The  $\delta^{13}\text{C}$  value of microbes in the mineral soil compartment is, as expected, even heavier compared to mineral-associated C. The increase with depth of the  $\delta^{13}\text{C}$  value of mineral-associated OC is the consequence of the fact that the contribution of leached OC to total OC increases with depth. In topsoil layers, less processes OC (which has not passed through the ‘microbial loop’ in the rhizosphere) can be readily transferred to the mineral soil to be adsorbed to minerals, while the C present in the mineral soil in deeper soil layers has gone through the ‘microbial loop’ multiple times and is thus isotopically enriched in  $^{13}\text{C}$ .

When all the mechanisms which are attributed to affect the  $\delta^{13}\text{C}$  value of SOC are included in the SOILcarb – RM model (isotopic differences between litter and roots, the  $^{13}\text{C}$  – Suess effect and microbial effects), the results show how the model simulates the  $\delta^{13}\text{C}$  profile of a natural undisturbed forest soil (Figure 7-2f). The simulated  $\delta^{13}\text{C}$  value of total OC shows an increase with depth throughout the soil profile while the steepest increase takes place in the topsoil. The heavier  $\delta^{13}\text{C}$  value ( $^{13}\text{C}$ -enriched, less negative) of topsoil OC compared to litter (ca. 1.5 ‰) is a feature which is generally observed in natural ecosystems (Acton et al., 2013; Balesdent et al., 1993; Boström et al., 2007; Powers and Schlesinger, 2002). The  $\delta^{13}\text{C}$  value of the mineral-associated OC pool dominates the total value while it’s larger compared to C inputs and increases with depth, as was also observed for measured mineral-associated C pools in undisturbed forest soils in Europe (Schrumpf et al., 2013, see Figure 6.1 in the previous chapter). Moreover, the isotopic signature of microbes in the mineral soil is heavier compared to the signature of total OC, which is also in line with empirical data (Dijkstra et al., 2006; Werth and Kuzyakov, 2010). The  $\delta^{13}\text{C}$  value of the OC pools in the rhizosphere compartment, in contrast, are similar to the  $\delta^{13}\text{C}$  value of C inputs, which is in line with observations that the  $\delta^{13}\text{C}$  value of unprocessed particulate OC is constant with depth and more negative compared to the  $\delta^{13}\text{C}$  value of total SOC (Schrumpf et al., 2013).

The characteristics of respired  $\text{CO}_2$  (‘C losses’ in Figure 7-2) show that respired C has a fraction modern  $^{14}\text{C} > 1$ , indicating that at least down to 0.6 m of the simulated soil profile relatively fresh SOC served as the main source for bacterial metabolism, rather than bulk SOC, which has a smaller fraction modern  $^{14}\text{C}$  (Figure 7-2b). This is in line with empirical studies which came to similar conclusions (Trumbore, 2000). The  $\delta^{13}\text{C}$  value of respired  $\text{CO}_2$  is slightly less negative compared to the  $\delta^{13}\text{C}$  value of roots, and substantially depleted in  $^{13}\text{C}$  compared to the total SOC (Figure 7-2f). This is in line with studies showing that the  $\delta^{13}\text{C}$  value of respired  $\text{CO}_2$  is slightly enriched in  $^{13}\text{C}$  compared to C inputs (Werth and Kuzyakov, 2010), but is contradictory to other studies which have reported respired  $\text{CO}_2$  which was enriched in  $^{13}\text{C}$  compared to bulk SOM (Boström et al., 2007). The combined results for total OC,  $F^{14}\text{C}$  and  $\delta^{13}\text{C}$  suggest that the structure of the SOILcarb – RM model adequately represent the dynamics of SOC along soil profiles, as influenced by vertical OC transport, microbial interactions and the stabilization of OC on mineral surfaces.

## 7.4 Discussion

### 7.4.1 Novelties of the SOILcarb – RM model

Over the past years, a new paradigm on the preservation mechanisms of SOC has emerged (Cotrufo et al., 2013; Lehmann and Kleber, 2015; Schmidt et al., 2011), as discussed in the introduction of this dissertation (section 1.2). In the historical view, the preservation of soil organic matter was a consequence of the preferential processing and preservation of plant inputs whose chemical complexity rendered them inert to microbial degradation. According to the new view, the preservation of soil organic matter is governed by ecosystem properties such as a physical disconnection between microbes and substrates and the sorption of organic matter on mineral surfaces. In addition, it has been shown that a large portion of stabilized SOC has a microbial origin (Miltner et al., 2012). Together with the advent of this new paradigm, new SOC models have been developed to simulate soil organic matter dynamics in accordance to the proposed mechanisms of soil organic matter formation and preservation. A complete overview of these models is beyond the scope of this study, but reference to these models will be made where appropriate. Together with the emergence of this new paradigm, deep SOC is being increasingly recognized to be an important part of the global carbon cycle (Jobbágy and Jackson, 2000; Rumpel and Kögel-Knabner, 2010) and to be vulnerable to climatic and anthropogenic disturbances (Harrison et al., 2011; Hobbey et al., 2017; Shi et al., 2013). Given that both these views on SOC cycling have been widely accepted, it is surprising that the incorporation of the proposed mechanisms in SOC models has been largely limited to models that do not account for the distribution of SOC with depth (e.g. Allison et al., 2010; Davidson et al., 2012; Luo et al., 2017; Sulman et al., 2014; Wang et al., 2013; Wieder et al., 2014), while the number of models that do so is limited (e.g. Ahrens et al., 2015; Dwivedi et al., 2017; Riley et al., 2014; Wieder et al., 2013). However, the development and testing of SOC models simulating deep SOC is an important prerequisite to simulate how total SOC stocks will change in the face of climatic and anthropogenic changes.

SOILcarb – RM is a process-based SOC model that simulates depth profiles of SOC,  $\delta^{13}\text{C}$  and  $\text{F}^{14}\text{C}$ , while accounting for depth-dependent OC inputs and stabilization of SOC by interactions with minerals. The model explicitly simulates depolymerisation of plant inputs by enzymes produced by microbes (although the former are not explicitly modelled but are assumed to be proportional to microbial biomass) using reverse Michaelis-Menten kinetics (similar to Ahrens et al. (2015) and Schimel and Weintraub (2003)) and microbial uptake of bio-available C using traditional Michaelis-Menten kinetics (similar to other recently developed SOC models (e.g. COMMISSION (Ahrens et al., 2015); DAMM (Davidson et al., 2012); MEND (Wang et al., 2013); BAMS1 (Riley et al., 2014) and MIMICS (Wieder et al., 2014))). The major novelty of the SOILcarb – RM model is that there is an explicit separation between the rhizosphere and the mineral soil. To the best of my knowledge, this has only been done in one other process-based SOC model (CORPSE; Sulman et al. (2014)), but there both soil compartments receive direct OC from litter and roots, while also protected C is present in both compartments. Similar to the COMMISSION model, SOILcarb-RM allows for the cycling of microbial necromass. This is done in two separate ‘microbial loops’, one in the rhizosphere, where a portion of microbial necromass is transferred to the DOC pool, and another one in the mineral soil, where

microbial necromass is can be adsorbed on minerals or again be used by living microbes as a source of energy (Figure 7-1). It is noted that despite a microbial loop is also present in the COMMISSION model (Figure 6-4), this loop did not led to the enrichment of  $^{13}\text{C}$  with depth. This is attributed to the direct input of both microbial necromass and fresh inputs to the DOC pool, with the magnitude of the former flux being smaller compared to the latter. This only caused a limited increase in the  $\delta^{13}\text{C}$  value of DOC, and thus mineral-associated OC, with depth. The model set-up that is proposed here offers two main advantages compared to set-ups where the soil is viewed as a homogenous continuum in which OC cycles.

First, the proposed approach does not assume a direct coupling between OC inputs through roots stabilized OC in the subsoil. The wide range of empirical evidence that OC below ca. 0.2 m depth is on average up to millennia old implies that there is no direct input of root C to stabilized SOC, as earlier pointed out by Kaiser and Kalbitz (2012). Moreover, observations that  $\text{CO}_2$  in the soil pore space is derived from recent OC (although this might also include  $\text{CO}_2$  from root respiration) suggest that stabilized, old OC is not a major source for microbial respiration in subsoils. Both features are simulated by the SOILcarb – RM model, as (i) OC inputs are processed by soil microbes before they can be adsorbed to minerals to be preserved over long timescales (Figure 7-1) while (ii) OC in the rhizosphere is the main source for microbial respiration, as indicated by the high  $^{14}\text{C}$  content of respired  $\text{CO}_2$  (Figure 7-2f).

Second, the proposed model set-up has the result that OC has to be processed by soil microbes before it can be stored in the soil over centennial timescales by adsorption to minerals. This is in line with multiple studies which have argued that microbial necromass (dead microbes) is an important precursor of stable SOC (Cotrufo et al., 2013; Liang et al., 2017; Rumpel and Kögel-Knabner, 2010; Schmidt et al., 2011; Six et al., 2006). Specifically, Miltner et al. (2012) proposed a framework of stable soil organic matter formation by stabilization of cell wall material from bacteria and fungi on mineral surfaces, while this organic matter can again be desorbed and used by the soil microbial community. In addition, based on an analysis of the  $\delta^{13}\text{C}$  value of phospholipid fatty acids from bacteria and fungi along a soil profiles, Kohl et al. (2015) concluded that the contribution of microbial necromass to the total SOC stock increases with increasing soil depth. Their conclusion was based on the observation that soil bacteria are on average enriched in  $^{13}\text{C}$  compared to OC inputs, which is in accordance with earlier observations (Dijkstra et al., 2006). The proposed mainly microbial origin of mineral-associated OC is also in line with the low C:N ratio that is generally observed for this fraction (Miltner et al., 2012; Schrumpf et al., 2013). This value is slightly higher compared to the C:N ratios observed for bacteria (3-6, Wallander et al. (2003) and references therein), and is substantially lower compared to the C:N ratio of e.g. free particulate organic matter in soils (Schrumpf et al., 2013). As a consequence of these lines of evidence, Miltner et al. (2012) concluded that “soil C turnover models should reflect that stabilisation of microbial biomass, an inherently biodegradable material, is much more important than recalcitrance of plant residues”.

One of the most important differences between SOC models with conceptual pools with pre-defined turnover rates and recently developed process-based SOC models is that in the first type of models, decomposition rates are generally assumed to decrease exponentially with

depth (Jenkinson and Coleman, 2008; Van Dam et al., 1997; Wang et al., 2015a), although exceptions exist (Baisden et al., 2002; Elzein and Balesdent, 1995; see previous chapter). In the second type of models, in contrast, this modelled decrease in OC decomposition with depth (which has been referred to as an 'arbitrary function' (Riley et al., 2014)) is not included and other mechanisms are responsible for the slower turnover rates of SOC with increasing soil depth. For example, in BAMS1 (Riley et al., 2014),  $\Delta^{14}\text{C}$  values decrease with depth because of a decreasing decomposition rate with depth associated with decreasing OC substrate concentration and thus microbial biomass. In the COMMISSION model (Ahrens et al., 2015), similar results were obtained as a consequence of the limited depolymerisation of OC by microbes and stabilization of OC on mineral surfaces in the subsoil. In the model formulation of SOILcarb – RM, an additional mechanism to reduce the decomposition rate with increasing soil depth is introduced in the form of a decreasing rate of OC desorption from minerals ( $K_{\text{des}}$ ) with depth. This mechanism was introduced to the model to represent the effect of decreased desorption with depth, as it is generally observed in undisturbed soils that the turnover rate of mineral-associated OC in topsoils is much faster compared to subsoils. However, despite efforts to quantify the effect of different controls on the desorption of mineral-associated OC, such as biotic priming (Fontaine et al., 2007, 2003), abiotic release of OC by interactions with root exudates (Keiluweit et al., 2015) and soil moisture content (Blankinship and Schimel, 2018), information on the effect of these factors on the desorption of mineral-associated OC along the soil profile is very limited. Therefore, it was chosen to include an exponentially decreasing  $K_{\text{des}}$  value with depth. In the original formulation of the COMMISSION model,  $K_{\text{des}}$  was assumed to be constant with depth, although the maximum sorption capacity of the soil ( $q_{\text{max}}$ ) was assumed to decrease substantially with depth. This also results in a decreasing turnover rate of adsorbed OC with depth, because when the maximum sorption capacity is reached and under steady state, the rate of adsorption and desorption scales with the maximum sorption capacity ( $q_{\text{max}}$ ). The validity of the assumption of a decreasing desorption rate with depth is, however, to be tested in further research.

Another difference between SOILcarb – RM and other process-based SOC models is the addition of a bio-available SOC pool, although this has been done for some other models (Lawrence et al., 2009). This addition was based on the fact that it has been shown that only a portion of DOC is readily available for microbial uptake (Andreasson et al., 2009; Risse-Buhl et al., 2013; Shen et al., 2015). In addition, a direct coupling between a DOC pool and minerals, as is the case in COMMISSION, does not allow microbes to be the main source of stabilized soil organic matter (see above).

#### **7.4.2 The added value of the simulation of $\delta^{13}\text{C}$ values**

Another novelty of SOILcarb – RM is that it allows to calculate realistic depth profiles of stable carbon isotopes by linking isotopic discrimination explicitly to SOC dynamics. To the best of my knowledge, this has to date not been done based in another process based SOC model. Therefore, a comparison of the performance of SOILcarb – RM with similar models is not possible. In the current version of the SOILcarb – RM model, the following processes lead to the relative  $^{13}\text{C}$  enrichment of SOC with depth: (1) differences in the isotopic signature between aboveground litter and roots, (2) the  $^{13}\text{C}$  – Suess effect and (3) the preferential

respiration of  $^{12}\text{C}$  by soil microbes. It is noted that potential isotopic discrimination related to interactions between SOC and soil minerals are not accounted for in the model, as these effects have been less documented in literature. Noteworthy here is the study by Kaiser et al. (2001), in which lab experiments of DOC sorption on synthetic minerals were performed in addition to measurements of the  $\delta^{13}\text{C}$  value of DOC in forest soils. These authors reported that the hydrophobic fraction of DOC, which is typically depleted in  $^{13}\text{C}$  compared to total DOC (see also Nakanishi et al. (2012)), is preferentially adsorbed on soil minerals in the topsoil, while the ( $^{13}\text{C}$ -enriched) hydrophilic fraction is preferentially adsorbed in subsoils. In their experiments, the authors used DOC extracted from forest floor litter. Based on the above provided arguments that a substantial portion of mineral-associated OC in soils has been processed by soil microbes and consists for a large portion of microbial necromass, it can be argued that the experiments performed by Kaiser et al. (2001), although informative on how plant-derived DOC reacts with minerals, do not resemble the situation of OC-mineral interactions in soils. In addition, it can be argued that the increase in the  $\delta^{13}\text{C}$  value of DOC with soil depth in forest soils, as observed by Kaiser et al. (2001), is a consequence of interactions between soil water and SOC, which is typically more enriched in  $^{13}\text{C}$  with increasing depth as a consequence of an increasing contribution of microbial-derived OC with increasing soil depth. Because of these uncertainties, no isotopic discrimination was assumed for interactions between OC and soil minerals in the SOILcarb – RM model. The structure of the model, however, allows to include these mechanisms in future studies.

As the model runs performed here were not validated against field measurements, further research has to quantify the accuracy with which  $\delta^{13}\text{C}$  depth profiles can be simulated. If the confrontation of model results with measurements shows that accurate  $\delta^{13}\text{C}$  depth profiles can be simulated using SOILcarb - RM, simulated  $\delta^{13}\text{C}$  profiles of the total OC stock and the different pools can be used as an additional calibration criterion for model evaluation in the future, as argued in the introduction.

### **7.4.3 Increasing model complexity implies a trade-off with data availability**

When developing models simulating natural environmental systems, which are very heterogeneous in space and time, special attention has to be paid to the trade-off between model complexity and data-availability (e.g. Schindler and Hilborn, 2015). Based on the framework proposed by Van Rompaey and Govers (2002), the error associated with the model structure decreases when more well-described processes are represented in the model ('model error'). However, this increase in model complexity will lead to an increasing error associated with uncertainties with input data, or the lack thereof ('input error'), as shown in Figure 7-4 (hereafter called the model complexity – error graph). This trade-off between model complexity and data availability is important to consider when developing models simulating SOC dynamics. Over the past decades, there has been an evolution from relatively simple SOC models with one or more conceptual pools, to very complex models included microbial dynamics and related enzyme production, protection mechanisms of OC, vertical soil mixing and sometimes even subdividing SOC in different molecular classes with different characteristics. Although it is difficult to place different SOC model on the horizontal axis of

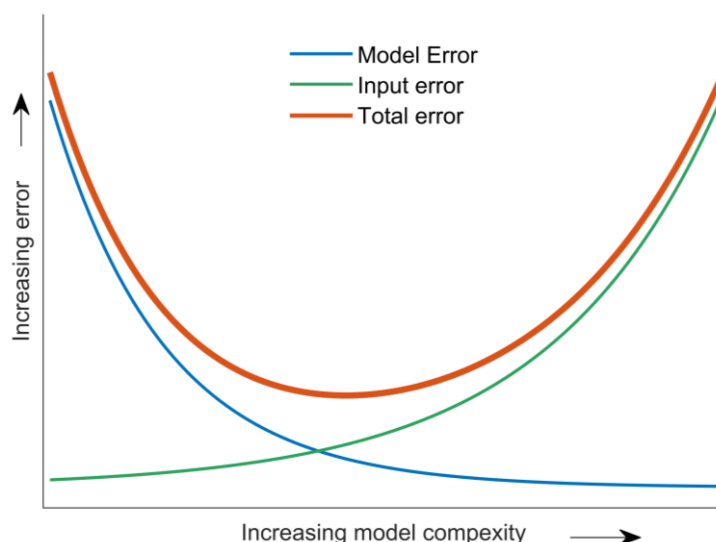


**Figure 7-4** The trade-off between complexity of environmental models and data availability results in an optimal model complexity with a minimal error (Van Rompaey and Govers, 2002)

the model complexity – error graph, it can be hypothesized that model using conceptual pools (e.g. ICBM, RothC and Century) are located to the left of the optimal model complexity, due to the minimalistic process representation, while the most complex process based models (e.g. BAMS1; Riley et al. (2014)), can be placed to the right of the optimal complexity (of course depending on the purpose for which these models are used). The rationale for the latter is that Riley et al. (2014) state that ‘to our knowledge, observations do not exist to fully test such a complicated model structure [...]’.

This indicates that, while models representing detailed mechanisms are a great advance as they allow to test multiple hypothesis regarding SOC cycling in a numerical framework, applying SOC models with such complexities to different soil environments will be difficult due to the lack of validation possibilities. The location of less complex process-based models, such as COMMISSION and SOILcarb – RM, lies somewhere in between on the model complexity – error graph, yet probable to the right of the optimal complexity, as some of the parameters in both model formulations are very difficult to measure in natural soil environments (e.g. parameters regarding the rate of depolymerisation or microbial uptake of OC), while the effect of environmental factors, e.g. temperature and soil moisture are currently not even included. It is noted that the assessment of the relation between model complexity and error of an environmental model depends on the purpose for which the model is used. If the aim of the model is to simulate very detailed processes for which numerous parameter values can be obtained under controlled lab conditions, a very complex model can be applied with a reasonable error. In contrast, when this model is used to simulate spatially distributed processes at the landscape scale, a very large uncertainty on parameter values can be expected.

#### 7.4.4 Considerations for future work

The following recommendations for future work regarding the SOILcarb – RM model are made:

- Although there is considerable evidence that mineral-associated OC consists mainly of microbial necromass (e.g. Miltner et al., 2012), assuming that this is the only source of stable OC in soils, as is currently done in SOILcarb – RM, is clearly a simplification of reality as mineral-associated OC consists of a mixture of sources (Angst et al., 2017; Kleber et al., 2015). Therefore, changes to the current model structure could be made to assess model results when also other OC sources are transferred from the rhizosphere compartment to the mineral soil compartment. Also, the current assumption that a portion of dead microbes in the rhizosphere is transferred to the DOC pool and needs to be depolymerised before it can be used by microbes, while the remainder is transferred to a bio-available OC pool, should be checked. This is currently justified by the fact that a portion of necromass (the cytosol) has been hypothesized to be more easily adsorbed to minerals compared to more resistant material (e.g. the cell wall) (Miltner et al., 2012), but assuming that the cytosol is transferred to the mineral soil while cell walls remain in the rhizosphere might be an oversimplification of reality.
- In the current model simulations, the maximum sorption capacity of OC to soil minerals ( $q_{max}$ ) is assumed to be constant with depth. It has, however, been shown that this capacity varies among different soil horizons (Kaiser and Guggenberger, 2003; Kothawala et al., 2009), so a correct formulation of this depth-dependence could improve model simulations. In addition, different formulations of OC adsorption to minerals could be assessed (Kothawala et al., 2008). However, the currently applied Langmuir sorption has the advantage that the rate of OC adsorption decreases with a decreasing available surface area for sorption, in line with empirical evidence (Kaiser and Guggenberger, 2003).
- Also the current formulation of desorption of OC from minerals as a first-order process ( $k_{Des} \cdot C_q$ ) is probably too simplistic. According to this formulation, the rate of desorption is independent of environmental factors which could lead to a rapid loss of OC. This is, however, likely not to be the case in soils, as it is generally observed that e.g. deforestation leads to substantial losses of previously stable and old SOC along the entire soil profile (e.g. Hobbey et al., 2017). In addition, it has recently been shown that the 'priming effect' might not only lead to accelerated SOC losses through microbial mechanisms (Fontaine et al., 2007, 2003) but might also be the result of enhanced liberation of mineral-associated OC through interactions with root exudates (Keiluweit et al., 2015). These mechanisms could be included in a future version of the model by making  $K_{des}$  a function of environmental disturbances given that an appropriate amount of empirical evidence is present to support this.
- An important SOC preservation mechanism, the protection of SOC inside microaggregates (Six et al., 2000), is currently absent in the model. This is the case in most SOC models, but efforts have been made to represent aggregates as a protection mechanism of SOC (Abramoff et al., 2018; Segoli et al., 2013). As a correct representation of SOC cycling in SOILcarb – RM would benefit from the incorporation of aggregates as a protection mechanism of OC, this is a promising direction for future research.

## 7.5 Conclusions

The aim of this study was to develop and present a new process-based model to simulate depth profiles of total OC, stable carbon isotopes ( $\delta^{13}\text{C}$ ) and  $^{14}\text{C}$ , based on the conclusions drawn from attempts to include  $\delta^{13}\text{C}$  simulations in two well-established SOC models (see chapter 6). Based on a literature review and the conclusion in the previous chapter, SOILcarb – RM was developed based on the principles of the COMMISSION model (Ahrens et al., 2015) as presented in chapter 6. The novelty of SOILcarb – RM lies in the separation of the rhizosphere (which receives direct OC inputs from aboveground litter and roots) and the mineral soil (which receives OC inputs from the rhizosphere in the form of dead microbes). This de-coupling of fresh OC inputs and long-term OC storage is in accordance with empirical observations that a substantial portion of stable OC in soils has a microbial origin. In addition, the new model structure allowed to simulate reliable depth profiles of total OC,  $^{14}\text{C}$  and  $\delta^{13}\text{C}$ . As the SOILcarb – RM model is currently still in its conceptual phase, future validations with field data need to quantify its accuracy.



## Chapter 8 Conclusions

---

### 8.1 Implications for future soil organic carbon research

#### 8.1.1 Assessment of the organic carbon sink capacity of intertidal vegetated ecosystems

The results presented in this PhD dissertation have shown that there are clear gradients in the origin of OC that is stored in tidal marsh sediments along the Scheldt estuary. One of the conclusions of chapter 3 of this dissertation was that on a decadal time scale, the amount of locally fixed atmospheric CO<sub>2</sub> that is effectively buried in saltmarsh sediments is limited. In freshwater marsh sediments, in contrast, a substantial amount of locally produced biomass is buried on a decadal and potentially longer timescale. As a consequence, it was concluded that freshwater tidal marshes are a more substantial sink for atmospheric CO<sub>2</sub> compared to salt marshes in the estuary of the Scheldt river.

The sequestration of atmospheric CO<sub>2</sub> is defined here as the capacity of an ecosystem to remove CO<sub>2</sub> from the atmosphere and store it in a stable organic form, in order for this CO<sub>2</sub> to not act as a greenhouse gas for a considerable amount of time. Although not explicitly considered in the studies presented in chapters 2 and 3 of this dissertation, the assessment of the potential of tidal marsh sediments to sequester CO<sub>2</sub> depends to a large extent on the spatial and temporal scales that are considered. The studies presented here were focussed on OC dynamics at the spatial scale of the soil profile (i.e. the local scale). Considering this scale, the results showed that the amount of CO<sub>2</sub> that is effectively removed from the atmosphere and sequestered in tidal marsh sediments depend on the preservation of locally produced organic matter upon burial. The rationale not to consider allochthonous OC (i.e. OC deposited on the tidal marsh platform during tidal inundations) to contribute to CO<sub>2</sub> sequestration at the local scale is that this OC has been transported to these tidal marshes after having been sequestered in other ecosystems (e.g. terrestrial or marine).

On the spatial scale of the entire Scheldt estuary (the regional scale), in contrast, the transport of OC through the landscape, as a consequence of its association with minerals, is an important aspect of the regional OC cycle. On this spatial scale, tidal marsh sediments can be considered to act as important stores for OC, as the results presented in this dissertation have shown that OC that is being deposited on the platform of tidal marshes along the entire estuary is efficiently preserved on a decadal (and probably longer) timescale. Although it is not clear what the fate of this OC would be if it had not been deposited on these tidal marsh platforms (preservation versus mineralization after deposition in the estuary or on the continental shelf), tidal marshes act as important stores for OC on the regional spatial scale.

These findings have important implications for national and international policy, as carbon trading systems are being developed that provide a reward for the amount of CO<sub>2</sub> that is being withdrawn from the atmosphere, in addition to taxes imposed for CO<sub>2</sub> emissions, based on a carbon price (e.g. Baranzini et al., 2017). As it is well established that tidal marsh sediments contain large amounts of OC (Duarte et al., 2013, 2005), proposals have been made to include OC buried in tidal marsh sediments in carbon trading systems (Macreadie et al., 2017; Thomas, 2014). However, the results presented here pose an important consideration concerning the ‘reward’ of OC that is being buried in tidal marsh sediments. On the one hand, it can be argued that only CO<sub>2</sub> that is withdrawn from the atmosphere in-situ should be rewarded, as the main aim of carbon trading systems is to control the amount of atmospheric CO<sub>2</sub>. The reason not to reward deposited OC in this reasoning is that this OC has already been sequestered in another ecosystem and has subsequently been transported to the tidal marsh. As the withdrawal of atmospheric CO<sub>2</sub> from which this OC originated happened in another ecosystem, it should be ‘rewarded’ at that location. On the other hand, it can be argued that all OC buried in tidal marsh sediments should be rewarded, as our results have shown that allochthonous OC, although it is not sequestered at the tidal marsh, is efficiently preserved in these sediments. This mechanisms should, however, not be addressed as ‘carbon sequestration’, but rather as ‘carbon preservation’.

In addition to the discussion whether OC in tidal marsh sediments should be rewarded, it should be noticed that every initiative that promotes the preservation of tidal marshes should be encouraged, as these ecosystems are under great pressure around the globe (Bauer et al., 2013; Halpern et al., 2008; Hopkinson et al., 2012), while they deliver a range of valuable ecosystem services far beyond carbon sequestration (Barbier et al., 2011; Temmerman and Kirwan, 2015).

### **8.1.2 Assessing the influence of environmental changes on future tidal marsh organic carbon stocks: the role of organic carbon models**

Current and predicted environmental changes have been hypothesized to affect the store of OC in tidal marsh sediments in multiple ways. First, the preservation of OC stored in tidal marsh sediment depends primarily on the stability of these sediments in the near future. It has been hypothesized that when the rate of sea level rise exceeds the rate of sediment deposition, the vegetation growing on a tidal marsh platform may die, resulting in a substantial decrease in sediment cohesion and the subsequent erosion of the tidal marsh (referred to as ‘marsh drowning’) (Kirwan et al., 2010). Evidently, this process would lead to the loss of the OC stored in these sediments (Kirwan and Mudd, 2012). However, a recent assessment of the potential of marsh drowning has shown that previous reports may have overestimated this threat to tidal marshes (Kirwan et al., 2016). Nevertheless, the geomorphological stability of these sediments is a prerequisite for these ecosystems to store OC in the future. Secondly, other environmental factors related to sea level rise can cause the loss of previously stored OC, such as the intrusion of salt water further into estuaries. This has been shown to lead to enhanced decomposition of organic carbon stored in freshwater tidal marsh sediments (Morrissey et al., 2014; Weston et al., 2011, 2006). It should be noted that salinity as such only indirectly controls increases in the decomposition rate of organic carbon.

Other consequences of this salinity intrusion are resulting in this process, such as increasing microbial activity (Morrissey et al., 2014; Weston et al., 2011) and changing mineralization pathways from methanogenesis to sulphate reduction (Chambers et al., 2011; Weston et al., 2006). Also spatial restrictions on the possibility of tidal marshes to migrate to other locations will determine the total amount of OC stored in tidal marshes along an estuary. In the Scheldt estuary, for example, the estuary is completely embanked. This prohibits the possibility of tidal marshes to migrate to higher elevations after sea level rise and enhances the risk of 'marsh drowning'. In addition, the tidal wave in the Scheldt estuary is stopped by sluices near the city of Ghent, thereby preventing tidal marshes to migrate upstream beyond this location.

Although the assessment of the potential effects of both sediment deposition rate and saltwater intrusion should be based on empirical evidence, predictions of these effects on the rate at which tidal marshes will store OC over the coming decades are made using numerical models. Existing models simulating SOC dynamics in tidal marsh sediments have divided organic matter in a labile and refractory pool, which decay according to first-order kinetics (Kirwan and Mudd, 2012; Mudd et al., 2009) similar to the ICBM – DE (chapter 6). To the best of my knowledge, no mechanistic models of SOC dynamics in tidal marsh sediments have been developed.

The application of both conceptually-based and mechanistic models, such as SOILcarb – RM, to simulate SOC dynamics in tidal marsh sediments has advantages and disadvantages. The most important advantages of a conceptual SOC model (such as ICBM – DE) are associated with the limited amount of input data needed. The most important inputs to apply such a model are the amount of OC entering the marsh annually (both originating from local vegetation and deposited OC) and the decay rates of OC in different pools. Despite the relatively low data requirements, the application of such a model to a tidal marsh environment by Mudd et al. (2009) relied on the calibration of multiple essential parameters, such as the subdivision of OC inputs in a labile and refractory portion and the rate at which labile OC decays.

The simulation of OC dynamics in tidal marsh sediments using such a concept-based model is complicated by the empirical character of the SOC pools. First, there is a limited physical basis to define OC in a tidal marsh ecosystem into 'labile' and 'refractory'. Although it can be argued that locally-produced plant inputs can be assigned to the labile pool, while allochthonous sediment-associated OC can be assigned to the refractory pool, this approach can e.g. not include why freshwater marshes preserve more locally-produced OC compared to salt marshes (as shown in chapter 3), or include a mechanism to explain why sediment-associated OC is rapidly mineralized upon marsh embankment (as shown in chapter 4). Second, these type of models rely on a depth-dependent decay rate of OC (Kirwan and Mudd, 2012; Mudd et al., 2009). The rate at which the decay of labile OC is assumed to decrease with depth has a large influence on the model results when the rate of sediment deposition at the marsh surface is high (Mudd et al., 2009), and is site-dependent. The application of a concept-based SOC model to tidal marsh environments is thus associated with substantial uncertainties. The limited ability to link the modelled pools to measured OC fractions thus contributes substantially to this uncertainty.

The application of a mechanistic SOC model to tidal marsh environments provides a promising alternative to account for these shortcomings, although also this approach is prone to uncertainties, as discussed below. A first advantage of mechanistic models, such as SOILcarb – RM (chapter 7), is that inputs of OC originating from different sources can be explicitly linked to measured OC fractions. For example, allochthonous sediment-associated OC can be assigned to the mineral-associated OC pool, while locally produced biomass can be assigned to the ‘residual OC’ pool (representing unprocessed plant material). Second, a mechanistic model approach can explicitly account for the effect of water fluctuations on SOC dynamics in tidal marsh sediments, while also DOC losses (which are explicitly modelled in SOILcarb – RM) can be accounted for. Next, modelled SOC pools can more easily be linked to OC fractions as measured in the lab, which facilitates model validation. Last, the effect of microbes and enzymes on the decomposition of OC in tidal marsh sediments can be explicitly simulated, as this has been hypothesized to at least partly explain different decomposition rates observed in tidal marshes at different salinities (e.g. Morrissey et al., 2014).

There are also drawbacks associated with the application of a mechanistic SOC model, such as SOILcarb – RM, to a dynamic environment such as tidal marshes. The most important one is related to data availability. As discussed in chapter 7, a common problem with mechanistic SOC models is that there is no data available for all simulated processes, such as the decay and growth rates of soil microorganisms, the efficiency of their metabolism and the rate of adsorption and desorption of OC to mineral surfaces, all of which are essential for a successful application of the model. When deciding which type of model to use to simulating SOC dynamics in tidal marsh sediments (conceptually-based versus mechanistic), the trade-off between process representation and data availability is one of the main determinants to take into account.

During the course of this PhD, a substantial effort has been invested in the application of a conceptually-based SOC model to the studied tidal marshes (these results are not shown in this dissertation). This exercise showed that irrelevant of the decay rates that were chosen for the different pools (young, old and passive), adjusting the rate at which the ‘r’ parameter (representing the effect of external conditions on the decay of OC) decreased with depth generally resulted in an accurate reconstruction of the observed SOC profile. However, a physical basis for the choice of this decay rate with depth could never be assigned, which greatly limited (i) the value of the model application and (ii) the potential to apply the obtained model to tidal marshes in other environments. Based on this experience, it seems worth the effort to assess the potential of mechanistic models (such as COMMISSION or SOILcarb – RM, see chapters 6 and 7) to simulate SOC dynamics in tidal marsh sediments. This would allow to make an objective assessment of the potential of both models to reliably assess how future environmental changes will affect the OC stock of tidal marsh sediments.

### **8.2 Concluding summary**

The objectives of this PhD dissertation were focussed on improving the current understanding of the mechanisms controlling long-term soil organic carbon storage. First, a general overview of the work presented in this dissertation is provided, after which an answer on the research

questions, as posed in section 1.6, is given. The first part of this dissertation (chapters 2 and 3) was empirically-oriented and studied soil organic carbon dynamics in tidal marsh sediments along the salinity gradient of a temperate estuary (Scheldt, Belgium and The Netherlands). The basis of this work was an intensive field campaign, during which soil depth profiles for 18 locations on 10 different tidal marshes were collected, together with above-ground vegetation, roots and sediments that were deposited during inundation events. The obtained data allowed to gain important insights in the mechanisms controlling the fate of organic carbon in these intertidal sediments. The main finding was that the amount of organic carbon that is stored on a centennial (or longer) timescale in the studied tidal marsh sediments depends to a large extent on the amount of organic carbon that is associated with deposited sediments. Moreover, organic carbon in these tidal marsh sediments has an average age of up to thousands of years, indicating that the majority of preserved organic carbon has not been fixed from atmospheric CO<sub>2</sub> in-situ, given that the studied sediments were deposited during the past century. Previously calculated rates of organic carbon burial in tidal marsh sediments, however, do not account for the fact that a substantial portion of organic carbon that is present in these sediments has not been sequestered in-situ and therefore does not contribute to atmospheric CO<sub>2</sub> sequestration in these coastal ecosystems. These findings thus show that previously calculated rates of sequestration of atmospheric CO<sub>2</sub> in tidal marsh sediments are potentially greatly overestimated.

The next part of this dissertation (chapter 4) focussed on the fate of organic carbon present in tidal marsh sediments after these are converted to polders in the brackish and salt portion of the Scheldt estuary. This process includes the construction of an embankment at the seaward side of the tidal marsh and subsequent drainage in order to use this newly created land for agricultural purposes. The results of this study showed that in both brackish and salt polders, ca. 60 % of previously stored sedimentary organic carbon is lost upon embankment on a timescale of several decades. In addition, a numerical landscape model was constructed to reconstruct the historical distribution of tidal marshes, sand flats and polders in the study areas. This showed that despite large local losses of soil organic carbon from tidal marsh sediments upon embankment, accounting for additional organic carbon storage in newly formed tidal marshes results in an increase in the average soil organic carbon stock in these intertidal landscapes.

As intertidal landscapes are characterized by a high variability in soil organic carbon concentration, both spatially and temporally, a large number of sediment samples has to be analysed for organic carbon concentration in order to reliably estimate total sedimentary organic carbon stocks in these landscapes. Therefore, in a next chapter (chapter 5) it was shown that predictions of the organic carbon concentration of sediment samples using mid-infrared spectroscopy can be used to accurately calculate soil organic carbon stocks of tidal marsh sediments. As predictions of soil bulk density are not possible using this soil sensing technique, measurements of this soil property are currently still necessary to calculate total sedimentary organic carbon stocks.

The last two chapters of this PhD dissertation were focussed on the numerical representation of soil organic carbon dynamics in soil organic carbon models. Specifically, the aim was to

include stable carbon isotopes ( $\delta^{13}\text{C}$ ) in a soil organic carbon model, in order to assess (i) if the structure of two existing models allows to simulate realistic depth profiles of  $\delta^{13}\text{C}$  and (ii) to assess the potential of using modelled  $\delta^{13}\text{C}$  data as an additional criterion for model validation. The first chapter focussing on this topic (chapter 6) showed that both an empirically-based (ICBM) and a processes-based soil organic carbon model (COMISSION) were not able to realistically simulate the effect of microbial processing of organic matter on depth profiles of  $\delta^{13}\text{C}$ . Therefore, in the last chapter of this dissertation (chapter 7), the insights obtained in the previous chapter were used to construct a new process-based soil organic carbon model, based on the rationale behind the COMISSION model. The novelty of this model is that it distinguishes organic carbon dynamics in the rhizosphere and the mineral soil. This approach allowed to simulate realistic depth profiles of total soil organic carbon,  $\delta^{13}\text{C}$  and the  $^{14}\text{C}$  content of soil organic carbon.

The research questions, as posed in section 1.6, are answered as follows:

*RQ 1: How do organic carbon stocks vary in tidal marsh sediments along the salinity gradient of a temperate estuary and which factors control the observed variations?*

For the tidal marshes along the Scheldt estuary, sedimentary organic carbon stocks are the highest in freshwater marshes ( $19.4 \pm 1.2 \text{ kg OC m}^{-2}$ ) and decrease towards the coast (brackish marshes:  $17.3 \pm 0.9 \text{ kg OC m}^{-2}$ , salt marshes:  $12.6 \pm 0.8 \text{ kg OC m}^{-2}$ ). The results show that this pattern is not related to gradients in biomass production on tidal marshes along the estuary, but rather to (i) differences in the amount of deposited organic carbon, which decreases towards the coast and consists mainly of very old organic carbon and (ii) to a better preservation of locally-produced organic carbon on freshwater marshes, compared to brackish and salt marshes.

*RQ 2: At which rate is organic carbon lost from tidal marsh sediments after these are embanked and how do spatial variations in the area of tidal marshes and polders affect regional soil organic carbon stocks?*

This study has shown that polders (embanked tidal marshes) originating from both salt and brackish marshes lose a substantial amount of sedimentary organic carbon after they are embanked. The relative loss of sedimentary organic carbon is similar for brackish and salt polders, ca. 60 %, but absolute losses differ: brackish marshes lose on average  $8.7 \pm 0.5 \text{ kg OC m}^{-2}$  while salt marshes lose  $6.8 \pm 0.3 \text{ kg OC m}^{-2}$ . Also the rates at which these losses occur differ, with new equilibrium soil organic carbon stocks in brackish polders being reached approximately a century after embankment, while in salt polders this takes < 64 years. Despite these local losses, the application of a numerical landscape model showed that the average landscape scale soil organic carbon stock increased in both the brackish and salt polder regions. The model results showed that, compared to the initial sand flat situation centuries ago, to average soil organic carbon stocks has increased by ca.  $2 \text{ kg OC m}^{-2}$  in the brackish region and ca.  $1.4 \text{ kg OC m}^{-2}$  in the salt region.

*RQ 3: Can mid-infrared spectroscopy be used to accurately predict organic carbon stocks of tidal marsh sediments?*

The results showed that the organic carbon concentration of soil samples collected along the entire salinity range can be reliably predicted using mid-infrared spectroscopy combined with partial least squared regression (PLSR) ( $R^2 = 0.94$ ; absolute error = 0.40 % OC). These predictions of organic carbon concentration can be combined with measured depth profiles of bulk density to calculate total sedimentary organic carbon stocks. The relative error on these predicted total sedimentary organic carbon stocks (predicted versus measured organic carbon stock) was very low for freshwater and brackish marshes (< 3 %), while it was substantially higher for salt marshes (20 - 42 %). Although mid-infrared spectroscopy has been shown to be an accurate alternative to predict sedimentary organic carbon stocks in tidal marshes, constructing PLSR calibration models for different salinity zones is recommended to obtain optimal results.

*RQ 4: Can realistic depth profiles of stable carbon isotopes ( $\delta^{13}\text{C}$ ) be modelled using two soil organic carbon models build on different principles?*

A comparison of the ability of an empirically-based model (ICBM) and a process-based model (COMISSION) has shown that despite the observation that both models simulate realistic depth profile of total soil organic carbon and its  $^{14}\text{C}$  content, they did not realistically simulate the effect of microbial processes on isotopic discrimination of stable carbon isotopes. The reason was the internal structure of both models. As ICBM requires a decrease in the rate of organic matter processing with depth in order to simulate an increasing age of organic matter with depth, deep soil organic carbon is less processed compared to topsoil organic carbon, leading to a decrease in  $\delta^{13}\text{C}$  with depth. In the COMISSION model, the direct coupling between dissolved organic carbon (DOC) and mineral-associated carbon prevented to simulation of increasing  $\delta^{13}\text{C}$  values with depth as too much fresh organic carbon was adsorbed onto minerals. This model evaluation pointed to the need of an alternative model structure to correctly simulate depth profiles of stable carbon isotopes in soils.

*RQ 5: Can insights gained from the incorporation of stable carbon isotopes in established models be used to construct a soil organic carbon model that simulates realistic depth profiles of total soil organic carbon,  $\delta^{13}\text{C}$  and  $^{14}\text{C}$ ?*

Based on the conclusions drawn from the incorporation of  $\delta^{13}\text{C}$  in existing soil organic carbon models, combined with a literature review on the mechanisms controlling soil organic carbon cycling, a new soil organic carbon model (SOILcarb – RM) was proposed to simulate realistic depth profiles of total organic carbon,  $\delta^{13}\text{C}$  and the  $^{14}\text{C}$  content of soil organic carbon. The novelty of the model is two-fold: (i) the model distinguishes organic carbon cycling in the rhizosphere (where rapid carbon cycling is caused by the rapid uptake of carbon inputs by soil microbes) and the mineral soils (where slow carbon cycling is caused by the protection of carbon on mineral surfaces) and (ii) the fact that only organic carbon that has been processed by soil microbes can be adsorbed onto soil minerals. This model structure results in soil organic carbon which is older with increasing depth, despite inputs of fresh organic carbon by roots in deeper soil layers. Moreover, the downward advection of processed organic carbon results in an increase in the  $\delta^{13}\text{C}$  value of soil organic carbon with depth. Although a confrontation with field data needs to quantify the accuracy of results obtained with the SOILcarb – RM model, its structure is in line with the current understanding on soil organic

carbon cycling and allows to simulate realistic depth profiles of total organic carbon, its  $^{14}\text{C}$  content and  $\delta^{13}\text{C}$ .

### **8.3 Future research perspectives**

Based on the results obtained in this PhD dissertation, the following recommendations for further research are made, grouped per subject that has been addressed:

#### **Organic carbon cycling in tidal marsh sediments**

Despite the large research attention tidal marshes have received over the past decades, there are still substantial knowledge gaps which hamper an accurate assessment of (i) how much organic carbon is globally stored in these intertidal sediments, (ii) which processes control long-term sedimentary organic carbon storage and (iii) how these organic carbon stores will respond to environmental changes such as sea level rise and increasing atmospheric temperature. A first important future research direction should address the extent to which deposited allochthonous organic carbon contributes to the total sedimentary organic carbon stock in other estuaries. This will allow to assess if the conclusions drawn here are valid for other estuaries and to which extent this influences calculations of global rates of long-term atmospheric  $\text{CO}_2$  removal by tidal marshes. Secondly, as tidal marshes occur in a wide range of environments, a modelling approach will be necessary to estimate the potential of these ecosystems to store additional organic carbon in the future. As models simulating organic carbon dynamics are scarce and existing models are based on the historical view on soil organic carbon cycling (as explained in section 1.2.3) (Kirwan and Mudd, 2012; Mudd et al., 2009), there is an urgent need for the development of new models which account for the characteristics of organic carbon inputs and the different protection mechanism of organic carbon in tidal marsh sediments. In addition, as tidal marsh experience regular flooding, a correct representation of the effect of soil moisture on the preservation of organic carbon could increase the reliability with which organic carbon dynamics are simulated.

The results of this PhD dissertation have shown that unprotected particular organic matter is better preserved in sediments of freshwater marshes compared to salt marshes, but the mechanisms behind this observation could not be explained. This is a third important direction for future research, as understanding this observation will help to better constrain how future environmental changes might influence the amount of organic carbon stored in these environments. For example, as sea level rises, the intrusion of salt water further into estuaries could cause the decay of previously buried particulate organic carbon, releasing additional greenhouse gases to the atmosphere. Which greenhouse gases are released from tidal marsh sediments depend on the mineralization pathway followed by microorganisms, with saltwater marshes releasing mainly  $\text{CO}_2$  due to the sulfate reduction pathway, while the methanogenesis pathway in freshwater marshes causes a substantial amount of  $\text{CH}_4$  to the atmosphere. A fourth important research direction is therefore a better quantification of the magnitude at which different greenhouse gases (e.g.  $\text{CO}_2$ ,  $\text{CH}_4$  and  $\text{N}_2\text{O}$ ) are released from tidal marshes at different salinities. Including this in models is challenging, but nonetheless necessary in order to quantify the contribution of microbial respiration to total greenhouse gas emission from tidal marsh sediments.

### **Organic carbon dynamics in reclaimed tidal marshes**

Around the globe, a substantial area of land has been gained from the reclamation of tidal marshes, mangroves and peatlands. Despite the fact that it has been shown that these land use changes cause the emission of a large amount of greenhouse gases to the atmosphere (Pendleton et al., 2012), research addressing land use change has been relatively limited up till now. However, as the conversion of coastal vegetated ecosystems to arable land is currently still going on in large parts of southeast Asia (Ma et al., 2014; Wang et al., 2014), a better understanding of the magnitude of the amount of soil organic carbon losses and the rate at which this occurs is necessary to correctly quantify the environmental impact of these land use changes.

One of the hypotheses that were formulated in our study was that the construction of embankments triggered the formation of a new tidal marsh at the seaward side of the embankment, which acts as a new sedimentary organic carbon store. Although multiple indications suggested that this was the case in the Scheldt estuary, there is no conclusive evidence to confirm this hypothesis at this point. Therefore, assessing if the construction of embankments indeed triggers the formation of a new tidal marshes is an important line for further research concerning this topic. To this end, for example, hydro-morphological models or experiments in the lab, simulating these environments, could be used.

Our study did also not resolve the question as to why organic carbon in tidal marsh sediments is so rapidly mineralized upon the conversion to arable land. This is intriguing, as this organic carbon has been hypothesized to be very stable as it has travelled a long way, from terrestrial ecosystems, through rivers and into the estuary, while it has not been mineralized. A process-based assessment of the mechanisms leading to this rapid mineralization upon tidal marsh embankment could contribute to our general understanding of soil organic carbon preservation.

A last issue that should be addressed in future research is the rate at which sedimentary organic carbon is lost during the first years/decades after the embankment of salt marshes. This was not possible in our study, as a new equilibrium soil organic carbon stock was already reached in the youngest salt polder along the chronosequence. Analysing soil samples from young polders can thus resolve this issue. As large embankment projects are currently going on in e.g. China, analysing these embanked tidal marsh sediments could resolve this issue.

### **Mid-infrared spectroscopy as a tool to predict soil organic carbon stocks**

Soil sensing techniques (e.g. using mid-infrared spectroscopy) to predict the soil organic carbon concentration of sediments have been used intensively over the past decade and are relatively well established (Baldock et al., 2013; Bellon-Maurel and McBratney, 2011; Minasny et al., 2008; Reeves et al., 1999; Reeves III, 2010; Viscarra Rossel and Bouma, 2016; Viscarra Rossel et al., 2006). Important advances that can still be made in this field are related to the construction of global libraries of soil spectra (e.g. Stevens et al., 2013; Viscarra Rossel et al., 2016) and efficient techniques to sample them (e.g. Lobsey et al., 2017). This is a prerequisite to use soil sensing as a standard technique to predict the organic carbon concentration of soil samples at a large scale. One of the factors complicating the assessment of accuracy of

predicted organic carbon concentrations using proximal soil sensing is that most studies only report an  $R^2$  value as a measure of accuracy, which can, however, not be interpreted in terms of the absolute error on the predictions of organic carbon concentrations. It is therefore recommended that future studies using soil sensing techniques to predict organic carbon concentrations report both the absolute and relative error associated with their predictions.

### **Numerical modelling of soil organic carbon**

Despite the fact that a large scientific community is focussing on soil organic carbon modelling, both related to model development and application, major advances in this field of research can currently still be achieved. This is related to the heterogeneity of soilscapes and the complex nature of soil organic carbon cycling, which is to date not completely understood.

Concerning the SOILcarb – RM model, which is presented in chapter 7 of this dissertation, a first recommendation for further research is the confrontation of model results with field data, in order to assess the accuracy of model results and the extent to which the proposed model structure reflects natural processes. Furthermore, the hypothesis that only dead microbial biomass can be adsorbed to soil minerals is probably an oversimplification of reality. Therefore, the adsorption of e.g. litter-derived DOC to mineral in topsoil sediments could be included in the model.

With regard to the general field of soil organic carbon modelling, multiple recommendations for further research can be made. First, one of the major challenges of future model development is finding the optimal trade-off between model complexity (thus the extent of process representation) and data availability. This optimal complexity should on the one hand represent sufficient processes to correctly model soil organic carbon dynamics (e.g. mechanisms leading to both carbon mineralization and preservation) but, on the other hand, result in simulated pools that can be confronted with measured field data. A next line of future research should concern the representation of mechanisms causing destabilization of protected organic carbon in soils. Most current models, among which the proposed SOILcarbon – RM model, assume that desorption of stabilized organic carbon is a first-order process. However, empirical research has shown that e.g. deforestation causes the loss of previously stabilized organic carbon down to the subsoil (> 1 m depth). This process could be caused by e.g. priming effects and increased leaching of dissolved organic carbon, but can currently not be simulated with state-of-the-art biogeochemical models. A next direction of future research is the representation of the effect of temperature on decay of organic carbon. Most models currently assume that an increase in temperature will result in an increasing rate of organic matter decay. However, as long-term field experiments have shown that this effect is often only observed in the first years after warming, the representation of this process in biogeochemical models should be improved. Also the representation of the  $\text{CO}_2$  fertilization effect should be better incorporated into models, as a recent synthesis paper has shown that increased inputs of organic matter (due to  $\text{CO}_2$ -stimulated biomass growth) do not necessarily lead to increases in the amount of stabilized organic carbon (van Groenigen et al., 2017). In addition, a better representation of the effect of soil moisture on soil organic carbon dynamics is a major prerequisite for a more accurate simulation of soil organic carbon

dynamics, as temperature and soil moisture content are environmental factors which are intimately coupled and can have opposite effect on the preservation and decay of organic carbon (Carey et al., 2016).

This brief overview of shortcomings of current biogeochemical models simulating soil organic carbon dynamics is to a large extent the result of an incomplete understanding of the effect of multiple environmental factors on soil organic carbon cycling. There is thus a great need for an intimate collaboration between empirical researchers and modellers in order to improve the representation of soil organic carbon in numerical models, which is in turn necessary to obtain reliable estimates of future climatic changes.



## Data availability

---

The data associated with chapters 2, 3, 4 and 5 can be found at  
<http://dx.doi.org/10.17632/fv7szwyj9k.1>



## Supporting figures and tables

**Note** The colour versions of the supplementary figures can be found in the online supplement of this PhD (<http://dx.doi.org/10.17632/fv7szwyj9k.1>).

### Chapter 2

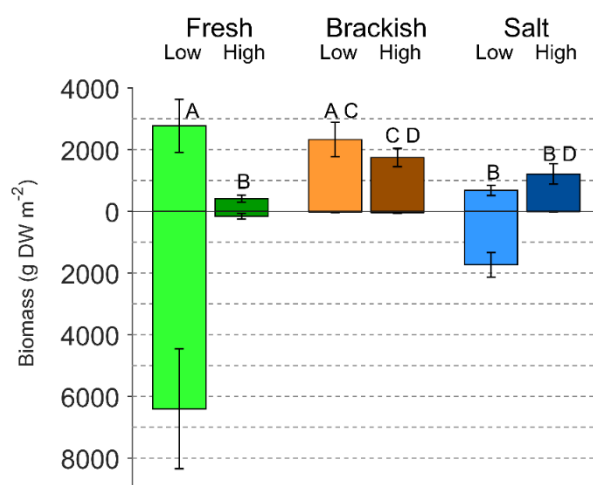


**Figure S2-1** Total above- and belowground biomass for the study sites (g dry weight m<sup>-2</sup>), with upward pointing bars representing aboveground biomass and downward pointing bars representing belowground biomass (data is provided in table S2). Standard deviations for aboveground biomass are calculated based on 5 replicates, for root biomass on 3 replicates. Sample locations that do not share a letter have significantly ( $p < 0.05$ ) different aboveground biomass.

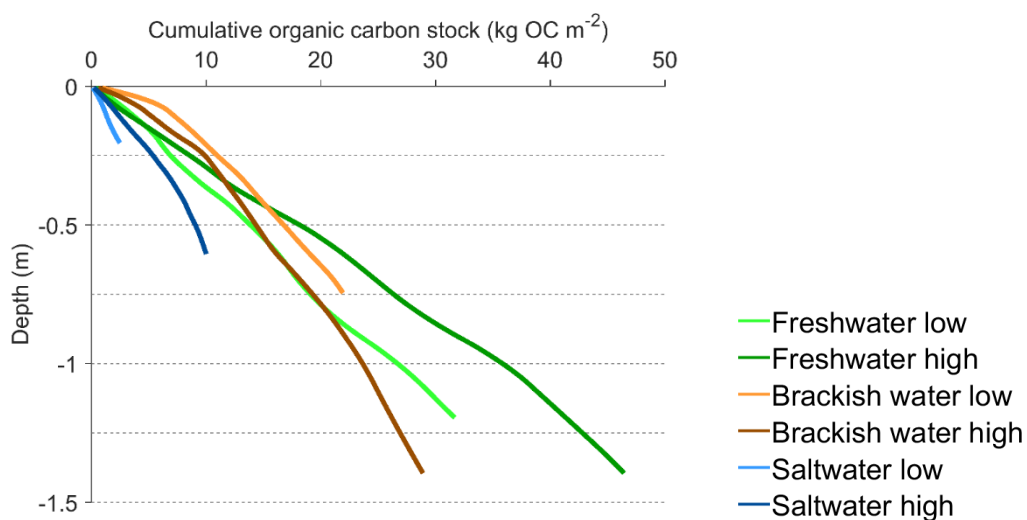


**Figure S2-2** Depth profiles of the cumulative organic carbon stock for depth intervals of 0.01m. No standard deviations are shown to improve readability.

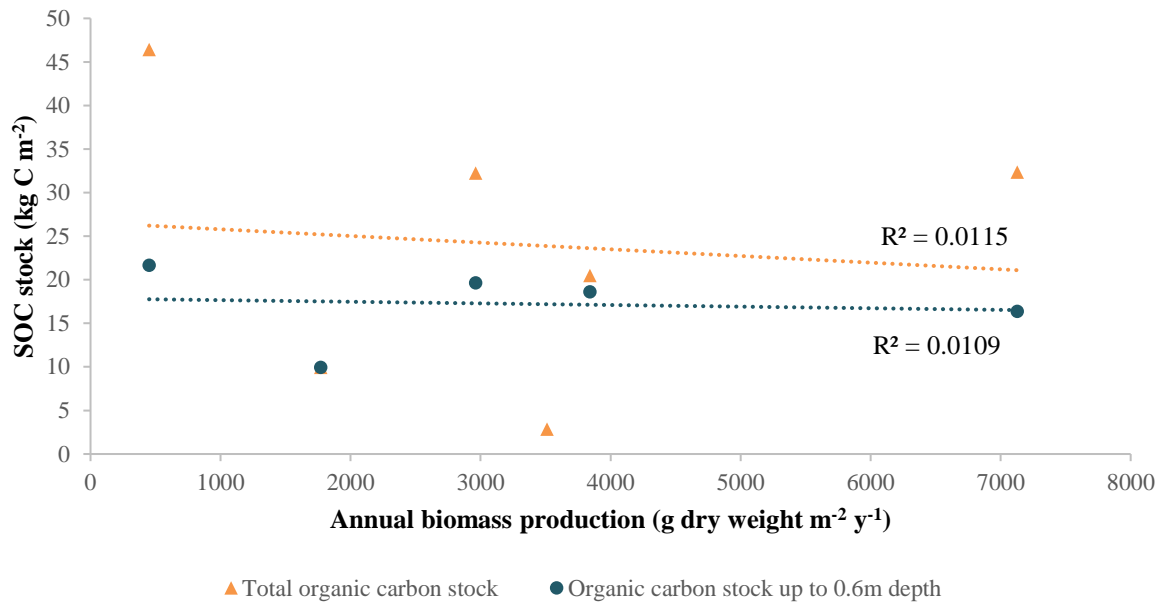


**Figure S2-3** Relationship between the total annual biomass production (above- and belowground) and soil organic carbon stocks, for both total stocks and stocks down to 0.6m depth.

**Table S2-1** GPS coordinates of the sample locations

	Low marsh	High marsh
Freshwater marsh	51° 7' 3.12" N 4° 16' 5.42" E	51° 7' 5.78" N 4° 16' 17.75" E
Brackish marsh	51° 24' 10.71" N 4° 6' 22.18" E	51° 24' 17.47" N 4° 6' 22.46" E
Saltmarsh	51° 21' 0.08" N 3° 43' 14.81" E	51° 20' 59.15" N 3° 43' 10.60" E

**Table S2-2** Average values ( $\pm$  standard deviation) for aboveground, belowground (maximum root depth is given in brackets (m)) and total biomass, biomass production, organic carbon and nitrogen concentration (%), C:N ratio as well as the  $\delta^{13}\text{C}$  signal (‰) for vegetation at the study sites.

	Vegetation type	Biomass (g DW m <sup>-2</sup> )	Annual biomass production (g DW m <sup>-2</sup> yr <sup>-1</sup> ) <sup>A</sup>	Organic carbon %	Nitrogen %	C:N	$\delta^{13}\text{C}$ (‰)
Freshwater low	<i>P. australis</i>	2775 $\pm$ 858	2775 $\pm$ 858	45.7 $\pm$ 0.5	1.12 $\pm$ 0.03	47.5 $\pm$ 2.0	-26.3 $\pm$ 0.2
	Litter	-	-	45.2 $\pm$ 0.8	1.00 $\pm$ 0.10	53.3 $\pm$ 7.6	-26.6 $\pm$ 0.2
	Below-ground	6400 $\pm$ 1943 (0.8m)	4352 $\pm$ 1321	42.1 $\pm$ 1.0	0.83 $\pm$ 0.11	61.3 $\pm$ 9.6	-26.2 $\pm$ 0.2
Freshwater high	Total	9175 $\pm$ 2124	215 $\pm$ 72	42.9 $\pm$ 1.6	1.60 $\pm$ 0.02	31.9 $\pm$ 1.2	-30.5 $\pm$ 0.5
	<i>Salix</i> (leaves)	202 $\pm$ 146	202 $\pm$ 146	43.1 $\pm$ 0.6	1.25 $\pm$ 0.03	40.7 $\pm$ 1.8	-29.6 $\pm$ 0.3
	<i>U. dioica</i>	160 $\pm$ 92 (0.35m)	34 $\pm$ 19	42.1 $\pm$ 0.7	1.33 $\pm$ 0.01	36.8 $\pm$ 0.2	-29.8 $\pm$ 0.1
Brackish water low	Total	577 $\pm$ 187	3754 $\pm$ 902	45.0 $\pm$ 0.4	0.96 $\pm$ 0.03	54.6 $\pm$ 2.6	-26.9 $\pm$ 0.3
	<i>E. athericus</i>	2331 $\pm$ 560	88 $\pm$ 28	34.4 $\pm$ 4.0	0.55 $\pm$ 0.03	73.1 $\pm$ 7.8	-28.3 $\pm$ 0.4
	Below-ground	25 $\pm$ 8 (0.40m)	2356 $\pm$ 560	44.4 $\pm$ 0.7	0.96 $\pm$ 0.06	54.4 $\pm$ 2.1	-27.0 $\pm$ 0.3
Brackish water high	Total	1746 $\pm$ 295	2811 $\pm$ 475	35.2 $\pm$ 3.5	0.58 $\pm$ 0.04	68.5 $\pm$ 10.8	-27.9 $\pm$ 0.4
	<i>E. athericus</i>	680 $\pm$ 163	1333 $\pm$ 319	39.5 $\pm$ 0.8	1.56 $\pm$ 0.10	29.6 $\pm$ 2.7	-14.0 $\pm$ 0.02
	Below-ground	43 $\pm$ 14 (0.20m)	1728 $\pm$ 399 (0.45m)	40.4 $\pm$ 1.7	1.19 $\pm$ 0.12	40.0 $\pm$ 4.8	-13.5 $\pm$ 0.3
Saltwater low	Total	2408 $\pm$ 431	1748 $\pm$ 477	40.3 $\pm$ 0.3	1.75 $\pm$ 0.04	26.9 $\pm$ 0.9	-24.7 $\pm$ 0.3
	<i>S. anglica</i>	1214 $\pm$ 331	22 $\pm$ 10	36.8 $\pm$ 1.9	1.67 $\pm$ 0.07	25.7 $\pm$ 0.9	-27.4 $\pm$ 0.2
	Below-ground	11 $\pm$ 5 (0.45m)	1225 $\pm$ 331				
Saltwater high	Total	1225 $\pm$ 331					
	Mixed vegetation <sup>B</sup>						
	Below-ground						

Notes: <sup>A</sup>Turnover rates are presented in table S2, <sup>B</sup>*Atriplex portulacoides*, *Limonium vulgare*, *Triglochin maritima*, *Elymus athericus*, *Puccinellia maritima*

**Table S2-3** Turnover rates for above- and belowground biomass at the study sites. Vegetation type is given in table S2-2.**Aboveground biomass**

Site	Turnover time (yr <sup>-1</sup> )	Reference	Remark
Freshwater low	1	Soetaert <i>et al.</i> (2004)	-
Freshwater high	1	-	As only fallen vegetation is sampled the turnover rate is assumed to be 1 /yr
Brackish water low and high	1.61	Groenendijk (1984) Wolff <i>et al.</i> (1979)	Marsh near Krabbendijke (Eastern Scheldt), calculated based on the paired-plot data Marsh near Stroodorpepolder (Eastern Scheldt), based on max biomass and biomass production
Saltwater low	1.96	Gray & Benham (1990) Groenendijk (1984)	Tidal marsh in the UK, based on primary production Marsh near Krabbendijke (Eastern Scheldt), calculated based on the paired-plot data
Saltwater high	1.44	Groenendijk (1984) Wolff <i>et al.</i> (1979)	<i>Triglochin maritima</i> , marsh near Krabbendijke (Eastern Scheldt), calculated based on the single-plot data <i>Elymus athericus</i> , marsh near Stroodorpepolder (Eastern Scheldt), based on max biomass and biomass production

**Belowground biomass**

Site	Turnover time (yr <sup>-1</sup> )	Reference	Remark
Freshwater low	0.68	Soetaert <i>et al.</i> , 2004)	Average value for roots and rhizomes
Freshwater high	0.21	Gill & Jackson (2000)	<i>Salix bebbiana</i> (Canada); <i>Salix spp.</i> (Alaska)
Brackish water low and high	3.5	Bouma <i>et al.</i> (2002)	Based on root ingrowth cores, marsh near Waarde (Western Scheldt)
Saltwater low	1.26	Bouma <i>et al.</i> (2002) Gray & Benham (1990)	Based on root ingrowth cores, marsh near Waarde (Western Scheldt) Tidal marsh in the UK, based on primary production
Saltwater high	1.99	Bouma <i>et al.</i> (2002) Groenendijk & Vink-Lievaart (1987)	<i>E. athericus</i> , based on root ingrowth cores, marsh near Waarde (Western Scheldt) <i>Triglochin maritima</i> , average for 0-60 cm depth, Eastern Scheldt, based on biomass production / max. biomass

## Chapter 3

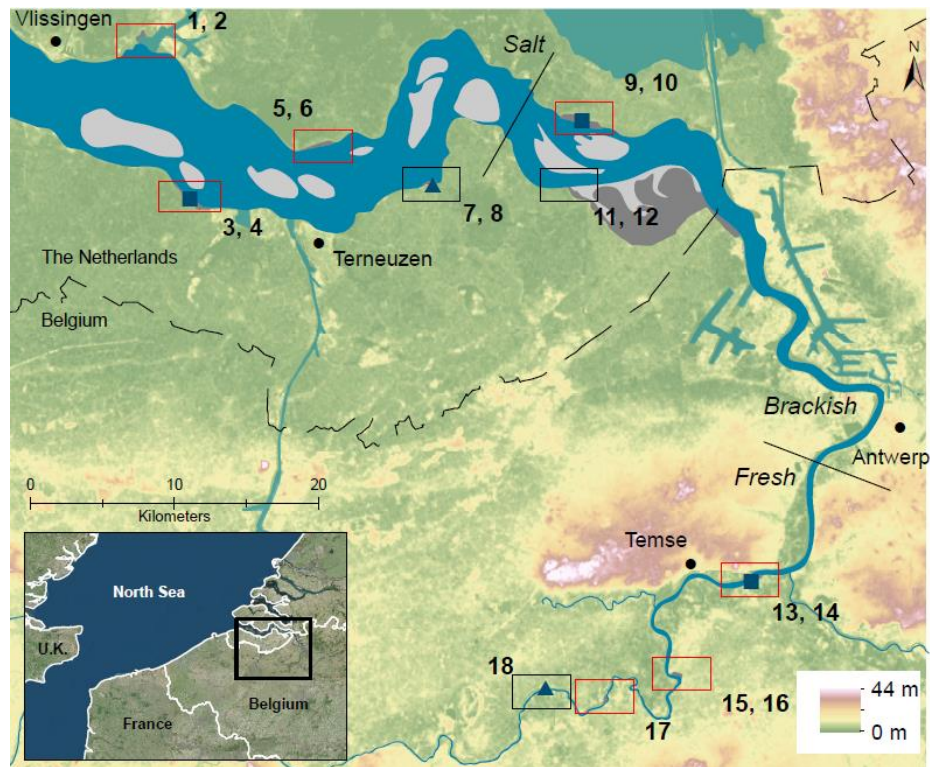


**Figure S3-1** Map of the study area showing the location of the tidal marshes at which OC fractionation was carried out (red rectangles) and sediment traps in both summer 2016 and winter 2017 (blue squares) and only in winter 2017 (blue triangles)



**Figure S3-2** Pictures of the sediment traps used to collect sediments deposited on the tidal marsh during inundation events. The blue lid floats on the water when the marsh is inundated, so that sediments are deposited in the grey tray (right picture). After inundation, the blue lid drop on the tray, to prevent contamination of deposited sediments and loss of sediment due to potential raindrop impact (left picture).

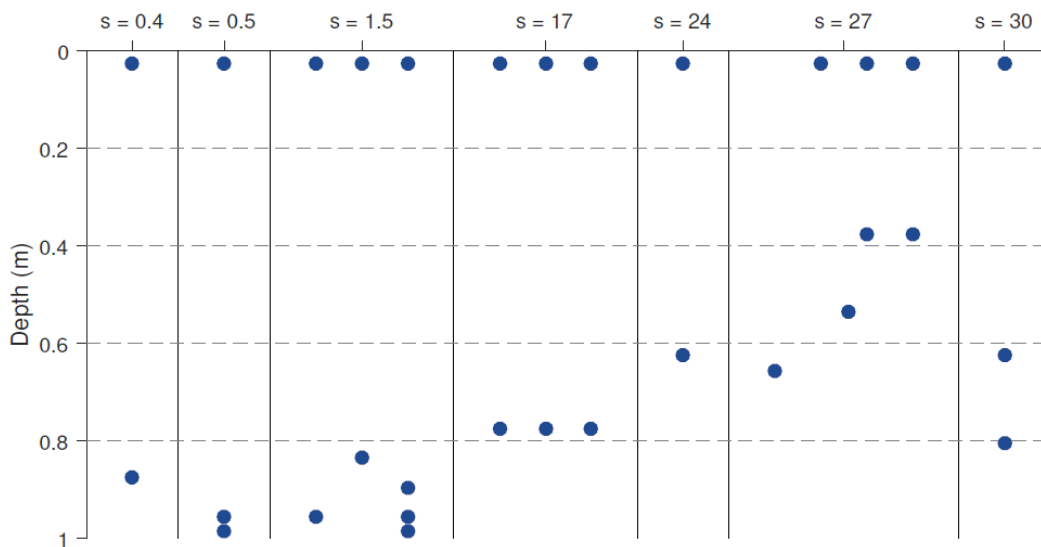


**Figure S3-3** Depth at which soil samples for organic carbon fractionation were collected at different tidal marshes. Dots located at the same vertical location denote samples from the same soil core. When samples from that same marsh are located at different horizontal locations, this denotes that multiple soil cores were collected. S (salinity) denotes the salinity of the tidal marshes.

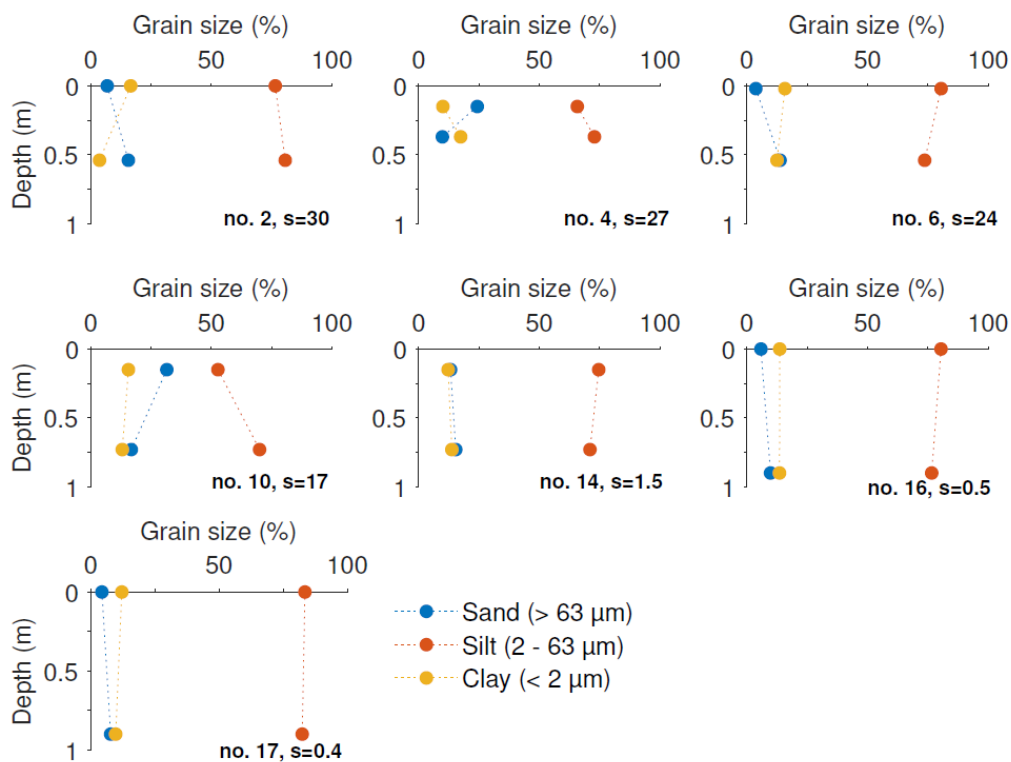


**Figure S3-4** Grain size of the samples analyzed for organic carbon fractions. Detailed grain size depth profiles are provided in the supplementary information. No. is the marsh number in Table 1 in the main manuscript, s is salinity.

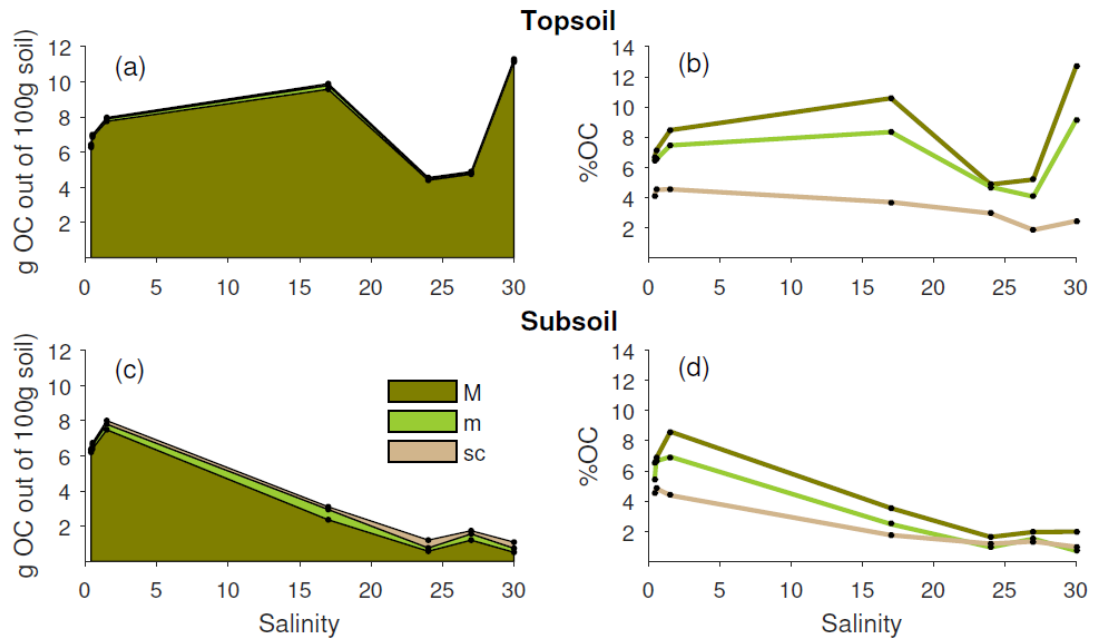


**Figure S3-5** Derived OC fractions after wet sieving (first fractionation step) of topsoil (a, b) and subsoil (c, d) tidal marsh sediments along the estuary. a) and c) show the contribution of each fraction to a total soil mass of 100 g, b) and d) show the OC concentration of the different fractions. M = macroaggregates and POM, m = microaggregates, sand and POM, sc = free silt and clay. Dots denote the location of tidal marshes for which OC fractionation has been carried out along the estuary.

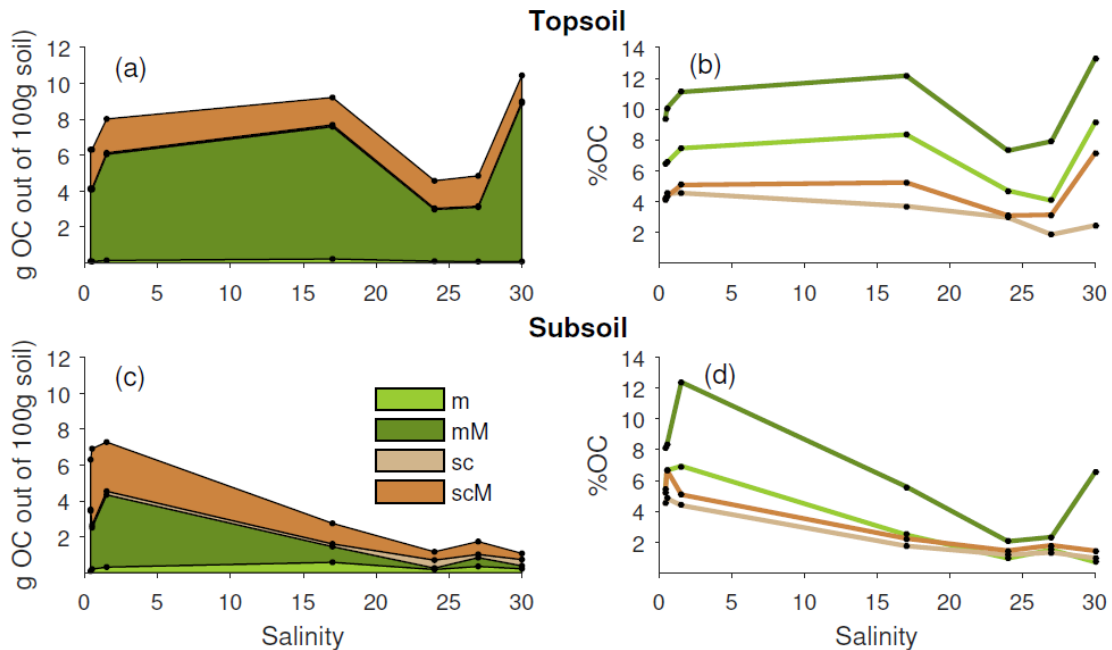


**Figure S3-6** Derived OC fractions after wet sieving and sonication (second fractionation step) of topsoil (a, b) and subsoil (c, d) tidal marsh sediments along the estuary. a) and c) show the contribution of each fraction to a total soil mass of 100 g, b) and d) show the OC concentration of the different fractions. m = microaggregates sand and POM, mM = microaggregates and POM inside macroaggregates, sc = free silt and clay, scM = silt and clay inside macroaggregates. Dots denote the location of tidal marshes for which OC fractionation has been carried out along the estuary.

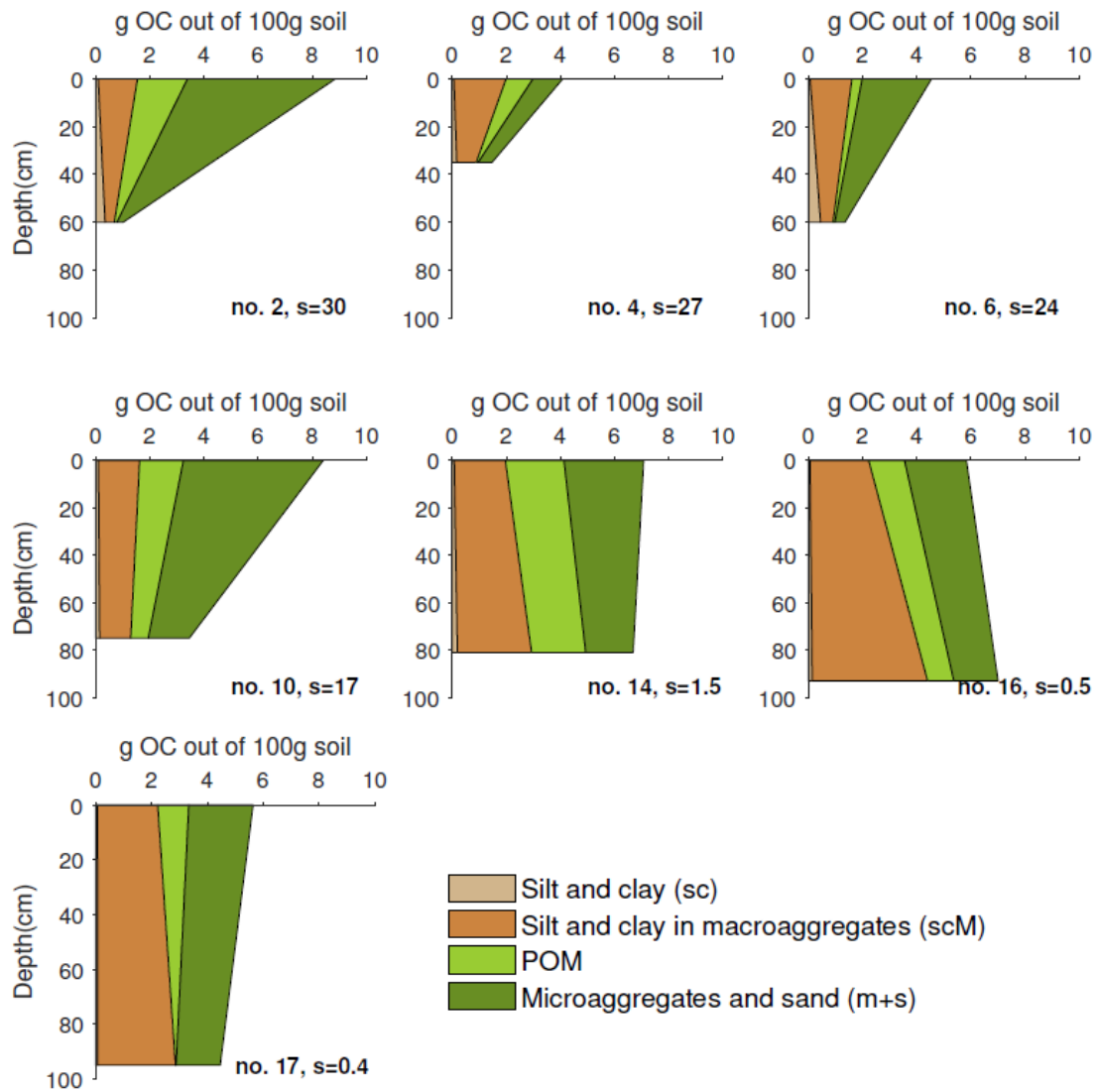


**Figure S3-7** Depth profiles of the final organic carbon fractions in tidal marsh sediments along the estuary. No. is the marsh number in Table 1 in the main manuscript, s is salinity. Note: these profiles are constructed by linear interpolation between 1 measurement in the topsoil and 1 measurement at depth.

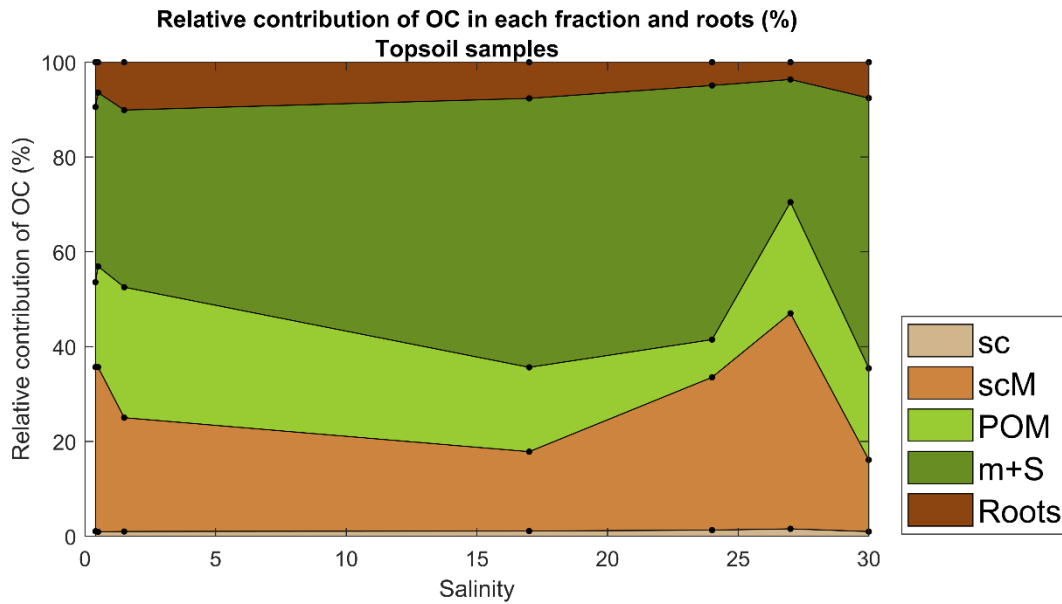


**Figure S3-8** Relative contribution of OC from each final fraction and roots to the total amount of OC in the fractionated topsoil samples. The sum of OC in each fraction is transformed so that the total amount of OC in each sample represents 100%.

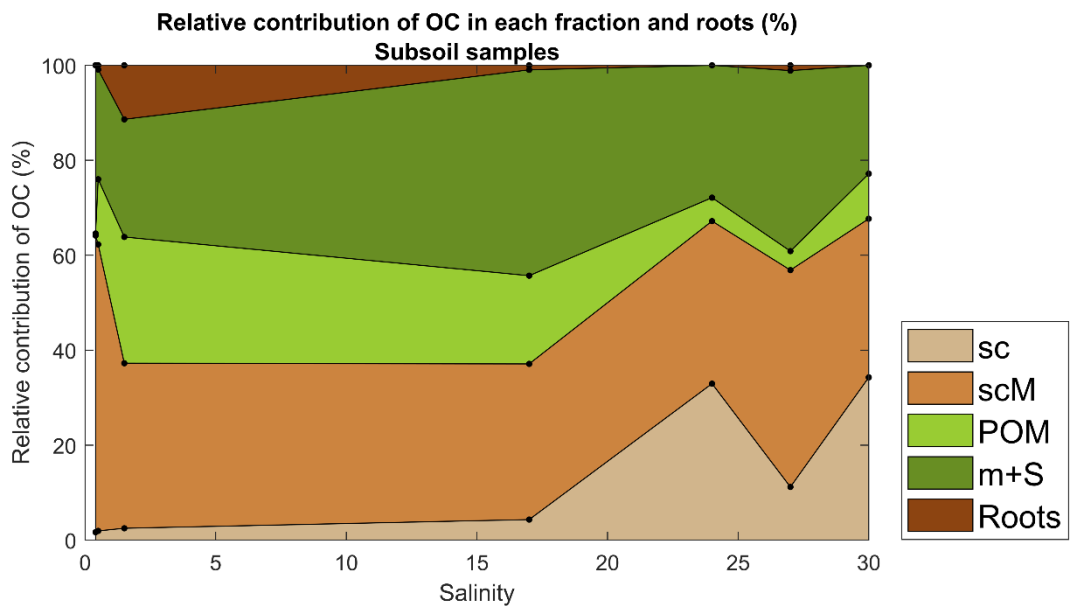


**Figure S3-9** Relative contribution of OC from each final fraction and roots to the total amount of OC in the fractionated subsoil samples. The sum of OC in each fraction is transformed so that the total amount of OC in each sample represents 100%.

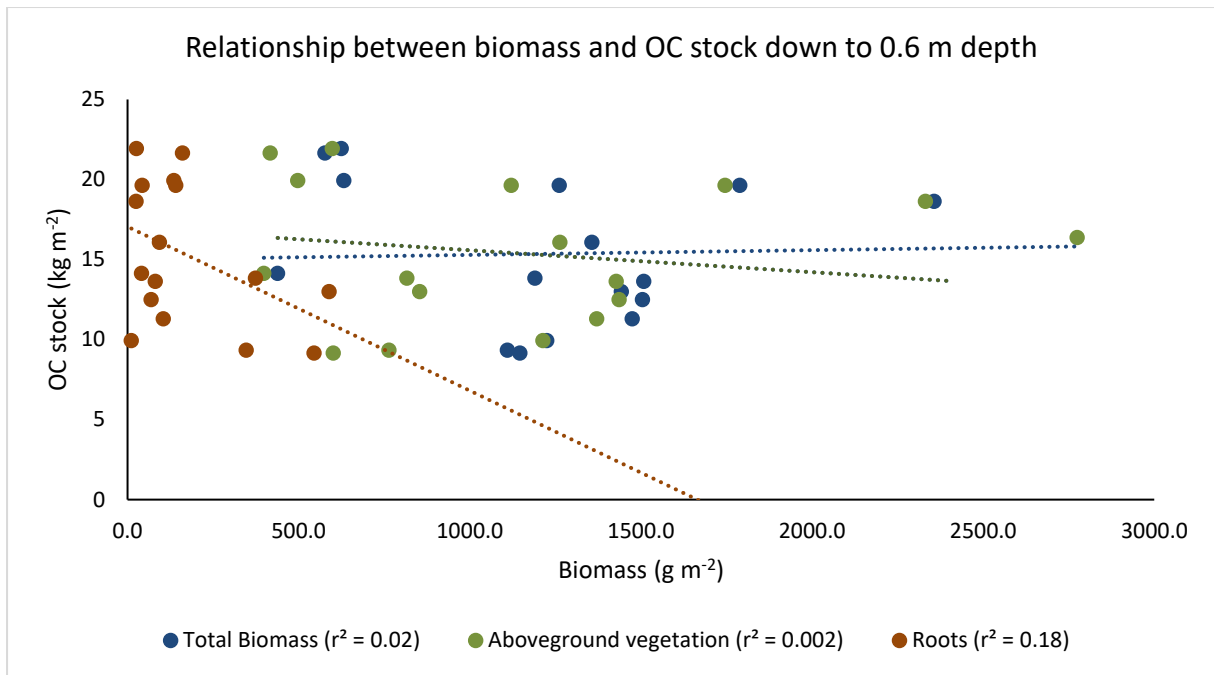


**Figure S3-10** Relation between the OC stock down to a depth of 0.6 m ( $\text{kg OC m}^{-2}$ ) and aboveground-, belowground- and total biomass ( $\text{g DW m}^{-2}$ ). The exceptionally high root biomass at the low marsh at salinity 1.5 (no. 13) is disregarded in this analysis

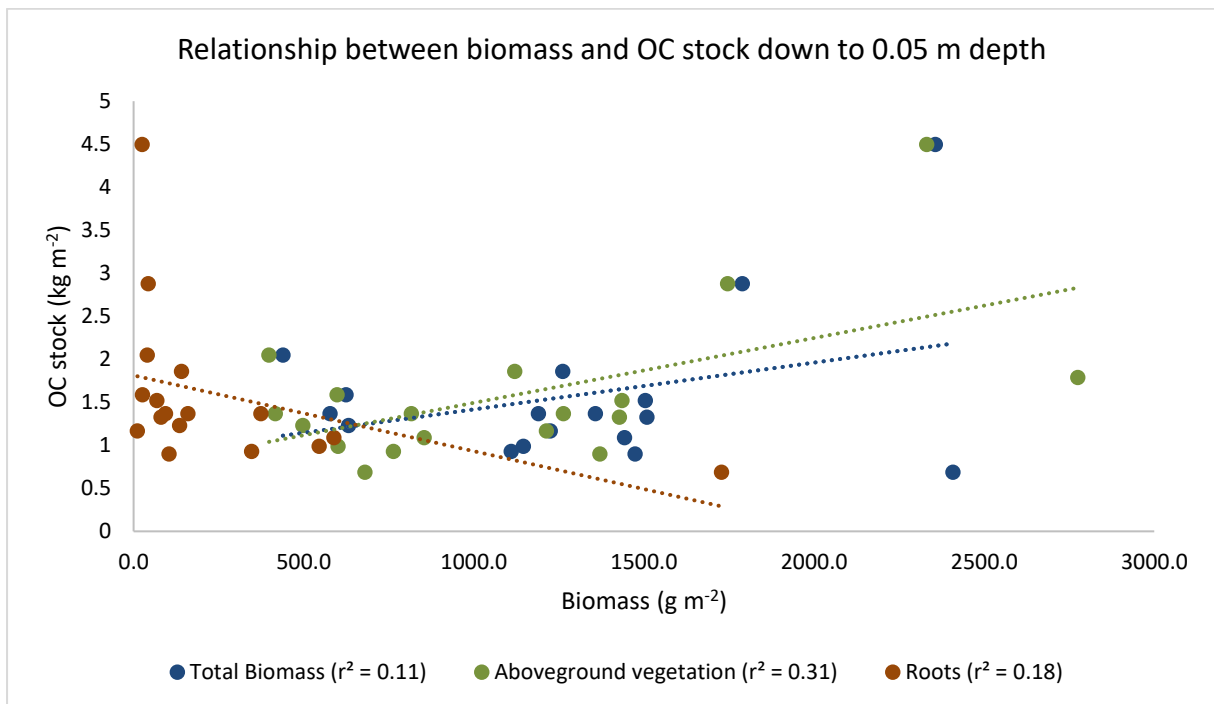


**Figure S3-11** Relation between the OC stock down to a depth of 0.05 m ( $\text{kg OC m}^{-2}$ ) and aboveground-, belowground- and total biomass ( $\text{g DW m}^{-2}$ ). The exceptionally high root biomass at the low marsh at salinity 1.5 (no. 13) is disregarded in this analysis

**Table S3-1** Characteristics of the sampled tidal marshes: name, salinity, dominant vegetation species, depth of silt-size marsh sediments and coordinates of the locations where soil cores were collected.

Location	Salinity	Dominant vegetation species	Depth of silt-size marsh sediments (m)	Coordinates
<b>Saltmarshes</b>				
Sloehaven low	30	<i>Atriplex Portulacoides</i>	0.25	51°27'23.13"N 03°39'49.12"E
Sloehaven high	30	<i>Spartina anglica</i>	> 1.4	51°27'19.86"N 03°39'20.60" E
Paulina low	27	<i>Spartina anglica</i>	0.20	51°21'0.08"N 03°43'14.81"E
Paulina high	27	<i>Atriplex Portulacoides</i> , <i>Limonium vulgare</i> , <i>Triglochin maritima</i> , <i>Elymus athericus</i> , <i>Puccinellia maritima</i>	0.60	51°20'59.15"N 03°43'10.60"E
Zuidgors low	24	<i>Elymus athericus</i>	0.75	51°23'16.85"N 03°49'41.79" E
Zuidgors high	24	<i>Atriplex Portulacoides</i>	0.69	51°23'22.74"N 03°50'09.92" E
Hellegat low	22	<i>Atriplex Portulacoides</i> , <i>Atriplex Patula</i> , <i>Solidago Sempervirens</i>	0.93	51°22'00.09"N 03°57'12.77" E
Hellegat high	22	<i>Solidago Sempervirens</i>	0.75	51°21'57.09"N 03°57'10.53" E
<b>Brackish marshes</b>				
Waarde low	17	<i>Elymus athericus</i>	0.75	51°24'10.71"N 04° 06'22.18" E
Waarde high	17	<i>Elymus athericus</i>	> 1.4	51°24'17.47"N 04° 06'22.46" E
Kruispolder low	15	<i>Scirpus maritimus</i>	1.53	51°21'27.25"N 04° 05'55.87" E
Kruispolder high	15	<i>Scirpus maritimus</i>	> 1.23	51°21'35.31"N 04° 05'35.63" E
<b>Freshwater marshes</b>				
Notelaar low	1.5	<i>Phragmites australis</i>	1.20	51° 07'3.12"N 04°16'05.42" E
Notelaar high	1.5	<i>Salix spp</i> , <i>Urtica Diocia</i>	> 1.4	51° 07'5.78"N 04°16'17.75" E
Mariekerke low	0.5	<i>Salix spp</i>	> 1.83	51° 03'35.78"N 04°11'29.49" E

## Supporting figures and tables

Mariekerke high	0.5	<i>Salix spp, Urtica Diocia, Impatiens Glandulifera</i>	1.41	51° 03'36.37"N 04°11'56.55" E
Grembergen high	0.4	<i>Salix spp</i>	> 1.47	51° 02'39.56"N 04° 07'29.67" E
Appels low	0.3	<i>Salix spp, Impatiens glandulifera</i>	0.99	51° 02'53.17"N 04° 04'8.93" E

**Table S3-2** Coordinates of the locations at which sediment traps were placed during summer 2016 and winter 2017

Name	Salinity	Coordinates summer 2016	Coordinates winter 2017
Paulina high	27	51°20'58.86"N 03°43'13.71"E	51°20'59.96"N 03°43'13.50"E
Hellegat high	22	-	51°21'58.60"N 03°57'11.50"E
Waarde high	17	51°24'16.34"N 04°06'22.50"E	51°24'12.19"N 04°06'17.53"E
Notelaar high	1.5	51°07'4.90"N 04°16'18.30"E	51°07'04.90"N 04°16'18.30"E
Appels low	0.3	-	51°02'53.30"N 04°04'09.10"E

## Chapter 4

**Note** Detailed maps of the sampling locations and a detailed description of the m-IR spectroscopy methods are provided in the online supplementary information

### ***Description of the landscape-scale SOC model***

#### *Model rationale*

To assess the effect of stepwise embankments on regional SOC stocks, a 2-D model was constructed to simulate the most important spatial processes occurring during step-wise embankments of tidal marshes and their effect on SOC stocks. The simulated processes are:

- Growth of tidal marshes, both vertically and laterally, and the accumulation of OC in these sediments.
- The embankment of tidal marshes and potentially part of the sandflat in front of the marsh, depending on the rate of lateral marsh expansion.
- The subsequent soil compaction and loss of OC from the embanked sediments.

These spatial processes are simulated for a region consisting solely of embanked tidal marshes over a timescale of centuries, with the initial condition being a tidal sandflat. As the model simulates vertical tidal marsh accretion through time for every tidal marsh cell, the depth of OC-rich tidal marsh sediments on top of OC-poor former sandflat sediments is calculated for every grid cell, allowing for a realistic calculation of SOC stocks down to a user-defined depth. By tracking the amount of OC present in every simulated grid cell for every time step, both the spatial variation in OC stocks as well as the total amount of SOC present in the simulated region are tracked for every simulated timestep.

#### *Input data*

- The spatial extent of embankments, the resulting polders and contemporary tidal marshes was digitized from the topographic map from the Netherlands (freely available on [www.opentopo.nl](http://www.opentopo.nl)) using ArcMap®.
- Historical data on marsh reclamations and dates of historical constructions were obtained from Wilderom (1968) for the brackish polders and Wilderom (1973) for the salt polders.
- The rate of lateral marsh expansion ( $\text{m yr}^{-1}$ ) was obtained from (Jongepier et al., 2015), who calculated this rate for a polder region in the Scheldt estuary at the Dutch – Belgian border.
- The rate of vertical marsh accretion due to sediment deposition ( $\text{m yr}^{-1}$ ) is varied as a function of time since marsh initiation
  - For marshes which accrete in equilibrium with mean high water level (MHWL; ‘high marshes’, (Temmerman et al., 2004)) historical data on MHW is used to calculate the annual accretion rate.
    - For the period 1935 – 2014, tidal gauge data from Vlissingen and Bath are used for the salt- and brackish polders respectively.
    - For earlier time periods, calculated data from van der Spek (1997) for 1650 and 1800 are used to interpolate MHWL from 1500 to 1935.

- For the period 2014 – 2100, the average increase in MHWL for the period 1984 – 2014 was used for extrapolation.
- Recently established tidal marshes accrete at a rate higher than MHWL (Temmerman et al., 2004). Therefore, data from Temmerman et al. (2004) were used to derive that the initial rate of tidal marsh accretion is 3 times higher than the rise in MHWL. In addition, Jongepier et al. (2015) established that it took between 60 and 96 years for historical tidal marshes in the Scheldt estuary to accrete in equilibrium with MHWL.
- These data were combined to construct time series of sediment accretion rates of tidal marshes. The rate of sediment deposition in the first year after marsh establishment is 3 times the rate of the rise in MHWL of that year, after which sediment deposition rates decline exponentially to be equal to the rise in MHWL after 100 years.
- The amount of OC accumulating in tidal marsh sediments was obtained from Van de Broek et al. (2016) for the ‘marsh near Waarde’ and ‘Paulina marsh’ for the modelled brackish- and salt polder region respectively. The measured depth profiles of OC at these locations, expressed as  $\text{g m}^{-2}$ , were used as the amount of OC accumulating in developing tidal marsh sediments.
- After embankment of tidal marshes, the OC stock declined exponentially through time until the average amount of OC measured for the polder soils in brackish and salt polder region was reached respectively. The rate at which OC declined through time was calculated based on the empirical results obtained in this study for the first century after reclamation (see main manuscript).
- Soil compaction after tidal marsh embankment was simulated by decreasing the depth of silty marsh sediments through time. As a consequence, bulk density increases through time. The rate of this decrease was calculated based on the increase in bulk density reported in the main manuscript, until the average measured bulk density was reached.

### *Model description*

The simulated landscape is represented in the model as a raster with a spatial resolution of 10 m, where the land use of every cell in the simulated region evolves through time. For every cell, SOC depth profiles are simulated down to a depth of 3 m at a vertical resolution of 0.01 m. For the brackish polder region, the model was ran between 1500 and 2100 AD, for the salt polder region between 1700 and 2100 AD. The model parameter values that were used are shown in Table S1, other data series are included with the model codes.

### Tidal marsh evolution

In the model, tidal marshes are always initiated against an embankment. In the first year after the construction of a new embankment, the amount of newly initiated tidal marsh is calculated as

$$N_{\text{marsh}(0)} = N_{\text{embankment}} * F_{\text{init}}$$

With  $N_{\text{marsh}(0)}$  being the number of new marsh cells,  $N_{\text{embankment}}$  the number of embankment cells bordering the tidal flat at which the tidal marsh is established and  $F_{\text{init}}$  the ratio between embankment cells and new marsh cells to be initiated. The newly initiated marsh cells are chosen by randomly accessing the sandflat cells bordering the embankment and assigning tidal marsh cells until the required number of tidal marsh cells is initiated.

After the establishment of a tidal marsh cell, sediments are deposited on this cell by multiplying the current rate in MHWL with a time-dependent factor, to simulate declining sediment deposition rates through time. This factor ( $F_{\text{depo}}$ ) is calculated as follows:

$$F_{\text{depo}}(t) = 1 + (F_{\text{depo}}(1)-1) \cdot \exp(-b \cdot t)$$

With  $t$  the time since the initiation of the marsh cell (year),  $F_{\text{depo}}(1)$  the factor in the first year after initiation of the marsh on that cell and  $b$  a constant determining the rate of decline ( $\text{year}^{-1}$ ). Note the '+1', which ensures that when the second part of the equation becomes 0,  $F_{\text{depo}}$  equals 1.

Every year, tidal marshes are allowed to expand laterally. Therefore, every year, all tidal marsh cells which share a boundary with the sandflat are accessed in a random order and a random cardinal neighboring sandflat cell is accessed. Subsequently, this sandflat cell will become a tidal marsh cell with a probability  $p_{\text{marsh}}$ . In addition, the rate of tidal marsh expansion cannot be larger than the user-defined rate:

$$\text{dist} < \text{expRate}_{\text{max}} \cdot t_{\text{marsh}}$$

with  $\text{dist}$  the shortest distance between a marsh cell the nearest dike (m),  $t_{\text{marsh}}$  the time since the initiation of the marsh (year) and  $\text{expRate}_{\text{max}}$  the user-defined maximum rate of lateral marsh expansion ( $\text{m year}^{-1}$ ).

Annually, the depth profile of OC for every tidal marsh cell is updated and is equal to the user-defined depth OC profile, down to the depth of simulated tidal marsh sediments.

### Embanked tidal marshes

After a tidal marsh is embanked, its bulk density increases. This is simulated by decreasing the depth of the deposited marsh sediments through time until the user-defined bulk density is obtained. The rate at which the sediment depth is reduced after embankment is defined as:

$$\text{Depth}(t) = \text{Depth}(0) \cdot \exp(-\text{BD}_{\text{rate}} \cdot t)$$

With  $t$  being the time since the cell was converted to a polder (year),  $\text{Depth}$  being the depth of the deposited marsh sediments (m) and  $\text{BD}_{\text{rate}}$  a factor determining the rate at which compaction occurs ( $\text{year}^{-1}$ ). This process is repeated annually until the user-defined equilibrium bulk density ( $\text{BD}_{\text{eq}}$ ) is reached.

After embankment, the total amount of SOC in every polder cell is reduced, until the user-defined equilibrium SOC ( $\text{SOC}_{\text{eq}}$ ) is reached. Note that the reduction in SOC content is applied to the total amount of SOC and is therefore independent of depth. This is calculated using the following equation:

$$\text{SOC}_{\text{polder}}(t) = \text{SOC}_{\text{polder}}(0) * \exp(-\text{SOC}_{\text{rate}} * t)$$

With  $t$  being the time since the cell was converted to a polder (year),  $\text{SOC}_{\text{polder}}$  being the SOC stock of the deposited marsh sediments (m) and  $\text{SOC}_{\text{rate}}$  a factor determining the rate at SOC declines through time ( $\text{year}^{-1}$ ).

The concentration of OC in sandflat sediments ( $\text{OC}_{\text{sandflat}}$ ) is kept constant through time, and is converted to total stocks using a constant bulk density value ( $\text{BD}_{\text{sandflat}}$ ). At the start of the model run, the simulated region is assumed to consist of sandflat sediments of the entire simulated depth (3 m). As tidal marsh sediments are deposited on top of sandflat sediments, the sediments below the deposited marsh sediments are assumed to be sandflat sediments, down to the maximum simulation depth.

As a result, the model simulates the average amount of OC in the area of interest, expressed as  $\text{OC m}^{-2}$ , down to a user-defined depth ( $\text{OC}_{\text{depth}}$ ).

**Table S4-1** Model parameter values

Parameter name	Brackish region	Salt region	Reference
$F_{\text{init}}$	0.2	0.2	
$\text{expRate}_{\text{max}}$	40 m $\text{year}^{-1}$	40 m $\text{year}^{-1}$	(Jongepier et al., 2015)
$\rho_{\text{marsh}}$	0.5	0.5	
$b$	0.05 $\text{year}^{-1}$	0.05 $\text{year}^{-1}$	Own data
$F_{\text{depo}}$	3	3	(Temmerman et al., 2004)
$\text{BD}_{\text{rate}}$	0.005 $\text{year}^{-1}$	0.006 $\text{year}^{-1}$	Own data
$\text{BD}_{\text{eq}}$	1.4 $\text{g cm}^{-3}$	1.5 $\text{g cm}^{-3}$	Own data
$\text{SOC}_{\text{rate}}$	0.01 $\text{year}^{-1}$	0.011 $\text{year}^{-1}$	Own data
$\text{SOC}_{\text{eq}}$	1.4 %	1.1 %	Own data
$\text{OC}_{\text{sandflat}}$	0.7 %	0.15 %	(1)
$\text{BD}_{\text{sandflat}}$	1.5 $\text{g cm}^{-3}$	1.5 $\text{g cm}^{-3}$	Own data (2)

(1) Salt region: (Moens et al., 2005, 2002); brackish region: (Boschker et al., 1999; Middelburg et al., 1996). (2) Bulk density measured in polders in the sandy layer below the silt layer.

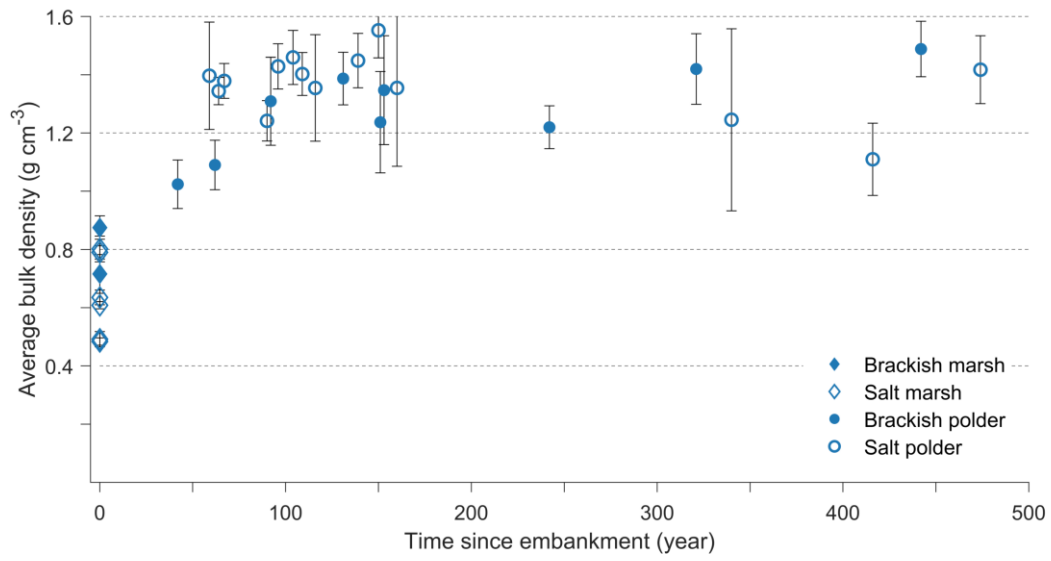


**Figure S4-1** Average bulk density in the top 0.3 m of present-day tidal marsh sediments and embanked polders (g cm<sup>-3</sup>).

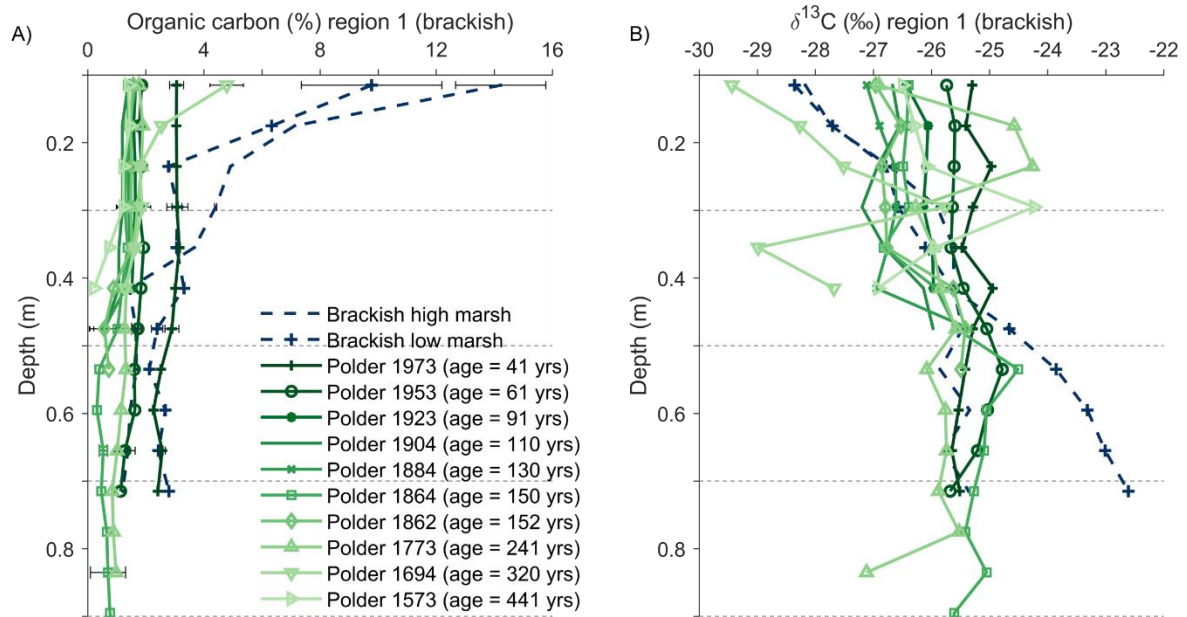


**Figure S4-2** Depth profiles of organic carbon (A) and  $\delta^{13}\text{C}$  values (B) for the sampled polders and a low and high marsh in region 1 (see Figure 1 in the main manuscript). Age refers to the time between embankment and sampling.

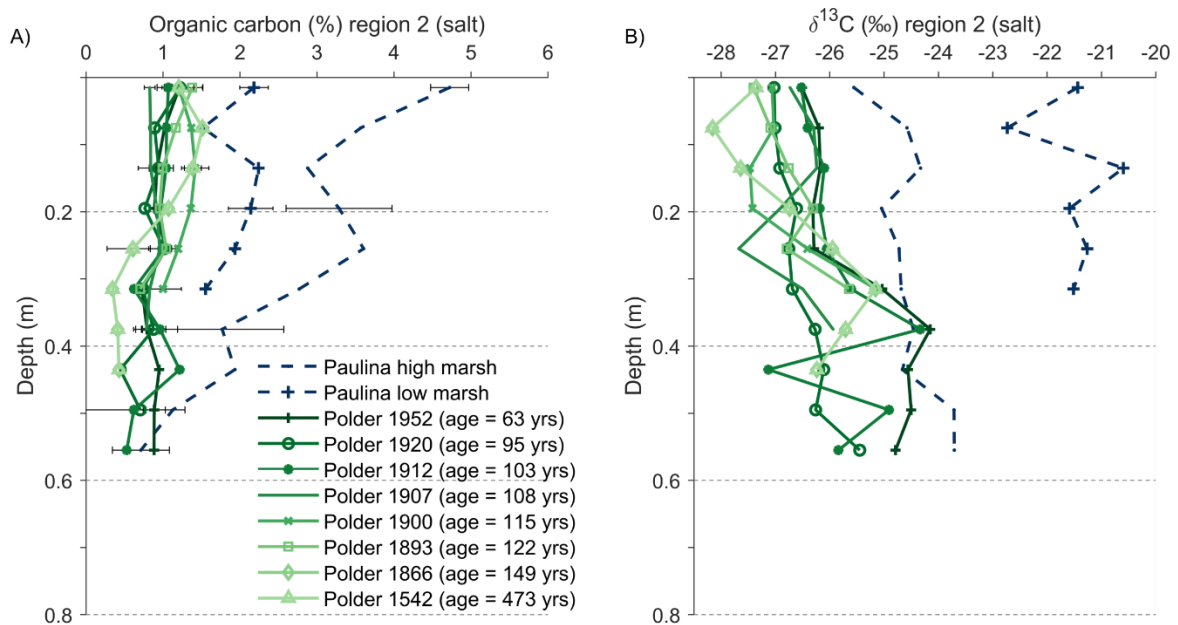


**Figure S4-3** Depth profiles of organic carbon (A) and  $\delta^{13}\text{C}$  values (B) for the sampled polders and a low and high marsh in region 2 (see Figure 1 in the main manuscript). Age refers to the time between embankment and sampling.

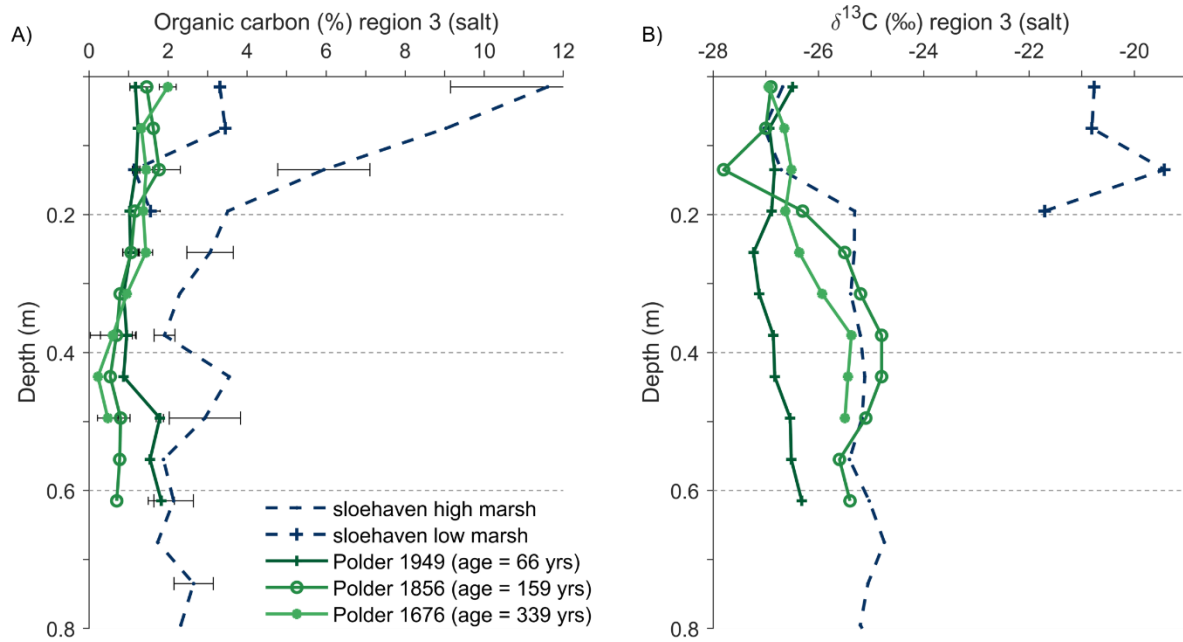


**Figure S4-4** Depth profiles of organic carbon (A) and  $\delta^{13}\text{C}$  values (B) for the sampled polders and a low and high marsh in region 3 (see Figure 1 in the main manuscript). Age refers to the time between embankment and sampling.

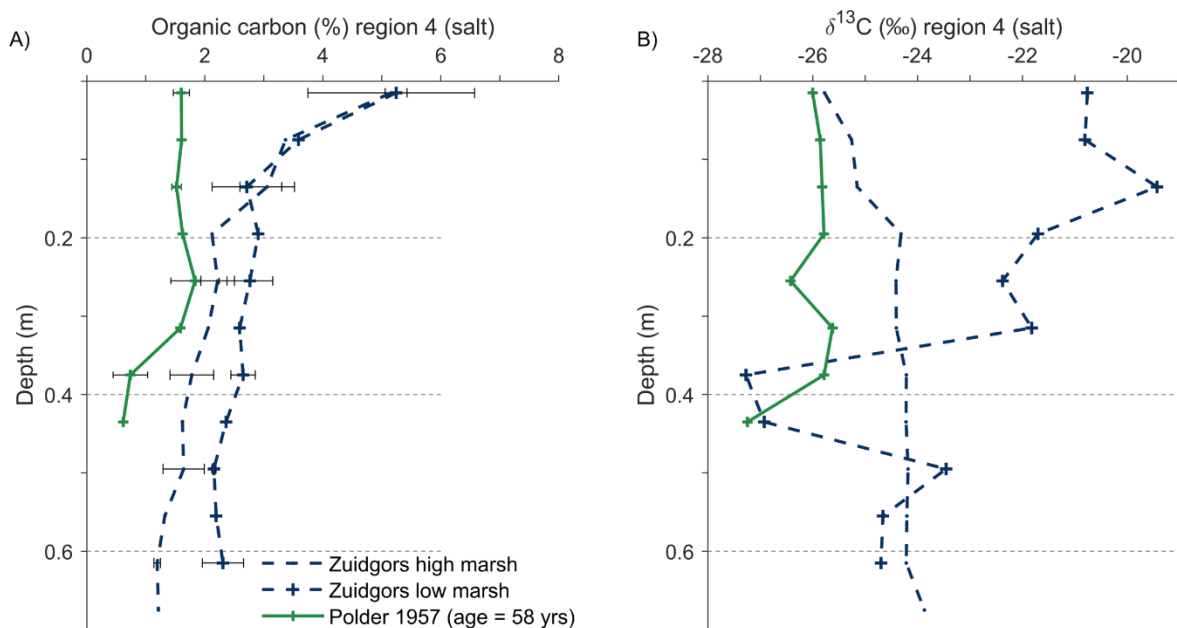


**Figure S4-5** Depth profiles of organic carbon (A) and  $\delta^{13}\text{C}$  values (B) for the sampled polders and a low and high marsh in region 4 (see Figure 1 in the main manuscript). Age refers to the time between embankment and sampling.

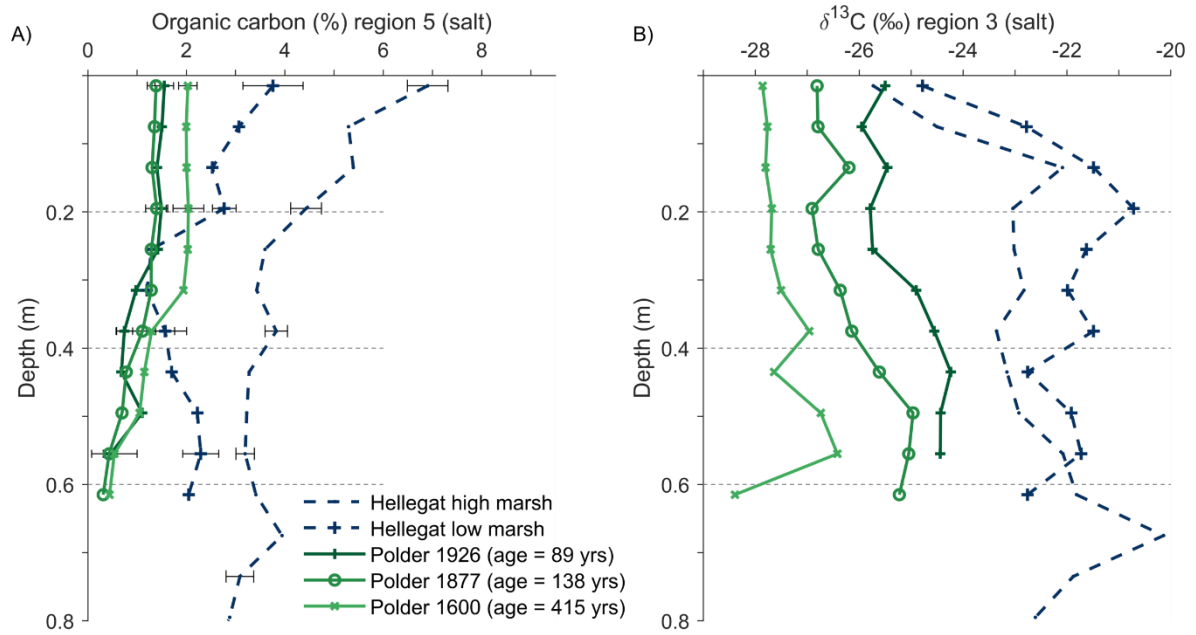


**Figure S4-6** Depth profiles of organic carbon (A) and  $\delta^{13}\text{C}$  values (B) for the sampled polders and a low and high marsh in region 5 (see Figure 1 in the main manuscript). Age refers to the time between embankment and sampling.

**Table S4-2** topsoil pH, inorganic carbon content and average grain size for the sampled polders and tidal marshes (the latter is from Van de Broek et al. (2018)). <sup>1</sup>See main manuscript for site names, <sup>2</sup>average for the top 0.3 m, <sup>3</sup>average for the silt-rich topsoil layer, <sup>4</sup>Total stock for the upper 400 kg m<sup>-2</sup> of soil.

Site (year) <sup>1</sup>	Topsoil pH <sup>2</sup>	% clay (< 2 μm) (%) <sup>3</sup>	% silt (2 – 63 μm) (%) <sup>3</sup>	% sand (> 63 μm) (%) <sup>3</sup>	Inorganic carbon (kg m <sup>-2</sup> ) <sup>4</sup>
<i>Region 1</i>					
Low marsh	7.7	13.8	66.0	20.2	4.87
High marsh	7.5	14.0	66.7	19.3	4.45
1571	7.14	13.2	59.6	27.2	4.06
1694	-	9.9	47.3	42.8	2.89
1773	7.07	18.8	66.8	14.4	4.82
1862	-	17.1	69.0	13.9	3.55
1864	-	17.0	71.1	11.9	4.81
1884	7.13	16.9	53.4	26.7	4.9
1904		13.5	49.5	37.0	3.72
1923	7.13	14.9	57.0	28.1	
1953	7.28	23.5	69.1	7.4	5.84
1973	7.45	21.2	71.9	6.9	5.45
<i>Region 2</i>					
Low marsh	7.87	8.9	47.6	43.5	-
High marsh	7.93	12.5	65.4	22.1	-
1542	7.76	11.7	77.7	10.6	-
1866	7.59	10.7	58.4	30.9	-
1893	7.84	6.2	42.0	51.8	-
1900	7.44	9.6	48.1	42.2	-
1907	7.44	5.5	49.0	45.4	-
1912	7.79	8.2	56.0	35.8	-
1920	4.67	5.3	35.8	58.9	-
1952	7.64	6.2	49.6	44.2	-
<i>Region 3</i>					
High marsh	7.24	15.0	79.5	5.5	-
1676	7.63	11.2	57.5	31.3	-
1856	7.84	14.5	76.3	9.2	-
1949	7.78	8.1	57.1	34.8	-
<i>Region 4</i>					
Low marsh	7.89	12.4	79.9	7.7	-
High marsh	7.64	9.3	77.6	13.1	-
1957	7.78	9.9	65.5	24.6	-
<i>Region 5</i>					
Low marsh	7.60	11.5	61.9	26.6	-
High marsh	7.50	14.1	73.4	12.5	-
1600	7.50	8.4	62.4	29.2	-
1877	7.51	12.2	72.0	15.8	-
1926	7.57	10.2	70.6	19.2	-

**Table S4-3** Coordinates of the locations at which the polders were sampled. Coordinates of the sampling locations on the tidal marshes are provided in the supplementary data of chapters 2 and 3.

Site (year) <sup>1</sup>	Coordinates
1571	51°25'52.86"N; 4° 3'20.88"E
1694	51°25'5.28"N; 4° 7'38.28"E
1773	51°24'55.02"N; 4° 8'33.12"E
1862	51°26'1.74"N; 4°10'10.74"E
1864	51°24'29.88"N; 4° 6'36.90"E
1884	51°24'39.54"N; 4°15'49.86"E
1904	51°24'31.20"N; 4°15'30.18"E
1923	51°25'4.44"N; 4°14'52.20"E
1953	51°24'30.00"N; 4°11'17.10"E
1973	51°24'33.42"N; 4°14'48.48"E
<i>Region 2</i>	
1542	51°19'26.80"N; 3°45'24.01"E
1866	51°17'30.63"N; 3°45'4.37"E
1893	51°18'2.41"N; 3°41'9.71"E
1900	51°17'6.52"N; 3°44'56.63"E
1907	51°17'44.90"N; 3°41'20.08"E
1912	51°17'20.98"N; 3°47'52.19"E
1920	51°17'50.42"N; 3°43'45.80"E
1952	51°17'55.54"N; 3°43'29.30"E
<i>Region 3</i>	
1676	51°28'23.26"N; 3°44'6.29"E
1856	51°28'29.39"N; 3°43'36.61"E
1949	51°29'47.77"N; 3°42'36.94"E
<i>Region 4</i>	
1957	51°23'24.63"N; 3°49'48.22"E
<i>Region 5</i>	
1600	51°19'8.12"N; 3°56'10.48"E
1877	51°19'32.07"N; 3°56'54.87"E
1926	51°21'48.53"N; 3°56'33.65"E

## Chapter 5

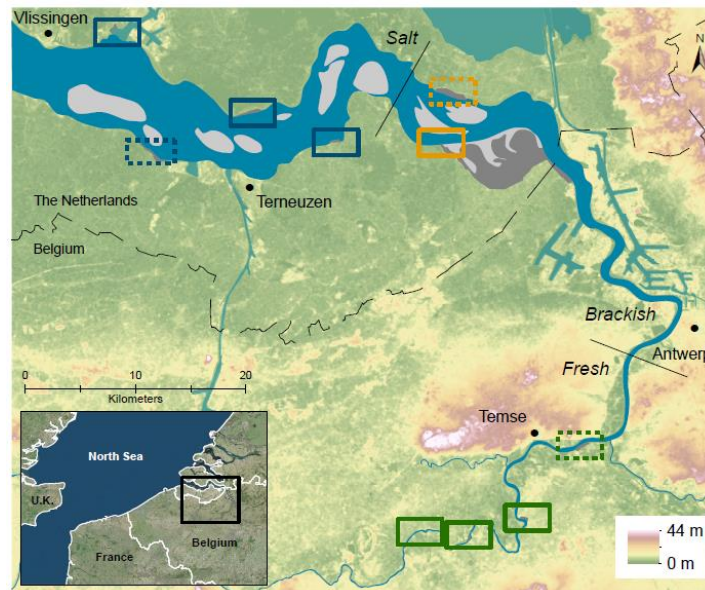


**Figure S5-1** Map of the Scheldt estuary showing the locations of the studied saltmarshes (blue rectangles), brackish marshes (orange rectangles) and freshwater marshes (green rectangles). For the marshes depicted with dashed rectangles, the SOC concentration has been determined with the elemental analyzer for three replicate depth profiles, samples from these marshes have been used to calculate the total SOC stocks using m-IR data. Adapted from Van de Broek et al. (2018)

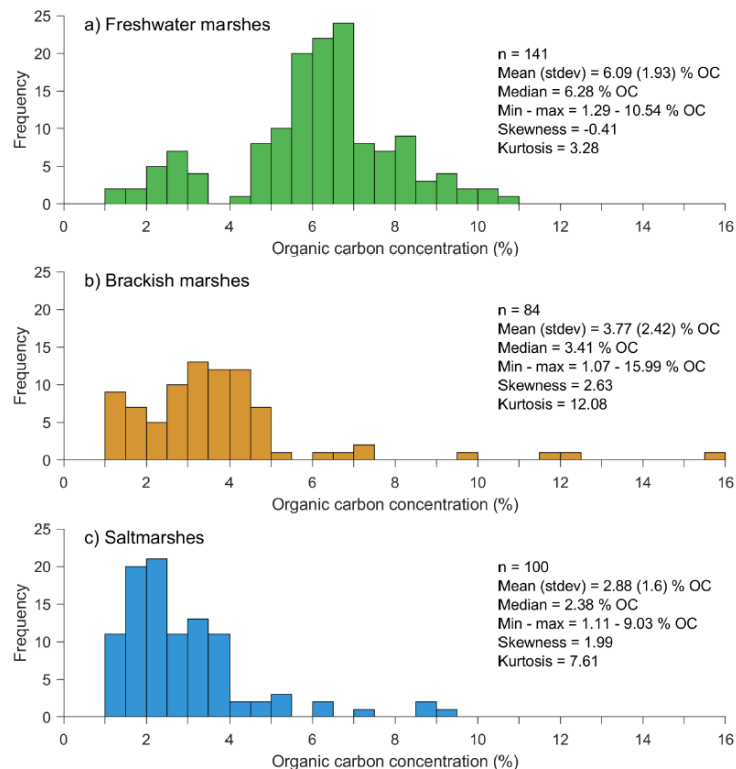


**Figure S5-2** Frequency histograms of the organic carbon concentration of the sediment samples in the studied tidal marshes and descriptive statistics of the organic carbon concentration of the samples per salinity zone.

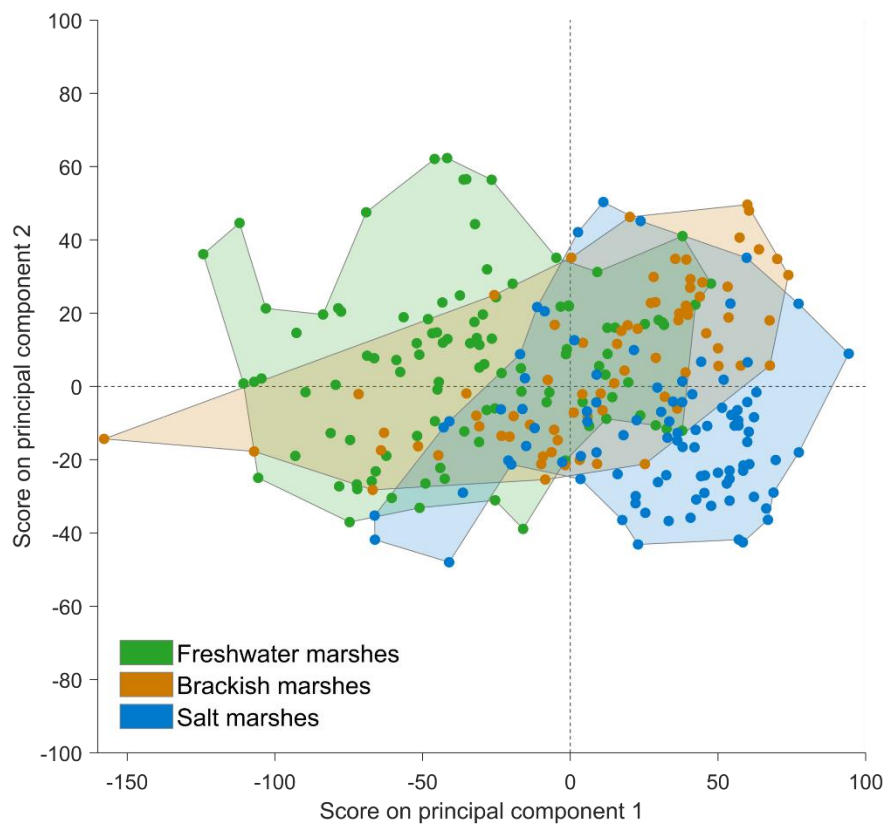


**Figure S5-3** Scores of the m-IR spectra on the first two principal components, grouped for soil samples per salinity zone.

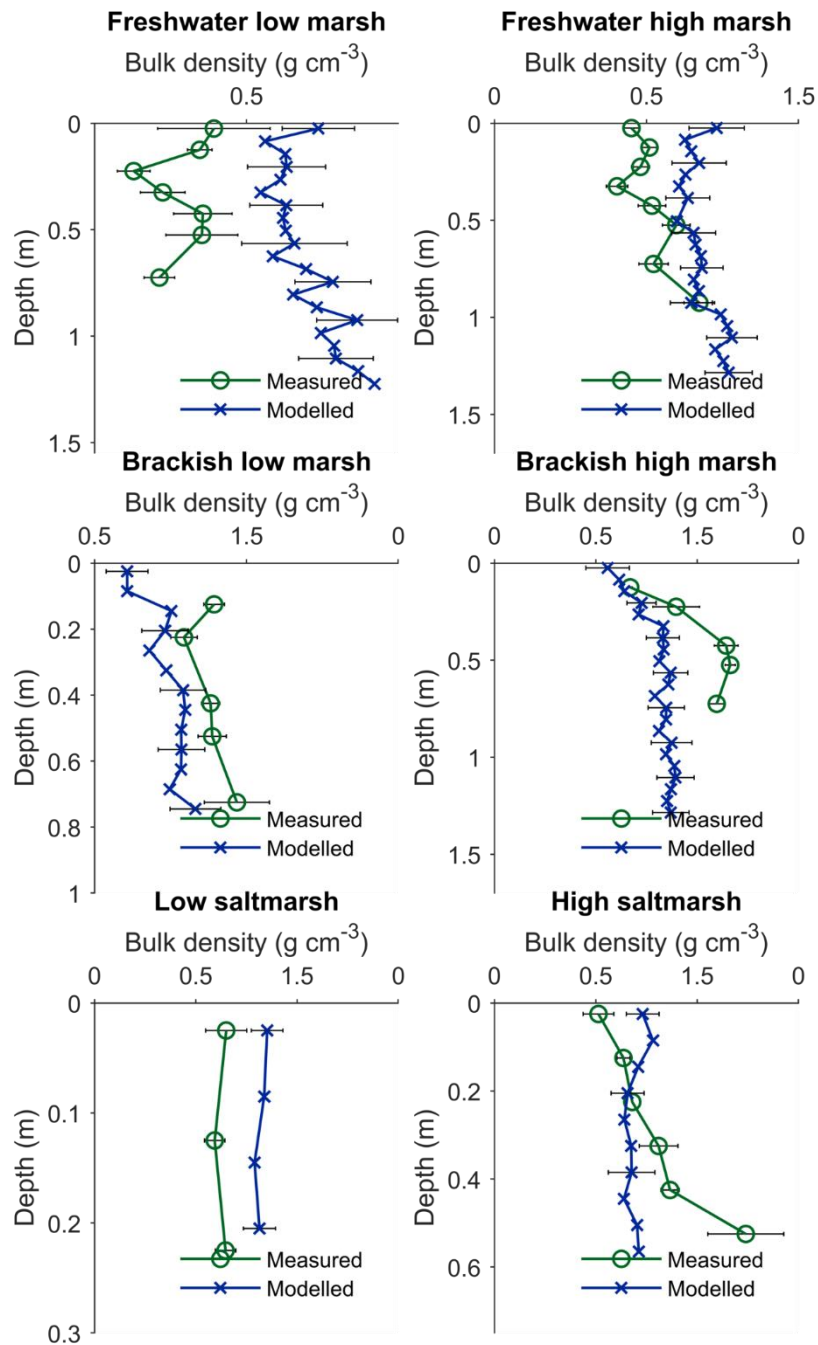


**Figure S5-4** Depth profiles of predicted and measured bulk density values (g cm<sup>-3</sup>). Error bars for the measured values show the standard deviation ( $\sigma$ ) representing the spatial variation between 3 replicate soil cores, the error bars for the modelled values show the  $\sigma$  for spatial variations plus the uncertainty associated with the m-IR predictions.

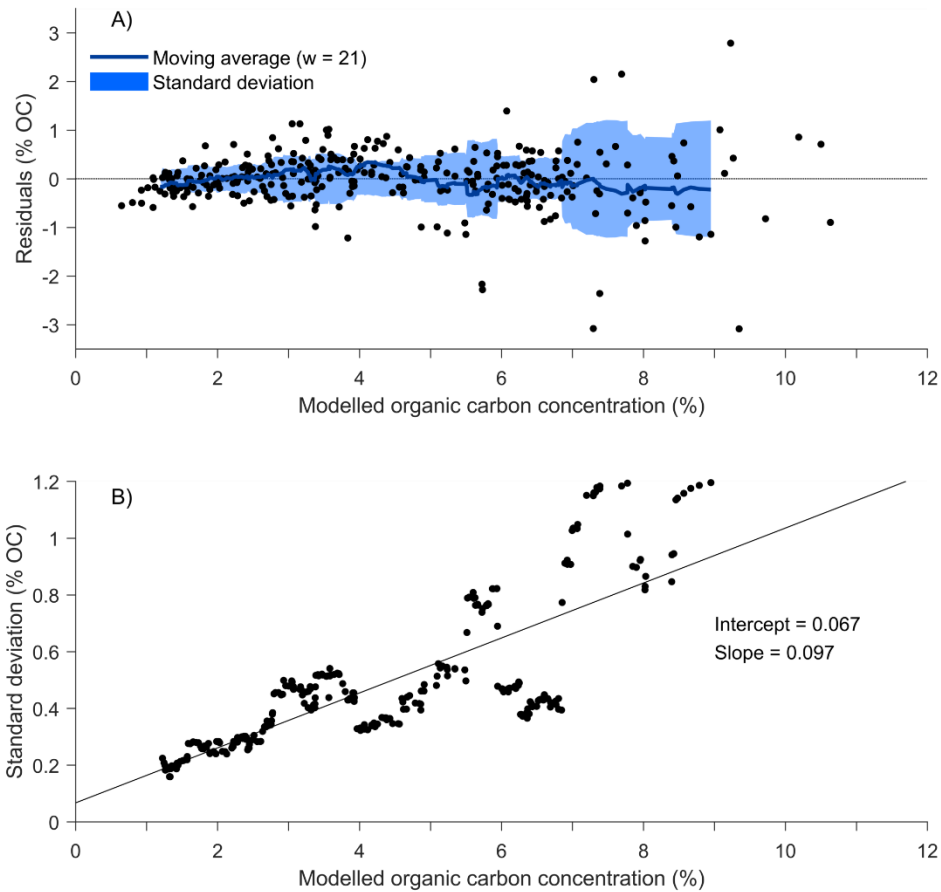


**Figure S5-5** Analyses of the absolute residuals (measured - modelled organic carbon concentration) for the independent validation results of the general model which was calibrated based on 70 samples. Plot A) shows the residuals, the moving average (window size ( $w$ ) = 21) and the standard deviation ( $w$  = 21) in function the predicted OC concentration. Plot B) shows the standard deviation in function of the predicted OC concentration.

---

## References

---

- Abramoff, R., Xu, X., Hartman, M., O'Brien, S., Feng, W., Davidson, E., Finzi, A., Moorhead, D., Schimel, J., Torn, M., Mayes, M.A., 2018. The Millennial model: in search of measurable pools and transformations for modeling soil carbon in the new century. *Biogeochemistry* 137, 51–71. <https://doi.org/10.1007/s10533-017-0409-7>
- Abril, G., Nogueira, M., Etcheber, H., Cabeçadas, G., Lemaire, E., Brogueira, M., 2002. Behaviour of Organic Carbon in Nine Contrasting European Estuaries. *Estuar. Coast. Shelf Sci.* 54, 241–262. <https://doi.org/10.1006/ecss.2001.0844>
- Accoe, F., Boeckx, P., van Cleemput, O., Hofman, G., Zhang, Y., Li, R., Guanxiong, C., 2002. Evolution of the  $\delta^{13}\text{C}$  signature related to total carbon contents and carbon decomposition rate constants in a soil profile under grassland. *Rapid Commun. mass Spectrom.* 16, 2184–2189. <https://doi.org/10.1002/rcm.767>
- Acton, P., Fox, J., Campbell, E., Rowe, H., Wilkinson, M., 2013. Carbon isotopes for estimating soil decomposition and physical mixing in well-drained forest soils. *J. Geophys. Res. Biogeosciences* 118, 1532–1545. <https://doi.org/10.1002/2013JG002400>
- Ahrens, B., Braakhekke, M.C., Guggenberger, G., Schrumpf, M., Reichstein, M., 2015. Contribution of sorption, DOC transport and microbial interactions to the  $^{14}\text{C}$  age of a soil organic carbon profile: Insights from a calibrated process model. *Soil Biol. Biochem.* 88, 390–402. <https://doi.org/10.1016/j.soilbio.2015.06.008>
- Ahrens, B., Reichstein, M., Borcken, W., Muhr, J., Trumbore, S.E., Wutzler, T., 2014. Bayesian calibration of a soil organic carbon model using  $\Delta^{14}\text{C}$  measurements of soil organic carbon and heterotrophic respiration as joint constraints. *Biogeosciences* 11, 2147–2168. <https://doi.org/10.5194/bg-11-2147-2014>
- Allen, J.R.L., 1990. The formation of coastal peat marshes under an upward tendency of relative sea-level. *J. Geol. Soc. London.* 147, 743–745.
- Allison, S.D., Romero-Olivares, A.L., Lu, Y., Taylor, J.W., Treseder, K.K., 2018. Temperature sensitivities of extracellular enzyme  $V_{\text{max}}$  and  $K_m$  across thermal environments. *Glob. Chang. Biol.* <https://doi.org/10.1111/gcb.14045>
- Allison, S.D., Wallenstein, M.D., Bradford, M.A., 2010. Soil-carbon response to warming dependent on microbial physiology. *Nat. Geosci.* 3, 336–340. <https://doi.org/10.1038/ngeo846>
- An, S., Li, H., Guan, B., Zhou, C., Wang, Z., Deng, Z., Zhi, Y., Liu, Y., Xu, C., Fang, S., Jiang, J., Li, H., 2007. China's natural wetlands: Past problems, current status, and future challenges. *Ambio* 36, 335–342. [https://doi.org/10.1579/0044-7447\(2007\)36\[335:CNWPPC\]2.0.CO;2](https://doi.org/10.1579/0044-7447(2007)36[335:CNWPPC]2.0.CO;2)
- Anderson, J.D., 1995. *Computational fluid dynamics : the basics with applications*. McGraw-Hill, Inc., New York.
- Andreasson, F., Bergkvist, B., Bååth, E., 2009. Bioavailability of DOC in leachates, soil matrix solutions and soil water extracts from beech forest floors. *Soil Biol. Biochem.* 41, 1652–1658. <https://doi.org/10.1016/j.soilbio.2009.05.005>
- Andrén, O., Kätterer, T., 1997. ICBM: The introductory carbon balance model for exploration of soil carbon balances. *Ecol. Appl.* [https://doi.org/10.1890/1051-0761\(1997\)007\[1226:ITICBM\]2.0.CO;2](https://doi.org/10.1890/1051-0761(1997)007[1226:ITICBM]2.0.CO;2)
- Angst, G., Mueller, K.E., Kögel-Knabner, I., Freeman, K.H., Mueller, C.W., 2017. Aggregation controls the stability of lignin and lipids in clay-sized particulate and mineral associated organic matter. *Biogeochemistry* 132, 307–324. <https://doi.org/10.1007/s10533-017-0304-2>

## References

---

- Anon, 2010. Soil interfering activities. Indicators for the Scheldt estuary. Commissioned by the Maritime Access Division, project group EcoWaMorSe, Flemish-Dutch Scheldt Commission. VLIZ Inf. sheets, 223. Flanders Mar. Inst. Oostende. 11 pp.
- Artigas, F., Shin, J.Y., Hobbie, C., Marti-Donati, A., Schäfer, K.V.R., Pechmann, I., 2015. Long term carbon storage potential and CO<sub>2</sub> sink strength of a restored salt marsh in New Jersey. *Agric. For. Meteorol.* 200, 313–321. <https://doi.org/10.1016/j.agrformet.2014.09.012>
- Bai, J., Xiao, R., Zhang, K., Gao, H., Cui, B., Liu, X., 2013. Soil organic carbon as affected by land use in young and old reclaimed regions of a coastal estuary wetland, China. *Soil Use Manag.* 29, 57–64. <https://doi.org/10.1111/sum.12021>
- Baisden, W.T., Amundson, R., Brenner, D.L., Cook, A.C., Kendall, C., Harden, J.W., 2002. A multiisotope C and N modeling analysis of soil organic matter turnover and transport as a function of soil depth in a California annual grassland soil chronosequence. *Global Biogeochem. Cycles* 16. <https://doi.org/10.1029/2001GB001823>
- Baldock, J.A., Hawke, B., Sanderman, J., Macdonald, L.M., 2013. Predicting contents of carbon and its component fractions in Australian soils from diffuse reflectance mid-infrared spectra. *Soil Res.* 51, 577. <https://doi.org/10.1071/SR13077>
- Balesdent, J., Girardin, C., Mariotti, A., 1993. Site-related  $\delta^{13}\text{C}$  of tree leaves and soil organic matter in a temperate forest. *Ecology* 74, 1713–1721.
- Baranzini, A., van den Bergh, J.C.J.M., Carattini, S., Howarth, R.B., Padilla, E., Roca, J., 2017. Carbon pricing in climate policy: seven reasons, complementary instruments, and political economy considerations. *Wiley Interdiscip. Rev. Clim. Chang.* 8, 1–17. <https://doi.org/10.1002/wcc.462>
- Barbier, E.B., Hacker, S.D., Kennedy, C., Koch, E.W., Stier, A.C., Silliman, B.R., 2011. The value of estuarine and coastal ecosystem services. *Ecol. Monogr.* 81, 169–193. <https://doi.org/10.1890/10-1510.1>
- Barendregt, A., Swarth, C.W., 2013. Tidal Freshwater Wetlands: Variation and Changes. *Estuaries and Coasts* 36, 445–456. <https://doi.org/10.1007/s12237-013-9626-z>
- Bauer, J.E., Cai, W.-J., Raymond, P. a, Bianchi, T.S., Hopkinson, C.S., Regnier, P. a G., 2013. The changing carbon cycle of the coastal ocean. *Nature* 504, 61–70. <https://doi.org/10.1038/nature12857>
- Bauska, T.K., Joos, F., Mix, A.C., Roth, R., Ahn, J., Brook, E.J., 2015. Links between atmospheric carbon dioxide, the land carbon reservoir and climate over the past millennium. *Nat. Geosci.* 8, 383–387. <https://doi.org/10.1038/ngeo2422>
- Beke, G.J., 1990. Soil development in a 100-year dike near grand pré, Nova Scotia. *Can. J. Soil Sci.* 70, 683–692.
- Bellon-Maurel, V., Fernandez-Ahumada, E., Palagos, B., Roger, J.-M., McBratney, A., 2010. Critical review of chemometric indicators commonly used for assessing the quality of the prediction of soil attributes by NIR spectroscopy. *Trends Anal. Chem.* 29, 1073–1081. <https://doi.org/10.1016/j.trac.2010.05.006>
- Bellon-Maurel, V., McBratney, A., 2011. Near-infrared (NIR) and mid-infrared (MIR) spectroscopic techniques for assessing the amount of carbon stock in soils - Critical review and research perspectives. *Soil Biol. Biochem.* 43, 1398–1410. <https://doi.org/10.1016/j.soilbio.2011.02.019>
- Bianchi, T.S. (Ed.), 2007. *Biogeochemistry of Estuaries*. Oxford University Press, Inc., Oxford. <https://doi.org/10.1007/s13398-014-0173-7.2>
- Billen, G., Garnier, J., Rousseau, V., 2005. Nutrient fluxes and water quality in the drainage network of the Scheldt basin over the last 50 years. *Hydrobiologia* 540, 47–67. <https://doi.org/10.1007/s10750-004-7103-1>
- Blankinship, J., Schimel, J., 2018. Biotic versus Abiotic Controls on Bioavailable Soil Organic Carbon. *Soil Syst.* 2, 2–13. <https://doi.org/10.3390/soilsystems2010010>
- Bornemann, L., Welp, G., Amelung, W., 2010. Particulate Organic Matter at the Field Scale: Rapid Acquisition Using Mid-Infrared Spectroscopy. *Soil Sci. Soc. Am. J.* 74, 1147. <https://doi.org/10.2136/sssaj2009.0195>
- Boschker, H.T.S., de Brouwer, J.F.C., Cappenberg, T.E., 1999. The contribution of macrophyte-derived organic matter to microbial biomass in salt-marsh sediments: Stable carbon isotope analysis of microbial biomarkers. *Limnol. Oceanogr.* 44, 309–319. <https://doi.org/10.4319/lo.1999.44.2.0309>

- Boström, B., Comstedt, D., Ekblad, A., 2007. Isotope fractionation and  $^{13}\text{C}$  enrichment in soil profiles during the decomposition of soil organic matter. *Oecologia* 153, 89–98. <https://doi.org/10.1007/s00442-007-0700-8>
- Bouillon, S., Boschker, H.T.S., 2006. Bacterial carbon sources in coastal sediments: a cross-system analysis based on stable isotope data of biomarkers. *Biogeosciences* 3, 175–185. <https://doi.org/10.5194/bg-3-175-2006>
- Bouma, T.J., Hengst, K., Koutstaal, B.P., Soelen, J. Van, 2002. Estimating root lifespan of two grasses at contrasting elevation in a salt marsh by applying vitality staining on roots from in-growth cores. *Plant Ecol.* 165, 235–245.
- Bowling, D.R., Pataki, D.E., Randerson, J.T., 2008. Carbon Isotopes in Terrestrial Ecosystem Pools and  $\text{CO}_2$  Fluxes. *New Phytol.* 178, 24–40. <https://doi.org/10.2307/30147703>
- Braakhekke, M., Beer, C., Schrumph, M., Ekici, A., Ahrens, B., Hoosbeek, M.R., Kruijt, B., Kabat, P., Reichstein, M., 2014. The use of radiocarbon to constrain current and future soil organic matter turnover and transport in a temperate forest. *J. Geophys. Res. Biogeosciences* 119, 372–391. <https://doi.org/10.1002/2013JG002420>
- Braakhekke, M., Wutzler, T., Beer, C., Kattge, J., Schrumph, M., Schöning, I., Hoosbeek, M.R., Kruijt, B., Kabat, P., Reichstein, M., 2013. Modeling the vertical soil organic matter profile using Bayesian parameter estimation. *Biogeosciences Discuss.* 9, 11239–11292. <https://doi.org/10.5194/bgd-9-11239-2012>
- Bradford, M.A., Wieder, W.R., Bonan, G.B., Fierer, N., Raymond, P.A., Crowther, T.W., 2016. Managing uncertainty in soil carbon feedbacks to climate change. *Nat. Clim. Chang.* 6, 751–758. <https://doi.org/10.1038/nclimate3071>
- Bridgman, S.D., Megonigal, J.P., Keller, J.K., Bliss, N.B., Trettin, C., 2006. The carbon balance of North American wetlands. *Wetlands* 26, 889–916.
- Bu, N.-S., Qu, J.-F., Li, G., Zhao, B., Zhang, R.-J., Fang, C.-M., 2015. Reclamation of coastal salt marshes promoted carbon loss from previously-sequestered soil carbon pool. *Ecol. Eng.* 81, 335–339. <https://doi.org/10.1016/j.ecoleng.2015.04.051>
- Buth, G.J.C., de Wolf, L., 1985. Decomposition of *Spartina anglica*, *Elytrigia pungens* and *Halimione portulacoides* in a Dutch salt marsh in association with faunal and habitat influences. *Vegetatio* 62, 337–355. <https://doi.org/10.1007/BF00044761>
- Callaway, J.C., Borgnis, E.L., Turner, R.E., Milan, C.S., 2012. Carbon Sequestration and Sediment Accretion in San Francisco Bay Tidal Wetlands. *Estuaries and Coasts* 35, 1163–1181. <https://doi.org/10.1007/s12237-012-9508-9>
- Cambou, A., Cardinael, R., Kouakoua, E., Villeneuve, M., Durand, C., Barthès, B.G., 2016. Prediction of soil organic carbon stock using visible and near infrared reflectance spectroscopy (VNIRS) in the field. *Geoderma* 261, 151–159. <https://doi.org/10.1016/j.geoderma.2015.07.007>
- Campbell, E.E., Paustian, K., 2015. Current developments in soil organic matter modeling and the expansion of model applications: a review. *Environ. Res. Lett.* 10, 1–36. <https://doi.org/10.1088/1748-9326/10/12/123004>
- Carey, J.C., Tang, J., Templer, P.H., Kroeger, K.D., Crowther, T.W., Burton, A.J., Dukes, J.S., Emmett, B., Frey, S.D., Heskell, M.A., Jiang, L., Machmuller, M.B., Mohan, J., Panetta, A.M., Reich, P.B., Reinsch, S., Wang, X., Allison, S.D., Bamming, C., Bridgman, S., Collins, S.L., de Dato, G., Eddy, W.C., Enquist, B.J., Estiarte, M., Harte, J., Henderson, A., Johnson, B.R., Larsen, K.S., Luo, Y., Marhan, S., Melillo, J.M., Peñuelas, J., Pfeifer-Meister, L., Poll, C., Rastetter, E., Reinmann, A.B., Reynolds, L.L., Schmidt, I.K., Shaver, G.R., Strong, A.L., Suseela, V., Tietema, A., 2016. Temperature response of soil respiration largely unaltered with experimental warming. *Proc. Natl. Acad. Sci.* 113, 13797–13802. <https://doi.org/10.1073/pnas.1605365113>
- Chambers, L.G., Reddy, K.R., Osborne, T.Z., 2011. Short-Term Response of Carbon Cycling to Salinity Pulses in a Freshwater Wetland. *Soil Sci. Soc. Am. J.* 75, 2000–2007. <https://doi.org/10.2136/sssaj2011.0026>
- Chen, M.S., Wartel, S., Van Eck, B., Van Maldegem, D., 2005. Suspended matter in the Scheldt estuary. *Hydrobiologia* 540, 79–104. <https://doi.org/10.1007/s10750-004-7122-y>
- Chen, S., Torres, R., Goñi, M. a., 2016. The Role of Salt Marsh Structure in the Distribution of Surface Sedimentary

## References

---

- Organic Matter. *Estuaries and Coasts* 39, 108–122. <https://doi.org/10.1007/s12237-015-9957-z>
- Cherry, J.A., McKee, K.L., Grace, J.B., 2009. Elevated CO<sub>2</sub> enhances biological contributions to elevation change in coastal wetlands by offsetting stressors associated with sea-level rise. *J. Ecol.* 97, 67–77. <https://doi.org/10.1111/j.1365-2745.2008.01449.x>
- Chmura, G.L., Aharon, P., 1995. Stable Carbon-Isotope Signatures of Sedimentary Carbon in Coastal Wetlands As Indicators of Salinity Regime. *J. Coast. Res.* 11, 124–135.
- Chmura, G.L., Anisfeld, S.C., Cahoon, D.R., Lynch, J.C., 2003. Global carbon sequestration in tidal, saline wetland soils. *Global Biogeochem. Cycles* 17, 12. <https://doi.org/10.1029/2002gb001917>
- Choi, Y., Hsieh, Y., Wang, Y., 2001. Vegetation succession and carbon sequestration in a coastal wetland in northwest Florida: Evidence from carbon isotopes. *Global Biogeochem. Cycles* 15, 311–319.
- Choi, Y.R., 2014. Modernization, Development and Underdevelopment: Reclamation of Korean tidal flats, 1950s–2000s. *Ocean Coast. Manag.* 102, 426–436. <https://doi.org/10.1016/j.ocecoaman.2014.09.023>
- Ciais, P., Sabine, C., Bala, L., Bopp, L., Brovkin, V., Canadell, J., Chhabra, A., Defries, R., Galloway, J., Heimann, M., Jones, C., Le Quéré, C., Myneni, R.B., Piao, S., Thornton, B., 2013. Carbon and Other Biogeochemical Cycles, in: Stocker, T.F., Qin, D., Plattner, G.-K., Tignor, M., Allen, S.K., Boschung, J., Nauels, A., Xia, Y., Bex, V., Midgley, P.M. (Eds.), *Climate Change 2013: The Physical Science Basis. Contribution of Working Group I to the Fifth Assessment Report of the Intergovernmental Panel on Climate Change*. Cambridge University Press, Cambridge, United Kingdom and New York, NY, USA.
- Coen, I., 1988. Ontstaan en ontwikkeling van de Westerschelde. *Water* 156–162.
- Coleman, K., Jenkinson, D.S., 1999. RothC - 26.3 - A model for the turnover of carbon in soil, Model description and windows user guide.
- Cotrufo, M.F., Soong, J.L., Horton, A.J., Campbell, E.E., Haddix, M.L., Wall, D.H., Parton, W.J., 2015. Formation of soil organic matter via biochemical and physical pathways of litter mass loss. *Nat. Geosci.* 8, 776–779. <https://doi.org/10.1038/ngeo2520>
- Cotrufo, M.F., Wallenstein, M.D., Boot, C.M., Deneff, K., Paul, E., 2013. The Microbial Efficiency-Matrix Stabilization (MEMS) framework integrates plant litter decomposition with soil organic matter stabilization: Do labile plant inputs form stable soil organic matter? *Glob. Chang. Biol.* 19, 988–995. <https://doi.org/10.1111/gcb.12113>
- Cousins, I.T., Mackay, D., Jones, K.C., 1999. Measuring and modelling the vertical distribution of semi-volatile organic compounds in soils. II: model development. *Chemosphere* 39, 2519–2534.
- Craft, C., 2007. Freshwater input structures soil properties, vertical accretion, and nutrient accumulation of Georgia and U.S. tidal marshes. *Limnol. Oceanogr.* 52, 1220–1230. <https://doi.org/10.4319/lo.2007.52.3.1220>
- Crowther, T.W., Todd-Brown, K.E.O., Rowe, C.W., Wieder, W.R., Carey, J.C., Machmuller, M.B., Snoek, B.L., Fang, S., Zhou, G., Allison, S.D., Blair, J.M., Bridgman, S.D., Burton, A.J., Carrillo, Y., Reich, P.B., Clark, J.S., Classen, A.T., Dijkstra, F.A., Elberling, B., Emmett, B.A., Estiarte, M., Frey, S.D., Guo, J., Harte, J., Jiang, L., Johnson, B.R., Kröel-Dulay, G., Larsen, K.S., Laudon, H., Lavelle, J.M., Luo, Y., Lupascu, M., Ma, L.N., Marhan, S., Michelsen, A., Mohan, J., Niu, S., Pendall, E., Peñuelas, J., Pfeifer-Meister, L., Poll, C., Reinsch, S., Reynolds, L.L., Schmidt, I.K., Sistla, S., Sokol, N.W., Templer, P.H., Treseder, K.K., Welker, J.M., Bradford, M.A., 2016. Quantifying global soil carbon losses in response to warming. *Nature* 540, 104–108. <https://doi.org/10.1038/nature20150>
- Cui, J., Li, Z., Liu, Z., Ge, B., Fang, C., Zhou, C., Tang, B., 2014. Physical and chemical stabilization of soil organic carbon along a 500-year cultivated soil chronosequence originating from estuarine wetlands: Temporal patterns and land use effects. *Agric. Ecosyst. Environ.* 196, 10–20. <https://doi.org/10.1016/j.agee.2014.06.013>
- Cui, J., Liu, C., Li, Z., Wang, L., Chen, X., Ye, Z., Fang, C., 2012. Long-term changes in topsoil chemical properties under centuries of cultivation after reclamation of coastal wetlands in the Yangtze Estuary, China. *Soil Tillage Res.* 123, 50–60. <https://doi.org/10.1016/j.still.2012.03.009>
- Cuvilliez, A., Deloffre, J., Lafite, R., Bessineton, C., 2009. Morphological responses of an estuarine intertidal

- mudflat to constructions since 1978 to 2005: The Seine estuary (France). *Geomorphology* 104, 165–174. <https://doi.org/10.1016/j.geomorph.2008.08.010>
- Dausse, A., Garbutt, A., Norman, L., Papadimitriou, S., Jones, L.M., Robins, P.E., Thomas, D.N., 2012. Biogeochemical functioning of grazed estuarine tidal marshes along a salinity gradient. *Estuar. Coast. Shelf Sci.* 100, 83–92. <https://doi.org/10.1016/j.ecss.2011.12.037>
- Davidson, E.A., Janssens, I.A., 2006. Temperature sensitivity of soil carbon decomposition and feedbacks to climate change. *Nature* 440, 165–73. <https://doi.org/10.1038/nature04514>
- Davidson, E.A., Samanta, S., Caramori, S.S., Savage, K., 2012. The Dual Arrhenius and Michaelis-Menten kinetics model for decomposition of soil organic matter at hourly to seasonal time scales. *Glob. Chang. Biol.* 18, 371–384. <https://doi.org/10.1111/j.1365-2486.2011.02546.x>
- De Brabandere, L., Dehairs, F., Van Damme, S., Brion, N., Meire, P., Daro, N., 2002.  $\delta^{15}\text{N}$  and  $\delta^{13}\text{C}$  dynamics of suspended organic matter in freshwater and brackish waters of the Scheldt estuary. *J. Sea Res.* 48, 1–15. [https://doi.org/10.1016/S1385-1101\(02\)00132-6](https://doi.org/10.1016/S1385-1101(02)00132-6)
- De Clercq, T., Heiling, M., Dercon, G., Resch, C., Aigner, M., Mayer, L., Mao, Y., Elsen, A., Steier, P., Leifeld, J., Merckx, R., 2015. Predicting soil organic matter stability in agricultural fields through carbon and nitrogen stable isotopes. *Soil Biol. Biochem.* 88, 29–38. <https://doi.org/10.1016/j.soilbio.2015.05.011>
- De Leeuw, J., Olf, H., Bakker, J.P., 1990. Year-to-Year variation in peak above-ground biomass of six salt-marsh angiosperm communities as related to rainfall deficit and inundation frequency. *Aquat. Bot.* 36, 139–151.
- De Vos, B., Cools, N., Ilvesniemi, H., Vesterdal, L., Vanguelova, E., Carnicelli, S., 2015. Benchmark values for forest soil carbon stocks in Europe: Results from a large scale forest soil survey. *Geoderma* 251–252, 33–46. <https://doi.org/10.1016/j.geoderma.2015.03.008>
- Deng, X., Zhan, Y., Wang, F., Ma, W., Ren, Z., Chen, X., Qin, F., Long, W., Zhu, Z., Lv, X., 2016. Soil organic carbon of an intensively reclaimed region in China: Current status and carbon sequestration potential. *Sci. Total Environ.* 565, 539–546. <https://doi.org/10.1016/j.scitotenv.2016.05.042>
- Dijkema, K.S., 1987. Changes in salt-marsh area in the Netherlands Wadden Sea after 1600, in: Huiskes, A.H.L., Blom, C.W.P.M., Rozema, J. (Eds.), *Vegetation between Land and Sea*. Geobotany, Vol 11. Springer, Dordrecht. [https://doi.org/10.1007/978-94-009-4065-9\\_4](https://doi.org/10.1007/978-94-009-4065-9_4)
- Dijkstra, P., Ishizu, A., Doucett, R., Hart, S.C., Schwartz, E., Menyailo, O. V., Hungate, B.A., 2006.  $^{13}\text{C}$  and  $^{15}\text{N}$  natural abundance of the soil microbial biomass. *Soil Biol. Biochem.* 38, 3257–3266. <https://doi.org/10.1016/j.soilbio.2006.04.005>
- Diachon, A., Kellman, L., 2008. Natural abundance measurements of  $^{13}\text{C}$  indicate increased deep soil carbon mineralization after forest disturbance. *Geophys. Res. Lett.* 35, 1–5. <https://doi.org/10.1029/2008GL034795>
- Doetterl, S., Stevens, A., Six, J., Merckx, R., Oost, K. Van, Pinto, M.C., Casanova-katny, A., Muñoz, C., Boudin, M., Venegas, E.Z., Boeckx, P., 2015. Soil carbon storage controlled by interactions between geochemistry and climate. *Nat. Geosci.* 8. <https://doi.org/10.1038/NNGEO2516>
- Don, A., Schu, J., Freibauer, A., 2011. Impact of tropical land-use change on soil organic carbon stocks - a meta-analysis. *Glob. Chang. Biol.* 17, 1658–1670. <https://doi.org/10.1111/j.1365-2486.2010.02336.x>
- Donato, D.C., Kauffman, J.B., Murdiyarso, D., Kurnianto, S., Stidham, M., Kanninen, M., 2011. Mangroves among the most carbon-rich forests in the tropics. *Nat. Geosci.* 4, 293–297. <https://doi.org/10.1038/ngeo1123>
- Dotto, A.C., Dalmolin, R.S.D., ten Caten, A., Grunwald, S., 2018. A systematic study on the application of scatter-corrective and spectral-derivative preprocessing for multivariate prediction of soil organic carbon by Vis-NIR spectra. *Geoderma* 314, 262–274. <https://doi.org/10.1016/j.geoderma.2017.11.006>
- Duarte, C.M., Losada, I.J., Hendriks, I.E., Mazarrasa, I., Marbà, N., 2013. The role of coastal plant communities for climate change mitigation and adaptation. *Nat. Clim. Chang.* 3, 961–968. <https://doi.org/10.1038/nclimate1970>
- Duarte, C.M., Middelburg, J.J., Caraco, N., 2005. Major role of marine vegetation on the oceanic carbon cycle. *Biogeosciences* 2, 1–8. <https://doi.org/10.5194/bgd-1-659-2004>

## References

---

- Dümig, A., Schad, P., Rumpel, C., Dignac, M.F., Kögel-Knabner, I., 2008. Araucaria forest expansion on grassland in the southern Brazilian highlands as revealed by  $^{14}\text{C}$  and  $\delta^{13}\text{C}$  studies. *Geoderma* 145, 143–157. <https://doi.org/10.1016/j.geoderma.2007.06.005>
- Dungait, J.A.J., Hopkins, D.W., Gregory, A.S., Whitmore, A.P., 2012. Soil organic matter turnover is governed by accessibility not recalcitrance. *Glob. Chang. Biol.* 18, 1781–1796. <https://doi.org/10.1111/j.1365-2486.2012.02665.x>
- Dwivedi, D., Riley, W.J., Torn, M.S., Spycher, N., Maggi, F., Tang, J.Y., 2017. Mineral properties, microbes, transport, and plant-input profiles control vertical distribution and age of soil carbon stocks. *Soil Biol. Biochem.* 107, 244–259. <https://doi.org/10.1016/j.soilbio.2016.12.019>
- Eertman, R.H.M., Kornman, B.A., Stikvoort, E., Verbeek, H., 2002. Restoration of the sieperda tidal marsh in the Scheldt estuary, The Netherlands. *Restor. Ecol.* 10, 438–449. <https://doi.org/10.1046/j.1526-100X.2002.01034.x>
- Ehleringer, J.R., Buchmann, N., Flanagan, L.B., 2000. Carbon isotope ratios in belowground carbon cycle processes. *Ecol. Appl.* 10, 412–422. [https://doi.org/10.1890/1051-0761\(2000\)010\[0412:CIRIBC\]2.0.CO;2](https://doi.org/10.1890/1051-0761(2000)010[0412:CIRIBC]2.0.CO;2)
- Ellis, S., Atherton, J.K., 2003. Properties and development of soils on reclaimed alluvial sediments of the Humber estuary, eastern England. *CATENA* 52, 129–147. [https://doi.org/10.1016/S0341-8162\(02\)00179-0](https://doi.org/10.1016/S0341-8162(02)00179-0)
- Elschot, K., Bakker, J.P., Temmerman, S., Van De Koppel, J., Bouma, T.J., 2015. Ecosystem engineering by large grazers enhances carbon stocks in a tidal salt marsh. *Mar. Ecol. Prog. Ser.* 537, 9–21. <https://doi.org/10.3354/meps11447>
- Elzein, A., Balesdent, J., 1995. Mechanistic Simulation of Vertical Distribution of Carbon Concentrations and Residence Times in Soils. *Soil Sci. Soc. Am. J.* 59, 1328. <https://doi.org/10.2136/sssaj1995.03615995005900050019x>
- Ewers Lewis, C.J., Carnell, P.E., Sanderman, J., Baldock, J.A., Macreadie, P.I., 2017. Variability and Vulnerability of Coastal “Blue Carbon” Stocks: A Case Study from Southeast Australia. *Ecosystems* 1–17. <https://doi.org/10.1007/s10021-017-0150-z>
- Fagherazzi, S., Kirwan, M.L., Mudd, S.M., Guntenspergen, G.R., Temmerman, S., Rybczyk, J.M., Reyes, E., Craft, C., Clough, J., 2012. Numerical models of salt marsh evolution: Ecological, geomorphic, and climatic factors. *Rev. Geophys.* 50, 1–28. <https://doi.org/10.1029/2011RG000359.1>
- Falloon, P., Jones, C.D., Ades, M., Paul, K., 2011. Direct soil moisture controls of future global soil carbon changes: An important source of uncertainty. *Global Biogeochem. Cycles* 25, 1–14. <https://doi.org/10.1029/2010GB003938> <<http://dx.doi.org/10.1029/2010GB003938>>
- Fan, J., McConkey, B., Wang, H., Janzen, H., 2016. Root distribution by depth for temperate agricultural crops. *F. Crop. Res.* 189, 68–74. <https://doi.org/10.1016/j.fcr.2016.02.013>
- Farquhar, G., O’Leary, M., Berry, J., 1982. On the Relationship Between Carbon Isotope Discrimination and the Intercellular Carbon Dioxide Concentration in Leaves. *Aust. J. Plant Physiol.* 9, 121. <https://doi.org/10.1071/PP9820121>
- Fernández, S., Santín, C., Marquínez, J., Álvarez, M.A., 2010. Saltmarsh soil evolution after land reclamation in Atlantic estuaries (Bay of Biscay, North coast of Spain). *Geomorphology* 114, 497–507. <https://doi.org/10.1016/j.geomorph.2009.08.014>
- Fontaine, S., Barot, S., Barré, P., Bdioui, N., Mary, B., Rumpel, C., 2007. Stability of organic carbon in deep soil layers controlled by fresh carbon supply. *Nature* 450, 277–280. <https://doi.org/10.1038/nature06275>
- Fontaine, S., Mariotti, A., Abbadie, L., 2003. The priming effect of organic matter: a question of microbial competition? *Soil Biol. Biochem.* 35, 837–843. [https://doi.org/10.1016/S0038-0717\(03\)00123-8](https://doi.org/10.1016/S0038-0717(03)00123-8)
- Friedlingstein, P., Cox, P., Betts, R., Bopp, L., von Bloh, W., Brovkin, V., Cadule, P., Doney, S., Eby, M., Fung, I., Bala, G., John, J., Jones, C., Joos, F., Kato, T., Kawamiya, M., Knorr, W., Lindsay, K., Matthews, H.D., Raddatz, T., Rayner, P., Reick, C., Roeckner, E., Schnitzler, K.-G., Schnur, R., Strassmann, K., Weaver, A.J., Yoshikawa, C., Zeng, N., 2006. Climate–Carbon Cycle Feedback Analysis: Results from the C 4 MIP Model Intercomparison. *J. Clim.* 19, 3337–3353. <https://doi.org/10.1175/JCLI3800.1>

- Fu, Q., Ding, N., Liu, C., Lin, Y., Guo, B., 2014. Soil development under different cropping systems in a reclaimed coastal soil chronosequence. *Geoderma* 230–231, 50–57. <https://doi.org/10.1016/j.geoderma.2014.03.026>
- Fuchs, R., Schulp, C.J.E., Hengeveld, G.M., Verburg, P.H., Clevers, J.G.P.W., Schelhaas, M.-J., Herold, M., 2016. Assessing the influence of historic net and gross land changes on the carbon fluxes of Europe. *Glob. Chang. Biol.* 22, 2526–2539. <https://doi.org/10.1111/gcb.13191>
- Garten, C.T.J., 2006. Relationships among forest soil C isotopic composition, partitioning, and turnover times. *Can. J. For. Res.* 36, 2157–2167. <https://doi.org/10.1139/x06-115>
- Gaudinski, J.B., Trumbore, S.E., Davidson, E.A., Zheng, S., 2000. Soil carbon cycling in a temperate forest: radiocarbon-based estimates of residence times, sequestration rates and partitioning of fluxes. *Biogeochemistry* 51, 33–69. <https://doi.org/10.1023/A:1006301010014>
- Gerino, M., Stora, G., Durbec, J.-P., 1994. Quantitative estimation of bioturbative and bioadvective sediment mixing : In situ experimental approach. *Oceanol. Acta* 17, 547–554.
- Ghashghaie, J., Badeck, F.-W., Lanigan, G., Nogués, S., Tcherkez, G., Deléens, E., Cornic, G., Griffiths, H., 2003. Carbon isotope fractionation during dark respiration and photorespiration in C3 plants. *Phytochem. Rev.* 2, 145–161. <https://doi.org/10.1023/B:PHYT.0000004326.00711.ca>
- Ghashghaie, J., Badeck, F.W., 2014. Opposite carbon isotope discrimination during dark respiration in leaves versus roots—a review. *New Phytol.* 201, 751–769.
- Gill, R.A., Jackson, R.B., 2000. Global patterns of root turnover for terrestrial ecosystems. *New Phytol.* 147, 13–31.
- Goeldner, L., 1999. The German Wadden Sea coast: reclamation and environmental protection. *J. Coast. Conserv.* 5, 23–30. <https://doi.org/10.1007/BF02802736>
- Govers, G., Merckx, R., Van Oost, K., van Wesemael, B., 2013. Managing Soil Organic Carbon for Global Benefits: A STAP Technical Report. Global Environmental Facility, Washington, D.C.
- Gray, A.J., Benham, P.E.M. (Eds.), 1990. *Spartina anglica - a research review*, Institute of Terrestrial Ecology. HMSO, London.
- Gregory Hood, W., 2004. Indirect environmental effects of dikes on estuarine tidal channels: Thinking outside of the dike for habitat restoration and monitoring. *Estuaries* 27, 273–282. <https://doi.org/10.1007/BF02803384>
- Groenendijk, A.M., 1984. Primary production of 4 dominant salt-marsh angiosperms in the southwestern Netherlands. *Vegetatio* 57, 143–152.
- Groenendijk, A.M., Vink-Lievaart, M.A., 1987. Primary production and biomass on a Dutch salt marsh: emphasis on the below-ground component. *Vegetatio* 70, 21–17.
- Guo, L.B., Gifford, R.M., 2002. Soil carbon stocks and land use change: a meta analysis. *Glob. Chang. Biol.* 8, 345–360. <https://doi.org/10.1046/j.1354-1013.2002.00486.x>
- Gypens, N., Delhez, E., Vanhoute-Brunier, A., Burton, S., Thieu, V., Passy, P., Liu, Y., Callens, J., Rousseau, V., Lancelot, C., 2013. Modelling phytoplankton succession and nutrient transfer along the Scheldt estuary (Belgium, The Netherlands). *J. Mar. Syst.* 128, 89–105. <https://doi.org/10.1016/j.jmarsys.2012.10.006>
- Halpern, B.S., Walbridge, S., Selkoe, K.A., Kappel, C. V., Micheli, F., D'Agrosa, C., Bruno, J.F., Casey, K.S., Ebert, C., Fox, H.E., Fujita, R., Heinemann, D., Lenihan, H.S., Madin, E.M.P., Perry, M.T., Selig, E.R., Spalding, M., Steneck, R., Watson, R., 2008. A Global Map of Human Impact on Marine Ecosystems. *Science* (80-. ). 319, 948–952. <https://doi.org/10.1126/science.1149345>
- Hansen, K., Butzeck, C., Eschenbach, A., Gröngroft, A., Jensen, K., Pfeiffer, E.M., 2016. Factors influencing the organic carbon pools in tidal marsh soils of the Elbe estuary (Germany). *J. Soils Sediments* 17, 47–60. <https://doi.org/10.1007/s11368-016-1500-8>
- Harrison, R.B., Footen, P.W., Strahm, B.D., 2011. Deep Soil Horizons : Contribution and Importance to Soil Carbon Pools and in Assessing Whole-Ecosystem Response to Management and Global Change. *For. Sci.* 57, 67–76.

## References

---

- Hartnett, H.E., Keil, R.G., Hedges, J.I., Devol, A.H., 1998. Influence of oxygen exposure time on organic carbon preservation in continental margin sediments. *Nature* 391, 572–574.
- Hatton, R.S., Delaune, R.D., Patrick, W.H.J., 1983. Sedimentation, accretion, and subsidence in marshes of Barataria Basin, Louisiana. *Limnol. Oceanogr.* 28, 494–502. <https://doi.org/10.4319/lo.1983.28.3.0494>
- Hayes, M.A., Jesse, A., Hawke, B., Baldock, J., Tabet, B., Lockington, D., Lovelock, C.E., 2017. Dynamics of sediment carbon stocks across intertidal wetland habitats of Moreton Bay, Australia. *Glob. Chang. Biol.* 0, 1–13. <https://doi.org/10.1111/gcb.13722>
- He, Q., Bertness, M.D., Bruno, J.F., Li, B., Chen, G., Coverdale, T.C., Altieri, A.H., Bai, J., Sun, T., Pennings, S.C., Liu, J., Ehrlich, P.R., Cui, B., 2015. Economic development and coastal ecosystem change in China. *Sci. Rep.* 4, 1–9. <https://doi.org/10.1038/srep05995>
- He, Y., Trumbore, S.E., Torn, M.S., Harden, J.W., Vaughn, L.J.S., Allison, S.D., Randerson, J.T., 2016. Radiocarbon constraints imply reduced carbon uptake by soils during the 21st century. *Science* (80-. ). 353, 1419–1424. <https://doi.org/10.1126/science.aad4273>
- Healy, M.G., Hickey, K.R., 2002. Historic land reclamation in the intertidal wetlands of the Shannon estuary , western Ireland. *J. Coast. Res.* 365–373.
- Heimann, M., Reichstein, M., 2008. Terrestrial ecosystem carbon dynamics and climate feedbacks. *Nature* 451, 289–292. <https://doi.org/10.1038/nature06591>
- Hellings, L., Dehairs, F., Tackx, M., Keppens, E., Baeyens, W., 1999. Origin and fate of organic carbon in the freshwater part of the Scheldt Estuary as traced by stable carbon isotope composition. *Biogeochemistry* 47, 167–186.
- Hemminga, M.A., Buth, G.J.C., 1991. Decomposition in Salt Marsh Ecosystems of the S.W. Netherlands: The Effects of Biotic and Abiotic Factors. *Vegetatio* 92, 73–83.
- Hemminga, M.A., De Leeuw, J., De Munck, W., Koutstaal, B.P., 1991. Decomposition in estuarine salt marshes: the effect of soil salinity and soil water content. *Vegetatio* 94, 25–33.
- Hobley, E., Baldock, J., Hua, Q., Wilson, B., 2017. Land-use contrasts reveal instability of subsoil organic carbon. *Glob. Chang. Biol.* 23, 955–965. <https://doi.org/10.1111/gcb.13379>
- Hoeksema, R.J., 2007. Three stages in the history of land reclamation in the Netherlands. *Irrig. Drain.* 56, S113–S126. <https://doi.org/10.1002/ird.340>
- Hood, W.G., 2004. Indirect environmental effects of dikes on estuarine tidal channels: Thinking outside of the dike for habitat restoration and monitoring. *Estuaries* 27, 273–282. <https://doi.org/10.1007/BF02803384>
- Hopkinson, C.S., Cai, W.J., Hu, X., 2012. Carbon sequestration in wetland dominated coastal systems—a global sink of rapidly diminishing magnitude. *Curr. Opin. Environ. Sustain.* 4, 186–194. <https://doi.org/10.1016/j.cosust.2012.03.005>
- Horváth, B., Opara-Nadi, O., Beese, F., 2005. A simple method for measuring the carbonate content of soils. *Soil Sci. Soc. Am. J.* 69, 1066. <https://doi.org/10.2136/sssaj2004.0010>
- Houghton, R.A., House, J.I., Pongratz, J., Van Der Werf, G.R., Defries, R.S., Hansen, M.C., Le Quéré, C., Ramankutty, N., 2012. Carbon emissions from land use and land-cover change. *Biogeosciences* 9, 5125–5142. <https://doi.org/10.5194/bg-9-5125-2012>
- Hua, Q., Barbetti, M., Rakowski, A.Z., 2013. Atmospheric radiocarbon for the period 1950–2010. *Radiocarbon* 55, 2059–2072. [https://doi.org/10.2458/azu\\_js\\_rc.v55i2.16177](https://doi.org/10.2458/azu_js_rc.v55i2.16177)
- Huang, Y., Sun, W., Zhang, G., W., Yu, Y., Su, Y., Song, C., 2010. Marshland conversion to cropland in northeast China from 1950 to 2000 reduced the greenhouse effect. *Glob. Chang. Biol.* 16, 680–695. <https://doi.org/10.1111/j.1365-2486.2009.01976.x>
- IAEA, 2001. *Environmental Isotopes in the Hydrological Cycle: Principles and Applications*, vol. 1 315. <https://doi.org/10.1007/978-3-319-25643-6>
- Igne, B., Reeves, J.B., McCarty, G., Hively, W.D., Lund, E., Hurburgh, C.R., 2010. Evaluation of spectral pretreatments, partial least squares, least squares support vector machines and locally weighted

- regression for quantitative spectroscopic analysis of soils. *J. Near Infrared Spectrosc.* 18, 167–176. <https://doi.org/10.1255/jnirs.883>
- lost, S., Landgraf, D., Makeschin, F., 2007. Chemical soil properties of reclaimed marsh soil from Zhejiang Province P.R. China. *Geoderma* 142, 245–250. <https://doi.org/10.1016/j.geoderma.2007.08.001>
- IPCC, 2013. IPCC, 2013: Climate Change 2013: The Physical Science Basis. Contributions of Working Group I of the Fifth Assessment Report of the Intergovernmental Panel on Climate Change. Cambridge University Press, Carmbridge, United Kingdom and New York, NY, USA.
- Janzen, H.H., 2006. The soil carbon dilemma: Shall we hoard it or use it? *Soil Biol. Biochem.* 38, 419–424. <https://doi.org/10.1016/j.soilbio.2005.10.008>
- Jenkinson, D.S., Coleman, K., 2008. The turnover of organic carbon in subsoils. Part 2. Modelling carbon turnover. *Eur. J. Soil Sci.* 59, 400–413. <https://doi.org/10.1111/j.1365-2389.2008.01026.x>
- Jeuken, C., Tánczos, I., Wang, Z.B., 2003. Jeuken, C. Evaluatie van het beleid voor vaargeulonderzoek en zandwinning sinds de tweede vaargeulverdieping op basis van veldwaarnemingen en het verbeterde Cellenconcept Westerschelde. WL | Delft Hydraulics, Rapportnr. Z346. Delft, The Netherlands (in Dutch).
- Jia, X., Chen, S., Yang, Y., Zhou, L., Yu, W., Shi, Z., 2017. Organic carbon prediction in soil cores using VNIR and MIR techniques in an alpine landscape. *Sci. Rep.* 7, 1–9. <https://doi.org/10.1038/s41598-017-02061-z>
- Jin, Y., Yang, W., Sun, T., Yang, Z., Li, M., 2016. Effects of seashore reclamation activities on the health of wetland ecosystems: A case study in the Yellow River Delta, China. *Ocean Coast. Manag.* 123, 44–52. <https://doi.org/10.1016/j.ocecoaman.2016.01.013>
- Jobbágy, E.G., Jackson, R.B., 2000. The vertical distribution of soil organic carbon and its relation to climate and vegetation. *Ecol. Appl.* 10, 423–436. [https://doi.org/10.1890/1051-0761\(2000\)010\[0423:TVDOSO\]2.0.CO;2](https://doi.org/10.1890/1051-0761(2000)010[0423:TVDOSO]2.0.CO;2)
- Johnson, M.O., Mudd, S.M., Pillans, B., Spooner, N.A., Keith Fifield, L., Kirkby, M.J., Gloor, M., 2014. Quantifying the rate and depth dependence of bioturbation based on optically-stimulated luminescence (OSL) dates and meteoric  $^{10}\text{Be}$ . *Earth Surf. Process. Landforms* 39, 1188–1196. <https://doi.org/10.1002/esp.3520>
- Jones, J.A., Cherry, J.A., Mckee, K.L., 2016. Species and tissue type regulate long-term decomposition of brackish marsh plants grown under elevated  $\text{CO}_2$  conditions. *Estuar. Coast. Shelf Sci.* 169, 38–45. <https://doi.org/10.1016/j.ecss.2015.11.033>
- Jongepier, I., Wang, C., Missiaen, T., Soens, T., Temmerman, S., 2015. Intertidal landscape response time to dike breaching and stepwise re-embankment: A combined historical and geomorphological study. *Geomorphology* 236, 64–78. <https://doi.org/10.1016/j.geomorph.2015.02.012>
- Juston, J., Andrén, O., Kätterer, T., Jansson, P.-E., 2010. Uncertainty analyses for calibrating a soil carbon balance model to agricultural field trial data in Sweden and Kenya. *Ecol. Modell.* 221, 1880–1888. <https://doi.org/10.1016/j.ecolmodel.2010.04.019>
- Kaiser, K., Guggenberger, G., 2003. Mineral surfaces and soil organic matter. *Eur. J. Soil Sci.* 54, 219–236. <https://doi.org/10.1046/j.1365-2389.2003.00544.x>
- Kaiser, K., Guggenberger, G., Zech, W., 2001. Isotopic fractionation of dissolved organic carbon in shallow forest soils as affected by sorption. *Eur. J. Soil Sci.* 52, 585–597. <https://doi.org/10.1046/j.1365-2389.2001.00407.x>
- Kaiser, K., Kalbitz, K., 2012. Cycling downwards – dissolved organic matter in soils. *Soil Biol. Biochem.* 52, 29–32. <https://doi.org/10.1016/j.soilbio.2012.04.002>
- Kang, H., Gao, H., Yu, W., 2017. Evaluation of spectral pretreatments, spectral range, and regression methods for quantitative spectroscopic analysis of soil organic carbon composition. *Spectrosc. Lett.* 50, 143–149. <https://doi.org/10.1080/00387010.2017.1297956>
- Kaplan, J.O., 2015. Climate or humans? *Nat. Geosci.* 8, 335–336. <https://doi.org/10.1038/ngeo2432>
- Keeling, C.D., 1979. The Suess effect:  $^{13}\text{C}$ – $^{14}\text{C}$  interrelations. *Environ. Int.* 2, 229–300. [https://doi.org/10.1016/0160-4120\(79\)90005-9](https://doi.org/10.1016/0160-4120(79)90005-9)

## References

---

- Keeling, R.F., Graven, H.D., Welp, L.R., Resplandy, L., Bi, J., Piper, S.C., Sun, Y., Bollenbacher, A., Meijer, H.A.J., 2017. Atmospheric evidence for a global secular increase in carbon isotopic discrimination of land photosynthesis. *Proc. Natl. Acad. Sci.* 114, 10361–10366. <https://doi.org/10.1073/pnas.1619240114>
- Keil, R.G., Montluçon, D.B., Prahl, F.G., Hedges, J.I., 1994. Sorptive preservation of labile organic matter in marine sediments. *Nature* 370.
- Keiluweit, M., Bougoure, J.J., Nico, P.S., Pett-Ridge, J., Weber, P.K., Kleber, M., 2015. Mineral protection of soil carbon counteracted by root exudates. *Nat. Clim. Chang.* 5, 588–595. <https://doi.org/10.1038/nclimate2580>
- Keller, K.M., Lienert, S., Bozbiyik, A., Stocker, T.F., Churakova (Sidorova), O. V., Frank, D.C., Klesse, S., Koven, C.D., Leuenberger, M., Riley, W.J., Saurer, M., Siegwolf, R., Weigt, R.B., Joos, F., 2017. 20th century changes in carbon isotopes and water-use efficiency: tree-ring-based evaluation of the CLM4.5 and LPX-Bern models. *Biogeosciences* 14, 2641–2673. <https://doi.org/10.5194/bg-14-2641-2017>
- Kelleway, J.J., Saintilan, N., Macreadie, P.I., Ralph, P.J., 2016. Sedimentary Factors are Key Predictors of Carbon Storage in SE Australian Saltmarshes. *Ecosystems* 19, 865–880. <https://doi.org/10.1007/s10021-016-9972-3>
- Kennard, R.W., Stone, L.A., 1969. Computer Aided Design of Experiments. *Technometrics* 11, 137–148. <https://doi.org/10.2307/1266770>
- Kiem, R., Kögel-Knabner, I., 2003. Contribution of lignin and polysaccharides to the refractory carbon pool in C-depleted arable soils. *Soil Biol. Biochem.* 35, 101–118. [https://doi.org/10.1016/S0038-0717\(02\)00242-0](https://doi.org/10.1016/S0038-0717(02)00242-0)
- Kindler, R., Miltner, A., Richnow, H., Kästner, M., 2006. Fate of gram-negative bacterial biomass in soil—mineralization and contribution to SOM. *Soil Biol. Biochem.* 38, 2860–2870. <https://doi.org/10.1016/j.soilbio.2006.04.047>
- Kirwan, M.L., Blum, L.K., 2011. Enhanced decomposition offsets enhanced productivity and soil carbon accumulation in coastal wetlands responding to climate change. *Biogeosciences* 8, 987–993. <https://doi.org/10.5194/bg-8-987-2011>
- Kirwan, M.L., Guntenspergen, G.R., 2012. Feedbacks between inundation, root production, and shoot growth in a rapidly submerging brackish marsh. *J. Ecol.* 100, 764–770. <https://doi.org/10.1111/j.1365-2745.2012.01957.x>
- Kirwan, M.L., Guntenspergen, G.R., Alpaos, A., Morris, J.T., Mudd, S.M., Temmerman, S., 2010. Limits on the adaptability of coastal marshes to rising sea level. *Geophys. Res. Lett.* 37, 1–5. <https://doi.org/10.1029/2010GL045489>
- Kirwan, M.L., Megonigal, J.P., 2013. Tidal wetland stability in the face of human impacts and sea-level rise. *Nature* 504, 53–60. <https://doi.org/10.1038/nature12856>
- Kirwan, M.L., Mudd, S.M., 2012. Response of salt-marsh carbon accumulation to climate change. *Nature* 489, 550–553. <https://doi.org/10.1038/nature11440>
- Kirwan, M.L., Temmerman, S., Skeehan, E.E., Guntenspergen, G.R., Faghe, S., 2016. Overestimation of marsh vulnerability to sea level rise. *Nat. Clim. Chang.* 6, 253–260. <https://doi.org/10.1038/nclimate2909>
- Klap, V.A., Boon, J.J., Hemminga, M.A., van Soelen, J., 1996. Assessment of the molecular composition of particulate organic matter exchanged between the Saeftinghe salt marsh (southwestern Netherlands) and the adjacent water system. *Mar. Chem.* 54, 221–243. [https://doi.org/10.1016/0304-4203\(96\)00043-6](https://doi.org/10.1016/0304-4203(96)00043-6)
- Kleber, M., Eusterhues, K., Keiluweit, M., Mikutta, C., Mikutta, R., Nico, P.S., 2015. Mineral–Organic Associations: Formation, Properties, and Relevance in Soil Environments, in: *Advances in Agronomy*. Elsevier Ltd, pp. 1–140. <https://doi.org/10.1016/bs.agron.2014.10.005>
- Kleber, M., Nico, P.S., Plante, A., Filley, T., Kramer, M., Swanston, C., Sollins, P., 2011. Old and stable soil organic matter is not necessarily chemically recalcitrant: implications for modeling concepts and temperature sensitivity. *Glob. Chang. Biol.* 17, 1097–1107. <https://doi.org/10.1111/j.1365-2486.2010.02278.x>
- Kögel-Knabner, I., Guggenberger, G., Kleber, M., Kandeler, E., Kalbitz, K., Scheu, S., Eusterhues, K., Leinweber, P., 2008. Organo-mineral associations in temperate soils: Integrating biology, mineralogy, and organic

- matter chemistry. *J. Plant Nutr. Soil Sci.* 171, 61–82. <https://doi.org/10.1002/jpln.200700048>
- Kohl, L., Laganière, J., Edwards, K.A., Billings, S.A., Morrill, P.L., Van Biesen, G., Ziegler, S.E., 2015. Distinct fungal and bacterial  $\delta^{13}\text{C}$  signatures as potential drivers of increasing  $\delta^{13}\text{C}$  of soil organic matter with depth. *Biogeochemistry* 124, 13–26. <https://doi.org/10.1007/s10533-015-0107-2>
- Kohn, M.J., 2010. Carbon isotope compositions of terrestrial C3 plants as indicators of (paleo)ecology and (paleo)climate. *Proc. Natl. Acad. Sci. U. S. A.* 107, 19691–19695. <https://doi.org/10.1073/pnas.1004933107>
- Kopp, R.F., Abrahamson, L.P., White, E.H., Volk, T.A., Nowak, C.A., Fillhart, R.C., 2001. Willow biomass production during ten successive annual harvests. *Biomass and Bioenergy* 20, 1–7. [https://doi.org/10.1016/S0961-9534\(00\)00063-5](https://doi.org/10.1016/S0961-9534(00)00063-5)
- Kothawala, D.N., Moore, T.R., Hendershot, W.H., 2009. Soil Properties Controlling the Adsorption of Dissolved Organic Carbon to Mineral Soils. *Soil Sci. Soc. Am. J.* 73, 1831–1842. <https://doi.org/10.2136/sssaj2008.0254>
- Kothawala, D.N., Moore, T.R., Hendershot, W.H., 2008. Adsorption of dissolved organic carbon to mineral soils: A comparison of four isotherm approaches. *Geoderma* 148, 43–50. <https://doi.org/10.1016/j.geoderma.2008.09.004>
- Koven, C.D., Riley, W.J., Subin, Z.M., Tang, J.Y., Torn, M.S., Collins, W.D., Bonan, G.B., Lawrence, D.M., Swenson, S.C., 2013. The effect of vertically resolved soil biogeochemistry and alternate soil C and N models on C dynamics of CLM4. *Biogeosciences* 10, 7109–7131. <https://doi.org/10.5194/bg-10-7109-2013>
- Krull, E.S., Skjemstad, J.O., Burrows, W.H., Bray, S.G., Wynn, J.G., Bol, R., Spouncer, L., Harms, B., 2005. Recent vegetation changes in central Queensland, Australia: Evidence from  $\delta^{13}\text{C}$  and  $^{14}\text{C}$  analyses of soil organic matter. *Geoderma* 126, 241–259. <https://doi.org/10.1016/j.geoderma.2004.09.012>
- Kuang, B., Mouazen, A.M., 2011. Calibration of visible and near infrared spectroscopy for soil analysis at the field scale on three European farms. *Eur. J. Soil Sci.* 62, 629–636. <https://doi.org/10.1111/j.1365-2389.2011.01358.x>
- Ladyman, S.J., Harkness, D.D., 1980. Carbon isotope measurements as an index of soil development. *Radiocarbon* 22, 885–891.
- Lal, R., 2018. Digging deeper: A holistic perspective of factors affecting soil organic carbon sequestration in agroecosystems. *Glob. Chang. Biol. O.* <https://doi.org/10.1111/gcb.14054>
- Lawrence, C.R., Neff, J.C., Schimel, J.P., 2009. Does adding microbial mechanisms of decomposition improve soil organic matter models? A comparison of four models using data from a pulsed rewetting experiment. *Soil Biol. Biochem.* 41, 1923–1934. <https://doi.org/10.1016/j.soilbio.2009.06.016>
- Le Quéré, C., Andrew, R.M., Friedlingstein, P., Sitch, S., Pongratz, J., Manning, A.C., Korsbakken, J.I., Peters, G.P., Canadell, J.G., Jackson, R.B., Boden, T.A., Tans, P.P., Andrews, O.D., Arora, V.K., Bakker, D.C.E., Barbero, L., Becker, M., Betts, R.A., Bopp, L., Chevallier, F., Chini, L.P., Ciais, P., Cosca, C.E., Cross, J., Currie, K., Gasser, T., Harris, I., Hauck, J., Haverd, V., Houghton, R.A., Hunt, C.W., Hurtt, G., Ilyina, T., Jain, A.K., Kato, E., Kautz, M., Keeling, R.F., Klein Goldewijk, K., Körtzinger, A., Landschützer, P., Lefèvre, N., Lenton, A., Lienert, S., Lima, I., Lombardozi, D., Metzl, N., Millero, F., Monteiro, P.M.S., Munro, D.R., Nabel, J.E.M.S., Nakaoka, S., Nojiri, Y., Padin, X.A., Pregon, A., Pfeil, B., Pierrot, D., Poulter, B., Rehder, G., Reimer, J., Rödenbeck, C., Schwinger, J., Séférian, R., Skjelvan, I., Stocker, B.D., Tian, H., Tilbrook, B., Tubiello, F.N., van der Laan-Luijkx, I.T., van der Werf, G.R., van Heuven, S., Viovy, N., Vuichard, N., Walker, A.P., Watson, A.J., Wiltshire, A.J., Zaehle, S., Zhu, D., 2018. Global Carbon Budget 2017. *Earth Syst. Sci. Data* 10, 405–448. <https://doi.org/10.5194/essd-10-405-2018>
- Lehmann, J., Kleber, M., 2015. The contentious nature of soil organic matter. *Nature* 528, 60–68. <https://doi.org/10.1038/nature16069>
- Lerch, T.Z., Nunan, N., Dignac, M.-F., Chenu, C., Mariotti, A., 2011. Variations in microbial isotopic fractionation during soil organic matter decomposition. *Biogeochemistry* 106, 5–21. <https://doi.org/10.1007/s10533-010-9432-7>
- Letten, S., Orshoven, J., Wesemael, B., Muys, B., 2004. Soil organic and inorganic carbon contents of landscape

## References

---

- units in Belgium derived using data from 1950 to 1970. *Soil Use Manag.* 20, 40–47. <https://doi.org/10.1111/j.1475-2743.2004.tb00335.x>
- Li, J., Pu, L., Zhu, M., Zhang, J., Li, P., Dai, X., Xu, Y., Liu, L., 2014. Evolution of soil properties following reclamation in coastal areas: A review. *Geoderma* 226–227, 130–139. <https://doi.org/10.1016/j.geoderma.2014.02.003>
- Li, M., Peng, C., Wang, M., Yang, Y., Zhang, K., Li, P., Yang, Y., Ni, J., Zhu, Q., 2017. Spatial patterns of leaf  $\delta^{13}C$  and its relationship with plant functional groups and environmental factors in China. *J. Geophys. Res. Biogeosciences* 122, 1564–1575. <https://doi.org/10.1002/2016JG003529>
- Liang, C., Balsler, T.C., 2011. Microbial production of recalcitrant organic matter in global soils: implications for productivity and climate policy. *Nat. Rev. Microbiol.* 9, 75–75. <https://doi.org/10.1038/nrmicro2386-c1>
- Liang, C., Balsler, T.C., 2008. Preferential sequestration of microbial carbon in subsoils of a glacial-landscape toposequence, Dane County, WI, USA. *Geoderma* 148, 113–119. <https://doi.org/10.1016/j.geoderma.2008.09.012>
- Liang, C., Schimel, J.P., Jastrow, J.D., 2017. The importance of anabolism in microbial control over soil carbon storage. *Nat. Microbiol.* 2, 1–6. <https://doi.org/10.1038/nmicrobiol.2017.105>
- Lobsey, C.R., Viscarra Rossel, R.A., 2016. Sensing of soil bulk density for more accurate carbon accounting. *Eur. J. Soil Sci.* 67, 504–513. <https://doi.org/10.1111/ejss.12355>
- Lobsey, C.R., Viscarra Rossel, R.A., Roudier, P., Hedley, C.B., 2017. RS-LOCAL data-mines information from spectral libraries to improve local calibrations. *Eur. J. Soil Sci.* 68, 840–852. <https://doi.org/10.1111/ejss.12490>
- Loomis, M.J., Craft, C.B., 2010. Carbon Sequestration and Nutrient (Nitrogen, Phosphorus) Accumulation in River-Dominated Tidal Marshes, Georgia, USA. *Soil Sci. Soc. Am. J.* 74, 1028–1036. <https://doi.org/10.2136/sssaj2009.0171>
- Lotze, H.K., 2006. Depletion, Degradation, and Recovery Potential of Estuaries and Coastal Seas. *Science* (80-. ). 312, 1806–1809. <https://doi.org/10.1126/science.1128035>
- Luo, Y., Ahlström, A., Allison, S.D., Batjes, N.H., Brovkin, V., Carvalhais, N., Chappell, A., Ciais, P., Davidson, E.A., Finzi, A., Georgiou, K., Guenet, B., Hararuk, O., Harden, J.W., He, Y., Hopkins, F., Jiang, L., Koven, C., Jackson, R.B., Jones, C.D., Lara, M.J., Liang, J., McGuire, A.D., Parton, W., Peng, C., Randerson, J.T., Salazar, A., Sierra, C.A., Smith, M.J., Tian, H., Todd-brown, K.E.O., Torn, M., Groenigen, K.J., Wang, Y.P., West, T.O., Wei, Y., Wieder, W.R., Xia, J., Xu, X., Xu, X., Zhou, T., 2015. Towards more realistic projections of soil carbon dynamics by Earth system models. *Global Biogeochem. Cycles* 30, 40–56. <https://doi.org/10.1002/2015GB005239>
- Luo, Z., Baldock, J., Wang, E., 2017. Modelling the dynamic physical protection of soil organic carbon: Insights into carbon predictions and explanation of the priming effect. *Glob. Chang. Biol.* 23, 5273–5283. <https://doi.org/10.1111/gcb.13793>
- Ma, Z., Melville, D.S., Liu, J., Chen, Y., Yang, H., Ren, W., Zhang, Z., Piersma, T., Li, B., 2014. Rethinking China's new great wall. *Science* (80-. ). 346, 912–914. <https://doi.org/10.1126/science.1257258>
- Macreadie, P.I., Ollivier, Q.R., Kelleway, J.J., Serrano, O., Carnell, P.E., Ewers Lewis, C.J., Atwood, T.B., Sanderman, J., Baldock, J., Connolly, R.M., Duarte, C.M., Lavery, P.S., Steven, A., Lovelock, C.E., 2017. Carbon sequestration by Australian tidal marshes. *Sci. Rep.* 7, 1–10. <https://doi.org/10.1038/srep44071>
- Manzoni, S., Porporato, A., 2009. Soil carbon and nitrogen mineralization: Theory and models across scales. *Soil Biol. Biochem.* 41, 1355–1379. <https://doi.org/10.1016/j.soilbio.2009.02.031>
- Mariotti, A., Lancelot, C., Billen, G., 1984. Natural isotopic composition as a tracer of origin for suspended matter in the Scheldt estuary. *Geochim. Cosmochim. Acta* 48, 549–555.
- Martin, A., Mariotti, A., Balesdent, J., Lavelle, P., Vuattoux, R., 1990. Estimate of organic matter turnover rate in a savanna soil by  $^{13}C$  natural abundance measurements. *Soil Biol. Biochem.* 22, 517–523. [https://doi.org/10.1016/0038-0717\(90\)90188-6](https://doi.org/10.1016/0038-0717(90)90188-6)
- Martinelli, L. a., Pessenda, L.C.R., Espinoza, E., Camargo, P.B., Telles, E.C., Cerri, C.C., Victoria, R.L., Aravena, R.,

- Richey, J., Trumbore, S., 1996. Carbon-13 variation with depth in soils of Brazil and climate change during the Quaternary. *Oecologia* 106, 376–381. <https://doi.org/10.1007/BF00334565>
- Mayer, L.M., 1994. Surface area control of organic carbon accumulation in continental shelf sediments. *Geochim. Cosmochim. Acta* 58, 1271–1284.
- Mcleod, E., Chmura, G.L., Bouillon, S., Salm, R., Björk, M., Duarte, C.M., Lovelock, C.E., Schlesinger, W.H., Silliman, B.R., 2011. A blueprint for blue carbon: toward an improved understanding of the role of vegetated coastal habitats in sequestering CO<sub>2</sub>. *Front. Ecol. Environ.* 9, 552–560. <https://doi.org/10.1890/110004>
- Mcowen, C., Weatherdon, L., Bochove, J.-W., Sullivan, E., Blyth, S., Zockler, C., Stanwell-Smith, D., Kingston, N., Martin, C., Spalding, M., Fletcher, S., 2017. A global map of saltmarshes. *Biodivers. Data J.* 5, e11764. <https://doi.org/10.3897/BDJ.5.e11764>
- Megonigal, J.P., Hines, M.E., Visscher, P.T., 2004. Anaerobic Metabolism: Linkages to Trace Gases and Aerobic Processes, in: Schlesinger, W.H. (Ed.), *Treatise on Geochemistry*. Elsevier-Pergamon, Oxford, UK, pp. 317–424. <https://doi.org/10.1016/B0-08-043751-6/08132-9>
- Meire, P., Ysebaert, T., Van Damme, S., Van Den Bergh, E., Maris, T., Struyf, E., 2005. The Scheldt estuary: A description of a changing ecosystem. *Hydrobiologia* 540, 1–11. <https://doi.org/10.1007/s10750-005-0896-8>
- Mendelssohn, I.A., Sorrell, B.K., Brix, H., Schierup, H.H., Lorenzen, B., Maltby, E., 1999. Controls on soil cellulose decomposition along a salinity gradient in a *Phragmites australis* wetland in Denmark. *Aquat. Bot.* 64, 381–398. [https://doi.org/10.1016/S0304-3770\(99\)00065-0](https://doi.org/10.1016/S0304-3770(99)00065-0)
- Menichetti, L., Katterer, T., Leifeld, J., 2016. Parametrization consequences of constraining soil organic matter models by total carbon and radiocarbon using long-term field data. *Biogeosciences* 13, 3003–3019. <https://doi.org/10.5194/bg-13-3003-2016>
- Middelburg, J.J., Herman, P.M.J., 2007. Organic matter processing in tidal estuaries. *Mar. Chem.* 106, 127–147. <https://doi.org/10.1016/j.marchem.2006.02.007>
- Middelburg, J.J., Klaver, G., Nieuwenhuize, J., Wielemaker, A., de Haas, W., Vlug, T., Van Der Nat, F.W.A., 1996. Organic matter mineralization in intertidal sediments along an estuarine gradient. *Mar. Ecol. Prog. Ser.* 132, 157–168.
- Middelburg, J.J., Nieuwenhuize, J., 1998. Carbon and nitrogen stable isotopes in suspended matter and sediments from the Schelde Estuary. *Mar. Chem.* 60, 217–225. [https://doi.org/10.1016/S0304-4203\(97\)00104-7](https://doi.org/10.1016/S0304-4203(97)00104-7)
- Middelburg, J.J., Nieuwenhuize, J., Lubberts, R.K., van de Plassche, O., 1997. Organic carbon isotope systematics of coastal marshes. *Estuar. Coast. Shelf Sci.* 45, 681–687. <https://doi.org/10.1006/ecss.1997.0247>
- Miltner, A., Bombach, P., Schmidt-Brücken, B., Kästner, M., 2012. SOM genesis: microbial biomass as a significant source. *Biogeochemistry* 111, 41–55. <https://doi.org/10.1007/s10533-011-9658-z>
- Minasny, B., McBratney, A.B., Tranter, G., Murphy, B.W., 2008. Using soil knowledge for the evaluation of mid-infrared diffuse reflectance spectroscopy for predicting soil physical and mechanical properties. *Eur. J. Soil Sci.* 59, 960–971. <https://doi.org/10.1111/j.1365-2389.2008.01058.x>
- Moens, T., Bouillon, S., Gallucci, F., 2005. Dual stable isotope abundances unravel trophic position of estuarine nematodes. *J. Mar. Biol. Assoc. UK* 85, 1401–1407. <https://doi.org/10.1017/S0025315405012580>
- Moens, T., Luyten, C., Middelburg, J., Herman, P., Vincx, M., 2002. Tracing organic matter sources of estuarine tidal flat nematodes with stable carbon isotopes. *Mar. Ecol. Prog. Ser.* 234, 127–137. <https://doi.org/10.3354/meps234127>
- Moreira, C.S., Brunet, D., Verneyre, L., Sá, S.M.O., Galdos, M. V., Cerri, C.C., Bernoux, M., 2009. Near infrared spectroscopy for soil bulk density assessment. *Eur. J. Soil Sci.* 60, 785–791. <https://doi.org/10.1111/j.1365-2389.2009.01170.x>
- Morrissey, E.M., Gillespie, J.L., Morina, J.C., Franklin, R.B., 2014. Salinity affects microbial activity and soil organic matter content in tidal wetlands. *Glob. Chang. Biol.* 20, 1351–1362. <https://doi.org/10.1111/gcb.12431>
- Mudd, S.M., Howell, S.M., Morris, J.T., 2009. Impact of dynamic feedbacks between sedimentation, sea-level

## References

---

- rise, and biomass production on near-surface marsh stratigraphy and carbon accumulation. *Estuar. Coast. Shelf Sci.* 82, 377–389. <https://doi.org/10.1016/j.ecss.2009.01.028>
- Murray, N.J., Clemens, R.S., Phinn, S.R., Possingham, H.P., Fuller, R.A., 2014. Tracking the rapid loss of tidal wetlands in the Yellow Sea. *Front. Ecol. Environ.* 12, 267–272. <https://doi.org/10.1890/130260>
- Muyllaert, K., Dasseville, R., De Brabandere, L., Dehairs, F., Vyverman, W., 2005. Dissolved organic carbon in the freshwater tidal reaches of the Schelde estuary. *Estuar. Coast. Shelf Sci.* 64, 591–600. <https://doi.org/10.1016/j.ecss.2005.04.010>
- Muyllaert, K., Sabbe, K., Vyverman, W., 2009. Changes in phytoplankton diversity and community composition along the salinity gradient of the Schelde estuary (Belgium/The Netherlands). *Estuar. Coast. Shelf Sci.* 82, 335–340. <https://doi.org/10.1016/j.ecss.2009.01.024>
- Muyllaert, K., Sabbe, K., Vyverman, W., 2000. Spatial and Temporal Dynamics of Phytoplankton Communities in a Freshwater Tidal Estuary (Schelde, Belgium). *Estuar. Coast. Shelf Sci.* 50, 673–687.
- Nakanishi, T., Atarashi-Andoh, M., Koarashi, J., Saito-Kokubu, Y., Hirai, K., 2012. Carbon isotopes of water-extractable organic carbon in a depth profile of forest soil imply a dynamic relationship with soil carbon. *Eur. J. Soil Sci.* 63, 495–500. <https://doi.org/10.1111/j.1365-2389.2012.01465.x>
- Nelleman, C., Corcoran, E., Duarte, E., Valdés, L., De Young, C., Fonseca, L., Grimsditch, G. (Eds.), 2009. Blue carbon. A Rapid Response Assessment. United Nations Environ. Program. GRID-Arendal, [www.grida.no](http://www.grida.no).
- Neubauer, S.C., 2008. Contributions of mineral and organic components to tidal freshwater marsh accretion. *Estuar. Coast. Shelf Sci.* 78, 78–88. <https://doi.org/10.1016/j.ecss.2007.11.011>
- Nierop, K.G.J., Verstraten, J.M., 2004. Rapid molecular assessment of the bioturbation extent in sandy soil horizons under pine using ester-bound lipids by on-line thermally assisted hydrolysis and methylation-gas chromatography/mass spectrometry. *Rapid Commun. Mass Spectrom.* 18, 1081–1088. <https://doi.org/10.1002/rcm.1449>
- Nolting, R.F., Helder, W., De Baar, H.J.W., Gerringa, L.J.A., 1999. Contrasting behaviour of trace metals in the Scheldt estuary in 1978 compared to recent years. *J. Sea Res.* 42, 275–290. [https://doi.org/10.1016/S1385-1101\(99\)00036-2](https://doi.org/10.1016/S1385-1101(99)00036-2)
- Okumura, Y., 2015. Package “rpsychi.”
- Omengo, F.O., Geeraert, N., Bouillon, S., Govers, G., 2016. Deposition and fate of organic carbon in floodplains along a tropical semiarid lowland river (Tana River, Kenya). *J. Geophys. Res. Biogeosciences* 121, 1131–1143. <https://doi.org/10.1002/2015JG003288>
- Oreskes, N., Shrader-Frechette, K., Belitz, K., 1994. Verification, Validation, and Confirmation of Numerical Models in the Earth Sciences. *Science* (80-). 263, 641–646. <https://doi.org/10.1126/science.263.5147.641>
- Orgiazzi, A., Bardgett, R.D., Barrios, E., Behan-Pelletier, V., Briones, M.J.I., Chotte, J.-L., De Deyn, G.B., Eggleton, P., Fierer, N., Fraser, T., Hedlund, K., Jeffery, S., Johnson, N.C., Jones, A., Kandeler, E., Kaneko, N., Lavelle, P., Lemanceau, P., Miko, L., Montanarella, L., Moreira, F.M.S., Ramirez, K.S., Scheu, S., Singh, B.K., Six, J., van der Putten, W.H., Wall, D.H., 2016. Global soil biodiversity atlas. <https://doi.org/10.2788/2613>
- Ota, M., Nagai, H., Koarashi, J., 2013. Root and dissolved organic carbon controls on subsurface soil carbon dynamics: A model approach. *J. Geophys. Res. Biogeosciences* 118, 1646–1659. <https://doi.org/10.1002/2013JG002379>
- Ouyang, X., Lee, S.Y., 2014. Updated estimates of carbon accumulation rates in coastal marsh sediments. *Biogeosciences* 11, 5057–5071. <https://doi.org/10.5194/bg-11-5057-2014>
- Ouyang, X., Lee, S.Y., Connolly, R.M., 2017. The role of root decomposition in global mangrove and saltmarsh carbon budgets. *Earth-Science Rev.* 166, 53–63. <https://doi.org/10.1016/j.earscirev.2017.01.004>
- Parton, B., Ojima, D., Del Grosse, S., Keough, C., 2001. CENTURY tutorial - Supplement to CENTURY User's Manual.
- Pendleton, L., Donato, D.C., Murray, B.C., Crooks, S., Jenkins, W.A., Sifleet, S., Craft, C., Fourqurean, J.W., Kauffman, J.B., Marbà, N., Magonigal, P., Pidgeon, E., Herr, D., Gordon, D., Baldera, A., 2012. Estimating Global “Blue Carbon” Emissions from Conversion and Degradation of Vegetated Coastal Ecosystems. *PLoS*

- One 7. <https://doi.org/10.1371/journal.pone.0043542>
- Pessenda, L.C.R., Aravena, R., Melfi, A.J., Telles, E.C.C., Boulet, R., Valencia, E.P.E., Tomazellos, M., 1996. The use of carbon isotope ( $^{13}\text{C}$ ,  $^{14}\text{C}$ ) in soil to evaluate vegetation changes during the Holocene in central Brazil. *Radiocarbon* 38, 191–201. <https://doi.org/10.1017/S0033822200017562>
- Pessenda, L.C.R., Gouveia, S.E.M., Aravena, R., Gomes, B.M., Boulet, R., Ribeiro, A.S., 1998.  $^{14}\text{C}$  dating and stable carbon isotopes of soil organic matter in forest-savanna boundary areas in the southern Brazilian Amazon region. *Radiocarbon* 40, 1013–1022.
- Poeplau, C., Don, A., 2014. Effect of ultrasonic power on soil organic carbon fractions. *J. Plant Nutr. Soil Sci.* 177, 137–140. <https://doi.org/10.1002/jpln.201300492>
- Poeplau, C., Don, A., Vesterdal, L., Le, J., van Wesemael, B., Schumacher, J., Gensior, A., 2011. Temporal dynamics of soil organic carbon after land-use change in the temperate zone - carbon response functions as a model approach. *Glob. Chang. Biol.* 17, 2415–2427. <https://doi.org/10.1111/j.1365-2486.2011.02408.x>
- Poffenbarger, H.J., Needelman, B. a., Megonigal, J.P., 2011. Salinity influence on methane emissions from tidal marshes. *Wetlands* 31, 831–842. <https://doi.org/10.1007/s13157-011-0197-0>
- Powers, J.S., Schlesinger, W.H., 2002. Geographic and vertical patterns of stable carbon isotopes in tropical rain forest soils of Costa Rica. *Geoderma* 109, 141–160.
- R Core Team, 2017. R: A language and environment for statistical computing. R Foundation for Statistical Computing, Vienna, Austria. URL <https://www.R-project.org/>.
- Raymond, P. a, Bauer, J.E., 2001. Riverine export of aged terrestrial organic matter to the North Atlantic Ocean. *Nature* 409, 497–500. <https://doi.org/10.1038/35054034>
- Reeves, J.B., McCarty, G.W., Meisinger, J.J., 1999. Near Infrared Reflectance Spectroscopy for the Analysis of Agricultural Soils. *J. Near Infrared Spectrosc.* 7, 179–193. <https://doi.org/10.1255/jnirs.248>
- Reeves, J.B., Smith, D.B., 2009. The potential of mid- and near-infrared diffuse reflectance spectroscopy for determining major- and trace-element concentrations in soils from a geochemical survey of North America. *Appl. Geochemistry* 24, 1472–1481. <https://doi.org/10.1016/j.apgeochem.2009.04.017>
- Reeves III, J.B., 2010. Near- versus mid-infrared diffuse reflectance spectroscopy for soil analysis emphasizing carbon and laboratory versus on-site analysis: Where are we and what needs to be done? *Geoderma* 158, 3–14. <https://doi.org/10.1016/j.geoderma.2009.04.005>
- Regnier, P., Wollast, R., 1993. Distribution of Trace-Metals in Suspended Matter of the Scheldt Estuary. *Mar. Chem.* 43, 3–19. [https://doi.org/10.1016/0304-4203\(93\)90212-7](https://doi.org/10.1016/0304-4203(93)90212-7)
- Reimer, P., Bard, E., Bayliss, A., Beck, J., Blackwell, P., Ramsey, C., Buck, C., Cheng, H., Edwards, R., Friedrich, M., Grootes, P., Guilderson, T., Hafliðason, H., Hajdas, I., Hatté, C., Heaton, T., Hoffmann, D., Hogg, A., Hughen, K., Kaiser, K., Kromer, B., Manning, S., Niu, M., Reimer, R., Richards, D., Scott, E., Southon, J., Staff, R., Turney, C., van der Plicht, J., 2013. Intcal13 and marine13 radiocarbon age calibration curves 0 – 50,000 years cal bp. *Radiocarbon* 55, 1869–1887. <https://doi.org/10.2458/rc.v51i4.3569>
- Riley, W.J., Maggi, F., Kleber, M., Torn, M.S., Tang, J.Y., Dwivedi, D., Guerry, N., 2014. Long residence times of rapidly decomposable soil organic matter: application of a multi-phase, multi-component, and vertically resolved model (BAMS1) to soil carbon dynamics. *Geosci. Model Dev.* 7, 1335–1355. <https://doi.org/10.5194/gmd-7-1335-2014>
- Risse-Buhl, U., Hagedorn, F., Dümig, A., Gessner, M.O., Schaaf, W., Nii-Annang, S., Gerull, L., Mutz, M., 2013. Dynamics, chemical properties and bioavailability of DOC in an early successional catchment. *Biogeosciences* 10, 4751–4765. <https://doi.org/10.5194/bg-10-4751-2013>
- Robins, P.E., Skov, M.W., Lewis, M.J., Giménez, L., Davies, A.G., Malham, S.K., Neill, S.P., McDonald, J.E., Whitton, T.A., Jackson, S.E., Jago, C.F., 2016. Impact of climate change on UK estuaries: A review of past trends and potential projections. *Estuar. Coast. Shelf Sci.* 169, 119–135. <https://doi.org/10.1016/j.ecss.2015.12.016>
- Rocha, A. V., Goulden, M.L., 2009. Why is marsh productivity so high? New insights from eddy covariance and biomass measurements in a *Typha* marsh. *Agric. For. Meteorol.* 149, 159–168. <https://doi.org/10.1016/j.agrformet.2008.07.010>

## References

---

- Ross, A.C., Najjar, R.G., Li, M., Mann, M.E., Ford, S.E., Katz, B., 2015. Sea-level rise and other influences on decadal-scale salinity variability in a coastal plain estuary. *Estuar. Coast. Shelf Sci.* 157, 79–92. <https://doi.org/10.1016/j.ecss.2015.01.022>
- Ruddiman, W.F., 2003. The Anthropogenic Greenhouse Era Began Thousands of Years Ago. *Clim. Change* 61, 261–293. <https://doi.org/10.1023/B:CLIM.0000004577.17928.fa>
- Rumpel, C., Kögel-Knabner, I., 2010. Deep soil organic matter—a key but poorly understood component of terrestrial C cycle. *Plant Soil* 338, 143–158. <https://doi.org/10.1007/s11104-010-0391-5>
- Rumpel, C., Kögel-Knabner, I., Bruhn, F., 2002. Vertical distribution, age, and chemical composition of organic carbon in two forest soils of different pedogenesis. *Org. Geochem.* 33, 1131–1142. [https://doi.org/10.1016/S0146-6380\(02\)00088-8](https://doi.org/10.1016/S0146-6380(02)00088-8)
- Saintilan, N., Rogers, K., Mazumder, D., Woodroffe, C., 2013. Allochthonous and autochthonous contributions to carbon accumulation and carbon store in southeastern Australian coastal wetlands. *Estuar. Coast. Shelf Sci.* 128, 84–92. <https://doi.org/10.1016/j.ecss.2013.05.010>
- Salomons, W., Mook, W.G., 1981. Field observations of the isotopic composition of particulate organic carbon in the southern north sea and adjacent estuaries. *Mar. Geol.* 41, M11–M20.
- Scharlemann, J.P., Tanner, E.V., Hiederer, R., Kapos, V., 2014. Global soil carbon: understanding and managing the largest terrestrial carbon pool. *Carbon Manag.* 5, 81–91. <https://doi.org/10.4155/cmt.13.77>
- Schile, L.M., Kauffman, J.B., Crooks, S., Fourqurean, J.W., Glavan, J., Megonigal, J.P., 2017. Limits on carbon sequestration in arid blue carbon ecosystems. *Ecol. Appl.* 27, 859–874. <https://doi.org/10.1002/eap.1489>
- Schimel, J.P., Schaeffer, S.M., 2012. Microbial control over carbon cycling in soil. *Front. Microbiol.* 3, 1–11. <https://doi.org/10.3389/fmicb.2012.00348>
- Schimel, J.P., Weintraub, M.N., 2003. The implications of exoenzyme activity on microbial carbon and nitrogen limitation in soil: a theoretical model. *Soil Biol. Biochem.* 35, 549–563. [https://doi.org/10.1016/S0038-0717\(03\)00015-4](https://doi.org/10.1016/S0038-0717(03)00015-4)
- Schindler, D.E., Hilborn, R., 2015. Prediction, precaution, and policy under global climate change. *Science* (80-. ). 347, 953–954.
- Schmidt, M.W.I., Torn, M.S., Abiven, S., Dittmar, T., Guggenberger, G., Janssens, I. a, Kleber, M., Kögel-Knabner, I., Lehmann, J., Manning, D. a C., Nannipieri, P., Rasse, D.P., Weiner, S., Trumbore, S.E., 2011. Persistence of soil organic matter as an ecosystem property. *Nature* 478, 49–56. <https://doi.org/10.1038/nature10386>
- Schrumpf, M., Kaiser, K., 2015. Large differences in estimates of soil organic carbon turnover in density fractions by using single and repeated radiocarbon inventories. *Geoderma* 239–240, 168–178. <https://doi.org/10.1016/j.geoderma.2014.09.025>
- Schrumpf, M., Kaiser, K., Guggenberger, G., Persson, T., Kögel-Knabner, I., Schulze, E.-D., 2013. Storage and stability of organic carbon in soils as related to depth, occlusion within aggregates, and attachment to minerals. *Biogeosciences* 10, 1675–1691. <https://doi.org/10.5194/bg-10-1675-2013>
- Schubert, B.A., Jahren, A.H., 2012. The effect of atmospheric CO<sub>2</sub> concentration on carbon isotope fractionation in C<sub>3</sub> land plants. *Geochim. Cosmochim. Acta* 96, 29–43. <https://doi.org/10.1016/j.gca.2012.08.003>
- Schuur, E.A.G., Druffel, E., Trumbore, S.E. (Eds.), 2016. Radiocarbon and Climate Change. Springer International Publishing. <https://doi.org/10.1007/978-3-319-25643-6>
- Schuur, E.A.G., McGuire, A.D., Schädel, C., Grosse, G., Harden, J.W., Hayes, D.J., Hugelius, G., Koven, C.D., Kuhry, P., Lawrence, D.M., Natali, S.M., Olefeldt, D., Romanovsky, V.E., Schaefer, K., Turetsky, M.R., Treat, C.C., Vonk, J.E., 2015. Climate change and the permafrost carbon feedback. *Nature* 520, 171–179. <https://doi.org/10.1038/nature14338>
- Segoli, M., De Gryze, S., Dou, F., Lee, J., Post, W.M., Denef, K., Six, J., 2013. AggModel: A soil organic matter model with measurable pools for use in incubation studies. *Ecol. Modell.* 263, 1–9. <https://doi.org/10.1016/j.ecolmodel.2013.04.010>
- Servais, P., Billen, G., M.-C., H., 1987. Determination of the biodegradable fraction of dissolved organic matter in waters 21, 445–450.

- Shen, Y., Chapelle, F.H., Strom, E.W., Benner, R., 2015. Origins and bioavailability of dissolved organic matter in groundwater. *Biogeochemistry* 122, 61–78. <https://doi.org/10.1007/s10533-014-0029-4>
- Shi, S., Zhang, W., Zhang, P., Yu, Y., Ding, F., 2013. A synthesis of change in deep soil organic carbon stores with afforestation of agricultural soils. *For. Ecol. Manage.* 296, 53–63. <https://doi.org/10.1016/j.foreco.2013.01.026>
- Sierra, C.A., Müller, M., Trumbore, S.E., 2014. Modeling radiocarbon dynamics in soils: SoilR version 1.1. *Geosci. Model Dev.* 7, 1919–1931. <https://doi.org/10.5194/gmd-7-1919-2014>
- Sierra, C.A., Trumbore, S.E., Davidson, E.A., Vicca, S., Janssens, I., 2015. Sensitivity of decomposition rates of soil organic matter with respect to simultaneous changes in temperature and moisture. *J. Adv. Model. Earth Syst.* 7, 335–356. <https://doi.org/10.1002/2014MS000358>
- Simpson, A.J., Simpson, M.J., Smith, E., Kelleher, B.P., 2007. Microbially Derived Inputs to Soil Organic Matter: Are Current Estimates Too Low? *Environ. Sci. Technol.* 41, 8070–8076. <https://doi.org/10.1021/es071217x>
- Six, J., Conant, R.T., Paul, E. a, Paustian, K., 2002. Stabilization mechanisms of soil organic matter: Implications for C-saturation of soils. *Plant Soil* 241, 155–176. <https://doi.org/10.1023/A:1016125726789>
- Six, J., Elliott, E., Paustian, K., 2000. Soil macroaggregate turnover and microaggregate formation: a mechanism for C sequestration under no-tillage agriculture. *Soil Biol. Biochem.* 32, 2099–2103. [https://doi.org/10.1016/S0038-0717\(00\)00179-6](https://doi.org/10.1016/S0038-0717(00)00179-6)
- Six, J., Frey, S.D., Thiet, R.K., Batten, K.M., 2006. Bacterial and Fungal Contributions to Carbon Sequestration in Agroecosystems. *Soil Sci. Soc. Am. J.* 70, 555. <https://doi.org/10.2136/sssaj2004.0347>
- Smith, P., Lutfalla, S., Riley, W.J., Torn, M.S., Schmidt, M.W.I., Soussana, J.-F., 2018. The changing faces of soil organic matter research. *Eur. J. Soil Sci.* 69, 23–30. <https://doi.org/10.1111/ejss.12500>
- Soetaert, K., Herman, P.M.J., 1995. Estimating estuarine residence times in the Westerschelde (The Netherlands) using a box model with fixed dispersion coefficients. *Hydrobiologia* 311, 215–224. <https://doi.org/10.1007/BF00008582>
- Soetaert, K., Hoffmann, M., Meire, P., Starink, M., Van Oevelen, D., Van Regenmortel, S., Cox, T., 2004. Modeling growth and carbon allocation in two reed beds (*Phragmites australis*) in the Scheldt estuary. *Aquat. Bot.* 79, 211–234. <https://doi.org/10.1016/j.aquabot.2004.02.001>
- Spahni, R., Joos, F., Stocker, B.D., Steinacher, M., Yu, Z.C., 2013. Transient simulations of the carbon and nitrogen dynamics in northern peatlands: from the Last Glacial Maximum to the 21st century. *Clim. Past* 9, 1287–1308. <https://doi.org/10.5194/cp-9-1287-2013>
- Spohn, M., Babka, B., Giani, L., 2013. Changes in soil organic matter quality during sea-influenced marsh soil development at the north sea coast. *Catena* 107, 110–117. <https://doi.org/10.1016/j.catena.2013.02.006>
- Stevens, A., Nocita, M., Tóth, G., Montanarella, L., Wesemael, B. Van, 2013. Prediction of Soil Organic Carbon at the European Scale by Visible and Near InfraRed Reflectance Spectroscopy. *PLoS One* 8, 1–13. <https://doi.org/https://doi.org/10.1371/journal.pone.0066409>
- Stevens, A., Ramirez Lopez, L., 2014. An introduction to the prospectr package.
- Still, C.J., Berry, J.A., Collatz, G.J., DeFries, R.S., 2003. Global distribution of C<sub>3</sub> and C<sub>4</sub> vegetation: Carbon cycle implications. *Global Biogeochem. Cycles* 17, 6-1-6–14. <https://doi.org/10.1029/2001GB001807>
- Stuiver, M., Polach, H. a, 1977. Reporting of <sup>14</sup>C Data. *Radiocarbon* 19, 355–363. [https://doi.org/10.2458/azu\\_js\\_rc.v.493](https://doi.org/10.2458/azu_js_rc.v.493)
- Sulman, B.N., Phillips, R.P., Oishi, A.C., Shevliakova, E., Pacala, S.W., 2014. Microbe-driven turnover offsets mineral-mediated storage of soil carbon under elevated CO<sub>2</sub>. *Nat. Clim. Chang.* 4, 1099–1102. <https://doi.org/10.1038/nclimate2436>
- Suzuki, T., 2003. Economic and geographic backgrounds of land reclamation in Japanese ports. *Mar. Pollut. Bull.* 47, 226–229. [https://doi.org/10.1016/S0025-326X\(02\)00405-8](https://doi.org/10.1016/S0025-326X(02)00405-8)
- Tang, J., Riley, W.J., 2015. Weaker soil carbon–climate feedbacks resulting from microbial and abiotic interactions. *Nat. Clim. Chang.* 5, 56–60. <https://doi.org/10.1038/nclimate2438>

## References

---

- Tanner, B.R., Uhle, M.E., Mora, C.I., Kelley, J.T., Schuneman, P.J., Lane, C.S., Allen, E.S., 2010. Comparison of bulk and compound-specific  $\delta^{13}\text{C}$  analyses and determination of carbon sources to salt marsh sediments using n-alkane distributions (Maine, USA). *Estuar. Coast. Shelf Sci.* 86, 283–291. <https://doi.org/10.1016/j.ecss.2009.11.023>
- Tarnocai, C., Canadell, J.G., Schuur, E.A.G., Kuhry, P., Mazhitova, G., Zimov, S., 2009. Soil organic carbon pools in the northern circumpolar permafrost region. *Global Biogeochem. Cycles* 23, n/a-n/a. <https://doi.org/10.1029/2008GB003327>
- Temmerman, S., Govers, G., Meire, P., Wartel, S., 2003. Modelling long-term tidal marsh growth under changing tidal conditions and suspended sediment concentrations, Scheldt estuary, Belgium. *Mar. Geol.* 193, 151–169. [https://doi.org/10.1016/S0025-3227\(02\)00642-4](https://doi.org/10.1016/S0025-3227(02)00642-4)
- Temmerman, S., Govers, G., Wartel, S., Meire, P., 2004. Modelling estuarine variations in tidal marsh sedimentation: response to changing sea level and suspended sediment concentrations. *Mar. Geol.* 212, 1–19. <https://doi.org/10.1016/j.margeo.2004.10.021>
- Temmerman, S., Kirwan, M.L., 2015. Building land with a rising sea. *Science* (80-. ). 349, 588–589. <https://doi.org/10.1126/science.aac8312>
- Thomas, S., 2014. Blue carbon: Knowledge gaps, critical issues, and novel approaches. *Ecol. Econ.* 107, 22–38. <https://doi.org/10.1016/j.ecolecon.2014.07.028>
- Tian, H., Lu, C., Yang, J., Banger, K., Huntzinger, D.N., Schwalm, C.R., Michalak, A.M., Cook, R., Ciais, P., Hayes, D., Huang, M., Ito, A., Jain, A.K., Lei, H., Mao, J., Pan, S., Post, W.M., Peng, S., Poulter, B., Ren, W., Ricciuto, D., Schaefer, K., Shi, X., Tao, B., Wang, W., Wei, Y., Yang, Q., Zhang, B., Zeng, N., 2015. Global patterns and controls of soil organic carbon dynamics as simulated by multiple terrestrial biosphere models: Current status and future directions. *Global Biogeochem. Cycles* 29, 775–792. <https://doi.org/10.1002/2014GB005021>.Received
- Todd-Brown, K.E.O., Hopkins, F.M., Kivlin, S.N., Talbot, J.M., Allison, S.D., 2012. A framework for representing microbial decomposition in coupled climate models. *Biogeochemistry* 109, 19–33. <https://doi.org/10.1007/s10533-011-9635-6>
- Todd-Brown, K.E.O., Randerson, J.T., Hopkins, F., Arora, V., Hajima, T., Jones, C., Shevliakova, E., Tjiputra, J., Volodin, E., Wu, T., Zhang, Q., Allison, S.D., 2014. Changes in soil organic carbon storage predicted by Earth system models during the 21st century. *Biogeosciences* 11, 2341–2356. <https://doi.org/10.5194/bg-11-2341-2014>
- Todd-Brown, K.E.O., Randerson, J.T., Post, W.M., Hoffman, F.M., Tarnocai, C., Schuur, E.A.G., Allison, S.D., 2013. Causes of variation in soil carbon simulations from CMIP5 Earth system models and comparison with observations. *Biogeosciences* 10, 1717–1736. <https://doi.org/10.5194/bg-10-1717-2013>
- Tolman, M.E., Pranger, D.P., 2012. Toelichting bij de Vegetatiekartering Westerschelde 2010. Rijkswaterstaat, Ministerie van verkeer en Waterstaat, Delft.
- Torn, M.S., Lapenis, A.G., Timofeev, A., Fischer, M.L., Babikov, P. V., Harden, J.W., 2003. Organic carbon and carbon isotopes in modern and 100-year-old soil archives of the Russian Steppe. *Glob. Chang. Biol.* 8, 941–953. <https://doi.org/10.1046/j.1365-2486.2002.00477.x>
- Treseder, K.K., Balsler, T.C., Bradford, M.A., Brodie, E.L., Dubinsky, E.A., Eviner, V.T., Hofmockel, K.S., Lennon, J.T., Levine, U.Y., MacGregor, B.J., Pett-Ridge, J., Waldrop, M.P., 2012. Integrating microbial ecology into ecosystem models: challenges and priorities. *Biogeochemistry* 109, 7–18. <https://doi.org/10.1007/s10533-011-9636-5>
- Trumbore, S., 2009. Radiocarbon and Soil Carbon Dynamics. *Annu. Rev. Earth Planet. Sci.* 37, 47–66. <https://doi.org/10.1146/annurev.earth.36.031207.124300>
- Trumbore, S., 2000. Age of soil organic matter and soil respiration: radiocarbon constraints on belowground C dynamics. *Ecol. Appl.* 10, 399–411. [https://doi.org/10.1890/1051-0761\(2000\)010\[0399:AOSOMA\]2.0.CO;2](https://doi.org/10.1890/1051-0761(2000)010[0399:AOSOMA]2.0.CO;2)
- Trumbore, S., Davidson, E., Barbosa de Camargo, P., Nepstad, D., Martinelli, L.A., 1995. Belowground cycling of carbon in forests and pastures of Eastern Amazonia. *Global Biogeochem. Cycles* 9, 515–528.

- Vågen, T.-G., Winowiecki, L.A., 2013. Mapping of soil organic carbon stocks for spatially explicit assessments of climate change mitigation potential. *Environ. Res. Lett.* 8, 1–9. <https://doi.org/10.1088/1748-9326/8/1/015011>
- Valery, L., Bouchard, V., Lefevre, J.C., 2004. Impact of the invasive native species *Elymus athericus* on carbon pools in a salt marsh. *Wetlands* 24, 268–276. [https://doi.org/10.1672/0277-5212\(2004\)024\[0268:IOTINS\]2.0.CO;2](https://doi.org/10.1672/0277-5212(2004)024[0268:IOTINS]2.0.CO;2)
- Van Braeckel, A., Coen, L., Peeters, P., Plancke, Y., Mikkelsen, J., Van den Bergh, E., 2012. Historische evolutie van Zeescheldehabitats. Kwantitatieve en kwalitatieve analyse van invloedsfactoren. Rapporten van het Instituut voor Natuur- en Bosonderzoek (59). Instituut voor Natuur- en Bosonderzoek, Brussel i.s.m. het Waterbouwkundig Laboratorium, Antwerpen.
- Van Dam, D., Veldkamp, E., Van Breemen, N., 1997. Soil organic carbon dynamics: Variability with depth in forested and deforested soils under pasture in Costa Rica. *Biogeochemistry* 39, 343–375. <https://doi.org/10.1023/A:1005880031579>
- Van Damme, S., De Winder, B., Ysebaert, T., Meire, P., 2001. Het “bijzondere” van de Schelde: de abiotiek van het Schelde-estuarium. *Levende Nat.* 102, 37–39.
- Van Damme, S., Struyf, E., Maris, T., Ysebaert, T., Dehairs, F., Tackx, M., Heip, C., Meire, P., 2005. Spatial and temporal patterns of water quality along the estuarine salinity gradient of the Scheldt estuary (Belgium and The Netherlands): results of an integrated monitoring approach. *Hydrobiologia* 540, 29–45. <https://doi.org/10.1007/s10750-004-7102-2>
- Van de Broek, M., Temmerman, S., Merckx, R., Govers, G., 2016. Controls on soil organic carbon stocks in tidal marshes along an estuarine salinity gradient. *Biogeosciences* 13, 6611–6624. <https://doi.org/10.5194/bg-13-6611-2016>
- Van de Broek, M., Vandendriessche, C., Poppelmonde, D., Merckx, R., Temmerman, S., Govers, G., 2018. Long-term organic carbon sequestration in tidal marsh sediments is dominated by old-aged allochthonous inputs in a macrotidal estuary. *Glob. Chang. Biol.* <https://doi.org/10.1111/gcb.14089>
- Van den Berg, J.H., Jeuken, C.J.L., Van der Spek, A.J.F., 1996. Hydraulic processes affecting the morphology and evolution of the Westerschelde estuary, in: Nordstrom, K.F., Roman, C.T. (Eds.), *Estuarine Shores: Evolution, Environments and Human Alterations*. John Wiley & Sons Ltd., pp. 157–184.
- Van Der Nat, F., Middelburg, J.J., 2000. Methane emission from tidal freshwater marshes. *Biogeochemistry* 49, 103–121. <https://doi.org/10.1023/A:1006333225100>
- van der Spek, A.J.F., 1997. Tidal asymmetry and long-term evolution of Holocene tidal basins in The Netherlands: simulation of palaeo-tides in the Schelde estuary. *Mar. Geol.* 141, 71–90. [https://doi.org/10.1016/S0025-3227\(97\)00064-9](https://doi.org/10.1016/S0025-3227(97)00064-9)
- van Groenigen, K.J., Osenberg, C.W., Terrer, C., Carrillo, Y., Dijkstra, F.A., Heath, J., Nie, M., Pendall, E., Phillips, R.P., Hungate, B.A., 2017. Faster turnover of new soil carbon inputs under increased atmospheric CO<sub>2</sub>. *Glob. Chang. Biol.* 1–10. <https://doi.org/10.1111/gcb.13752>
- van Kessel, T., Vanlede, J., van Holland, G., 2015. Human versus natural mud fluxes in the Scheldt estuary: are they significant and if so, how can they best be optimised?, in: *Scheldt Estuary: Physics and Integrated Management - Special Session on of the 36th IAHR WORLD CONGRESS, 28 June – 3 July, 2015, The Hague, the Netherlands*. pp. 34–37.
- Van Rompaey, A.J.J., Govers, G., 2002. Data quality and model complexity for regional scale soil erosion prediction. *Int. J. Geogr. Inf. Sci.* 16, 663–680. <https://doi.org/10.1080/13658810210148561>
- Vasques, G.M., Grunwald, S., Sickman, J.O., 2008. Comparison of multivariate methods for inferential modeling of soil carbon using visible/near-infrared spectra. *Geoderma* 146, 14–25. <https://doi.org/10.1016/j.geoderma.2008.04.007>
- Verhoeven, J.T.A., Setter, T.L., 2010. Agricultural use of wetlands: opportunities and limitations. *Ann. Bot.* 105, 155–163. <https://doi.org/10.1093/aob/mcp172>
- Viscarra Rossel, R.A., Behrens, T., Ben-Dor, E., Brown, D.J., Demattê, J.A.M., Shepherd, K.D., Shi, Z., Stenberg, B., Stevens, A., Adamchuk, V., Aichi, H., Barthès, B.G., Bartholomeus, H.M., Bayer, A.D., Bernoux, M., Böttcher,

## References

---

- K., Brodský, L., Du, C.W., Chappell, A., Fouad, Y., Genot, V., Gomez, C., Grunwald, S., Gubler, A., Guerrero, C., Hedley, C.B., Knadel, M., Morrás, H.J.M., Nocita, M., Ramirez-Lopez, L., Roudier, P., Campos, E.M.R., Sanborn, P., Sellitto, V.M., Sudduth, K.A., Rawlins, B.G., Walter, C., Winowiecki, L.A., Hong, S.Y., Ji, W., 2016. A global spectral library to characterize the world's soil. *Earth-Science Rev.* 155, 198–230. <https://doi.org/10.1016/j.earscirev.2016.01.012>
- Viscarra Rossel, R.A., Bouma, J., 2016. Soil sensing: A new paradigm for agriculture. *Agric. Syst.* 148, 71–74. <https://doi.org/10.1016/j.agry.2016.07.001>
- Viscarra Rossel, R. a., McBratney, A.B., Minasny, B. (Eds.), 2010. *Proximal Soil Sensing*, 1st ed. Springer N. <https://doi.org/10.1007/978-90-481-8859-8>
- Viscarra Rossel, R. a., Walvoort, D.J.J., McBratney, a. B., Janik, L.J., Skjemstad, J.O., 2006. Visible, near infrared, mid infrared or combined diffuse reflectance spectroscopy for simultaneous assessment of various soil properties. *Geoderma* 131, 59–75. <https://doi.org/10.1016/j.geoderma.2005.03.007>
- von Fischer, J.C., Tieszen, L.L., 1995. Carbon Isotope Characterization of Vegetation and Soil Organic Matter in Subtropical Forest in Luquillo, Puerto Rico. *Biotropica* 27, 138–148. <https://doi.org/10.2307/2388989>
- Wallander, H., Nilsson, L.O., Hagerberg, D., Rosengren, U., 2003. Direct estimates of C:N ratios of ectomycorrhizal mycelia collected from Norway spruce forest soils. *Soil Biol. Biochem.* 35, 997–999. [https://doi.org/10.1016/S0038-0717\(03\)00121-4](https://doi.org/10.1016/S0038-0717(03)00121-4)
- Wang, G., Post, W.M., Mayes, M.A., 2013. Development of microbial-enzyme-mediated decomposition model parameters through steady-state and dynamic analyses. *Ecol. Appl.* 23, 255–272. <https://doi.org/10.1890/12-0681.1>
- Wang, J.J., Dodla, S.K., Delaune, R.D., Hudnall, W.H., Cook, R.L., 2011. Soil carbon characteristics in two Mississippi river deltaic Marshland profiles. *Wetlands* 31, 157–166. <https://doi.org/10.1007/s13157-010-0130-y>
- Wang, W., Liu, H., Li, Y., Su, J., 2014. Development and management of land reclamation in China. *Ocean Coast. Manag.* 102, 415–425. <https://doi.org/10.1016/j.ocecoaman.2014.03.009>
- Wang, X., Chen, W., Zhang, L., Jin, D., Lu, C., 2010. Estimating the ecosystem service losses from proposed land reclamation projects: A case study in Xiamen. *Ecol. Econ.* 69, 2549–2556. <https://doi.org/10.1016/j.ecolecon.2010.07.031>
- Wang, Z., Doetterl, S., Vanclooster, M., Van Wesemael, B., Van Oost, K., 2015a. Constraining a coupled erosion and soil organic carbon model using hillslope-scale patterns of carbon stocks and pool composition. *J. Geophys. Res. Biogeosciences* 120, 452–465. <https://doi.org/10.1002/2014JG002768>
- Wang, Z., Van Oost, K., Govers, G., 2015b. Predicting the long-term fate of buried organic carbon in colluvial soils. *Global Biogeochem. Cycles* 29, 65–79. <https://doi.org/10.1002/2014GB004912>
- Webster, J.R., Benfield, E.F., 1986. Vascular Plant Breakdown in Freshwater Ecosystems. *Annu. Rev. Ecol. Syst.* 17, 567–594.
- Werth, M., Kuzyakov, Y., 2010. <sup>13</sup>C fractionation at the root–microorganisms–soil interface: A review and outlook for partitioning studies. *Soil Biol. Biochem.* 42, 1372–1384. <https://doi.org/10.1016/j.soilbio.2010.04.009>
- Weston, N.B., Dixon, R.E., Joye, S.B., 2006. Ramifications of increased salinity in tidal freshwater sediments: Geochemistry and microbial pathways of organic matter mineralization. *J. Geophys. Res. Biogeosciences* 111, 1–14. <https://doi.org/10.1029/2005JG000071>
- Weston, N.B., Neubauer, S.C., Velinsky, D.J., Vile, M. a., 2014. Net ecosystem carbon exchange and the greenhouse gas balance of tidal marshes along an estuarine salinity gradient. *Biogeochemistry* 120, 163–189. <https://doi.org/10.1007/s10533-014-9989-7>
- Weston, N.B., Vile, M.A., Neubauer, S.C., Velinsky, D.J., 2011. Accelerated microbial organic matter mineralization following salt-water intrusion into tidal freshwater marsh soils. *Biogeochemistry* 102, 135–151. <https://doi.org/10.1007/s10533-010-9427-4>
- Whigham, D.F., 2009. Primary Production in Tidal Freshwater Wetlands, in: Barendregt, A., Whigham, D.,

- Baldwin, A. (Eds.), *Tidal Freshwater Wetlands*. Margraf Publishers GmbH, p. 320.
- Wieder, W.R., Bonan, G.B., Allison, S.D., 2013. Global soil carbon projections are improved by modelling microbial processes. *Nat. Clim. Chang.* 3, 909–912. <https://doi.org/10.1038/nclimate1951>
- Wieder, W.R., Grandy, A.S., Kallenbach, C.M., Bonan, G.B., 2014. Integrating microbial physiology and physiochemical principles in soils with the Microbial-MIneral Carbon Stabilization (MIMICS) model. *Biogeosciences* 11, 3899–3917. <https://doi.org/10.5194/bg-11-3899-2014>
- Wieski, K., Guo, H.Y., Craft, C.B., Pennings, S.C., 2010. Ecosystem Functions of Tidal Fresh, Brackish, and Salt Marshes on the Georgia Coast. *Estuaries and Coasts* 33, 161–169. <https://doi.org/10.1007/s12237-009-9230-4>
- Wilderom, M.H., 1973. Tussen afsluitdammen en deltadijken IV: Zeeuwsch Vlaanderen.
- Wilderom, M.H., 1968. Tussen afsluitdijken en deltadammen III: Midden-Zeeland.
- Williams, E.K., Rosenheim, B.E., 2015. What happens to soil organic carbon as coastal marsh ecosystems change in response to increasing salinity? An exploration using ramped pyrolysis. *Geochemistry, Geophys. Geosystems* 16, 2322–2335. <https://doi.org/10.1002/2015GC005839>
- Williams, J., Dellapenna, T., Lee, G., Louchouart, P., 2014. Sedimentary impacts of anthropogenic alterations on the Yeongsan Estuary, South Korea. *Mar. Geol.* 357, 256–271. <https://doi.org/10.1016/j.margeo.2014.08.004>
- Wolff, W.J., Van Eeden, M.J., Lammens, E., 1979. Primary production and import of particulate organic matter on a salt marsh in The Netherlands. *Netherlands J. Sea Res.* 13, 242–255.
- Woodwell, G.M., Rich, P.H., Mall, C.S.A., 1973. Carbon in estuaries, in: Woodwell, G.M., Pecari, E.V. (Eds.), *Carbon and the Biosphere*. U.S. AEC. <https://doi.org/10.1017/CBO9781107415324.004>
- Wynn, J.G., Bird, M.I., Wong, V.N.L., 2005. Rayleigh distillation and the depth profile of  $^{13}\text{C}/^{12}\text{C}$  ratios of soil organic carbon from soils of disparate texture in Iron Range National Park, Far North Queensland, Australia. *Geochim. Cosmochim. Acta* 69, 1961–1973. <https://doi.org/10.1016/j.gca.2004.09.003>
- Xie, W., He, Q., Zhang, K., Guo, L., Wang, X., Shen, J., 2017. Impacts of Human Modifications and Natural Variations on Short-Term Morphological Changes in Estuarine Tidal Flats. *Estuaries and Coasts* 1–15. <https://doi.org/10.1007/s12237-017-0352-9>
- Yin, A., Zhang, M., Gao, C., Yang, X., Xu, Y., Wu, P., Zhang, H., 2016. Salinity evolution of coastal soils following reclamation and intensive usage, Eastern China. *Environ. Earth Sci.* 75, 1–11. <https://doi.org/10.1007/s12665-016-6095-2>
- Zetsche, E., Thornton, B., Midwood, A.J., Witte, U., 2011. Utilisation of different carbon sources in a shallow estuary identified through stable isotope techniques. *Cont. Shelf Res.* 31, 832–840. <https://doi.org/10.1016/j.csr.2011.02.006>
- Zhang, H., Wu, P., Yin, A., Yang, X., Zhang, X., Zhang, M., Gao, C., 2016. Organic carbon and total nitrogen dynamics of reclaimed soils following intensive agricultural use in eastern China. *Agric. Ecosyst. Environ.* 235, 193–203. <https://doi.org/10.1016/j.agee.2016.10.017>
- Zhu, G., Xu, X., Wang, H., Li, T., Feng, Z., 2017. The ecological cost of land reclamation and its enlightenment to coast sustainable development in the northwestern Bohai Bay, China. *Acta Oceanol. Sin.* 36, 97–104. <https://doi.org/10.1007/s13131-017-1016-0>
- Zimmermann, M., Leifeld, J., Schmidt, M.W.I., Smith, P., Fuhrer, J., 2007. Measured soil organic matter fractions can be related to pools in the RothC model. *Eur. J. Soil Sci.* 58, 658–667. <https://doi.org/10.1111/j.1365-2389.2006.00855.x>